GRAVITY DRAINAGE: MICROSCOPIC STUDIES AND FREE FALL IN FRACTURED RESERVOIRS

by

VALIAHMAD SAJJADIAN

BSc Pet. Eng., MSc Res. Eng.

Submitted for the Degree of Doctor of Philosophy in

PETROLEUM ENGINEERING

Department of Petroleum Engineering

Heriot-Watt University

Edinburgh, UK

May 1999

TABLE OF CONTENTS

LIST OF SYMBOLS

A	Cross-sectional area
a_1, a_2, a_3	Matrix block dimensions
A_f	Cross sectional area of fracture
A_s	Cross sectional area of sample
b	Fracture aperture
C_{et}	Total effective compressibility
C_{pf}	Fracture pore compressibility
C_{pm}	Matrix pore compressibility
D	Diffusion coefficient
d	Distance between hanging drop center and bottom surface of block
D1, D2, D3	One, two, and three dimensions
d_g	Mean grain diameter
g	Acceleration of gravity
H_b	Block height
H_{eb}	Equivalent block height
H_f	Fracture height
He	Heterogeneous model
Ho	Homogeneous model
h_t	Threshold height
k	Permeability
k'_{rg}	End-point gas relative permeability
k'_{ro}	End-point oil relative permeability
k'_{rw}	End-point water relative permeability

k_a	Absolute permeability
k_f	Permeability of fracture
k_g	Apparent gas permeability
k_r	Permeability of composite system
$k_{rg,\ dra}$	Gas drainage relative permeability
$k_{ro,\ imb}$	Oil imbibition relative permeability
$k_{rw,\ imb}$	Water imbibition relative permeability
L	Length of the system
L_x, L_y, L_z	Lengths of the matrix block
m	Cementation factor
M	Mass flow rate
mw	Molecular weight
n	Saturation exponent
V_{cri}	Critical gas velocity
N	Number of blocks in stack
N_b	Bond number
N_c	Capillary number
N_f	Number of normal sets of fractures
N_t	Number of tubes per unit cross-section
P_1	Upstream pressure
P_2	Downstream pressure
P_c	Capillary pressure
P_{cf}	Capillary pressure of the fracture
P_{cd}	Capillary pressure of the drop
P_{nw}	Pressure in non-wetting phase

P_w	Pressure in wetting phase
q_b	Gas flow rate at base pressure P_b
q_f	Flow rate of fluid
q_i	Initial flow rate
q_{inf}	Infiltration rate
$q_{o\text{-}max}$	Maximum drainage rate
Q_w	The cumulative water injection in pore volumes
r	Radius of curvature
R	Recovery
R_∞	Ultimate recovery
r_1, r_2	Radii of curvatures
R_a	Rayleigh number
r_h	Hydraulic radius
r_i	Inner radius
R_m	Radius of physical model
R_o	Resistivity of the saturated sample
R_w	Resistivity of the electrolyte solution
s	Length measured along the tube
S*	Normalized saturation
S_f	Fracture spacing
S_g	Gas saturation
S_{gc}	Critical gas saturation
S_m	Interstitial surface area based on unit mass of porous media
S_o	Oil saturation
S_{or}	Residual oil saturation

S_{org}	Residual oil saturation by gravity drainage
S_{rem}	Remain oil saturation
S_v	Interstitial surface area based on unit volume of porous media
S_w	Water saturation
S_{wc}	Connate water saturation
S_{wirr}	Irreducible water saturation
t	Actual time
t_f	Film thickness
t_D	Dimensionless time
T_{maf}	Interporosity transmissibility
U	Superficial velocity
V	Velocity
$V_{fracture}$	Fracture volume
V_{matrix}	Matrix total volume
V_{pore}	Matrix pore volume
V_{total}	Total volume of matrix and fracture
V_x	Velocity in x-direction
V_y	Velocity in y-direction
w	Width of fracture (as illustrated in Figure 2.1)
W_A	Adhesion work
W_C	Cohesion work
Z_D	Dimensionless length
P	Mean Pressure
$(P_c)_d$	Capillary pressure of drop
$\bar{r}$	Capillary radius or hydraulic radius

$\bar{v}$	Average velocity
1/f	Empirical factor to include the effect of surface roughness

Greek Letters

α	Rate of convergence
β	Forcheimer coefficient
θ	Contact angle measured through the denser phase
σ	Interfacial tension
σ_f	Shape factor
σ_{sw}	Interfacial tension between solid and water
σ_{so}	Interfacial tension between solid and oil
σ_{wo}	Interfacial tension between water and oil
σ_{lg}	Interfacial tension between liquid and gas
$\varnothing$	Average diameter of the lens
φ	Porosity
φ_{matrix}	Matrix porosity
μ_o	Oil viscosity
ρ	Density of the fluid
ω	Storativity coefficient
λ	Interporosity flow coefficient
$\Delta\rho$	Density difference

Abbreviations

+ve	Positive
-ve	Negative
Exp.	Experiment/experiments
GIZ	Gas invaded zone
GOC	Gas oil contact
Lab.	Laboratory
LHS	Left hand side
MM	Micromodel
OGOC	Original gas oil contact
OWOC	Original water oil contact
RHS	Right hand side
Sec.	Secondary recovery
T	Gas absolute temperature
Ter.	Tertiary recovery
WIZ	Water invaded zone
WOC	Water oil contact

GLOSSARY

Some of the terms related to fractured reservoirs frequently used throughout this thesis are explained for the benefit of reader.

Adhesion: The molecular force exerted across a surface of contact between unlike liquids or solids that resists "interfacial" separation.

Brecciation: Disruption of strata, and development of fitted clasts separated by fractures of chaotic clasts with or without matrix, formed as a result of tectonism, carbonate dissolution and collapse, or evaporite dissolution and collapse.

Capillary: The minute openings between rock particles through which fluids are drawn.

Capillary number: The ratio of viscous forces to capillary forces i.e. $N_c = (\mu.v) / \sigma$.

Carbonate: Carbonates are potential reservoir rocks, primarily limestone and dolomite. Types of carbonate textures include rhombic, sucrosic, microsucrosic, grainy, subcrystalline, slabby, oolitic and pseudo-oolitic. About one-forth of the world's sedimentary rocks are carbonates.

Chalk: Carbonate rock of low-magnesian calcite composition composed dominantly of the remains of coccoliths and coccospheres.

Clastic: Term used in reference to particles (carbonate, siliciclastic, or other minerallogies) that commonly are transported by fluids

Cohesion: The molecular force exerted across a surface within a liquid or a solid that resists "internal" rupture.

Composite grain: Aggregate carbonate grain composed of discrete particles bound together by cement or organic mucilage.

Composite system: System that consists of both matrix and fractures.

Connate water: In reference to evolved waters ultimately of marine origin that have entrapped in sediment pores after their burial, and which have been out of contact with the atmosphere for an appreciable period of geologic time.

Contractional fractures: Result of volume shrinkage, as in the case of shales that lose water, cooling of igneous rock, and desiccation of sedimentary rock.

Cross-axis fracture: Joint or faults which strike perpendicular to the associated anticlinal or synclinal axis.

Dissolution: Process of dissolving substances.

Dolomitization: Replacement of a pre-existing carbonate sediment or rock by dolomite.

Dolostone: Synonym for dolomite rock.

Dual Porosity: System consisting of matrix and fracture each having different but nearly constant porosity.

End effect: Influence of capillary forces on the flooding behaviour that causes a spreading of the displacement front and build-up of the wetting phase at the end of the core.

Fault: Fracture with displacement parallel to the fracture surface.

Fracture: Is usually created as a result of breaking; a crack, division, split etc. caused by geomechanical stresses. A fracture can be either natural or induced, caused by drilling or well stimulation. Fractures can be either open or closed to fluid flow due to healing or mineralization. Fractures can be described as tensile, extension or shear-based on the stress that formed the fracture.

Fracture aperture/Fracture thickness: Opening of fracture from side to side.

Fracture number: The number of fractures in a given length.

Fracture porosity: Porosity of voids in the rock produced by natural fractures. Fracture porosity tends to be small, usually 0.1% - 1%.

Fracture set: A group of parallel joints or fractures.

Fracture spacing: The average distance between two parallel fractures.

Fractured reservoir: A subsurface reservoir of oil, water, or gas in which there are many inter connected natural fractures.

Free gravity drainage (F.G.D.): When the only driving force is the gravity force without any external force, it is called free gravity drainage. By this definition the ultimate saturation distribution inside the block is governed by the capillary pressure force of the block, and there would be no breakthrough of gas.

Free water level: The level at which water saturation is 100% and capillary pressure is zero.

Gas
Gas cap: Pocket of free gas trapped in the reservoir, above the oil column.
Free gas: Gas present in a vapour state.
Solution gas: Gas dissolved (in solution) in reservoir liquids.

Joint: One of a group of parallel fractures which has no detectable displacement parallel to the fracture surface.

Kerogen: Insoluble organic matter (fossilized), which can be converted by distillation into petroleum products.
Lithology: Descriptive, physical characteristics of rocks.

Longitudinal fractures: Fractures whose strike is parallel to associated longitudinal anticlinal or synclinal axis.

Matrix porosity: Porosity in the fine-grained portion of the reservoir rock, excluding the fracture void.

Matrix: The continuous material (sediment, cement) composing rocks; the continuous material enclosing interstices in rocks, between fractures.

Maximum capillary pressure: Capillary pressure at irreducible wetting phase saturation.

Oblique fracture: A fracture whose strike is oblique to the associated anticlinal or synclinal axis.

Rectilinear fracture set (vertical): Two perpendicular sets of fractures.

Reef: An organic build-up.

Stylolite: A pressure-solution feature, generally formed in moderately to deeply-buried rocks, characterized by a thin seam or suture of irregular, interlocking, saw-toothed appearance.

Texture: General physical appearance or characteristics of a rock, including parameters such as size, shape, sorting, and packing of constituent particles.

Threshold pressure: The lowest differential pressure necessary for moving out a wetting phase fluid from a pore in a rock, by non-wetting fluid.

Transmissibility: The product of permeability and cross-section area divided to length of the producing zone (k.A/L).

Unconformity: A substantial break or gap in the geologic record where a rock unit is overlain by another that is not next in the stratigraphic succession.

LIST OF TABLES

LIST OF FIGURES

ACKNOWLEDGMENTS

The author would first and foremost like to express his heartfelt thanks to professor A. Danesh and professor D. H. Tehrani for their continuous support, encouragement and invaluable guidelines.

Gratitude is also extended to Prof. Adrian C. Todd, Prof. Brian Smart and Dr. A. Emamzadeh for their support and encouragement for many years now.

I would like to extend my thanks to Dr. A.M. Saidi for his guidance and for his experience, so freely given over the past four years. I owe a great deal to Dr. G. D. Henderson and Mr. S. Ireland for helping build the laboratory apparatus and running the micromodel experiments.

I am also indebted to other friends and colleagues who helped me in different stages of this work. In particular Mr. Eric Mackay who has always attempted to answer my questions politely and sympathetically.

Finally, for their everlasting love and support during this period of my life, I proudly, dedicate this work to my wife and my children.

ABSTRACT

A study has been undertaken where micromodels and physical models were used to make qualitative and quantitative investigations of free gravity drainage mechanism.

The micromodel experimental works are aimed to improve the understanding of the physical process involved in free gravity drainage at pore level scale. The effect of pore geometry, fluid properties, wettability, layering and spreading coefficient on gravity drainage mechanism were investigated.

In order to evaluate free gravity drainage in a fractured reservoir, it is necessary to have some knowledge of the behaviour of the block-to-block interaction. The effect of the degree of the block-to-block interaction on the drainage performance of a stack of two blocks is investigated by the contributions of infiltration process, effect of contact area, capillary continuity and fracture capillary pressure.

Infiltration has investigated by using physical models at different saturation, position and supplied oil rate. It was found that the conventional constriction coefficient definition can not be accurately applied in free gravity drainage process. Another definition based on the ratio of drainage time of the constricted and unconstricted cases was represented. An investigation was also conducted with the objective being to establish the effect of horizontal fracture on gravity drainage of stack block. The effect of oil saturation and distribution inside the lower block on capillary pressure of horizontal fracture was investigated for the first time (to the best of our knowledge). From the capillary point of view, the key parameter is the fracture aperture.

A commercial simulator, was calibrated and used to numerically model the experiments.

CHAPTER-1

INTRODUCTION

1.1 BACKGROUND

Naturally fractured reservoirs are formed by stress forces that occur in slow deformations of the earth's crust, with fractures frequently appearing in a reasonably regular pattern. Due to additional network of fractures in the porous medium, the internal architecture of fractured reservoir is more complex than that of conventional sandstone reservoirs. The carbonate rocks are important reservoirs, more than two-thirds of the major reservoirs in the Middle East and about one-third of the major North American oil and gas fields are in carbonates (Halbouty, 1969). Carbonate reservoir rocks show large variations in porosity and permeability between reservoirs, and even within the same reservoir.

The naturally fractured carbonate reservoirs, all behave the same from a high productivity point of view which is much more than is expected from their rock permeability. A fractured porous medium is comprised of two different systems: 1- a matrix porous medium with high porosity and low permeability, 2- a fracture network with high permeability and low porosity.

The performance of a fractured reservoir depends on the intensity of fracturing, the fracture volume and the degree of fracture communication. In its depletion period, a fractured reservoir may be divided vertically into several distinct zones. These zones are mainly: gas cap, gas invaded, gassing, undersaturated oil, water invaded and aquifer. The presence of vertical fractures causes the gas-oil contact inside the fracture network exceeds the corresponding contact in the matrix block, where the gas invaded zone (GIZ) is formed. When the gravitational forces exceed the capillary forces, causes the fluid in the matrix block become unstable and thus producing oil from the blocks. The oil

recovery in this zone is therefore dominated by gravity drainage mechanism, which is one of the most efficient recovery mechanisms in fractured reservoir.

When the gravity force is the only driving force, the process is called, "free gravity drainage". In a free gravity drainage the ultimate saturation distribution inside the matrix block is governed by the capillary pressure curve of the block. This work is concerned with free gravity drainage phenomena at microscopic, core and reservoir scales.

1.2 OBJECTIVES

The main objective of this work is to highlight the mechanisms of gravity drainage from microscopic considerations and the block-to-block interaction process, i.e. reinfiltration and capillary continuity. By having enough knowledge about gravity drainage at the pore scale, the gravity drainage at a large scale can be analyzed more effectively, and the related experimental data by physical models can be more reliably interpreted.

By using micromodels, the motion of fluids and menisci can be magnified, observed and investigated, qualitatively, in terms of microgeometry and the physical characteristics of the liquids, gases, and solids present. The results and findings from micromodel studies can be used to improve our understanding of microscopic as well as macroscopic behavior of displacement process, and for modeling of the flow mechanisms at larger scales. In micromodel studies, pore-level phenomena are visualized and investigated to understand how oil/water and/or oil/gas menisci move, why an oil phase becomes disconnected and trapped into ganglia or blobs, and what is required to mobilize it. Micromodels have been used to observe the effect of systematic changes in many variables such as pore geometry and wettability, interfacial tension, density difference and initial saturation. Often these studies have not succeeded in isolating individual variables, but have illustrated important interrelationship between them.

In an actual fractured reservoir the blocks are neither completely isolated from each other, nor they are in full capillary contact. Furthermore, it is often possible that due to precipitation of asphaltene materials over the surface of block, and erosion between two neighboring blocks, the outlet surface of the block would be impermeable.

Experimental results have revealed that, the draining flow rate and ultimate recovery of a stack block are strongly related to interaction between blocks. The block to block interaction consists of two phenomena: 1- reinfiltration, and 2- capillary continuity. The block to block interaction depends on the physical properties of the matrix blocks, fractures and fluids.

In 1989, Firoozabadi et al. have published the results of the sixth *SPE* comparative solution "A Comparison of Dual-porosity Simulations." They argued that, the difference between results of the cases with zero and non-zero fracture capillary pressure is noticeable, and further investigation and development of the physics was recommended.

The block-to-block interaction, and the role of horizontal fracture in gravity drainage have imposed a real challenge to researchers during the last three decades. So far, no final conclusive result on the physics of this process has emerged. The purpose of this work is to resolve some of the uncertainties about the block-to-block interaction.

1.3 THESIS CONTENT

A review of the nature of porous media is presented in Chapter 2. Related basic parameters, including pore structure and fluid/solid interaction are detailed. The fluid/solid interaction is discussed under the contact angle, spreading, wettability, capillary pressure and relative permeability topics.

Carbonate rocks are not homogeneous or isotropic in their properties. Hence, the porosity, fluid saturation, bed thickness and rock types show very little uniformity

throughout reservoirs. Chapter 3, focuses on the reservoir engineering aspects of fractured reservoir to obtain basic information on carbonate reservoirs, such as geological features, and reservoir classification schemes. These issues and recovery mechanisms in fractured reservoirs such as the convection-diffusion process, solution gas drive, imbibition and gravity drainage are explained in detail.

Glass micromodels were used in this work to study various aspects of micro displacement by qualitative visual observation of the gravity drainage as explained in Chapter 4. Micromodels provide better understanding of many pore-scale gravity drainage processes. The experimental facilities are demonstrated as well as a description of the experimental procedure. The procedure of manufacturing glass micromodels by etching process is also detailed. Two series of experiments have been performed with different initial water and oil saturation, i.e. connate water saturation and residual oil saturation, respectively. The results of these tests are also applicable for gravity drainage in secondary and tertiary recovery processes. Film flow drainage, phase trapping, gas finger propagation processes as well as the effect of wettability and spreading coefficient on oil drainage process at the microscopic scale are also illustrated.

In Chapter 5, the gravity drainage mechanisms have been experimentally investigated in fractured porous media by using physical models. After briefly reviewing different views about the block-to-block interaction, attention is focused upon the effect of horizontal fractures on gravity drainage of a stack block. The experiments were performed in a simple but fully characterized system: single and/or stack of two homogeneous blocks, free gravity drainage at controlled room conditions. Synthetic oil and air were used as test fluids and the porous/non-porous spacers artificially constructed were used to model fractures. The first series of experiments were designed to study the flow pattern inside a matrix block, providing necessary knowledge and better understanding of free gravity

drainage from a single block. The next four series of experiments investigate the effect of horizontal fracture between blocks, the reinfiltration phenomena, the effect of contact area, and the capillary continuity.

The different approaches for simulation of fractured reservoirs are detailed in Chapter 6. A commercial simulator is used to predict the amount of oil drainage rate and production from a single/stack block. The simulation outputs are compared with the experimental data, demonstrating a good match between the model output and experimental data, indicating the capability of the dual porosity dual permeability option for simulating the gravity drainage process in fractured reservoirs.

The overall conclusions obtained from the study, as well as some recommendations for future work are presented in Chapter 7.

CHAPTER-2

THE NATURE OF POROUS MEDIA

2.1 INTRODUCTION

A porous medium consists of a solid matrix and interconnected pore space. The solid matrix may be rigid or may undergo small deformations. With a proper definition on the pore scale "*d*", the theory of flow through porous media is concerned with the behaviour of samples of typical scale "*l*" much larger than "*d*".

A distinctive property of a natural porous media is the irregular distribution (shape, size) of its pores. The dimension "*l*" of the laboratory sample is of the order of ten to thousands of "*d*" and such samples are generally homogeneous, in the sense that the irregular pore structure reproduces itself in the various portion of the sample.

There are two main categories of porous media. 1- Porous and permeable: When most of the pores are interconnected to form flow channels, the porous bodies become permeable to fluids. The degree of permeability of porous media depends on these interconnected pores (effective pore space). 2- Porous and impermeable: When the pore space does not form flow channels from one end to another end of the porous media, the medium is nonpermeable and cannot transmit fluid. The most common natural rock in this category is shale.

The voids within porous bodies are also classified according to size. The smallest are called "Interstices", the largest are "Caverns". The intermediate voids between these two are generally referred to as pore space. In formations such as limestone and dolomite, some pores are often created by a very slow process of leaching by solution during geological time, and are referred to as vugs.

2.2 PORE STRUCTURE, MACROSCOPIC PARAMETERS

2.2.1 Porosity (ϕ)

Porosity is defined as the fraction of the bulk volume of the porous sample that is occupied by pore or void space. There are two kinds of pore space, one which forms a continuous phase within porous media, called interconnected or effective pore space, and the other which consists of isolated or non-interconnected void or pore space. Non-interconnected void cannot contribute to transport of matter across the porous medium. Dead-end or stagnant pockets are interconnected only from one side. Although they can often be penetrated, they usually contribute only negligibly to transport. In certain mechanisms of flow (e.g. diffusion and dispersion phenomena), it is important to take into consideration the effects of dead-end pores. When the effective pore volume is used, the value is called effective porosity. Otherwise it is referred to as total porosity. Many porous media are made of a mixture of discrete large and small grains or particles that are either loose (unconsolidated) or held together by compaction and cementing material (consolidated).

2.2.2 Permeability

Permeability of porous media is defined as the ability to let fluid flow through its interconnected pore network. The most common expression for linear flow was developed by Henri Darcy in (1856). The generalized form of Darcy's equation is:

$$q = \frac{k \cdot A}{\mu}\left(\frac{\Delta P}{L} - \rho g \right) \qquad (2.1)$$

where q, μ, $\Delta P/L$, k, g, ρ and A are fluid rate in volume per unit time, viscosity of the fluid, pressure differential across the horizontal porous media, permeability, acceleration of gravity, density of fluid and cross-sectional area, respectively.

2.2.3 Single Phase Flow in a Single Fracture

In 1956, Huitt, studied the effect of surface roughness and the friction factor on single phase fracture flow experimentally based on the analogy to fluid flow between parallel plates. He showed that in the region of turbulent flow, the surface roughness effect becomes prominent.

Because of the proportionality between the flow rate and cube of the aperture, in a fracture network, the flow is dominated by the largest aperture. The focus in the single fracture phase flow studies was basically to characterize the surface roughness and represent the effect of surface roughness on the flow properties.

Witherspoon et al. (1980) have demonstrated the validity of the cubic law (analogy of flow between parallel plates) for tension fractures. These authors, therefore, have shown that hydraulic apertures are a major parameter of single phase flow in the type of fractures that they have utilized. By using the Poiseuille equation, the volume flow rate through a fracture with an aperture of b and width of w (see Figure 2.1) is given by:

$$q = \frac{b^3 w}{12\mu} \cdot \frac{\Delta P}{L} \qquad (2.2)$$

where q, μ and $\Delta P/L$ *are* volume flow rate, viscosity of the fluid and pressure differential across the fracture, respectively.

By equating the Darcy equation with Equation 2.2, the apparent formation permeability of the matrix block which contains such fracture becomes:

$$k_a = \frac{wb^3}{12A} = \varphi_f \frac{b^2}{12} \qquad (2.3)$$

where A and φ_f are total matrix cross section area and fracture porosity, respectively.

2.3 FLUID/SOLID INTERACTION PARAMETERS

2.3.1 Contact Angle

When two fluid phases, say oil and water, are in contact with a solid at a point, equilibrium is defined by the following equation:

$$\cos 6 = (\sigma_{sw} - \sigma_{so}) / \sigma_{ow} \qquad (2.4)$$

where σ_{sw}, σ_{so}, and σ_{ow} are interfacial tension between solid and water (denser fluid), interfacial tension between solid and oil (light fluid) and interfacial tension between water and oil (dense and light fluids), respectively.

The angle 6, measured through the denser phase (in this case water), is called the contact angle (see Figure 2.2). If $\theta < 90°$ the solid is described as being water wet, whereas if $\theta > 90°$ it is oil wet. It has been determined experimentally that the contact angle is larger when the wetting phase is advancing over the solid surface than when retreating. The difference between advancing and retreating angles is attributed to the hysteresis of the contact angle (see Figure 2.3).

2.3.2 Spreading Coefficient

Before 1912, the corresponding theory persisted that a drop of one pure liquid would always spread completely over the surface of another pure liquid on which it was placed. When an experiment yielded no evidence of spreading, it was assumed either, the liquid surface was contaminated or the layer too thin to be detected, and the remainder of the drop was in equilibrium with this film. In 1912, Hardy reported that pure heavy paraffin did not spread on water. He was apparently the first to suggest that chemical affinities between the liquids might be important as a cause of spreading. For the spreading of a liquid over a solid, Hardy suggested the theory that spreading occurred through the

condensation of vapour from the liquid over the solid surface and the subsequent spreading of the bulk of the liquid over this film of condensed vapour. Subsequent experiments revealed that spreading was a function of interfacial tensions between each of the liquids and the adjacent gas as well as the *IFT* between the two liquids.

The spreading coefficient is a measure of the tendency of one liquid to spread over another and is defined as:

$$S = W_A - W_C \tag{2.5}$$

where W_A , and W_C are the work of adhesion, and the work of cohesion, respectively.

The spreading coefficient may be developed on thermodynamic basis, since only large scale motion is of importance in spreading, only the free surface energies are involved.

The work of adhesion W_A, between two immiscible liquids is defined as the work necessary to separate unit area of the liquid-liquid interface and form two separate liquid-air interface, and is given as:

$$W_A = \sigma_{ng} + \sigma_{wg} - \sigma_{wo} \tag{2.6}$$

where σ_{ij} represent the free energy of the surface or interface per unit surface area (i.e. interfacial tension) between phases *i* and *j*.

The work of cohesion for a single liquid is that required to pull apart a column of liquid of unit cross sectional area in such a way as to give two surfaces, each one unit area, and is given as:

$$W_C = 2\,\sigma_{ng} \tag{2.7}$$

A combination of Equations (2.5), (2.6), and (2.7) gives:

$$S_{wo} = W_A - W_C = \sigma_{wg} - (\sigma_{ng} + \sigma_{wo}) \tag{2.8}$$

Therefore spreading occurs if the adhesion between the two liquids is greater than the cohesion in the liquid which is in the position for spreading, while spreading does not occur if the cohesion is greater than the adhesion.

Experiment shows that in some cases where oil spreads as a thick film, the film later contracts to form lenses in equilibrium with monolayer on the water. It is probable that no other condition is thermodynamically stable. When the contraction of the thick film begins, the change is mainly due to the three phases coming into equilibrium by molecular transfer between them. Their compositions and *IFT* values will gradually change until equilibrium conditions are attained. The spreading coefficient has now become negative, usually because of a reduction of σ-oil with time.

The necessary condition for spreading of oil over water or solid is simply that the process shall involve a decrease in free energy. When spreading is possible, it is the mechanism of the process rather than the magnitude of the spreading coefficient that determines the rate of spreading. Harkins (1952) pointed out that spreading may be extremely rapid in spite of a small energy difference.

In case of non-spreading oil the addition of a minute quantity of some 'active' substance (e.g. dye) may produce spreading, because the adsorption of the active substance at interface reduces the value of σ_{o-w}, to such an amount which changes the sign of spreading coefficient from negative to positive.

The weak point is that the three tensions each have a magnitude much larger than that of *S* itself. It is not uncommon that the total uncertainty of each tension value is as large as the spreading coefficient. Langmuir (1917) showed theoretically that the equilibrium spreading coefficient *S* of an oil on water is related to the thickness of an infinitely large lens of the oil t_- on water as:

$$S = \frac{t_-^2 g (\rho_{o(w)} - \rho_v)(\rho_{w(o)} - \rho_{o(w)})}{2(\rho_{w(o)} - \rho_v)} \qquad (2.9)$$

where $\rho_{w,o}$, $\rho_{o,w}$, ρ_{v}, and g are the mass density of water saturated with the oil, the oil saturated with water, the mass density of the vapour phase which can be neglected in many cases, and the acceleration due to gravity, respectively.

For complete spreading or wetting of the solid, the contact angle must be zero (see Figure 2.4).

Referring to Equation 2.10 and Figure 2.5, a lens of oil can reside, unspread, on water surface when the spreading coefficient is negative, i.e.:

$$\sigma_{wg} < \sigma_{og} + \sigma_{wo} \qquad (2.10)$$

On the other hand when the spreading coefficient in non-negative, i.e.:

$$\sigma_{wg} \geq \sigma_{og} + \sigma_{wo} \qquad (2.11)$$

oil will spread over water in the form of a thin film.

In Chapter four, for micromodel study, 18 experiments were conducted by using dyed oil, the oil was dyed by Ferrosen and Sudan. To investigate the effect of dyes on the spreading coefficient, nine experiments were performed. In these experiments a drop of oil was added to the water surface, the results of experiments are presented in Table 2.1. Suppose for a particular, oil-gas-water system the spreading coefficient is positive before they come into equilibrium but clearly negative after equilibrium is achieved. What is expected to happen is that as soon as oil comes into contact with water (in presence of gas), oil will spread over the water as a thick film. The film later contracts to form lenses in equilibrium with mono-layer on the water (Test 9 in Table 2.1).

Conversely, if the initial value of spreading coefficient is negative but its final equilibrium value is non-negative, when oil is added to water a lens is formed initially and the oil spreads over water later when equilibration is achieved (Test 4, in Table 2.1).

The shape of lens will depend on the values of the three *IFT*s and the densities of gas and

Table 2.1 Experiments on spreading of decane on water (A drop of oil was added to the water surface).

Exp no	Oil (Cyclic)	Water	t = 0 min	t = 2 min	t = 5 min	t = 10 min	t = 20 min	t = 40 min	t = 12 hr
1	Pure	distilled	Circular shape stain (Ø=1.5 cm)	Ø=1.7 cm	Ø=2.0 cm	Ø=2.9 cm	Deformed, Ø=4.0 cm	Change to a small circular lens, Ø=0.5 cm, and then disappeared	
2		brine	Circular shape stain (Ø=1.5 cm)	Ø=1.7 cm	Ø=3.5cm	Ø=2.0 cm, shrunk to a lens	Ø=1.0 cm, shrunk further	Change to a small circular lens, Ø=0.2 cm, and then disappeared	
3		methyl-blue	A stain (Ø=1.0 cm) without specific geometry shape	Ø=2.0 cm	Ø=2.5 cm	Ø=2.5 cm	Ø=2.0 cm	Ø=2.5 cm	The stain disappeared
4	Ferrocene	distilled	Circular shape stain (Ø=1.0 cm)	Ø=1.7 cm	Ø=1.7 cm, small red spots at circumference	Ø=2.0 cm	Deformed, Ø=3.0 cm	The stain disappeared	
5		brine	Circular shape stain (Ø=1.0 cm)	Ø=1.7 cm	Ø=1.7 cm, small red spots at circumference	Ø=2.0 cm	Deformed, Ø=1.8 cm	Small knock would divided it in to several pieces and mostly disappeared	The stain disappeared, very little residual scattered on surface
6		methyl-blue	The stain spread quickly	Ø=4.0 cm, several coloured counter lines near circumference	Shrinkage (Ø=2.0 cm)	Disappeared			
7	Sudan Red	distilled	Circular shape stain (Ø=2.5 cm)	Ø=4.0 cm	Ø=4.5 cm, small red spots at circumference	The red spots modified to small chunks	Deformed to elliptical shape, Ø=4.0 & 6 cm		The main stain disappeared but some of those chunks remained on the surface
8		brine	Circular shape stain (Ø=2.5 cm)	Ø=4.0 cm	Ø=4.5 cm, small red spots at circumference	Main stain (Ø=2.0 cm), coloured lines (Ø=4.0 cm), brown crescent (Ø=2.0 cm)	No change		The main stain disappeared but some of those chunks remained on the surface
9		methyl-blue	Without specific geometry (Ø=5 cm) checkmate colour		A brown crescent outside and several coloured counter lines toward inside of its perimeter			No change and it seems stable	No change

Ø = Average diameter of the lens in cm.

oil. The more negative the spreading coefficient the thicker will be the lens, so the larger will be the angle between σ_{ow} and σ_{no}.

2.3.3 Wettability

A knowledge of reservoir wettability is an important prerequisite for success in any oil recovery operation. The relative distribution of oil and water as well as their flow behaviour within the porous rock matrix have been attributed to wettability. Reservoir wettability is understood to mean the relative preference of the rock surface to be in contact with oil and water. Wettability is determined by the interaction of rock and fluid properties.

A comprehensive review of literature pertaining to wettability was presented by McCaffery (1973) and the extensive survey articles by W.G. Anderson (1986A, 1986B, 1986C, 1987A, 1987B, and 1987C) are excellent sources for further information. The minerals from which reservoir rocks are formed are all high energy solids. Determination of reservoir wettability from contact angle measurements for reservoir fluids at smooth mineral surfaces might be regarded as a grossly over simplified approach to a complex problem. One main problem is that of obtaining a surface which is representative of the reservoir rock surface. Treiber et al. (1972) found that wettability, as determined from contact angle measurements on smooth crystal surfaces, was qualitatively consistent with wettability as judged by relative permeability measurements. Contact angle data were reported for 55 reservoirs, and these indicate that a wide range of wettability conditions may be encountered. They used water advancing contact angles in the range 0 to 75, 75 to 105, and 105 to 180 to classify reservoirs as respectively water-wet, intermediately-wet, or oil wet.

Mixed wet rock

Before the migration of oil into a formation, the rock is saturated with water and 100% water wet. After the entry of oil into the rock and displacement of water out of it, initially some residual water (connate water) stays in the corners and a film of water covers all the pore surfaces. The rock is still 100% water-wet.

By passage of time gradually some molecules of oil pass through the in-situ water towards the rock surface. In areas where the water film is thin the oil molecules reach the rock surface first, and depending on the oil-water-rock chemistry some oil molecules may adhere to the rock surface. This adhesion process gradually makes those parts of the rock surface oil wet. The areas still exposed to thick films of water and the tight corners remain water wet. Therefore, there is a correlation between the water wetness and S_{wc}; the higher the S_{wc} the higher the water wettability of the rock. Normally the rock near the crest of the reservoir has lower S_{wc} and is more oil-wet, and the rock close to *WOC* has higher S_{wc} and is more water-wet.

2.3.4 Capillary Pressure

The capillary pressure profiles determine ultimate economic oil recovery, location of gas-oil and water-oil contacts, and transition zones. The fundamental property of liquid surfaces is that they tend to contract to the smallest possible area. If a liquid surface is curved the pressure is greater on the concave side than on the convex. Young-Laplace equation, is the foundation of the classical theory of capillary pressure.

$$P_c = P_1 - P_2 = \sigma_{1,2}\left(\frac{1}{R_1} + \frac{1}{R_2}\right) \qquad (2.12)$$

where R_1 and R_2 are the principal radii of curvature, p_1 and p_2 are pressure in concave and convex sides respectively, and $\sigma_{1,2}$ is the interfacial tension between the two fluids.

Capillary pressure, is the differential pressure that exists between two fluid phases at their interface.

$$P_c = P_{nw} - P_w \qquad (2.13)$$

where P_{nw}, and P_w are pressure in non-wetting phase, and pressure in wetting phase, respectively, on either side of interface at one point.

For a fracture of aperture b, the aperture acts as diameter of the capillary tube, and its capillary pressure is calculated as:

$$P_c = \frac{2\,\sigma\,\cos\theta}{b} \qquad (2.14)$$

2.3.5 Relative Permeability

Petroleum reservoirs producing under primary, secondary, or tertiary processes usually involve the simultaneous flow of two or more fluids. Multiple-phase flow of fluids through porous media can be related to relative permeability of each phase, fluid viscosities, pressure drop, capillary pressure, and absolute permeability. Of these, relative permeabilities are the least understood and the most difficult quantities to measure.

Relative permeability is an extension of permeability concept as defined by Darcy's flow equation for single phase flow to simultaneous transport of two or three immiscible fluid phases through porous media. The concept which assumes that each of the flowing phases is continuous and noninteracting with the porous matrix, was first proposed by Bukingham (1907). Wyckoff et al. (1937) then, defined the term effective permeability for each of the flowing phases.

Two phase flow in a single fracture

The Romm's study (1966) showed that the straight line relative permeability which are commonly used in numerical simulations are valid for flow in two smooth parallel plates. He used kerosene-water and performed the experiments for different fractures.

In 1990, Pruess and Tsang measured gas-water relative permeability for a single fracture containing a certain degree of surface roughness. They verified their results numerically by assigning log-normally distributed apertures while neglecting the matrix contribution. They concluded that the behaviour of two phase flow in a fracture is similar to that in porous media i.e. not necessary straight lines.

Although these studies have provided an insight to the problem of two-phase flow in a fracture, understanding the two phase flow in a network of fractures including the matrix effect is much harder to handle experimentally. More experimentation to clarify and formulate the matrix-fracture process is required.

2.4 EFFECTS OF VISCOUS, CAPILLARY, AND GRAVITATIONAL FORCES ON IMMISCIBLE DISPLACEMENT EFFICIENCY

Immiscible displacements in porous media with capillary, gravity and viscous effects can be characterized by two dimensionless numbers, the capillary number N_c, and the Bond number N_b.

2.4.1 Capillary Number

One suitable criterion for correlating mobilization of residual oil is the capillary number; a dimensionless group, which is the ratio of viscous to interfacial forces. It has been used in the literature to demonstrate the dependence of ultimate recovery on viscous and capillary forces. For the case of water displacing oil:

$$N_c = \frac{\mu_w V_w}{\varphi \sigma_{ow}} \qquad (2.15)$$

where N_c is the capillary number, V_w and μ_w are water flow rate per unit cross sectional (Darcy velocity) and viscosity, respectively, φ is porosity and σ_{ow} is the oil/water interfacial tension. For a typical waterflood, its value is typically in the order of 10^{-6}.

Lefebvre du Prey (1973) and Foster (1973) observed that the microscopic displacement efficiency, E_M, defined as:

$$E_M = \frac{1 - S_{or} - S_{wi}}{1 - S_{wi}} \qquad (2.16)$$

was independent of N_c. Melrose and Brandner (1974), however, correlated E_M with capillary number and obtained a critical value of N_c which, when exceeded, will permit E_M to increase to unity. Based on the premise that when viscous forces begin to compete with capillary forces, the critical value for N_c is reached, they calculated $N_{c,\,critical}$ to be approximately 10^{-3} with a range of observed critical values of 10^{-6} to $3*10^{-2}$. The lower critical value corresponds to displacement of large oil ganglia occupying several pores formed during original water displacement, and the upper limit is associated with displacement of single pore droplets. According to them, it is the shape and size distribution of the pores rather than absolute size which controls the critical value of the capillary number. The easiest way to significantly increase capillary number is to lower interfacial tension.

The capillary number difference given in the equation below was used by Pavone (1989) instead of the capillary number.

$$\Delta N_c = \frac{(\mu_o - \mu_w)V_w}{\sigma_{ow}} \qquad (2.17)$$

The advantage of using the capillary number difference is that viscous forces of both the oil and water are accounted for in the displacement process.

2.4.2 Bond number

Buckley and Leverett (1942), in the derivation of their frontal advances equation, assumed both gravity and capillary forces to be negligible compared to viscous forces. Hovanessian and Fayers (1961) solved the one-dimensional displacement equation, which included a gravity function and a capillary function, using a finite difference scheme and

obtained the effect of inclusion of these terms in a linear waterflood. The gravity term included in their treatment is a gravitational force which, they concluded, had significant effect on saturations, pressure, and fractional flow profiles of an oil-wet system. Catchpole and Fulford (1966) obtained a dimensionless group, the Bond number, which is a ratio of gravitational to interfacial forces and is involved in multiple-phase flow of fluids:

$$N_B = \frac{\Delta\rho\, g\, R^2}{\sigma} \tag{2.18}$$

where N_B, $\Delta\rho$, g, and R are the Bond number, the fluid density difference, the acceleration due to gravity, and the particle radius, respectively. For low permeability porous media, this term is likely to have very little effect on relative permeability (Bardon and Longeron, 1980). However, in situations where interfacial tension is very low, such as during surfactant or microemulsion flooding miscible displacement, Bond numbers may be high enough to cause vertical segregation of oil and water and permit fingering of injection water through the lower portion of the core (Foster, 1973). Morrow and Songkran (1979) studied the effect of both capillary number and Bond number on trapping and mobilization of oil in random packing of equal spheres of glass. For a gas-oil system, they reported that gravity forces were important when the Bond number was in the range of 0.005 to 0.33. Below this range, these forces were negligible, and above 0.33, they dominated capillary forces.

In the case of three-phase flow, there will be two Bond numbers and two capillary numbers, and how these will affect three-phase relative permeabilities remains to be explored.

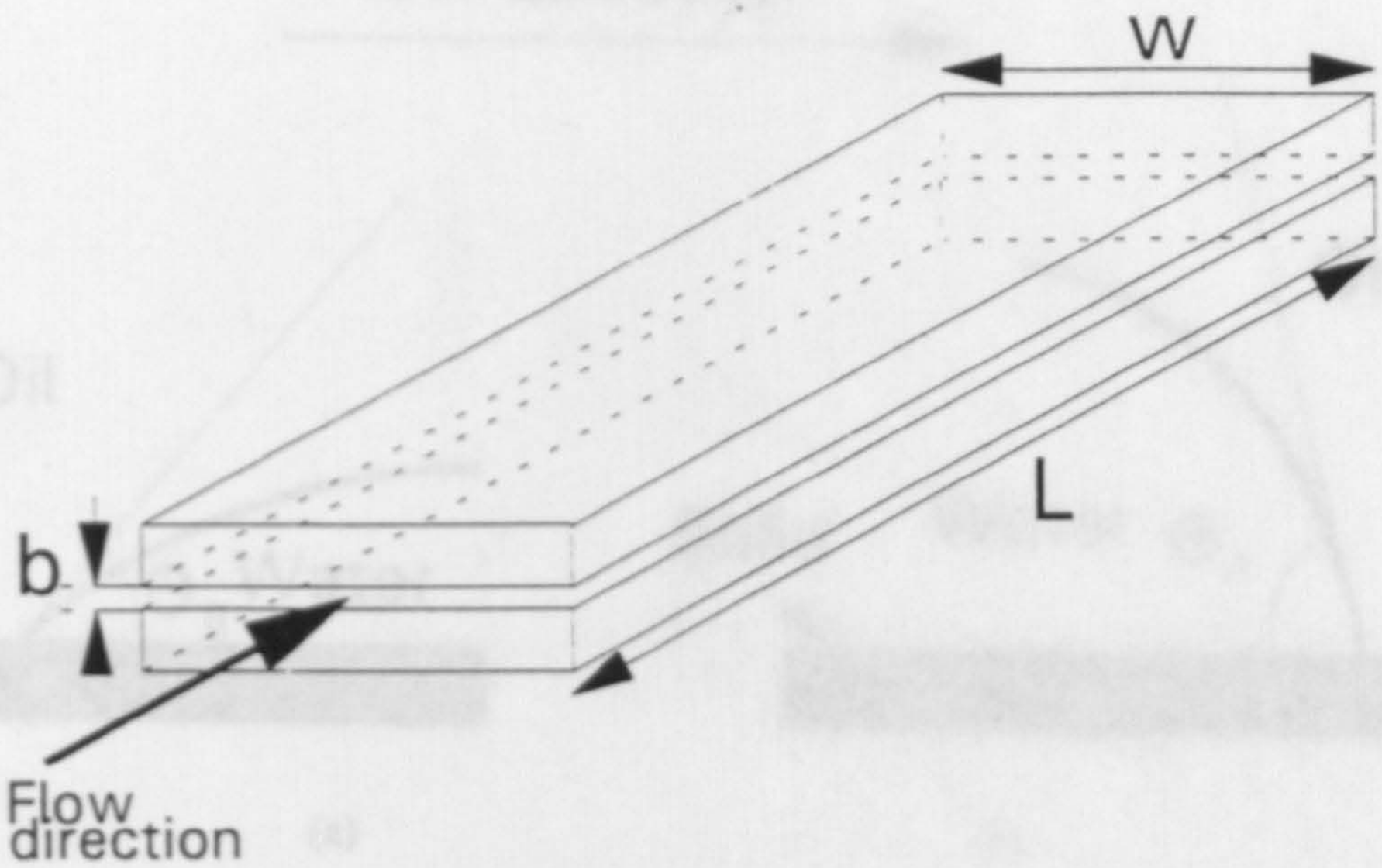

Figure 2.1 Schematic representation of slab matrix with its associated fracture.

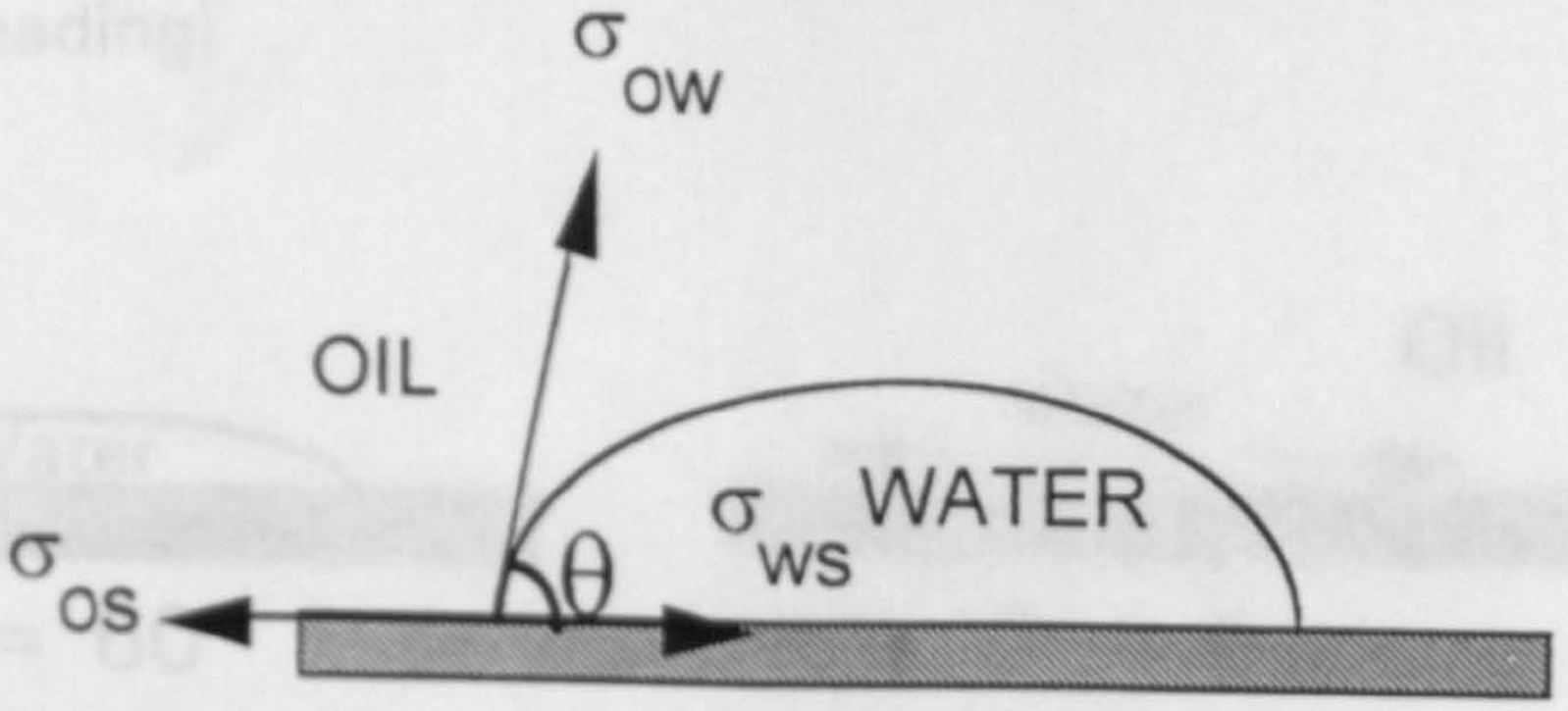

Figure 2.2 Contact angle between water and oil phases.

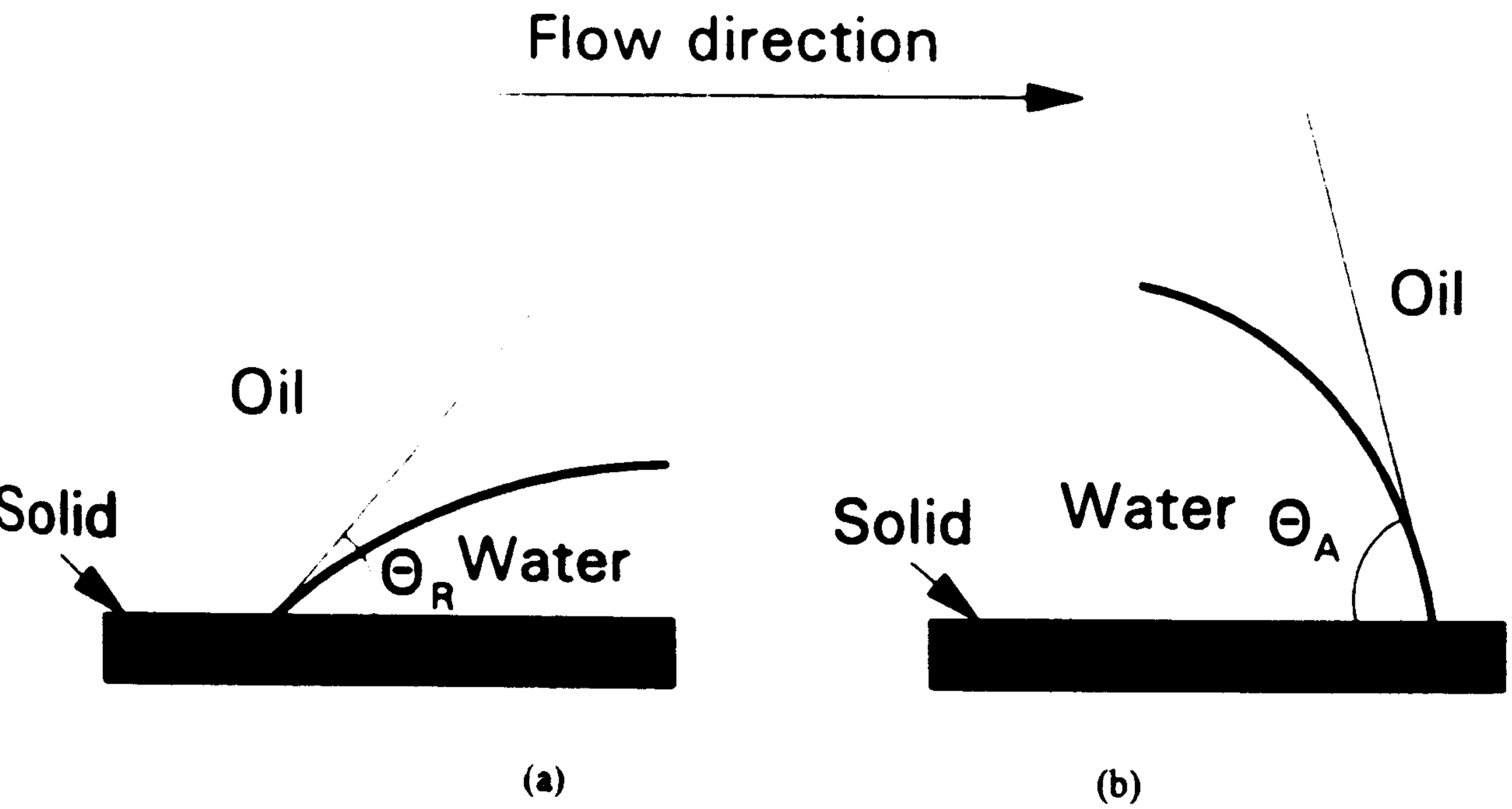

Figure 2.3 Hysteresis in contact angle, a-Drainage, b-Imbibition.

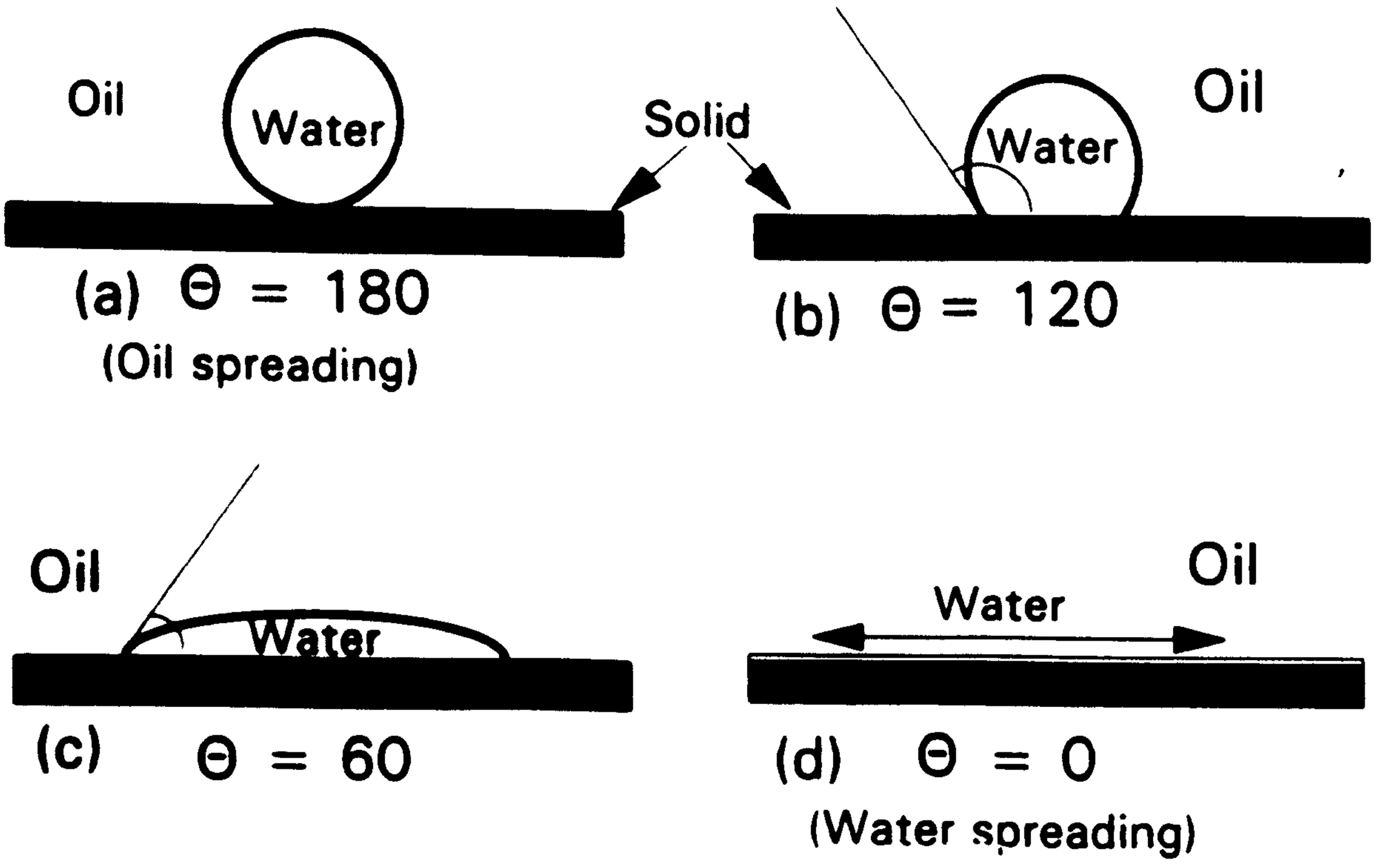

Figure 2.4 Examples of contact angles and spreading.

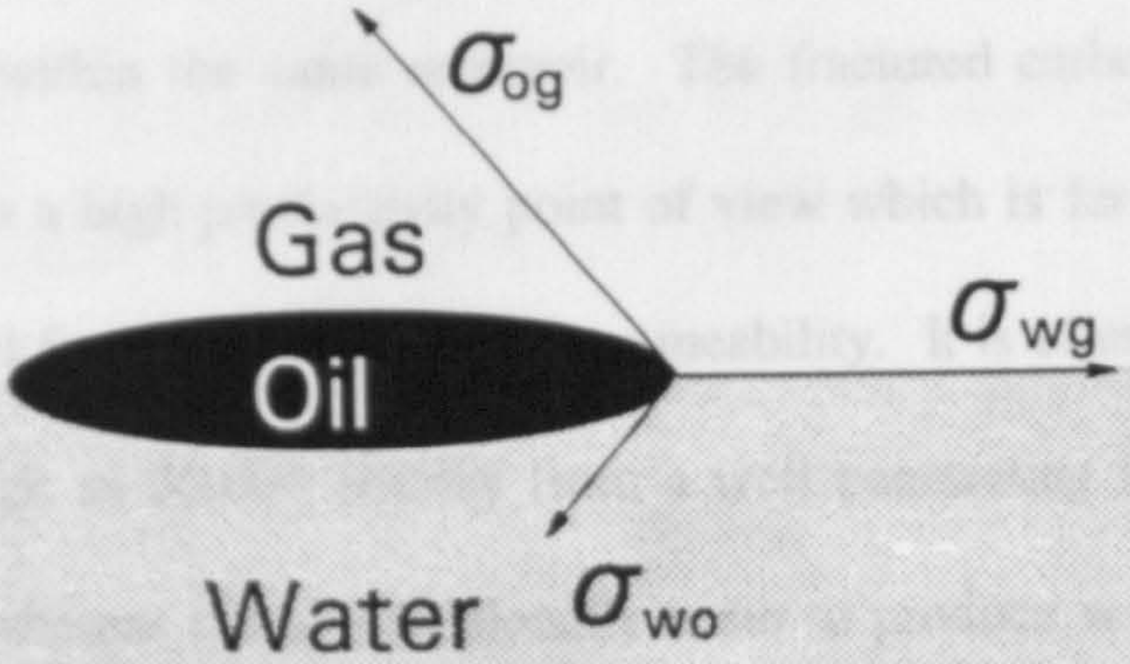

Figure 2.5 Spreading of oil on water.

CHAPTER-3

THE RESERVOIR ENGINEERING ASPECTS OF THE FRACTURED RESERVOIRS

3.1 INTRODUCTION

Carbonate reservoir rocks show large variations in porosity and permeability between reservoirs, and even within the same reservoir. The fractured carbonate reservoirs, all behave the same from a high productivity point of view which is far more in excess of that which is expected from their rock matrix permeability. It is often possible to have a production rate as high as 30,000 bbl/day from a well penetrating less than 10 feet of fractured carbonate, whereas it may occasionally occur to produce very little from a well which is penetrated more than 1000 feet in an unfractured carbonate reservoir. This opposite extreme, can only be described by the existence or absence of fissures and fractures in the formation. A fractured reservoir may be divided vertically into several distinct zones sometime in its depletion period. These zones are mainly: gas cap, gas-invaded, gassing, undersaturated oil, water invaded, and water zone (see Figure 3.1).

Gas and water-invaded zones are those portions of the reservoir in which blocks are surrounded by gas or water within the fractures. In a gas invaded zone, oil is draining out of these blocks essentially due to gravity drainage. In a water invaded zone, for the case of water and/or fractional wettability in addition to gravity segregation, capillary imbibition also influences the recovery performance. The gravity force is essentially the force resulting from the density difference between oil and gas, or water and oil, acting against the retention capillary forces. The gassing zone consists of the portion of the reservoir where the pressure of the matrix is below the prevailing bubble-point pressure. In the lower portion of this zone, where $S_g < S_{gc}$, a solution gas drive mechanism takes place in the known sense of it, except for the volume of gas transfer due to diffusion.

When free gas reaches its critical saturation in the upper portion of gassing zone, gas moves upward due to its lower density than oil. Therefore, the recovery due to the solution-gas drive mechanism is mainly a function of the rate of pressure drop and the resulting effect determines the final fluid saturation in the blocks.

In the under saturated portion of the reservoir two processes take place: a- expansion of the liquids and b- diffusion of gas through oil from matrix to the fracture. The diffusion process causes the oil in the matrix to lose some of its gas and therefore, oil from the fracture replaces the equivalent volume of lost gas.

The performance of the fractured reservoirs depends on the intensity of fracturing, the fracture volume and the degree of fracture communication. The oil content of the matrix blocks in a fractured limestone reservoir is normally much greater than the volume of the oil filled fissures. For the case of matrix porosity of 15%, and oil saturation of 90%, 13.5% of total bulk volume is occupied by oil. However, the fissure volume may only be 0.1% if 1 mm-wide fissures occur every 10 feet. In most conditions it is reasonable to assume that the oil recovery from the fissure is 100%, while the oil recovery from the matrix blocks, will depend on the balance of the gravitational, viscous, and capillary forces between the fluids and the rock. The gravitational forces are determined by the density difference between the oil and water or gas. The viscous forces will depend on the rock permeability, and fluid viscosity, whereas the capillary forces will depend on the characteristics of the rock and the fluids.

3.2 GEOLOGICAL FEATURES OF FRACTURED RESERVOIR

The internal architecture of a fractured reservoir is more complex than that of conventional sandstone reservoirs. This is due to the additional network of fractures in the porous medium, which results from tectonic forces which have broken the rock. The three discontinuous units are superimposed on the matrix, which are of variable

permeability. These units are: a- The fracture network, b- Channels in these fractures and cavities, and c- The network of stylolites.

The carbonate rocks are important reservoirs (see Table 3.1), more than two-thirds of the major reserves in the Middle East reside in carbonates, about one-third of the major North American oil and gas fields are in carbonates and they produce about half of the total oil produced from North American giant fields (Halbouty, 1969). In 1982, Nelson argued that, any fractured reservoir, should be treated as two systems i.e. matrix and fracture, communication or interaction between these two systems may be inhibited by mineralization within or deformation along the fracture plane surface.

It is well known that, the magnificent exposed Asmari limestone formations in south west Iran (see Figures 3.2 and 3.3), duplicate their buried counter parts, and provide a good situation for the study of reservoir fabric. In all of the structures studied the predominant faults are of the longitudinal and cross-axis type, resulting from the stretching of the Asmari limestone during folding of the anticlines. McQuillan et al. (1961) showed that fissures with wide aperture are filled in preference to tight "hair line" fractures and to matrix pores; this causes a breakdown of permeable channels to the well bore but does not destroy matrix porosity. Therefore, the most server effects of mineralization occur in the fault drainage system; the joint system seems to be less seriously affected. They conclude that, most of the tight fractures are either free of cement or are coated with a thin layer of drusy calcite. But because of the filling of the larger fissures, there may be no mechanism to drain these joints to wellbore. Anhydrite is the principal fracture-plugging agent; Calcites are of lesser importance. Pyrite and Celestite are present, in small amounts.

Birks (1957) in his study of the geology of the Asmari reservoirs, has recognized some fractures with apertures of up to 5 mm, which are usually partly filled with secondary minerals. He concludes that, the apertures of fracture remaining open is usually greater than 1 mm. These larger fractures result in capillary discontinuities while the hairline

fractures do not. His evidence from some part of the outcrop indicates that, the larger fractures are spaced at the most 20 feet apart while the hairline fractures are probably less than 10 feet apart.

Carbonate reservoir rocks include the following lithological types:

1. Dolomite. Dolomite limestone is generally accepted that is formed by molecular replacement of calcium by magnesium in the original limestone.

2. Accretionary limestone. These are formed in situ and include bioherms (or reefs), biostromes, and pelagic limestones.

3. Clastic limestones. These sediments are formed by mineral grain precipitation resulting from erosion and weathering of limestone originally deposited elsewhere.

4. Chemical limestones. This type of sediment is formed by the direct chemical precipitation of calcitic grains from carbonate solutions in shallow seas.

3.2.1 Types of Porosity in Carbonate Reservoirs

1. Inter crystalline or primary porosity results from interstitial voids inside individual crystal or grain. Primary porosity has the tendency to be discontinuous because of void spaces by fine material and cement. Primary porosity in limestones seldom gives economical oil reservoirs.

2. Inter granular porosity is specifically the pore development in heterogeneous packed clastic sediments. Chalk exhibits a typical inter granular porosity.

3. Oolitic porosity results from the packing of fossil spheres of almost uniform diameter. The original packing usually approaches the hexagonal pattern of 26 percent porosity.

4. Vuggy and fissure porosity results from leaching of carbonate rocks by solutions or circulating water and is characterized by channels and large openings inside the rocks.

5. Fracture porosity results from earth movements which create joints and faults through which solution waters may gain easy access throughout the massive rock.

6. Fossiliferous porosity is developed by leaching when fossils are more soluble than the rock.

7. Reef porosity is a type of fossiliferous porosity and results from decay of organic matter originally filling the openings.

3.3 RELATIONSHIP BETWEEN FRACTURE PARAMETERS

3.3.1 Nature of Fracture

The nature of fractures mainly concerns the state of fracture under observation with reference to opening, filling and wall characteristics. The discontinuity which breaks the rock beds into blocks along cracks, fissures, joints or whatever they may be referred to as, and along which there is no displacement parallel with the plane of discontinuity is referred to as a fracture. A fracture in which relative displacement has occurred can be defined as a fault. While a fracture in which no noticeable displacement has occurred can be defined as a joint. Macro-fracture corresponds to a fracture with a large aperture (over 100 microns) and micro-fracture applies to a fracture of limited length and aperture (below 100 microns).

Depending on circulating water and precipitation, which is capable of plugging the fracture with anhydrite, minerals..., a fracture may be *open* or *closed* (see Figure 3.4). On the other hand, fractures which are closed in surface conditions may often be open or partially open in reservoir conditions where pore pressure acts on fracture walls. The width of the opening may depend (at reservoir conditions) on depth, pore pressure and type of rock. The fracture aperture varies between 10-200 microns, but statistics have shown that the most frequent range is between 10-40 microns. The description has to mention whether, the opening is free (providing void space), or more or less filled up with various crystallized materials. Very narrow openings (≅100 microns) define fissures.

Single fracture parameters

A single fracture may be characterized by the following parameters:

a- Fracture aspect: The surface of fissure plane offers a surface either: rough, smooth, glassy, or grooved.

b- Fracture opening/fracture aperture: Fracture aperture is represented by the distance between the fracture walls.

c- Fracture size: Fracture size refers to the relationship between fracture length and layer thickness, especially if a qualitative evaluation is to be formulated.

i- minor fractures: have a length less than the width of a single layer.

ii- average fractures: extend to more layers.

iii- major fractures: have a very large extension, often tens or even hundreds of meters.

d- Fracture dip: Fracture dip is the angle between the fracture surface and the horizontal plane. The angle is measured in the direction of the steepest descent. The azimuth of the line representing the intersection of the fracture plane with a horizontal plane is termed the *strike* of the fracture (see Figure 3.5).

Fractures associated with folding

Based on the direction of folding axis, three types of fractures may be identified (see Figure 3.6);

a- *longitudinal fractures*: along the folding axis

b- *transversal fractures*: perpendicular to the folding axis

c- *diagonal fracture*: in relation with the folding axis

Fractures and stress state

If fractures are associated to one or more states of stress they are divided into two groups:

a- *conjugate fractures*: are those which have been developed from a unique state of stress.

b- *non-conjugate (orthogonal) fractures*: which are associated to more than one stress center.

The totality of the fractures

a- *a fracture system*: is formed by all fractures having the same mutually parallel direction.

b- *a fracture network*: is the result of various fracture systems.

Fractures associated with stratigraphy

The variation of dimensions and density of fractures depend on lithology and thickness of the layer in which the fractures are developed. The results obtained will divide the fractures into two categories:

a- first-order fractures: are those which cut through several layers of rock.

b- second-order fractures: are limited to a single layer of rock.

Analytical parameters

The length of that part of a fracture visible on a core is a function of its dip and core diameter.

$$L = D / \cos \alpha \qquad (3.1)$$

where D, and α are the core diameter, and the dip angle, respectively.

Fracture interval: represents the length of the matrix between two consecutive fracture:

$$e = d. \cos \alpha \qquad (3.2)$$

where d is the distance, measured on the core, between the considered fractures.

Fracture density: is the degree of rock fracturing through various relative ratio. If the ratio refers to the bulk volume, the area or to a length the fracture density is called volumetric, areal or linear respectively. The linear fracture density is also called fracturing rate, fracture frequency or linear frequency and is defined by:

$$F = 1/e = 1/(d. \cos \alpha) \qquad (3.3)$$

3.3.2 Fracture Porosity

The two types of pore-space within a fractured reservoir can be expressed as follows:

a- Matrix porosity (exclusive of fractures)

$$\phi_{matrix} = \frac{v_{pore}}{v_{matrix}} \tag{3.4}$$

b-Fracture porosity

$$\phi_{fracture} = \frac{v_{fracture}}{v_{total}} \tag{3.5}$$

Total porosity

$$\phi_{total} = \frac{v_{pore} + v_{fracture}}{v_{total}} = \frac{v_{pore}}{v_{total}} + \frac{v_{fracture}}{v_{total}} \tag{3.6}$$

Generally the fracture volume is very small compared with the total volume of the system ($\cong 1\%$), therefore it can be written as:

$$\phi_t = \phi_m + \phi_f \tag{3.7}$$

Apertures of "true" joints, as distinct from fault-associated fractures, were measured on polished surfaces of representative limestone cores (Kulander, 1979). They were found to range from submicroscopic tracers of very small "micro-joints" to a maximum of about 0.25 mm. The average is believed to be about 0.1 mm. This is a very small aperture, but it provides permeability at several orders of magnitude larger than that of the matrix.

Based on the spacing of fractures measured in exposed structures and upon the apertures measured in cores, fracture void volume is probably about one tenth of one percent of the total reservoir (bulk) volume. When the dimensions of the block are 0.9 * 0.9 * 1.5 feet i.e. each vertical face is cut by one vertical joint and one horizontal joint. The volume of these joints (assuming an average aperture of 0.1 mm) is 0.093 per cent of the bulk volume. If we assume that spacing is even as much as twice as close (because of micro-fractures not visible on the exposure) we still have less than 0.2 per cent of bulk volume in the joints.

Many of the microfractures are blind (do not intersect the interconnected joint network) and consequently are not effective drainage channels. If we consider only the larger joints

known to connect with the joint network, their volume is 0.056 per cent of bulk volume. Weighting these figures for local highly porous fault zones, we conclude that a reasonable total for effective fracture void porosity is about one tenth of one percent of bulk volume. The fracture porosity provides a channel for gas segregation and oil drainage. Also, all the oil in the fissures are fully displaced by either gas or water. In reservoirs with high matrix porosity only a small amount of the *IOIP* is inside the fissures, and the effects on displacement efficiency is not so important. However, in reservoirs with a small matrix porosity, the fracture porosity plays a more important role in recovery performance of the reservoir. The higher the fracture porosity results, the smaller the difference between *GOC* levels in matrix and fracture, therefore the lower the gas and water displacement efficiency in the matrix blocks.

3.3.3 Fracture Permeability

Fluid transmissibilities in fractures are governed by fracture aperture and relative permeabilities to flowing phases. Because of the proportionality between the flow rate and cube of the aperture, in a fracture network, the flow is dominated by the largest aperture. The focus in single fracture phase flow studies was basically to characterize the surface roughness and represent the effect of surface roughness on the flow properties.

For a system that is composed of a series of planer fractures of constant aperture b, height h, and spacing S, and negligible matrix porosity and permeability. The flow rate through a planer fracture is given by:

$$q_f = \frac{\Delta p.b^2.A_f}{12\mu L} \tag{3.8}$$

where ΔP, μ, q_f, L, and b are the pressure drop along the fracture, the viscosity of the fluid, the flow rate of the fluid, the length of the fracture, and the aperture of the fracture, respectively.

From Darcy's law,

$$q_s = \frac{\Delta p . k_s . A_s}{\mu L} \tag{3.9}$$

where q_s, A_s, and k_s are the flow rate, the cross-sectional area, and the permeability of the system, respectively.

If the matrix permeability is zero, and we assume only one fracture, then

$$q_f = q_s \quad \text{or} \quad k_s = (\frac{1}{12})(\frac{A_f}{A_s})(b^2) \tag{3.10}$$

Converting into Darcy's unit,

$$k_s = (84.4 * 10^5)(\frac{A_f}{A_s})(b^2) \tag{3.11}$$

where k_s, b, A_f, and A_s are the permeability of system in darcy, the aperture of the fracture in cm, the cross-sectional area of fracture in cm^2, and the cross-sectional area of the system in cm^2, respectively. If the sample width is assumed to be equal to the fracture spacing, then from Equation 3.11,

$$k_s = (84.4 * 10^5)(\frac{b^3}{a}) \tag{3.12}$$

and the porosity of the sample is given by:

$$\phi_s = \frac{b}{a}(100) \tag{3.13}$$

The permeability is related to the third power of the fracture aperture and is inversely related to the fracture spacing. Therefore, the aperture of the fracture has more influence on the sample permeability than the fracture spacing does.

Witherspoon (1980) have demonstrated the validity of the cubic law (analogy of flow through parallel plates) for tension fractures. This author, therefore, has shown that hydraulic aperture is a major parameter of single phase flow in the type of fractures that

they have utilized. He has also proposed the following empirical correlation between fracture flow rate and fracture aperture.

$$q = \left(\frac{wb^3}{12\mu}\right)\left(\frac{dP}{dx}\right)\left(\frac{1}{f}\right) \qquad (3.14)$$

where q, w, b, and dP/dx are the flow rate, the fracture width, the fracture aperture, and pressure gradient across the system, respectively. $1/f$ is empirical factor to include the effect of surface roughness.

For a rectangular element structure of matrix blocks with the dimensions 'a_1', 'a_2', 'a_3' and a fracture aperture of 'b' (see Figures 3.7 and 3.8), Reiss (1980) presented fracture porosity and permeability as:

$$f = w\left(\frac{1}{a_1} + \frac{1}{a_2} + \frac{1}{a_3}\right) \qquad (3.15)$$

and, $$k_f = f\frac{b^3}{12} \qquad (3.16)$$

Jones et al. (1988) suggested the following equations for open, rough fractures with single-phase flow:

$$q = 5.06 * 10^4 \, w[\Delta p \, b^3 / f L \rho]^{0.5} \qquad (3.17)$$

and

$$k = 5.39 * 10^5 \mu [b L / f \, \Delta p \, \rho]^{0.5} \qquad (3.18)$$

where q, b, Δp, w, L, μ, k, ρ, *and* f are the volumetric rate of flow (bbl/D), the aperture of the fracture (in), the pressure drop (psi), the width of the fracture face (ft), the length of the fracture (ft), the viscosity of the fluid (cp), the permeability (darcy), the density of fluid (lb/ft^3), and the friction factor (which is dimensionless), respectively.

In 1966, Parsons suggested the following expression, for the composite fractured rock:

$$k_f = k_r + \frac{b^3.\cos^2\alpha}{12h_b} \qquad (3.19)$$

where k_f, k_r, α, and h_b stand for permeability of the composite system, the matrix rock permeability, the angle between the pressure gradient and fracture plane, and the matrix block height , respectively.

The studies of Huitt (1956) and Parsons (1966) provided the following two equations for determining permeability of fracture-rock system, k_{rf}, in direction of pressure gradient. In their model, an idealized fracture-matrix system was considered, (i.e. a slab of rock, such that the slab faces are vertical and perpendicular to the pressure gradient). Every fracture has the same orientation and aperture, and there is a constant spacing between fractures.:

$$k_{fr} = k_m + (5.446 * 10^{10} b^3 \cos^2 \alpha) / a \qquad (3.20)$$

where k_m, b, a, and α are the matrix permeability (mD), the fracture aperture (in), the distance between fractures (in), and the angle of deviation of the fracture from the horizontal plane in degree, respectively. If b and a expressed in mm, then Equation 3.20 becomes:

$$k_{fr} = k_m + (8.44 * 10^{7} b^3 \cos^2 \alpha) / a \qquad (3.21)$$

3.3.4 Effect of Stress Change on Fracture Aperture

The permeability variation of fractures, as a function of pressure drop in reservoir is given generally by the following relation (Jones, 1975):

$$k_f = k_{fi}\left(1 - C_{pf} . \Delta P\right)^3 \qquad (3.22)$$

where $C_{pf} \cong 10^{-4}$ - 10^{-3} bar^{-1}, and ΔP is in bar.

Therefore for variation of fracture aperture, the equation will modify to :

$$b = b_i \left(1 - C_{pf} . \Delta P\right)^{\frac{3}{2}} \qquad (3.23)$$

For 200 bar, pressure drop and $C_{pf} = 5*10^{-4}$, the variation in b would be as; $b = 0.85\ b_i$.

Decreasing of the fracture aperture is in direction of having more stable liquid bridges and

stronger capillary continuity between blocks. The flow rate through the fracture i.e. in direction parallel to fracture plane is proportional to b^3, when the fracture aperture reduces by 0.85 the flow rate would decrease by a factor 0.61, which is considerable. Jones (1975) provides further explanation on this aspect (e.g. procedure of measuring the fracture pore compressibility).

3.4 RECOVERY MECHANISMS IN FRACTURED RESERVOIR

Initially there is a high production rate, and then a rapid decline in rates indicate fracture-controlled flow, in the first period of production performance. In the next step, i.e. matrix controlled, the decline in flow rate may be much steadier. Finally, the reservoir shows a decline curve, which is determined by the composite fracture-matrix system (see Figure 3.9). The main recovery mechanisms which contribute in fractured reservoir are as follows:

3.4.1 Natural Convection and Diffusion

Convection

The oil contained in the fissures of the gassing zone, will continuously reduce its dissolved gas during reservoir depletion. Consequently, during the depletion, the oil of the gassing zone will become heavier than the underlying oil in the fissures of the undersaturated zone. Additionally the temperature gradient of the formations helps to increase the inverse oil-density gradient inside the fracture network. The heavier oil on the top and lighter oil on the bottom will create an instability, and as a result, a convection mixing will take place. The dimensionless Rayleigh number, R_a, (Rayleigh, 1916) is an indication for how strong the convection process is in a reservoir (Saidi, 1987).

$$R_a = \frac{g.A.k}{\mu.D_e}.\frac{\partial \bar{o}\rho}{\partial z} \qquad (3.24)$$

where $\frac{\partial \rho_o}{\partial z}$, g, k, A, μ, and D_e are the density gradient in vertical direction, the acceleration of gravity, the permeability, the cross sectional area, the liquid viscosity, and the effective diffusion coefficient, respectively.

In most fractured reservoirs the magnitude of Rayleigh-number is fairly higher than its critical value i.e. the minimum Rayleigh-number which is necessary for initiating convection process. The convection is an effective flow mechanism inside the fractured reservoir. Because of the convection there is a continuous mixing of oil in a vertical direction inside the fracture network. To have nearly the same oil, from *PVT* properties point of view in different depths is a common case, in all well fractured reservoirs.

The density contrast between the oil in the matrix and fissures, in the case of a high permeable matrix, causes some local convectional mixing within the matrix. In well fractured reservoirs, the gas which comes out of solution from the reservoir oil, travels freely up to the crest of the reservoir, forming a secondary gas cap or expanding the existing gas cap. In most well fractured reservoirs the oil properties such as the saturation pressure, and gas oil ratio are extraordinarily constant with depth. The diffusion and convection process cause the stirring of the oil in fractured reservoir. Sajjadian (1989) provides further explanation on this aspect.

Diffusion

When the reservoir is put on production, convection currents in the vertical fractures, bring oil from near the gas-oil level where the saturation pressure is relatively low, in contact with matrix blocks which are saturated with oil of a higher saturation pressure. The matrix oil loses solution gas by diffusion from the matrix to the fracture which has a lower solution gas-oil ratio.

In the pressure range of interest, gas concentration in oil is linearly related to the solution gas-oil ratio. The saturation pressure (P_s) can be used in the differential equation for diffusion, instead of gas concentration.

$$D\left\{\frac{\partial^2 P_s}{\partial x^2}+\frac{\partial^2 P_s}{\partial y^2}+\frac{\partial^2 P_s}{\partial z^2}\right\}=\frac{\partial P_s}{\partial t} \qquad (3.25)$$

where D is the average diffusion coefficient of gas in oil.

Due to the convection process, there is a difference in the *PVT* properties of oil inside the matrix and oil in fracture, at the same level. The diffusion process is determined by the difference of solution gas in the fracture and matrix oil.

3.4.2 Solution Gas Drive

After the pressure falls below P_s, gas coming out of the solution in the matrix remains in the matrix and drives out the oil. When gas saturation exceeds the critical gas saturation (S_{gc}), gas becomes mobile and thereafter the gas saturation in the matrix stays constant and consequently no more oil is driven out of the matrix due to increase in free gas saturation.

During single-phase expansion, the pressure in the matrix block is higher than in the fractures, therefore, the matrix oil expands and is driven to the fractures as given in the following formula:

$$N\,C_{et}\,\Delta P = N_P \qquad (3.26)$$

where ΔP, N, and N_p are change in reservoir pressure, the original oil in place, and the cumulative oil produced, respectively. C_{et} is the total effective compressibility of the system and expressed as:

$$C_{et} = C_o + \frac{(C_w S_{wm} + C_{pm})\,\varphi_m + C_{pf}\,\varphi_f}{\varphi_m (1 - S_{wm}) + \varphi_f} \cong C_o + \frac{C_w S_{wm} + C_{pm}}{1 - S_{wm}} \qquad (3.27)$$

where ϕ_m, ϕ_f, S_{wm}, C_o, C_w, C_{pm}, and C_{pf} are the matrix porosity, the fracture porosity, the matrix water saturation, the oil compressibility, the water compressibility, the matrix compressibility, and the fracture pore compressibility, respectively.

The amount of critical gas saturation and the mechanism of gas accumulation is related to the rate of pressure reduction (i.e. oil production rate) of the reservoir. In the case of slow pressure drop after small super saturation, some clusters of oil with higher solution gas are formed randomly. The only required condition is that the size of the pores must be more than that of clusters. The first bubbles of gas are formed inside the pores containing larger clusters, which result in reduction of solution gas concentration nearby these gas bubbles. Due to a difference in concentration of solution gas, gas starts to migrate from other parts toward the nearest pores that containing free gas spheres inside them. By this process free gas is formed only in several points of matrix. Then, the volume of gas bubble gradually increases till due to the buoyancy force, its shape changes from spherical to cylindrical shape and moves upward. At the time that gas bubbles start moving toward nearby fractures, the gas saturation is called critical (i.e. S_{gc}) and from that time its amount inside the matrix block will remain almost constant. The free gas cylinders act as channels for gathering solution gas from the matrix oil and transfer it to the fracture.

When the reduction of reservoir pressure is fairly high, the time is not enough for the migration of solution gas toward pores containing free gas. Therefore the nucleation of gas bubbles are formed in the large and most of the medium size pores. At this condition the free gas distribution would be as dispersed mode and the critical gas saturation is higher compared to channel process. In Figure 3.10 the gas distribution for dispersed and localized modes are illustrated. Based on their experimental work, Botset and Muskat (1940) concluded that the same amount of free gas saturation would be achieved for pressure drop below 0.5 psi/min which corresponds to 262800 psi/yr. They have extrapolated their data from 0.5 psi/min to 0, while in actual case the trends of the curve

changes for pressure drop rate less below 0.5 psi/min. As was described in the above discussion the physics of free gas formation is changed when pressure drop is small, i.e. by decreasing the pressure depletion rate the amount of free gas saturation and its distribution changes. Results of laboratory measurements on reservoir conditions by Dumore (1970) indicates that the amount of immobile gas saturation is highly dependent on the rate of pressure depletion.

3.4.3 Imbibition

In the water-invaded zone, as the oil-water interface rises in the fractures, the matrix blocks become immersed in water and the oil in the matrix is displaced by water. Depending upon whether the system oil/water/matrix-rock is strongly water-wet or strongly oil-wet or of mixed wettability, the displacement process is either water imbibition, gravity segregation, or a combination of both.

Two sets of forces play a role in the substitution of oil within the matrix by the water or gas in the surrounding fractures, i.e. gravity force and capillary force. Gravity force is related to the difference in densities between oil and water, and the difference between the water-oil contact (*WOC*) level inside the matrix and fracture. Capillary force is caused by the interaction of surface forces within the pores. Assuming the rock is water-wet, if *WOC* inside the fracture is lower than *WOC* inside the matrix, the oil recovery will be governed mainly by the capillary force. If due to a high production rate the *WOC* in the fracture is higher than the *WOC* in the matrix, gravity and capillary forces will act simultaneously.

Oil recovery by an imbibition process is highly related to the ascending rate of oil-water interface in a vertical fracture. The critical rate of water advance in fractured-matrix reservoirs is the maximum rate of water advancement at which the water level in the fractures be lower than the water level in the matrix. At rates less than the critical value, the *WOC* in the matrix block is always ahead of that in the fracture. The displacement

process is concurrent, and all recoverable oil will be displaced from the matrix block. When the rate of water advance is greater than the critical value, the matrix block will be completely surrounded by water before imbibition is complete. As soon as water gets above a matrix block the displacement process inside the matrix is counter-current. Bourbiaux and Kalaydijian (1990) performed numerical and physical simulation for the concurrent and counter-current flow of oil and water. The experimental results showed that the counter-current oil production is much slower than that for concurrent flow. Concurrent flow resulted in a desaturation front with a relatively smooth profile. Counter-current flow resulted in a diffuse and an extended desaturation front. The final oil recovery was found to be slightly greater for concurrent flow conditions than that for counter-current flow. The numerical results found that relative permeability for concurrent flow conditions were not applicable to counter-current flow conditions. To correctly predict counter-current oil production, the oil and water concurrent relative permeabilities were required to be reduced by 20-40%.

In 1958, Aronofsky defined a simple relationship between recovery and time for a single matrix block as:

$$R = \frac{V_o(t)}{V_i(t)} = R_\infty (1 - e^{-\alpha t}) \qquad (3.28)$$

where $V_o(t)$, $V_i(t)$, α, and R_∞ are the volume of oil produced up to time t, the original oil in place, a constant giving the rate of convergence, and the limit toward which the recovery converges, respectively. They proposed this equation for imbibition controlled by capillary pressure for an oil saturated matrix, totally immersed in water. They also extended this relationship to the entire reservoir as follows (i.e. by assuming that N identical blocks are stacked vertically):

$$R = R_\infty \left[1 - \frac{1}{\alpha t} (1 - e^{-\alpha t}) \right] \qquad (3.29)$$

Due to the above relationship, recovery from the reservoir is lower than that from a single block, and depends on αt and R_∞. In 1978, de Swaan developed a relationship for the rate of water imbibition as:

$$q = \frac{R_\infty}{\tau}\int_0^t e^{\frac{-(t-\theta)}{\tau}} \frac{\partial S_w}{\partial \theta} d\theta \qquad (3.30)$$

where τ is the proposed imbibition constant, that is, time necessary to produce (1- 1/*e* =0.63) of the oil recoverable from the block and θ is the integration parameter. The exponential describes the rate of imbibition per unitary fracture length.

A number of methods have been employed to model matrix imbibition in an infinite medium where flow is capillary dominated and one-dimensional. Among these are the similarity transform method (Philip, 1955), boundary layer or integral methods (Zimmerman and Bodvarsson, 1989), and empirical methods (Rossen, 1987). All of these approaches are in general agreement that the imbibition flux and wetting front penetration are linearly related to $t^{1/2}$. The more realistic case of imbibition into three-dimensional porous blocks (i.e. converging matrix flow) has been investigated by Zimmerman et al. (1995). They found a linear imbibition to occur only at very early times (i.e., where penetration depth is small relative to the curvature of the block); however, significant deviation from linear behavior did not occur until the wetting front reached the mid-point of the block.

Depending on the wettability of the rock/fluid system, there are two types of oil flow process:

a- Water-wet rock: the water tends to penetrate spontaneously into the block by imbibition, and also by gravity from the top downward.

$$q_i = \frac{k_o}{\mu_o} \cdot \frac{h_b(\rho_w - \rho_o)g + P_d}{h_b} \qquad (3.31)$$

b- Oil wet rock: the capillary forces oppose the entry of the water into the block. Oil is produced only if the gravitational force exceeds the capillary force.

$$q_i = \frac{k_o}{\mu_o} . \frac{h_b(\rho_w - \rho_o)g - P_d}{h_b} \qquad (3.32)$$

where q_i, P_d, and h_b are oil flow rate leaving the block initially per unit area, displacement pressure due to capillary, and block height, respectively.

Mattax and Kyte (1962) presented experimental results on water/oil imbibition in laboratory core samples and defined a dimensionless group that relates recovery to time. Their work showed that recovery time is proportional to the square root of the matrix permeability divided by porosity and is inversely proportional to the square of the characteristic matrix length. They investigated the effect of the matrix block size on the recovery for reservoir scaling purposes. They showed that the imbibition time required to recover a specified fraction of oil from a single matrix block is proportional to the square root of the distance between the fractures. By neglecting the gravity effect, the following relation was presented by them for reservoir scaling purposes:

$$\left(t\sqrt{\frac{k}{\varphi}} \cdot \frac{\sigma}{\mu_w . L^2} \right)_{matrix} = \left(t\sqrt{\frac{k}{\varphi}} \cdot \frac{\sigma}{\mu_w . L^2} \right)_{reservoir} \qquad (3.33)$$

The importance of block height and different boundary conditions have been studied by Hammon and Vidal (1988), both numerically and experimentally for reservoir scaling. They showed that the boundary conditions of the matrix block, i.e. the fracture spacing and the geometry of the fracture networks have a strong influence on the oil recovery rate. In 1993 Babadagli and Ershaghi, showed that the capillary imbibition process under fracture flow is a strong function of fracture flow rate, matrix capillary pressure and matrix permeability.

3.4.4 Gravity Drainage

The gravity drainage takes place mainly when gas from gas-saturated fractures displaces the oil of the matrix. In a fractured reservoir the presence of vertical or inclined fractures could cause the *GOC* or *WOC* to advance ahead of corresponding contact in the matrix block. In the gravity drainage mechanism, the difference between the density of the fluids and the elevation of the two contacts are major parameters, that cause the fluid movement in the block and result in oil production from the matrix blocks. When surrounded by gas, the matrix blocks will release their oil as soon as the gravitational forces exceed the capillary forces.

When the only driving force is the gravity force without any external force, it is called free gravity drainage (*FGD*), by this definition the ultimate saturation distribution inside the block is governed by the capillary pressure curve of the block, and there would be no breakthrough of gas.

The connate water saturation also affects gravity drainage to some degree. Generally speaking, in most cases, the connate water occupies the dead-end and small pores. Therefore by assuming that connate water and residual oil occupy the same fraction of pore volume, an increase in connate water would cause a reduction in residual oil, which increases the ultimate oil recovery, Sajjadian (1990).

Oil relative permeability and matrix capillary pressure are key factors which control the recovery rate and ultimate recovery from a single block. Additionally the flow rate and ultimate recovery from stack-blocks also depend on capillary continuity, reinfiltration, and fracture transmissibility.

Unlike a conventional sandstone reservoir, in a well fractured reservoir the produced solution gas-oil ratio would gradually reduce with reduction in pressure as more gas is separated in the reservoir. The reason is that the separated gas freely percolate up the fracture system into the gas cap and very little of it, if any, will flow into the producing

wells. This producing gas-oil ratio, which is merely solution *GOR*, is a function of the saturation pressure profile in the reservoir.

Single block behavior

If a matrix block in a fractured reservoir is surrounded by gas, the gravity forces tend to expel the oil from the matrix and the capillary forces tend to retain the oil. Lowering of the interfacial tension by increasing the pressure or injecting appropriate fluids, can improve recovery as the result of reduction in P_c and/or swelling of oil. The saturation profile within the matrix block at the end of the production may be derived by equating gravity and capillary forces. When the total height of the matrix block is smaller than the capillary threshold height, the oil in the matrix cannot be produced by gravity drainage. If the total height is greater than the capillary height, the final oil recovery is governed by capillary pressure curve of the matrix rock.

Cardwell and Parsons (1948) published a paper describing, with a sound theoretical basis, the concept of gravity drainage. They used the data of Stahl et al. (1943) to check their theory. Laboratory studies of gravity drainage from unconsolidated sands were performed by Higgings and Shea (1949). The results of their study demonstrated that: 1- increasing volume of interstitial water decreased the percentage of recovery of original oil in place, 2- finer sand grains caused lower oil recoveries, and 3- less viscous oils and thicker sand pays promoted better drainage.

The results of Hagoort (1980) suggest that oil recovery from the gravity drainage mechanism is dependent on three factors: 1- the magnitude of gravitational forces relative to viscous forces, 2- the shape of oil relative permeability curve, and 3- the reservoir geometry and heterogeneity.

In fractured reservoir, there are two sets of conditions that favor single block (isolated) behavior:

1- When barriers have a considerable lateral extend without being cut by fractures. The oil leaving the upper block(s) will flow down and dip along the permeability barrier, passing only the producing ends of lower located blocks, without being sucked in (see Figure 3.11 c and d).

2- When no lateral, across fracture communication is present (i.e. wide, flat, open fracture).

Stack block behavior

Warren and Root (1963) presented an analytical solution for single-phase, unsteady state, radial flow in a naturally fractured reservoir. They also derived an equation for the shape factor for parallelepiped matrix blocks within an orthonormal fracture system of one, two or three dimensions.

Their double porosity domain assumes a continuous uniform fracture network oriented parallel to the principal axes of permeability. The matrix blocks in this system occupy the same physical space as the fracture network and are assumed to be identical rectangular parallelepiped with no communication between the matrix blocks. This assumption is the main weak point in their theory. It is obvious that, at actual reservoir conditions, there exists some degree of block/block interaction (see Figures 3.11 a and b). The interaction between the matrix blocks has strong effects on the ultimate recovery and oil flow rate of the fractured porous media, which must be considered in prediction of the reservoir performance.

Block/block interaction

When oil is draining from a block into the fracture via an open face, it tends to flow downwards in a liquid film along the outflow face of that block. The oil film will tend to maintain a flat surface due to the oil-gas interfacial tension, and the oil will fill up the

irregularly shaped roughness in the block's over the block's surface. When the film becomes thick enough, from several points (depending on roughness of the block surface), it tends to deform and gradually form pendent droplets alternatively. For the case that the fracture thickness is small enough, the surface of the adjacent block will easily make contact with the droplets and a liquid bridge between two blocks will be formed. The liquid bridges will cause capillary continuity between blocks. If the fracture thickness is more than required amount for forming liquid bridge, then oil movement from upper block into lower block is by formation and detachment droplet process of oil droplets.

The presence of rock material in the fractures (breccia) and location of close contact between adjacent blocks will further promote the formation of liquid bridges and, consequently, the capillary continuity between adjacent blocks.

When the contact points of two blocks (e.g. when fractures are partly cut, by porous spacers, breccia) have no restriction to oil flow, the capillary continuity will be achieved between two adjacent blocks, in vertical direction.

a- Fracture capillary pressure

The thickness of horizontal fractures determines the probability of the existence of stable liquid bridges. Porous spacers and stable liquid bridges have major roles in preparing the path for bulk flow processes of draining oil through the horizontal fracture. Concerning the effect of horizontal fracture on flow rate and the ultimate recovery of the stack block, most researchers use the fracture capillary pressure as a matching parameter.

There is no doubt, that since the fracture is part of a stack-system there is a pressure difference between the gas and oil phases inside the fracture. The problem is, what is the physics of this capillary pressure and what is its effect on the gravity drainage mechanism. In most cases a modified Laplace formula (i.e. $P_c = 2\sigma/b$) is used as a base of the theoretical approach to the problem. The weak point is that the above equation is

originally derived for the case of flow parallel to fracture surface not perpendicular to it. Therefore this type of fracture capillary pressure which is used by some researchers (e.g. Firoozabadi 1994-C) has no consistency with the actual physics of fracture capillary pressure, when oil drainage is perpendicular to fracture plane.

The fracture capillary pressure has already investigated by a few authors, however, all of them concerned themselves with mainly the horizontal fracture properties (i.e. fracture thickness and type of spacers). In 1987, Rossen and Shen, argued that pseudo capillary pressure curves for both the matrix and the fractures are able to represent the behavior in fractured reservoirs. Quandalle and Sabathier (1987) assumed zero fracture capillary pressure, but in a test example consisting of eight 30-ft cubic matrix block, they assumed a non-zero water/oil capillary pressure for fractures. Firoozabadi et al. (1994-A), and Tan et al. (1995) in their experimental and theoretical studies assumed that the fracture capillary pressure was a function of the oil saturation. In Chapter 5, we have studied the effect of horizontal fractures systematically. Our analysis indicates that, when the fracture aperture is more than its critical value b_c (as is defined in Section 5.7), the fracture capillary pressure may be assumed equal to zero. When the fracture aperture is less than b_c, the fracture capillary pressure is related to saturation profile inside the lower blocks (i.e. existence of oil continuous path), and the height of the fracture from the *GOC* level in the neighboring vertical fracture.

b- Reinfiltration

When oil is supplied at the top face or at the upper part of the side face of a block, this oil is sucked into that block at a rate comparable with the maximum gravity drainage rate of the block. When oil drains from the upper block into the fracture, the chance that it touches another matrix is very high, in that situation due to capillary force, it will be sucked by the imbibition mechanism (reinfiltration). Blocks in a stack that show this kind of interference will have a drainage performance as a function of time that differs

considerably from that of a stack of isolated blocks. Generally all or part of the draining oil from the upper block (s) reinfiltrate into the lower block (s) which causes a time delay in the recovery process compared to the single block process.

Lefebvre du Prey (1976), in his study on fissured reservoirs, assumed that the oil drained from an upper block is sucked completely by the block underneath. The results from the numerical study of de Silva et al. (1990), showed that the oil reinfiltration effect decreases as the fracture dip angle increases. They determined that, the influence of reinfiltration become negligible for a fracture dip angle of around 45°.

When oil is supplied at the top of the vertical side face of a block, it will flow downwards in a film along this face, while at the same time, part of it will be sucked into the matrix block (see Figure 3.12). To be sucked in, the wetting area must be above the threshold height of the matrix. Inside the block a liquid saturated region will be formed, through which the infiltrated oil will flow downwards. At the boundary of this region, the capillary pressure between oil and gas will tend to give the oil a lateral movement, whereas gravity acts in the vertical direction. The average horizontal capillary pressure gradient is equal to the capillary pressure P_c divided by the local width of the oil-filled zone while the vertical gravity gradient is equal to $\Delta\rho.g$. The vertical velocity and horizontal velocity of imbibed oil can be calculated as:

$$U_z = (k_z.\Delta\rho.g)/\mu \qquad (3.34a)$$

$$U_x = (k_x.\Delta\rho.g.h_c)/(\mu.x) \qquad (3.34b)$$

Where L, hc, k_z, and k_x are the block height, the threshold height, the horizontal permeability and the vertical permeability, respectively.

By dividing Equation 3.34a to Equation 3.34b, and integration, width of the oil filled region at the bottom of the block can be calculated from resulting formula:

$$X = (2L.h_c.\ k_x/k_z)^{1/2} \qquad (3.35)$$

c- Film flow process

An estimate of the film thickness and volumetric flow rate of a draining film over the vertical surface of the lower block under influence of gravity is necessary for calculating the transsmisibility of the vertical fracture.

By assuming that oil film drainage is viscous, unidirectional (i.e. vertical), and steady state, the Navier-Stokes equations reduce to:

$$\frac{\partial}{\partial x}\left[\frac{\mu_o.\bar{o}\,v}{\partial x}\right]=(\rho_o-\rho_g)(g) \qquad (3.36)$$

where ρ_o and ρ_g are oil and gas density, respectively.

For the boundary condition, $\frac{\bar{o}\,v}{\bar{o}\,x}=0$ at $x = t_f$ (the film thickness), Equation 3-36 can be integrated to give Equation 3-37 for the point velocity in which the constant of integration is zero, $v = 0$ at $x = 0$.

$$v=\frac{\Delta\rho.g}{\mu}\left[\frac{x^2}{2}-x.t_f\right] \qquad (3.37)$$

The film thickness in terms of the average velocity can be obtained by integrating Equation 3-37:

$$t_f=\left(\frac{3\mu.\bar{v}}{\Delta\rho.g}\right)^{1/2} \qquad (3.38)$$

$$q=\frac{\Delta\rho.g.\,t_f^3}{3\mu} \qquad (3.39)$$

where t_f, $\bar{v}$, and q are the film thickness in horizontal direction, the average velocity, and the volumetric flow rate per unit width of the film, respectively.

d- Capillary continuity

In an actual fractured reservoir the blocks are neither completely isolated from other blocks and nor are they in full capillary contact. When the blocks are isolated from each other they would act independently. The flow rate and ultimate recovery of N equal

blocks in one column would be *N* times the flow rate and ultimate recovery from one block (without considering the effect of reinfiltration). While if there is full capillary continuity between the *N* blocks in one column, the stack-block would act as one block with the height equal to the sum of *N* blocks (see Figure 3.13).

In an actual reservoir the gravity drainage phenomenon is more complicated, there are several other parameters that contribute to the amount of flow rate and ultimate recovery from a stack-block. Since the blocks in a vertical direction are laid on top of each other there exist some contact points between them. Due to the geological history of the reservoir, there is a variety in number and area of these contact point, not only in different sections of the reservoir but also between different blocks in a stack column. When the number and area of these contact points are restricted, due to the huge amounts of weight on these contact point, the permeability of these contact points and local region around them may be reduced considerably. Therefore in the worst conditions there will be no oil flow through these contact points. Although the chance of oil flow over the boundary surface of these contact points by film flow will never vanish. In some cases due to precipitation of asphaltene materials over the surface of the block, and erosion between the two neighboring blocks, the exit surface of the block can became impermeable.

The capillary continuity between blocks of a stack has already been investigated by a few authors with conflicting results. Some of the conflicting results are as follows: Saidi (1987), often assumed capillary discontinuity between a stack of matrix blocks. He also argued that if the fracture aperture is about 50 micron or more, capillary continuity between a stack of blocks can not be realized. Saidi did not argue about the effect of spacers on capillary continuity. Thomas et al. (1991), in their history match of the Ekofisk fractured reservoirs of the North Sea, observed that the use of measured matrix gas-oil capillary pressure function resulted in excess *GOR* production. They were forced to set this function to zero to match the *GOR*. They interpreted this action as a sign of

capillary continuity across the fractures in the Ekofisk field, and they reasoned that the existence of capillary continuity needs only a few contact sites across the fractures. When matrix blocks have a zero capillary pressure it means that there is full capillary continuity between them, and the stack block acts as a single block with an equilibrium height. The results of our study show that this situation will be achieved when the aperture of a fracture is fairly small, such that stable liquid bridges are responsible for capillary continuity (see Chapter 5 for details).

Gilman and Kazemi (1988) however, mentioned that a horizontal fracture will reduce recovery and cause capillary discontinuity between matrix blocks. Horie et at. (1988), performed gravity drainage experiments to study capillary continuity in a fractured reservoir. In case *I* of their study, they used four aluminium shims (0.2 mm * 0.2 mm), each with a thickness 0.3 mm, between matrix blocks, and in case *II*, matrix blocks were contacted directly. In cases *III* and *IV*, coarse and fine sand grains i.e. 0.35 and 0.18 mm in diameter respectively were used in separating the blocks. They concluded that the fracture capillary pressure of zero does not have a sound basis, while as they have mentioned in that paper, the results of case *I*, was consistently in the direction of zero capillary pressure. Since in cases *III*, and *IV* the fracture is partially filled with sand grain, it is obvious that its performance will be closer to porous media than to an open fracture. If the extra recovery from the top block in cases *III* and *IV* was due to capillary pressure of the fracture, there is no reason why the middle block was not being influenced by the capillary pressure of the fracture. By applying the concept of capillary continuity and equivalent oil relative permeability to the system instead of fracture capillary pressure the results will be interpreted more clearly. Festoy and van Golf-Racht (1987) concluded that partial physical connection between two blocks drastically improved the final recovery when compared with two blocks which had no physical connections.

Firoozabadi et al. (1992-B) believed that the fracture liquid transmissibility was the key to understanding the fractured petroleum reservoirs in which gravity drainage is the dominant recovery mechanism. In their experimental study, as in the case of most gravity drainage studies, the oil flow direction was perpendicular to the surface of the horizontal fracture, therefore the transmissibility of the fracture for a single fluid flow is high, (i.e. $k/\mu L = \infty/\mu b = \infty$). Although the horizontal fracture has high transmissibility, but its existence, as Firoozabadi et al. (1994-C) have observed in their experiments, will cause a reduction in the overall transmissibility of two phase flow in the fractured system. This phenomenon is due to a reduction in the degree of capillary continuity. When the fracture aperture is more than some critical value (40-50 microns as in their experiment) it causes some decrease in the ultimate recovery and variation of oil relative permeability. They also concluded that, the fracture-liquid flow is mainly film flow. This statement is correct only when the fracture aperture is high and/or the contact area of the porous spacers are small. Other wise, the liquid flow through the liquid and porous spacers can be comparable with film flow.

In a porous medium, the flow area is equal to the cross-sectional area perpendicular to the direction of flow, i.e. vertical flow occurs across the whole cross-sectional area. When fracture is invaded by gas, this becomes more problematic, since flow does not occur across all of the fracture plane, but rather over small regions which act as liquid bridges. These bridges will act as a continuous section of the porous medium, and their number and size depend on the amount of draining oil from the upper block.

In 1992-A, Stones et al. published the results of their experimental work on capillary continuity across horizontal fractures. They concluded that, capillary continuity exists even in highly fractured porous media. They proposed an effective cross sectional area as a parameter to fracture flow analogous to permeability in the porous media. They observed, a greater recovery, when overburden pressure has been used to reduce the

fracture aperture. In Section 5.7 it will be shown that a decrease in fracture aperture means that, there is more chance to form stable liquid bridges for longer time, i.e. more bulk flow period through the fracture.

Table 3.1 Major naturally fractured reservoirs in the world.

AREA	LOCATION	ROCK TYPE
Far East	Phillipines	Limestone
Canada	Alberta	Limestone
South America	Venzuela	Limestone - Basement
North Africa	SPLAJ	Sandstone -Limestone
Europe	North Sea	Chalk - Sandstone - Basement
Middle East	Iran, Iraq, Qatar	Limestone - Dolomite - Chalk
USA	Texas	Sandstone - Chalk
	California	Complex lithology (Siliceous)

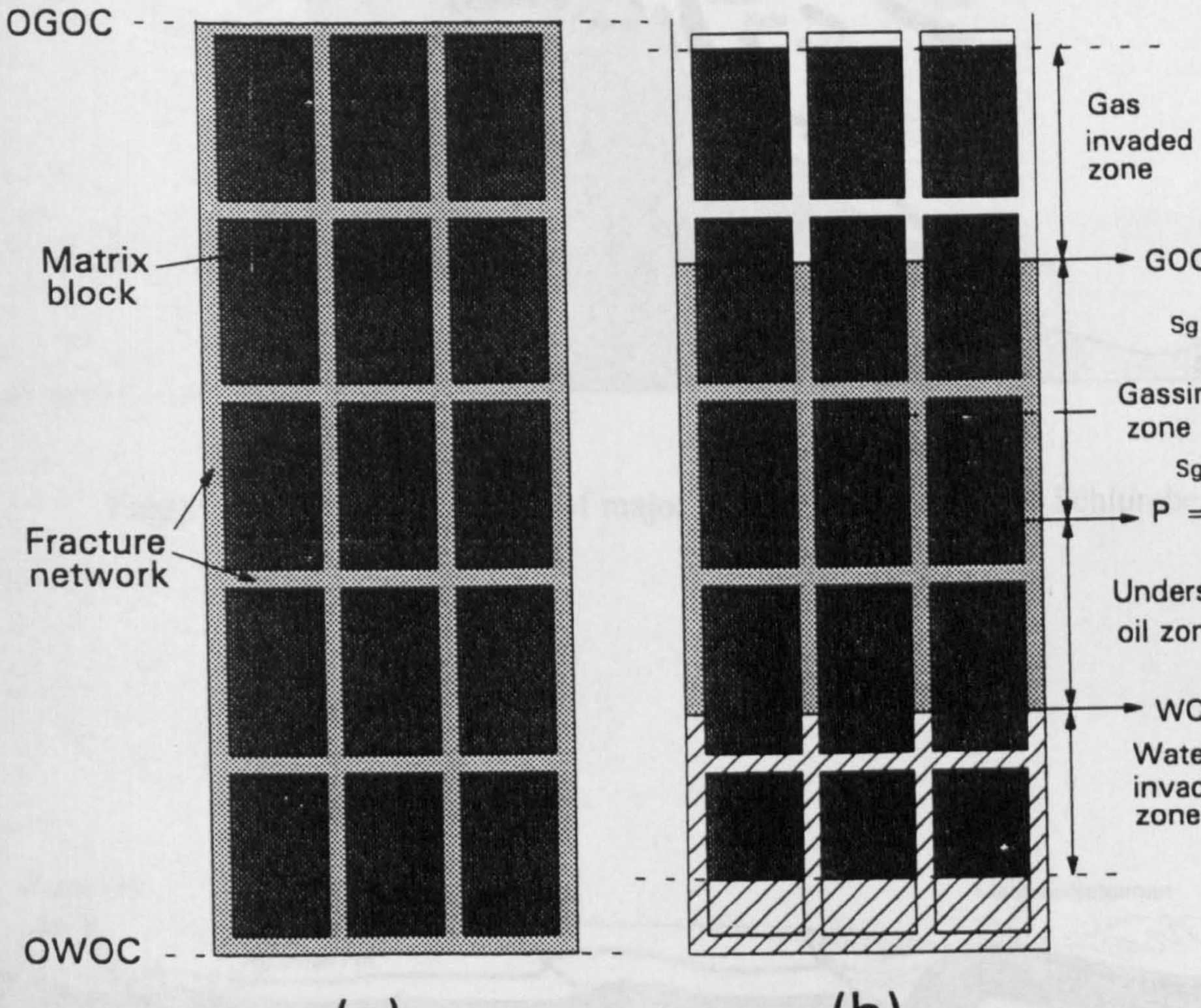

Figure 3.1 Schematisation of basic zones in fractured reservoir; (a) initial condition, (b) after some production.

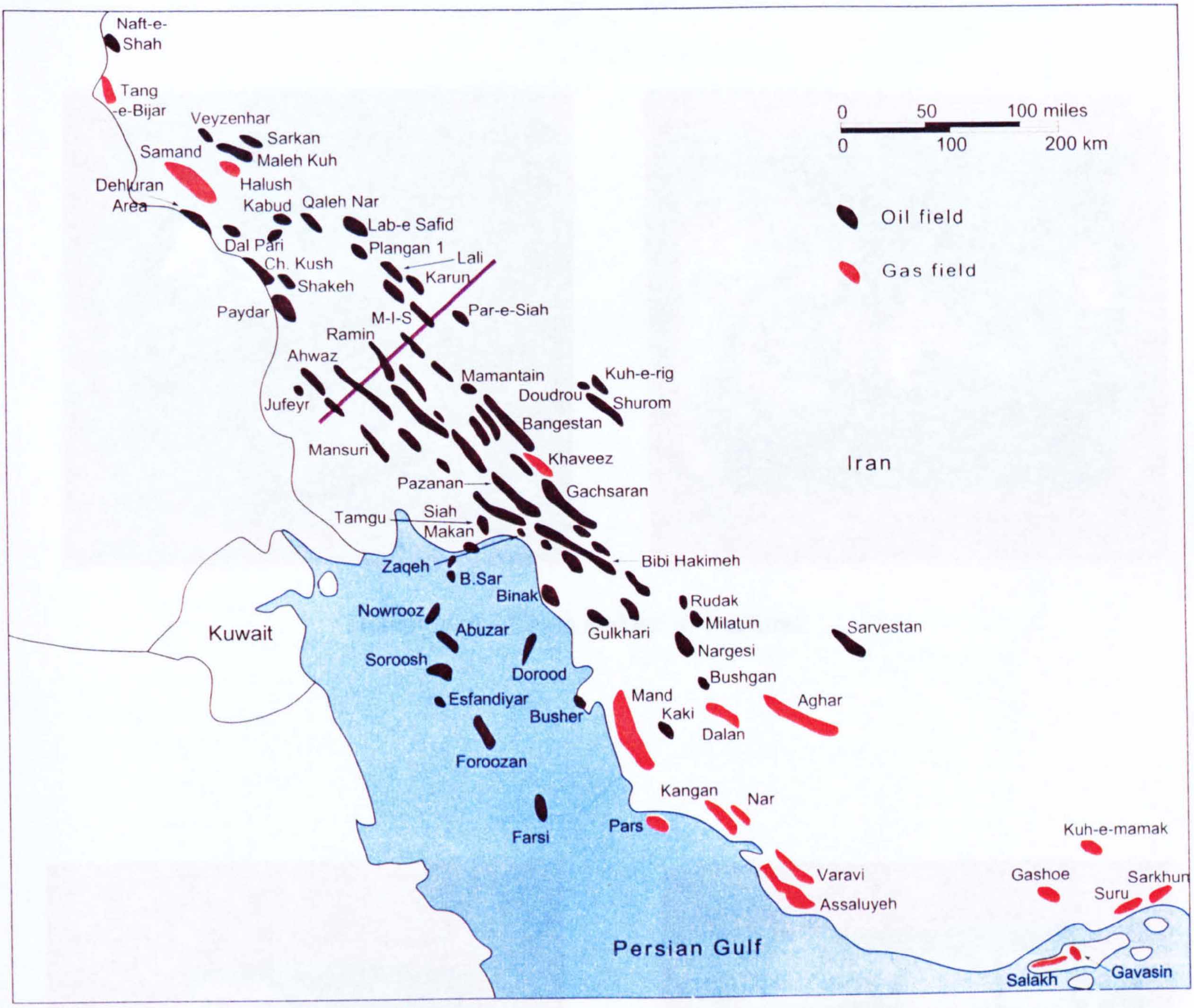

Figure 3.2 Areal distribution of major Asmari fields (courtesy Schlumberger).

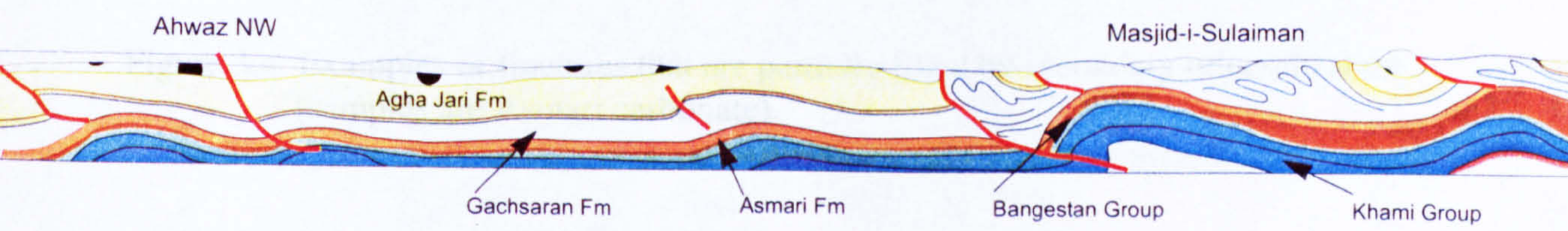

Figure 3.3 Geological cross-section across southwest Iran. The section follows the straight line on map of Figure 1.1, fields (courtesy Schlumberger).

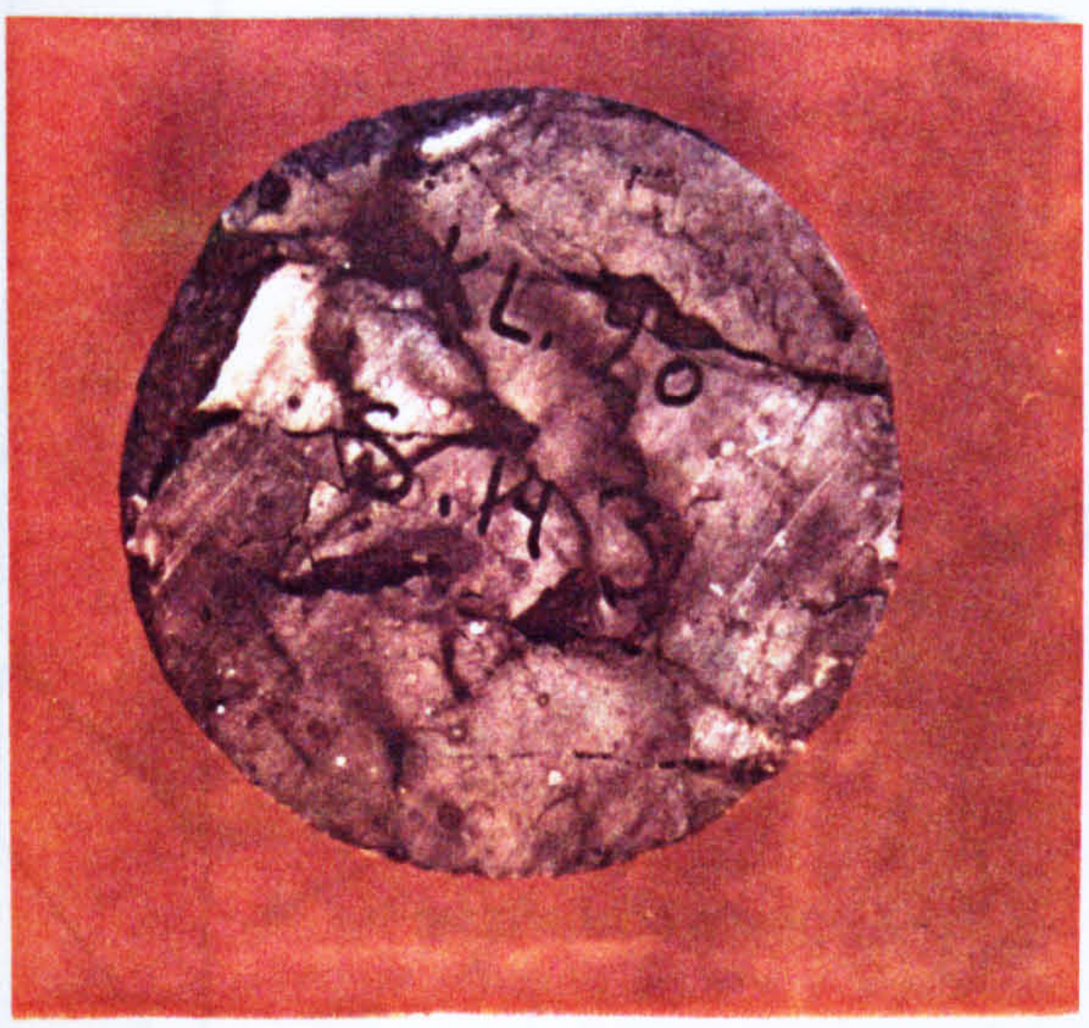

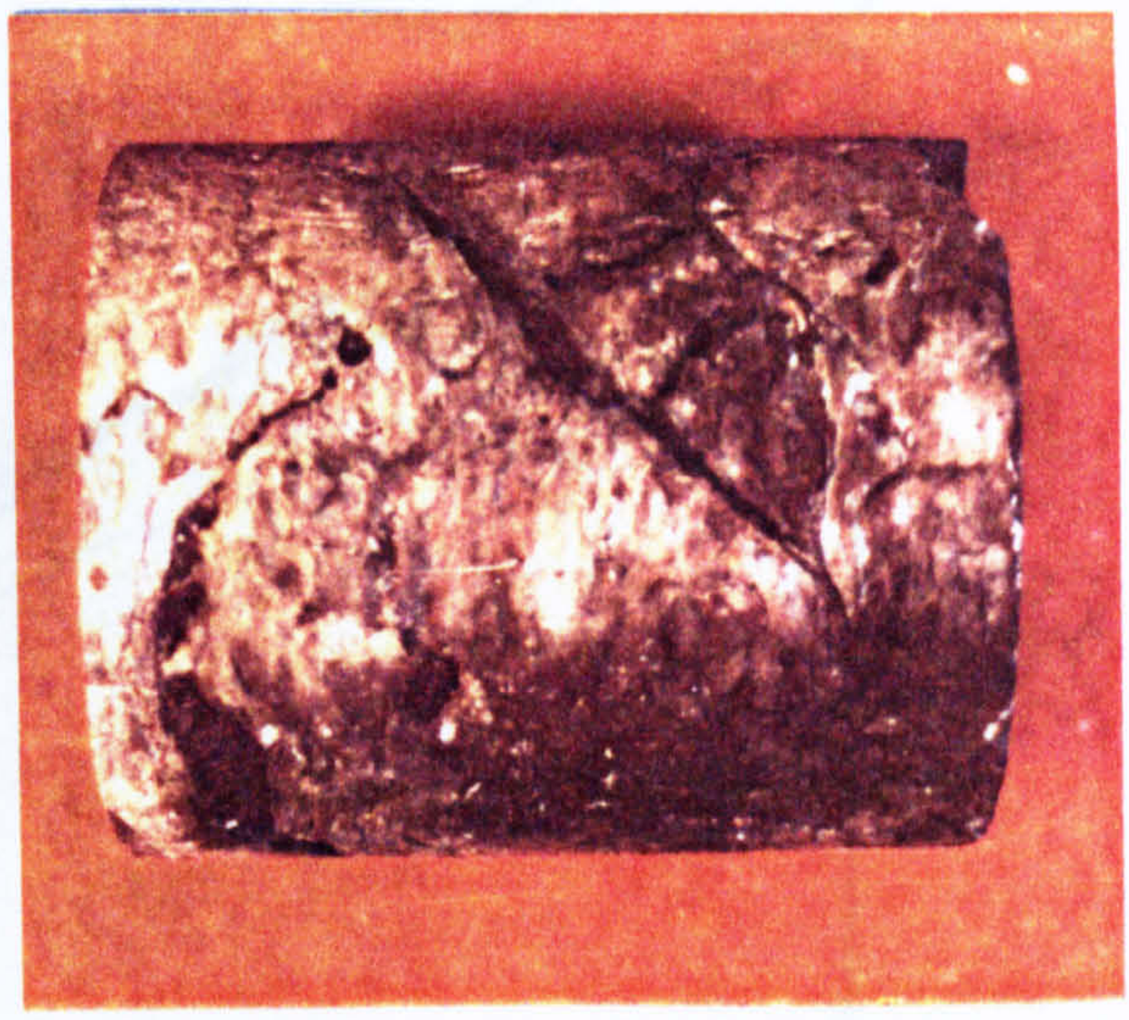

Note mineral-fill on surface of fractures.

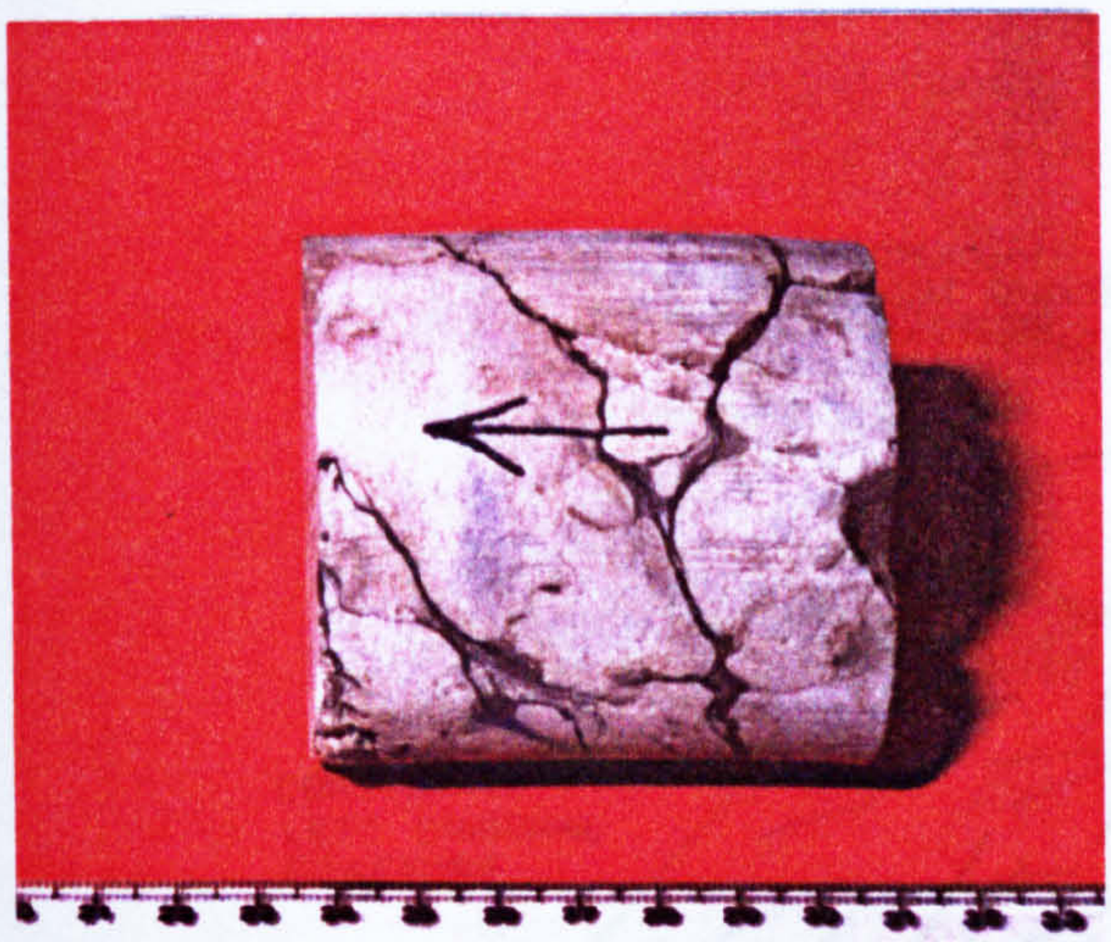

Figure 3.4 Examples of fractures that are partially filled by secondary mineralization (samples are Asmari carbonate).

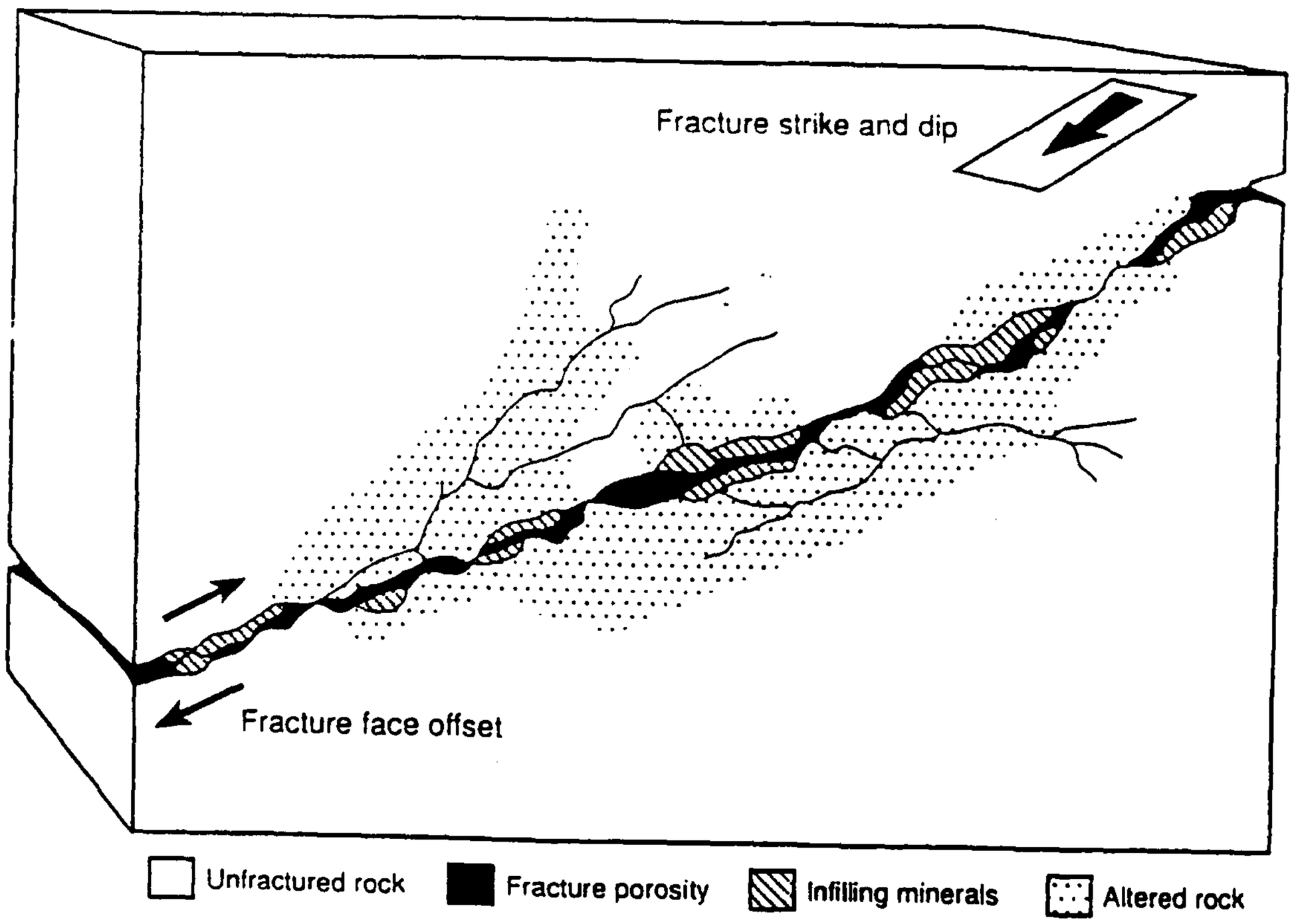

Figure 3.5 Graphical illustration of fracture properties (Paillet, 1985).

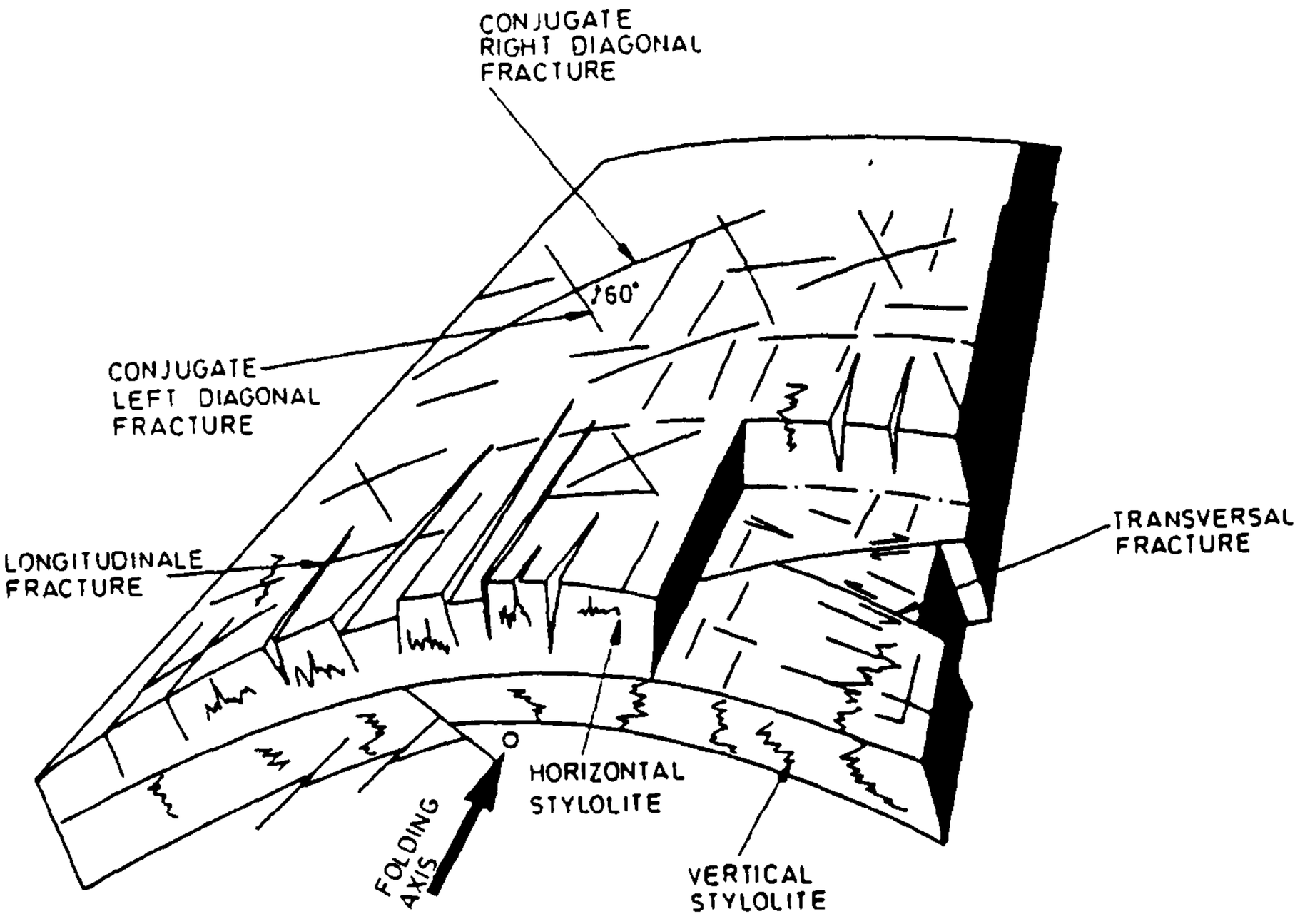

Figure 3.6 Various type of fractures generated by folding (Leroy, 1976).

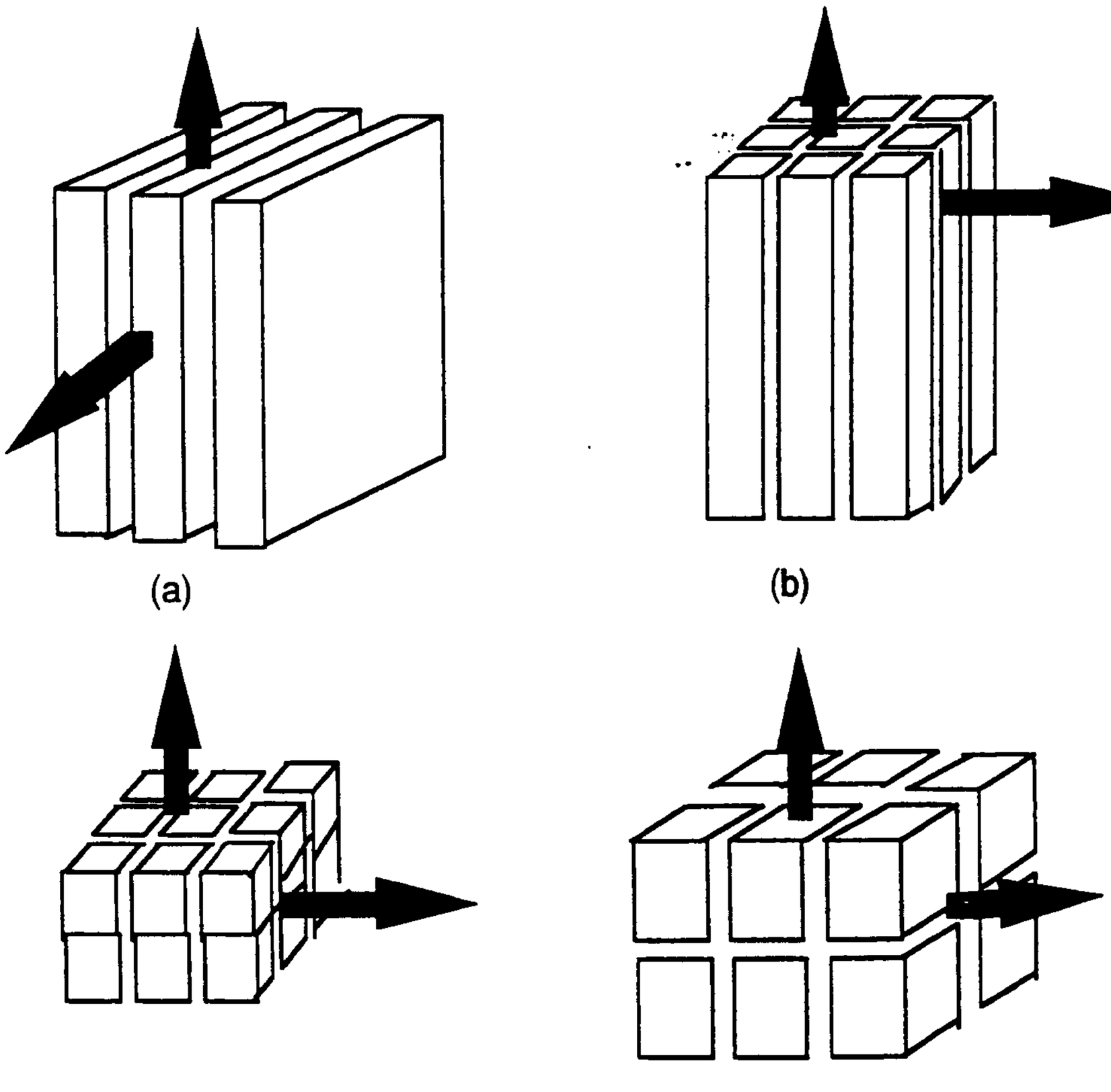

Figure 3.7 Typical fracture network, arrows indicate possible direction of flow (Reiss 1980).

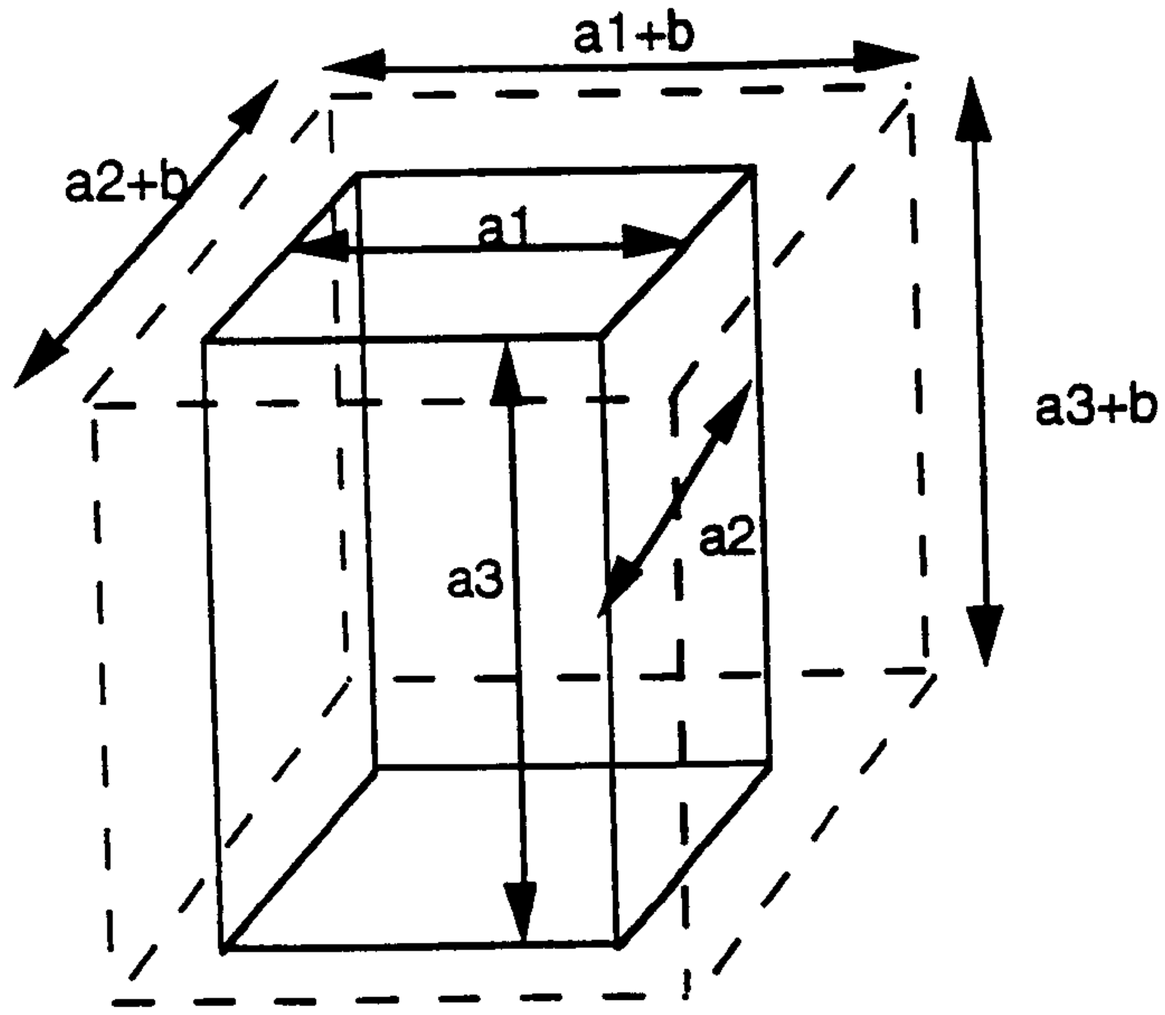

Figure 3.8 Definition of fracture porosity (Reiss 1980).

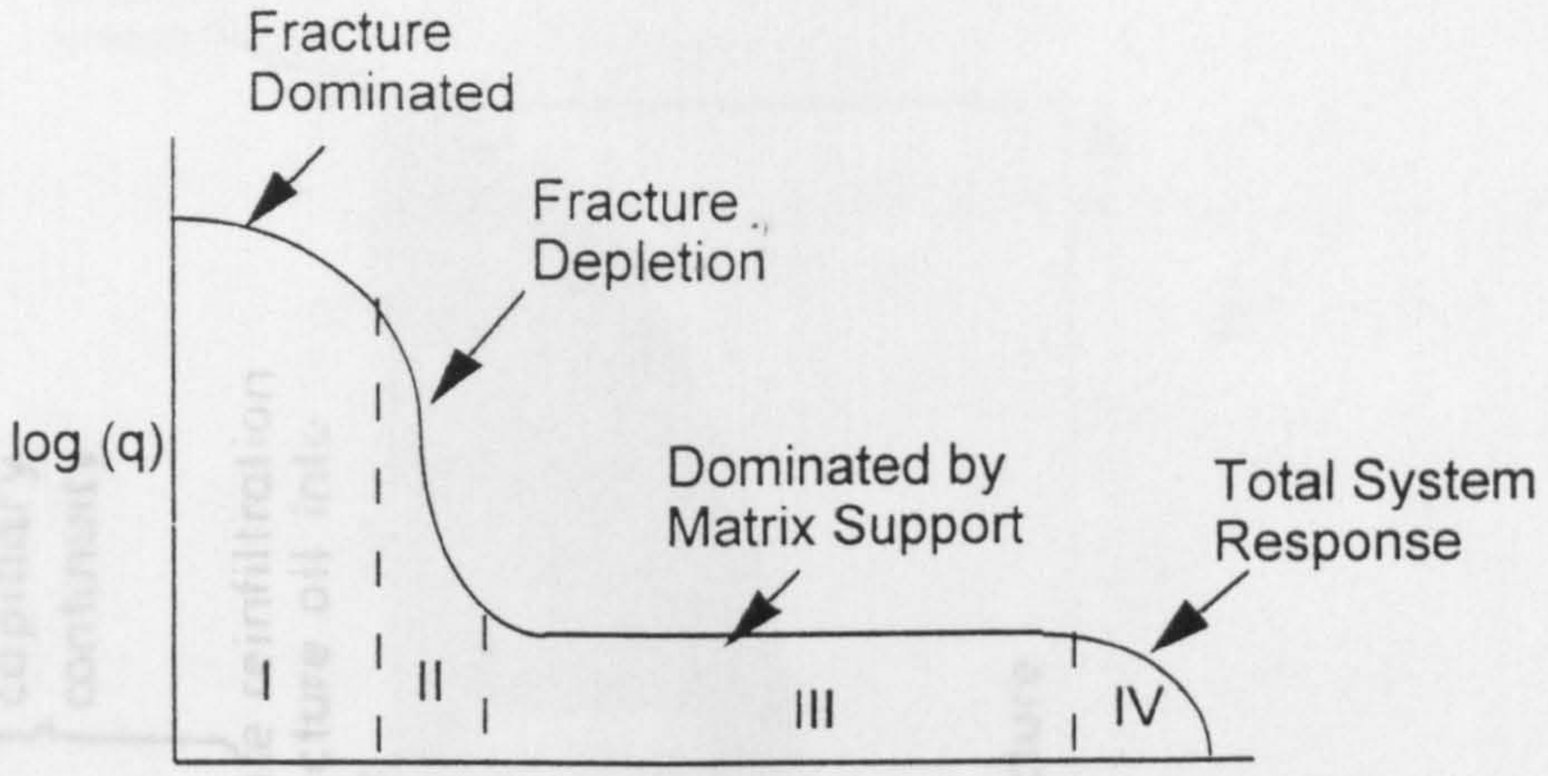

Figure 3.9 Typical production life performance for a fractured reservoir, constant pressure production (Qasem and Ershaghi, 1994).

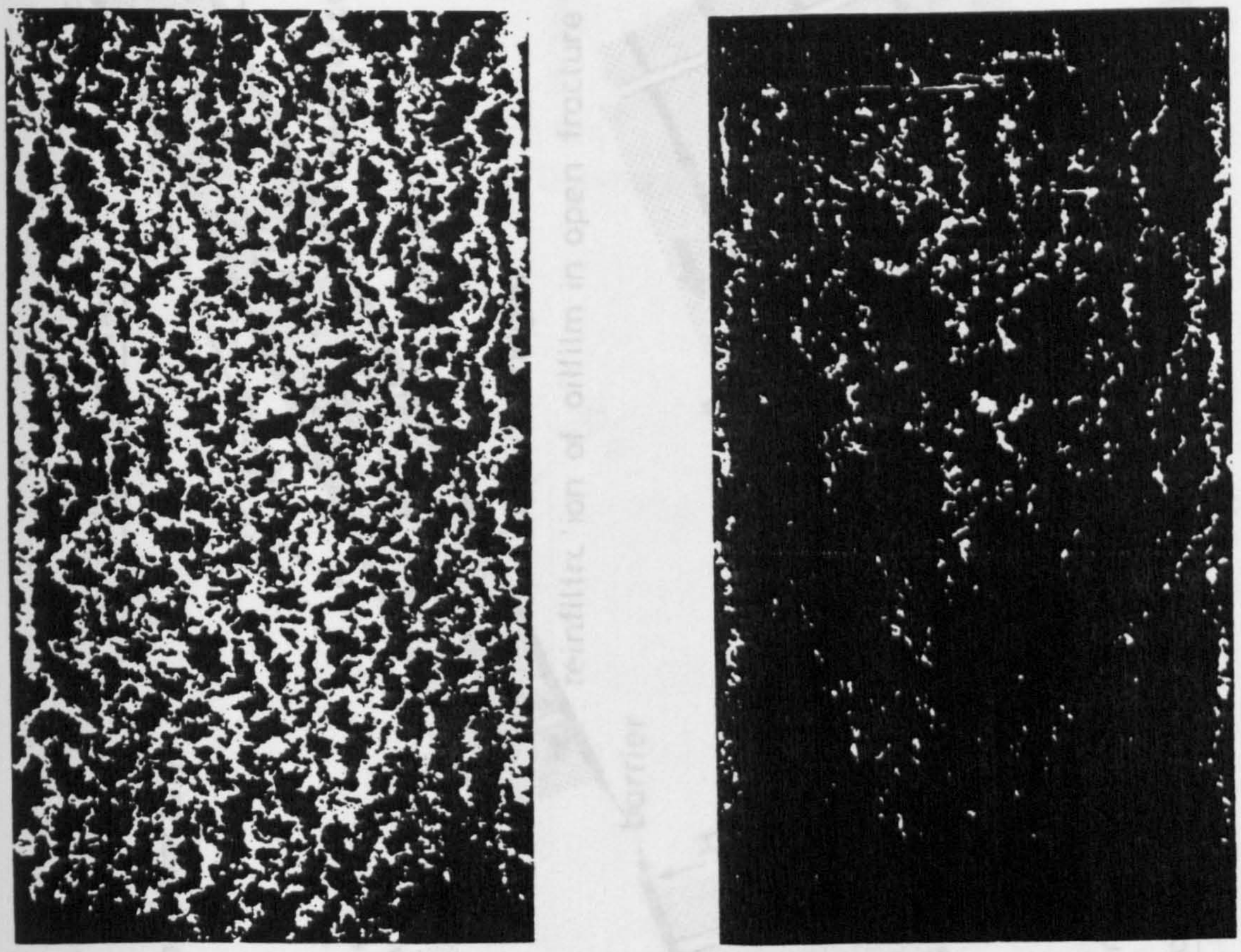

(a) Disperse gas distribution (b) Gas channels network

Figure 3.10 The build-up of a free-gas saturation in the 350-darcy pack, (Dumore 1970).

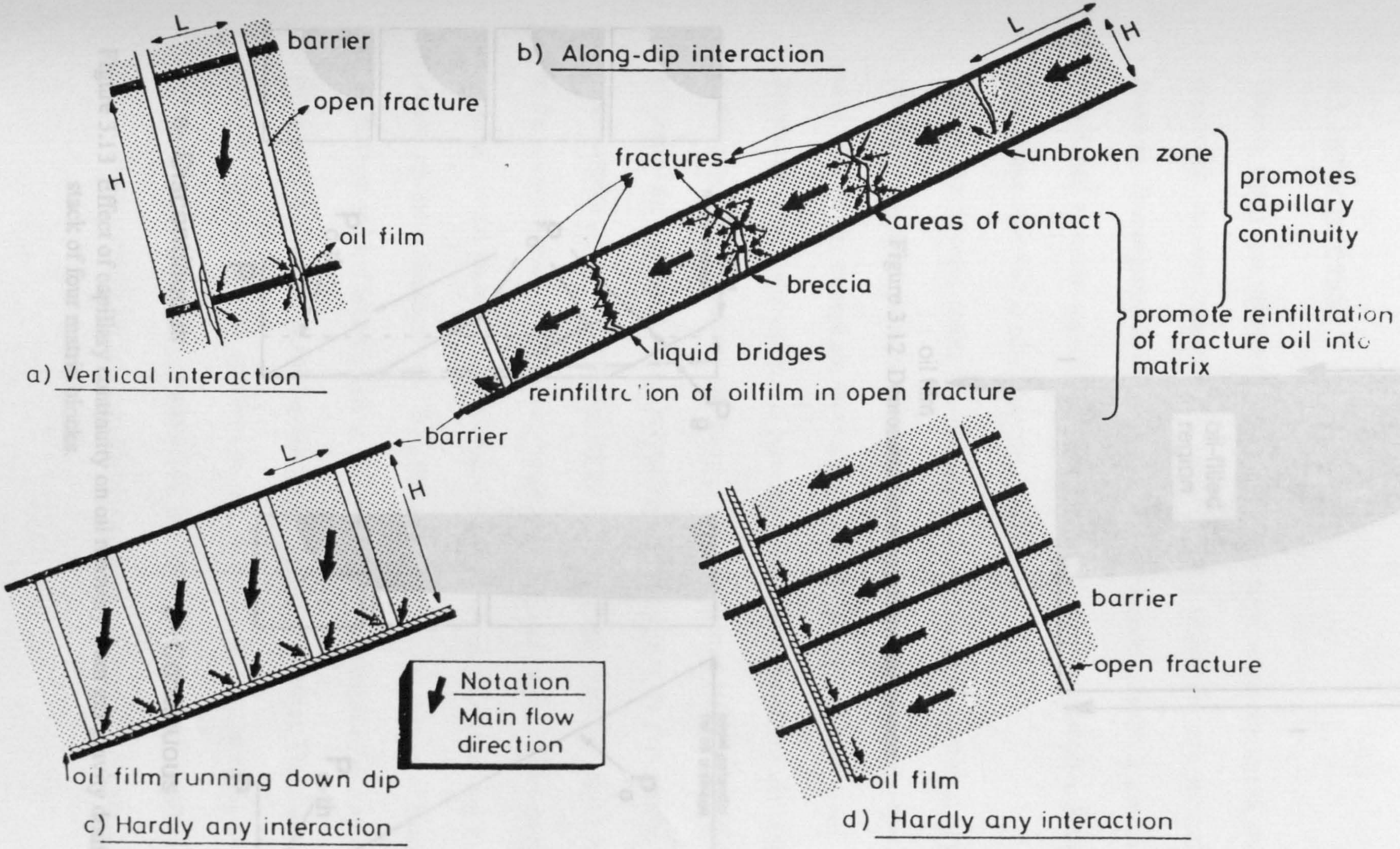

Figure 3.11 Schematic presentation of reservoir conditions that favour or prevent block/block interaction.

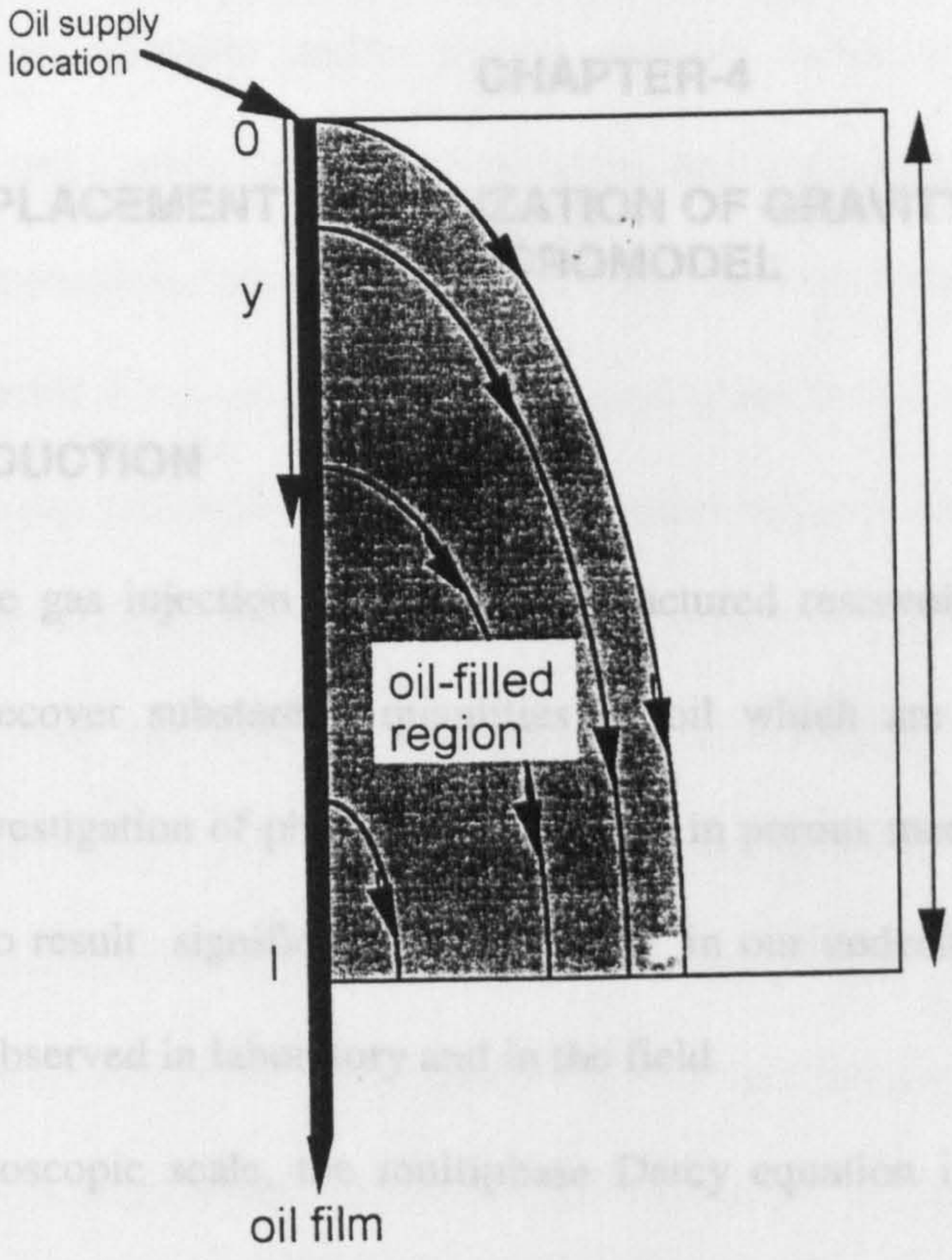

Figure 3.12 Demonstration of reinfiltration process.

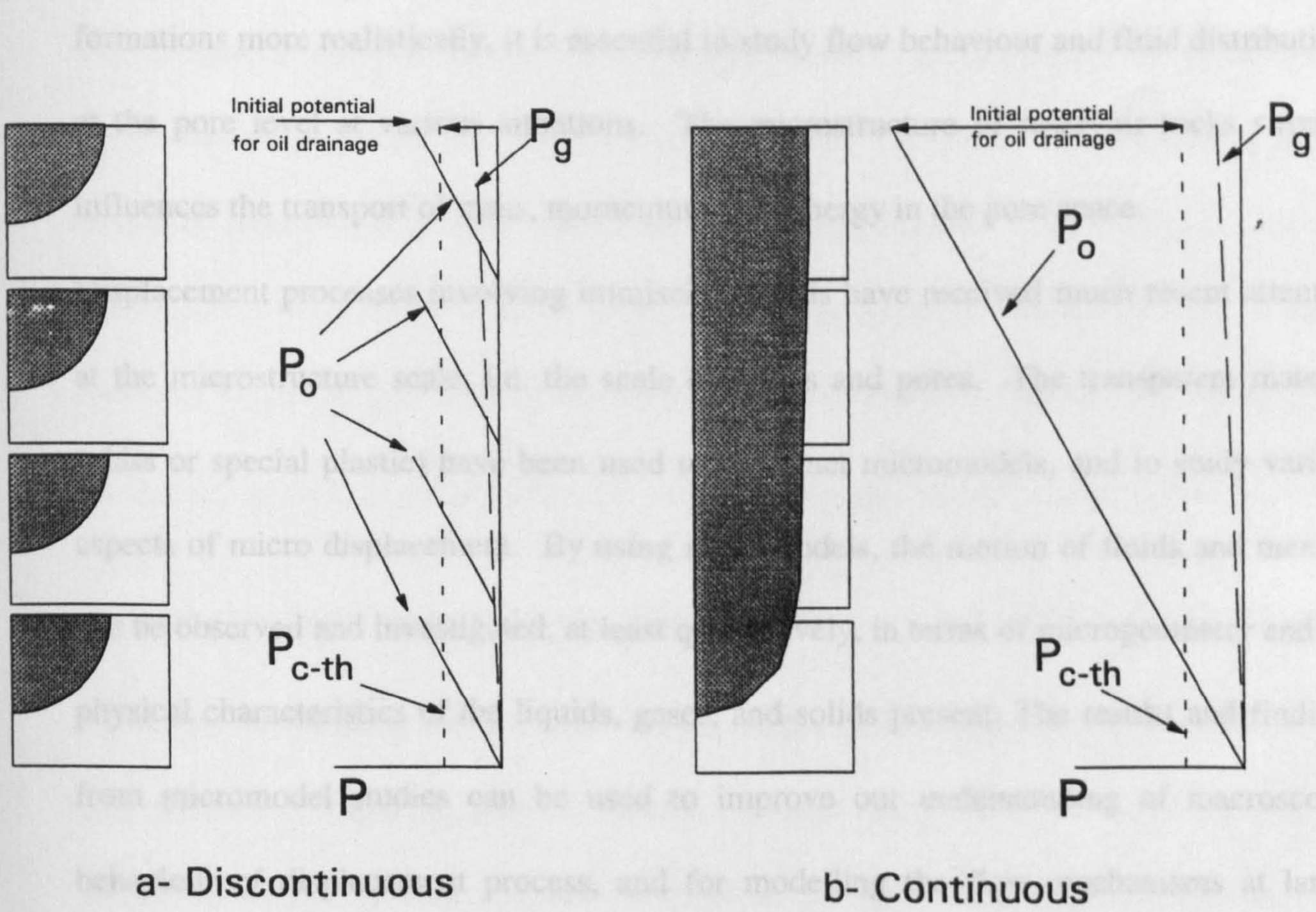

Figure 3.13 Effect of capillary continuity on oil recovery from gas gravity drainage for a stack of four matrix blocks.

CHAPTER-4

DISPLACEMENT VISUALIZATION OF GRAVITY DRAINAGE BY MICROMODEL

4.1 INTRODUCTION

Gravity stable gas injection into naturally fractured reservoirs could, under favourable conditions, recover substantial quantities of oil which are not recoverable by water flooding. Investigation of physics of fluid flow in porous media at the microscopic scale is expected to result significant improvement in our understanding of the macroscopic phenomena observed in laboratory and in the field.

On the macroscopic scale, the multiphase Darcy equation involving several empirical parameters relative permeabilities and average capillary pressures are conventionally used. To model multiphase flow and to predict ultimate oil recoveries from reservoir formations more realistically, it is essential to study flow behaviour and fluid distributions at the pore level at various situations. The microstructure of reservoir rocks strongly influences the transport of mass, momentum, and energy in the pore space.

Displacement processes involving immiscible fluids have received much recent attention at the microstructure scale, i.e. the scale of grains and pores. The transparent material (glass or special plastic) have been used to construct micromodels, and to study various aspects of micro displacement. By using micromodels, the motion of fluids and menisci can be observed and investigated, at least qualitatively, in terms of microgeometry and the physical characteristics of the liquids, gases, and solids present. The results and findings from micromodel studies can be used to improve our understanding of macroscopic behaviour of displacement process, and for modelling the flow mechanisms at larger scales. In micromodel studies, pore-level phenomena are visualized and measured to

understand how oil/water and/or oil/gas menisci move, why an oil phase becomes disconnected and trapped into ganglia or blobs, and what is required to mobilize it.

In glass micromodels, the depth is often the smallest pore dimension and thus the controlling factor for capillary forces. Etched glass models provide corners where the wetting fluid can accumulate, making them more appropriate models than a cylindrical tube, but they still do not reflect the three dimensional features of reservoir rocks. Nevertheless, they can be extremely valuable because they provide a means for direct observation of flow process. The ability to see the movement of fluid interfaces makes it possible to distinguish between a variety of mechanisms that may all lead to similar production behaviour. A great deal of effort has been put into understanding the importance of pore geometry and topology, fluid properties, and the interplay of capillary, viscous, and gravity forces in determining the mechanism of gravity drainage displacement.

The complex interaction between the effects of viscous, capillary, and gravity forces with pore network geometry and topology explains why two-phase flow in porous media cannot be described with a few macroscopic scale experiments.

Micromodels have been used to observe the effects of systematic change in many variables e.g. pore geometry, wettability, interfacial tension, density difference, initial saturation, as well as combination of variables like the capillary number i.e. $N_c = \frac{\mu.v}{\sigma}$ (ratio of viscous to capillary forces), Bond number i.e. $N_b = \frac{\Delta\rho.g.K}{\sigma}$ (ratio of gravity to capillary). Often these studies have not succeeded in isolating individual variables, but have illustrated important interrelationship between them. Dyes are often used in the interest of visibility, although most researchers recognize that dyes can influence the fluid/fluid/solid interactions.

Most often the contribution of micromodels is qualitative, rather than quantitative, because of the limits of accuracy in these very small samples, these results are of limited significance. Increased understanding of the importance of geometric and topologic factors helps to improve micromodel design. Larger models are difficult to make because of limitations on oven sizes, material properties, and problems with keeping the surface flat enough to ensure good sealing between two plates, but they might be helpful in reducing boundary effects and in providing better statistical samples for comparison with calculations.

Gas injection had been recognized as an effective means of enhancing the recovery of oil from petroleum reservoirs. The gravity stable gas injection studies conducted in this project are aimed to improve the understanding of the physical process involved in recovery of oil by this improved recovery technique. This study covers a total of 18 different experiments by using etched micromodel. Both the actual pore structure of rock, and the artificial network structure (homogeneous and layered), are used as flow patterns in construction of micromodels. A powerful camera enlarges the view of the fluid flow in the pores of the model, and transmits them to a *TV* monitor which can be magnified, observed and recorded.

Two major sets of experiments were conducted:

a- the model contained oil and irreducible water before the start of gas injection. These experiments were designed to simulate the "secondary recovery by stable gravity drainage, with immiscible gas injection".

b- the model which was saturated by oil and connate water, was initially flooded with water to simulate the process of secondary recovery by water injection. Gas was then injected as a means of "tertiary recovery by stable gravity drainage, with immiscible gas injection".

A number of parameters, such as pore geometry, fluid properties and the model wettability were investigated. The results obtained from the video-observations are presented in Section 4.3.

4.1.1 Literature Review

As early as 1952 Chatenever and Calhoun reported some micromodel observation of two-phase flow. They made bead packs from single layers of glass and Lucite beads and investigated immiscible displacement with brine and crude oil. Mattax and Kyte in 1962, fabricated the first etched "capillary glass micromodel" by coating a glass plate with wax, scribing lines on the wax coating to make the initial pattern, and finally, etching the pattern on the glass with hydrofluoric acid. This approach was improved by Davis et al. (1963) through replacing the wax coating with a photosensitive resist. In 1977, Bonnet and Lenormand reported a resin technique for making network geometries. Etched glass and moulded resin techniques, have been used to make most of the micromodels reported in the literature to date. A list of some of the previously published work on network micromodel is given in Table 4.1-1.

Micromodels have been used for studying a variety of oil recovery processes such as immiscible displacements (Touboul et al., 1987 and Mahers et al., 1985), surfactant floods (Paterson et al., 1984), solution gas drive (Danesh et al., 1987), and gas injection (Campbell et al., 1985). Micomodels have also been used to study specific phenomena relating to flow through porous media such as wettability (Morrow et al., 1986), asphaltene deposition (Danesh et al., 1988-A), retrograde condensation (Danesh et al., 1988-B), heterogeneity (Huh et al., 1988 and Bahralolom et al., 1988-A), mass transfer (Mahers et al., 1982), multiple contact miscibility (Bahralolom et al., 1988-B and Tiffin, 1983), and foam injection (Armitage, 1989).

Mattax and Kyte (1962) studied the motion of oil and water in a network consisting of a rectangular array of throats in etched glass micromodels. They reported residual oil saturation and relative permeability, and discussed various displacement mechanisms and the effects of wettability.

Chatzis, Morrow, and Lim (1983) discussed the residual oil distribution as a function of pore and throat geometry and network heterogeneity for free imbibition. Lenormand and Zarcone (1984) considered imbibition, drainage and the displacement of trapped fluid blobs as a function of pressure head in a network of ducts of square cross section, and discussed the various displacement mechanisms involved. Mahers and Dawe (1982, 1984, and 1985) studied mass transfer, diffusion, and dispersion in micromodels with regular flow patterns. Dead-end pores, and heterogeneous networks with different aspect ratios were included in their patterns. Morrow (1986), used a double-layer, cubic packing of Teflon beads to study forces required to mobilize trapped blobs of a nonwetting phase. The nonwetting blobs of varying length are trapped between the beads and cover so they contact only Teflon surfaces. The model can be tilted to study gravity forces, and the flow rate of the continuous wetting phase can be varied to change the viscous forces.

Peters and Reid (1990), presented a microcomputer-based imaging system used in conjunction with a square glass bead pack. They showed concentration profiles within the fingers, and demonstrated the stabilizing effect of gravity on finger growth.

Those studies dealing specifically with immiscible gas displacement are of particular interest in this work, and will be discussed. Kimber and Caudle (1957) improved visibility at both the microscopic level and the overall model view by the use of photographic enlarger in their studies of the distribution of gas and oil during and after two-phase flow. Saffman et al. (1958) studied penetration of a fluid into porous media or Hele-Shaw cell containing a more viscous liquid. They showed both experimentally and theoretically that; the ratio λ = (width of finger)/(spacing of fingers) is a function of

capillary number, i.e. $(\mu.v)/\sigma$, Where; μ- viscosity, v- the speed of advance, and σ is the interfacial tension.

Peden and Husein (1985) discussed, the scaling of micromodel experiments. Geometry of the flow paths (the sizes and shapes of the pores and pore throats), the dimensions of the model, end effects, flow behaviour were main factors involved in scaling. They used CO_2 to displace crude oil in glass micromodels. Precipitation of an asphaltic material at the fluids' interface was recognized during flooding. They developed, an improved micromodel system capable of operating at high pressure. In their paper a development in the micromodel processing, which were realistically scaled and geometrically representative of typical reservoir rock was presented. Peden (1985), emphasized that, as in the case of 3-D network, the high porosity and high coordination number will allow simultaneous parallel flow in 2-D models. Danesh et al. (1987, 1988 A, 1988B, and 1989) studied the effect of asphaltene precipitation and adsorption of surface active components of crude oils on glass micromodels. They noted wettability alteration from water-wet for clean surface to partially oil-wet for contaminated ones. They also observed that methane injection did not induce asphaltene precipitation. At some mixing conditions propane caused a considerable amount of asphaltenes to precipitate and thereby modified the flow patterns. Pore level mechanisms of gas propagation in immiscible conditions were also investigated by Danesh et al. for the case of both solution gas drive and gas injection. Thin section type micromodels and North Sea oil were used.

Mohanty et al. (1987), investigated the conditions that must be met for snap-off to occur in a flow channel. For the leading film of a bubble to advance into pore bodies considerably larger than the throats, a favorable pore-body-to-throat ratio must exist. In the homogeneous models, leading films are constrained by matrix grains on the downstream side before the curvature can expand enough to cause snap-off at the upstream pore neck. They also concluded that, when the statistical character of the pore

space in different porous media is the same, the statistical features of the residual saturation will also be the same. Bahralolom et al. (1988-B), investigated the effect of microscale heterogeneities on the gas injection process. They studied the effect of phase behaviour in the displacement of a crude oil with CO_2 and N_2. They concluded that the extractive power of CO_2 strongly affects the amount of oil production in secondary oil recovery. Tehrani et al. (1995) and Sajjadian et al. (1998-A) performed a series of secondary and tertiary gas injection experiments, using the high pressure etched glass micromodel (7 cm × 0.5 cm × 0.004 cm). They investigated a number of parameters, such as pore geometry and fluid properties and the model wettability.

They concluded that, no matter how low the gas injection rate is, gas never advances with a horizontally descending gas-oil contact within the pore structure. Gas will find the easiest path to move forward and initially the buoyancy effects are overshadowed by capillary forces. Also, they showed that, the penetration of gas phase, alters the balance of the governing forces and can result in redistribution of all phases, including connate water.

4.2 EXPERIMENTAL WORK

4.2.1 Equipment

A schematic diagram and photograph of the high pressure micromodel system is shown in Figures 4.2-1 and 4.2-2. The experiments were performed with the micromodels in vertical position for gravity drainage purposes. The basic elements of the apparatus are the pumping system, the micromodel in its temperature controlled high pressure holder,

Table 4.1-1 Summary of previously published work on network micromodel.

Author (s)	Micromodel	year
Michaels, A.S., et al.	Etched glass. Interconnecting capillary grooves. Pore width: 70 μm, Pore depth : 25 μm	1964
Davis, Jr., et al.	Etched glass, Pore opening : 0.001 to 0.003 in, pore depth: 0.001 in	1968
Mast, R.M.	Etched glass, Pore opening : 1.0 to 2.4 mm, Pore constriction: 0.3 to 0.6 mm, pore depth: 0.01 to 0.06 mm	1972
Wardlaw, N.C., et al.	Etched glass. Square lattice with 80 pores and coordination number of 4.	1978
Dullien, F.A.L., et al.	Etched glass. Square grid	1979
Wardlaw, N.C.	Etched glass. Non-random Heterogeneity	1980
Mahers, E.G., et al.	Etched nylon Pore diameter: 20 μm, Pore depth : 20-50 μm	1982
McKellar, M., et al.	Etched glass. Sizes : 13 * 5.5 mm and 14 * 5.5 mm	1982
Chatzis, I., et al.	Etched glass, Brick square and heterogeneous pattern coordination number from 2 to 8.	1983
Dawe, R.A., et al.	Epoxy resin Pore diameter : 10 μm	1983
Lenormand, R., et al.	Epoxy resin. Rectangular ducts. Constant depth : 1 mm, width > 0.1 mm	1984
Mahers, E. G., et al.	Epoxy resin. Regular network of pores and throats. Pore width: 20 μm, Pore depth : 20-50 μm	1985
Peden, J. M., et al.	Etched glass. Homogeneous and heterogeneous patterns. Pore throats : 25-100 μm, Pore bodies: 40-125 μm, Grains: 100-450 μm	1985
Campbell, B.T., et al.	Etched glass. Pore throats: 0.1-1.0 mm, Pore diameter: 0.7-4.0 mm, Pore thickness: 0.2-0.3 mm	1985
Morrow, N.T., et al.	Etched glass.	1986
Danesh, A., et al.	Etched glass, Pore throats: 35 μm, Grain diameter : 30-500 μm, Pore bodies: 40-150 μm, Pore depth : 10-35 μm	1987

Cont'd....

Table 4.1-1 (Cont'd...)

Williams, J.K., et al.	Etched glass. Pore throats: 100 µm, Grain diameter: 250 µm, Pore depth : 50 µm	1987
Bahralolom, I.M., et al.	Etched glass. Typical depth : 0.1 mm Model size : 6.3 * 4.3 cm	1988-A
Bahralolom, I.M., et al.	Etched glass. Thin section of San Andres carbonate Various model size : 7 * 4 cm	1988-B
Danesh, A., et al.	Etched glass. Grain diameter : 30-500 µm, Pore throats: 35 µm, Pore bodies: 40-150 µm, Pore depth : 10-35 µm	1988-A
Huh, D.G., et al.	Etched glass. Homogeneous and heterogeneous patterns.	1988
Kantzas, A., et al.	Etched glass. Grain diameter : 30-500 µm, Pore throats: 120-150 µm, Pore bodies: 200-1500 µm	1988
Martine, F.D., et al.	Etched glass. Pattern from a thin section of San Andres cores	1988
Shirley, A.I.	Etched glass, designed by petrographic image analysis. Pore sizes: 50-200 and 400-1300 µm	1988
Kuhlman, M.I.	Etched glass. Etched depth : 100 µm, Pore volume: 0.01 cc	1988
Gray, J.D., et al.	Etched glass. Coordination number of 3 and 8.	1989
Oren, P.E., et al.	Etched glass. Network with 4600 intersecting capillaries Pore widths: 400-500 µm, Pore throats: 100-300 µm, Depth :150 µm	1990
Tehrani, D.H., et al.	Etched glass, Pore throats: 35 µm, Grain diameter : 30-500 µm, Pore bodies: 40-150 µm, Pore depth : 10-35 µm	1995
Sajjadian, V.A. et al.	Etched glass, Pore throats: 35 µm, Grain diameter : 30-500 µm, Pore bodies: 40-150 µm, Pore depth : 10-35 µm	1998-A

and the visual system. A low rate flow-meter pump was used for injecting fluids into the micromodel. The overburden pressure was supplied with a high pressure cell, and the pressure in different parts of the system was controlled by four transducers housed in pressure console. The displacing network consists of fluid cylinders, lines and valves, and back pressure regulator (*BPR*). All of the experiments were observed, controlled and recorded by the visual system.

The micromodel

The micromodels used in the experiments are planar networks of pores and throats, created by photoetching of glass plates. The geometry of each network is characterized by the co-ordination number (i.e. number of connection to each pore), the throat size distribution, the aspect ratio (i.e. the ratio of the mean pore diameter to the mean throat diameter), and its porosity. The micromodel consists of a sealed pair of optically flat glass plates with the rock pore pattern etched on the side of one of the plates and the inlet/outlet holes drilled in the other plate. The micromodel allows the pore scale fluid flow under high pressure to be observed and recorded. Micromodels can be divided into two subgroups: a- high energy surface, initially water-wet (i.e. glass, silicon), and b- low energy surface, (i.e. Resin, Teflon). The typical procedure to fabricate etched glass model will be discussed in two dimensional etched model section.

After each experiment the micromodel plates are cleaned in solution of Decon 95 detergent, in an ultrasonic bath and finally rinsed with acetone and dried with nitrogen. The cleaned micromodel plates are then sealed (a vacuum between them is achieved). The model is then loaded in clamp (to ensure alignment between the two high pressure viewing windows of the pressure cell) and placed into the pressure cell (see Figure 4.2-3). In this study, two types of micromodel were used: those with homogeneous and those with heterogeneous network.

In heterogeneous model the grains, pores and channels are non-uniform in size, shape and distribution and resemble the pore geometry of natural rock. The composite homogeneous model was made of different types of homogeneous layers (see Table 4.2-2). Since flow pattern of each model in any direction differs from that in opposite direction, by using them in two modes (normal and upside down) actually, four types of flow patterns were studied (see Figure 4.2-4).

Characteristics of the models

The characteristics of both heterogeneous and homogeneous micromodels are given in Table 4.2-1.

Table 4.2-1 Characteristics of the micromodels.

Type of MM	Length cm	Width µm	Depth µm	V_b cc	V_p cc	k mD	Grain-size µm	Av. Pore & throat, µm
Heterogeneous	6.850	4800	30-50	0.013	0.0078	2300	30-50	35-95
Homogeneous	6.800	5000	30-50	0.013	0.0059	6000	96-115	150-200

Table 4.2-2 Dimensional characteristics of the layered homogeneous micromodel.

Layer No.	1	2	3	4	5	6	7	8	9	10	11	12	13
Coordin-ation No.	5	4, 5	4, 6	4, 5, 6	4, 5, 7	5, 6, 6	4, 5	4, 5, 6	4, 5, 7	4, 6, 8	4, 5, 6	4, 5, 7	5, 6, 8
Aspect Ratio	3	3	3, 4	3, 4	3, 4, 5	3, 4, 5	2	2	2, 3	2, 4	2, 3	2, 3	2, 4
Throat Size (µm)	96	96	96	96	96	96	115	115	115	115	115	115	115

The high pressure viewing cell

A high pressure cell has been designed and constructed to house the glass micromodel and to allow safe visual observation at high pressure, whilst providing the overburden pressure necessary to operate at any desired line pressure up to 6000 psig.

The cell is a thick walled stainless steel cylinder that opens at the top end, and is equipped with two viewing windows. The clamped micromodel is inserted inside the pressure cell through top hole and positioned in a vertical mode such that the surface of the

micromodel is parallel to the two windows of the high pressure cell. The cell and the clamp are designed such that after positioning the model, the top hole of the cell could be closed by the clamp which is then fastened by rotation of a treaded ring. Three stainless steel lines are connected to the cell, two of which are the inlet/outlet lines of the model (1/16 in) and the third one (1/8 in) is used to release the cell pressure. Glycerol is used to apply overburden pressure inside the high pressure cell, as this has the same refractive index as that of the glass and does not therefore distort the images to be viewed.

The displacement apparatus

The main elements of the displacement segment of the rig are a low flow metering pump, a back pressure regulator (*BPR*), five fluid storage vessels and the pressure monitoring and fluid flow lines.

Low flow metering pump

The unit comprises of a pump unit and a controller. The pump is mounted on a steel sub frame and is complete with fluid inlet and outlet hand operated valves. The controller is a free standing unit which can be situated remotely from the pump unit.

The pump can offer a wide range of precise flow rates.

Max. Operating Pressure:	20,000 psi
Min. Flow Rate	0.01 cc/hr
Max. Flow Rate	100 cc/hr

Back pressure regulator (BPR)

A dome *BPR* provided by D.B. Robinson has been used. The back-pressure regulator is essentially a pressure vessel filled with nitrogen at the desired back-pressure and connected to the outlet line of the flow system. Thus the back-pressure regulator vessel also acts as a collector for the produced fluids. Due to small amount of fluids used in any micromodel experiment, they do not cause an appreciable rise in nitrogen pressure.

After each run the liquids accumulated in the container are purged. The outlet pressure from the micromodel is maintained by back pressure regulator feed. The control level of the dome BPR has proved to be 1 psi for single phase flow.

Fluid cylinders and flow lines

Four stainless steel high pressure piston vessels are available for different fluids (oil, water and gas) and high pressure overburden cell (glycerol). Fluids on the outlet side of the piston can be transferred at the same rate that water is injected into the inlet side of the piston, by pump. There are two other high pressure cylinders; one is filled with distilled water and acts as a trap for collecting fluids from the outlet line and can discharge equal amounts of water to stabilize the volume balance of the system. The other cylinder is nitrogen reservoir that supplies adjusted pressure on BPR, no fluid could be drained from the system unless its pressure exceeded the nitrogen pressure.

To transfer fluids a network of stainless steel lines and valves has been designed and set up. The main point is to have a good facility for displacing individual fluids at very low volumes.

Pressure monitoring

A pressure console from ROP Electronics Ltd with 4-pressure transducers were used to control the system pressure (range 0-700 bar). The pressure of the high pressure cell, back-pressure regulator, the pump outlet, the micromodel outlet and confining fluid are monitored. The temperatures inside the pressure vessel and the oven are also monitored, in addition the micro-pump has pressure and flow rate displays.

The viewing equipment

The visual assembly consists of a close focusing lens, video camera and a tape recorder, a colour monitor and a high intensity light source. The lens is coupled to a video high resolution colour camera. This attachment can provide magnifications of up to 400X and therefore can focus specifically on a few grains in great detail or zoom out to allow magnification to observe a large area of the micromodel network. The assembly is coupled to a racking system enabling a precisely controlled scan across the width as well as along the length of the model. The light source guide cable moves simultaneously with

the camera, thus illuminating the area under observation. A special adjustable high intensity (400 watt) light source provides the strong illumination required.

4.2.2 Manufacturing of Glass Micromodel

Two dimensional etched model

The procedure followed to carry out the etching process (see Figure 4.2-5) is as follows:

1- A glass plate is thoroughly cleaned to ensure that proper chemical bonding of the silver coating to the glass surface occurs.

1.1- The glass is washed with detergent and cleaned with a soft cloth. It is then rinsed with hot water.

1.2- Immersing the glass plate in an oxidizing bath (sulphuric acid and ammonium persulphate - 200 gm/l) at 110 °C, for 1-2 hours removes the organic matter. The oxidant bath is changed once a week or after every four uses.

1.3- The glass plate is then rinsed with a large amount of hot water, followed by several rinses with deionised water.

2- A layer of silver is deposited on one of the glass plate surfaces so as to provide a substrate to which the photoresist can adhere (see Wheeler).

2.1- The clean glass plate is placed in a plastic tray and held in a clamp such that both of its surfaces can contact the solution to be added. The cold solutions (silver nitrate: 25 g/l, potassium hydroxide: 45 g/l) and (sucrose: 80 g, ethanol: 100 ml, concentrated nitric acid: 3.5 ml, and deionized (DI) water: 800 ml) are then poured into tray and mixed which initiates the reaction that results the precipitation of silver.

2.2- The glass plate is then rinsed with large amount of hot water, followed by several rinses with DI water.

2.3- The glass plate is then dried at 80° C for 10-20 minutes.

3- The silvered surface is coated with a layer of photoresist. This photoresist forms an acid resistant layer when it is polymerized by exposure to ultraviolet rays. The integrity of the silver coating and the photo resist film are critical to the success of etching process.

3.1- Photoresist solution is applied to the silvered surface with an eye dropper so as to wet the hole surface. It is then allowed to sit for about 15 seconds to permit any air to rise to the surface.

3.2- The glass plate is then dried at 80° C for 10-20 minutes.

4- The photoresist (or photosensitive resists) is exposed to UV rays through the mask of the micromodel flow pattern. Ultraviolet rays penetrate the clear portions of the mask and polymerize the photoresist lying underneath the images of the grains. The application is described by McKellar and Wardlaw (1982).

5- A developing step (using a solvent that dissolves the unexposed resist) is then carried out to remove the unpolymerised photoresist, thereby leaving the silver exposed in the areas that represent the flow paths.

5.1- Three dishes are filled with enough KTFR developer to cover the glass plate.

5.2- The glass plate is immersed in each of these dishes for the following times: sixty second in the first, ninety seconds in the second and third baths.

5.3- The glass is then washed in running warm tap water at 35-45 °C until the free resist has been washed off.

5.4-The glass plate is rinsed in DI water, and then is dried at 80° C for 10-20 minutes.

6- The exposed silver lying over the flow paths is removed using a modified Farmers reducing agent (75 gm potassium ferricyanide to 1000 ml, and 240 gr sodium thiosulphate diluted to 1000 ml).

6.1- A 250 ml, solution of (7.5 gm potassium ferricyanide and 24 gm sodium

thiosulphate diluted to 1000 ml) is poured into a dish, then the glass plate is placed into it with the coated side up.

6.2-The glass plate is rinsed in DI water, and then is dried at 80° C for 10-20 minutes.

7- The exposed flow paths are then etched into the glass plate surface using hydrofluoric acid (50% HF). Depending on the desired depth two different methods of etching can be used:

a- Shallow Etching: The glass plate is placed in acid, without agitation for 15 seconds. Gentle agitation is carried for an additional 20 seconds. Etches of this type achieve depths of 40-50 microns.

b- Deep Etching: The glass plate is placed in the acid for 5-10 seconds then gently washed with water to remove some of the reaction products. The glass is then put back into acid and process is repeated. The relation between the number of each etch/wash cycles to the depth of penetration is as follows:

Table 4.2-3 Relation between the number of each etch/wash cycles to the depth of penetration.

No. of Etch /Wash Cycle	Depth of Etch (μm)
1	10-20
2	30-40
5-6	40-60
6-10	60-80

4.2.3 Characteristics of Micromodel

Dimensions of the micromodel

Three different methods were used to measure the dimensions of used micromodel.

a- Direct measurement using a ruler

By this method a rough estimate has been made:

Length = 68.5 mm, Width = 4.8 mm.

b- Measuring by the magnification of the camera

A transparent ruler is put in place of the Micromodel and the size of 1 mm is measured on different parts of the monitor. Then dimension of the micromodel are obtained on monitor. To measure thickness of the model it was rotated 90° and the same procedure was used. Because the edges of the lines on monitor have not enough sharpness the accuracy is about 0.001 mm.

Length = 68.500 mm, Width = 4.802 mm, Depth = 0.045 mm.

c- Using the scanning electron microscope (SEM)

An *SEM* was used to measure the width of the model at different points. Due to the limitation of the microscope for the maximum movement of its lenses the length of the model was out of range, moreover no measurement of pore depth could be made.

Average width = 4.802 mm.

Measurements of physical properties

Porosity measurement

A 10 μL micro-syringe, was used to inject liquid into the micromodels to measure their pore volume, the measured values are:

Pore volume of heterogeneous model = 8.820 μL

Porosity of heterogeneous model = 59.6%

Permeability measurement

The absolute permeability (using Darcy's law) of the micromodels were measured, while it was placed horizontally. Then liquid was pumped through it using the micro-pump at six constant rates the measured values are:

Permeability = 2300 mD (heterogeneous model), and 6800 mD (homogeneous model).

Table 4.2-4 List and specification of micromodel experiments.

Exp. No.	Test Fluids			MM Type	(Process, Residual Sat.)		Wettability		Spreading Coefficient		Purpose Of Experiments
	Oil Decane	Water	Gas		Sec., S_{wr}	Ter., S_{orw}	Water	Mixed	+ve	-ve	
1	Red	Blue	C_1	1-Ht	*, h		*		*		To investigate the effects of residual oil saturation, and wettability on the recovery mechanism
2	Red	Blue	C_1	1-Ht	*, m		*		*		
3	Red	Distil	C_1	2-Ht	*, m			*	*		
4	Red	Blue	C_1	1-Ht		*, m	*		*		To study details of displacement mechanism and observing different phenomena during injection
5	Red	Blue	C_1	1-Ht		*, m	*		*		
6	Red	Blue	C_1	1-Ht		*, m	*		*		
7	Red	Blue	C_1	1-Ht		*, m	*		*		
8	Yellow	Brine	C_1	1-Ht		*, m	*		*		To identify the effect of different gases, brine, and dyed oil on recovery process.
9	Yellow	Brine	N_2	1-Ht		*, m	*		*		
10	Yellow	Brine	N_2	1-Ht		*, m	*		*		
11	Red	Brine	N_2	1-Ht		*, m	*		*		
12	Red	Brine	N_2	1-Ht		*, m	*		*		
13	Red	Brine	N_2	3-Ho		*, m	*		*		Study the influence of pore network on drainage process
14	Red	Brine	C_1	3-Ho		*, m	*		*		
15	Red	Alcohol	C_1	2-Ht		*, m	*			*	To investigate the effect of spreading. coefficient on recovery mechanism
16	Red	Alcohol	N_2	2-Ht		*, m	*			*	
17	Red	Distil	C_1	2-Ht		*, m		*	*		To observe the effect of mixed wettability on efficiency of recovery
18	Red	Brine	C_1	Lay	*, m		*		*		Study the influence of layered networked on efficiency of recovery

Red : Decane dyed by sudun red
Yellow : Decane dyed by frrocene yellow
Blue : Distilled water coloured with methyl-blue
Alcohol : Distilled water + 20 Wt% ethanol
MM : micromodel
(* = used in test)

1-Ht, 2-Ht : Heterogeneous model in position 1 and 2.
1-Ho, 2-Ho : Homogeneous model in position 1 and 2.
S_{wr}, S_{orw} : Residual oil and water saturation.
h, m : High and medium value.
$S_{sc.}$, S_{wr} : Residual water saturation for secondary gas injection.
$T_{er.}$, S_{orw} : Residual oil saturation to waterflood for tertiary gas injection.

4.2.4 Experiments and Test Fluids

Experiments

A list of Gravity Drainage experiments is given in Table 4.2-4. All experiments were conducted at 500 psig.

Test Fluids: Physical properties of test fluids are listed in Table 4.2-5, and spreading coefficient, (S) of the three phases (i.e. red-Decane, Methane and Water) are given in Table 4.2-6. The following fluids were used in the experiments:

A- Water: The following four different solutions, were used as the aqueous phase:

A.1- Distilled water (colourless),

A.2- Distilled water-dyed blue by methyl blue,

A.3- Brine 1% NaCl,

A.4- Ethanol, diluted with distilled water (20 wt %).

B- Oil: Dyed decane was used as oil phases:

B.1- Decane dyed in yellow by Ferrosene.

B.2- Decane dyed in red by Sudan red.

C- Gas: Pure methane, and pure nitrogen (99.995 %) were used as gas phase.

In all experiments, gas (methane or nitrogen) could be identified by dark shadows around it, water in blue colour or colourless, and oil (decane) is red or yellow.

Table 4.2-5 Properties of the test fluids.

Fluids	Density (gm/cc)		Viscosity (cp)	
	lab. condition ♥	500 psia	lab. condition ♥	500 psia
Methane	0.00066	0.0230	0.011	0.0125
Nitrogen	0.00115	0.0379	0.018	0.0197
Distilled Water	0.99980	0.9492 *	1.000	-
Water + Methyl blue	1.00800	0.9597 *	1.049	-
Brine (1% NaCl)	1.01000	0.9776 *	0.863	-
Decane + red, sudun	0.73180	0.6995 *	0.863	-
Decane + Ferrosene	0.73420	0.6995 *	0.901	-

*: live liquid, ♥: 1 atm & 22 °C

Table 4.2-6 Interfacial tensions and spreading coefficients for three phases at different conditions, red oil (B2) and methane were used as oil and gas in these measurements. [$S = \sigma_{gw} - (\sigma_{go} + \sigma_{ow})$].

	Lab. condition ♥	Test condition (distilled water, A.1)	Test condition (diluted ethanol, A.4)
σ (g-w)	68.87	56.20	38.00
σ (o-g)	16.26	14.50	14.50
σ (o-w)	50.66	42.80	32.3
S	+ 1.95	- 1.10	- 9.3

♥: 1 atm & 22 °C

4.2.5 Experimental Procedure

The mechanism of oil recovery by gravity stable gas injection into the micromodel, was observed and recorded by video tape for all the following experiments:

Free gravity drainage processes

a- Initial oil in place is a continuous phase in presence of connate water (S_{oi})

The secondary recovery referred to in this thesis applies to the recovery of oil by gravity stable gas injection in a micromodel, which has been initialized by establishing connate water saturation at about 500 psig. Gas was injected at very low rate, such that it never exceeded the critical velocity ($v_{crit.} = \frac{k \times k_{rg} \times \Delta\rho \times g \times Sin6}{1.0133 \times 10^6 \times \mu_g \times (M-1)} = 3.21 * 10^{-6}$ m/s), which indicates that the displacement was indeed gravity stable. The velocities were calculated by measuring fluid displacement within a given area.

b- Initial oil in place is a discontinuous phase (S_{ore})

In these experiments we have tried to simulate the gravity stable gas injection in a porous block which has already been flooded by water. The connate water and original oil saturation was initially established in the micromodel, then water was injected to establish the residual oil saturation.

Measurement of fluid production and injection rates

Two visual methods were used for measuring the average rate of fluid production or gas injection. In both methods the volume of displaced gas was measured in a given time period as follows:

a- Using the "U" tubes at the inlet and the outlet of the micromodel

The volume of "U" tubes (see Figures 4.2-4 and 4.2-7) were measured very accurately by an electronic microscope. Measuring the required time for gas to displace the liquid in the "U" tube, provided a good estimate of displacing rate, both at start and at breakthrough times. The average value of the two rates was used to calculate the gravity number for stability check.

b- Using a section of micromodel

The rate of gas flow was measured by calculating the gas volume inside a specific section of the model (see Figure 4.2-8) and the time that was taken for gas to occupy that section.

Displacement process

a- Secondary recovery process

In secondary recovery process, the gas/oil contact moves down-dip as oil is produced, leaving some oil behind in the gas-invaded zone. This oil drains downwards slowly, mostly by film flow process. In the gas-invaded region the flow of oil is dominated by gravity; gas is inserted to replace the voidage created by oil production down-dip. The amount of oil left behind the gas/oil contact depends primarily on the relative permeability to oil, the vertical permeability, and the oil viscosity. Thus for good recovery in a reasonable time period high oil mobility and high vertical permeability are needed. One further factor which should be considered is the gas/oil capillary pressure. The height of an individual block must exceed the capillary transition-zone height.

b- Tertiary recovery process

The formation and entrapment of oil ganglia i.e., residual oil saturation, depends on several parameters: the initial/boundary conditions, the geometry of the pore network, the

Bond number, the capillary number, the viscosity ratio, and the contact angle. Gas is injected to drive the oil rim down-dip and re-connect the oil ganglia trapped by waterflooding. Although connate water was immobile after water was displaced by oil, it was mobilized under gas injection (i.e. gas, oil and water all flow in the gas-invaded zone) so three-phase relative permeability to oil governs the drainage efficiency in this region. The mobility will be unfavourable where gas displaces the oil/water bank, so the displacement rate must be limited to allow gravity to stabilize the interface. In some circumstances, the gas replaces oil as the spreading phase.

4.2.6 Wettability Alteration

A clean water wet micromodel could be made preferentially oil-wet for oil/water displacement test by procedure presented in this section. Contact angle observation after alteration process showed that a coating of bitumen made the model mixed wet for gas/water and oil/water systems. The wettability effect apparently causes lower residual oil saturations to occur after water displacement.

In order to examine the effect of wettability, two experiments were performed with models that were aged using a North Sea oil to render them "mixed wet". One method of changing the core wettability is to age it with crude which is known to contain the required surface active agents. After some weeks of ageing one assumes that some change of wettability has taken place. Wettability change can be ascertained by some measurements like relative permeability or Amott test. With the help of micromodel we could actually observe the process of change of wettability of the model from water-wet to mixed-wet and see the change in contact angle and interface curvatures. The following steps were taken to age the heterogeneous model, (see Table 4.2-1), to alter the model from water-wet to mixed-wet:

. Saturated the micromodel with brine

. Flooded with decane to connate water saturation

. Displaced the decane with kerosene

. Flooded the model with the North Sea stock tank oil and aged it at laboratory conditions for 22 days.

. Displaced the stock tank oil by flooding the model with decane

The progress of changing the wettability was recorded by taking video tape at different time intervals. The change of oil-water curvatures (contact angle) in Figure 4.2-9 (a- after 2 days of ageing, b- after 22 days of ageing) and change of oil contact angle in Figure 4.2-10 (a-after 6 days, b-after 18 days of ageing) indicate alteration of wettability from completely water-wet to mixed-wetness. In most pores and throats due to deposition of some heavy components, part of the surface has been changed into oil wet while the rest of it still water-wet. If this process of alteration of wettability could extend over all parts of porous media then there would be the possibility of having both oil and water as continuous phase throughout the porous media (mixed-wettability).

4.3 RESULTS

Four experiments were conducted to simulate the secondary recovery of oil by gravity stable gas injection. These are listed as Experiments 1, 2, 3 and 18 in Table 4.2-4. The remaining fourteen experiments were performed to simulate mechanism of oil recovery by tertiary recovery with gravity stable gas injection. The influence of wettability on displacement process was considered only within the tertiary recovery experiments. The effect of interfacial tension, spreading coefficient, pore geometry, and pore size distribution were studied in both secondary and tertiary processes.

The highlight of a number of new and very interesting observations are given here, and details of the various features for each fluid phase are described in the subsequent section.

1- The connate water established in the porous media with initial oil saturation adjacent to it is normally assumed to be stable and immobile. Our observation indicated that this assumption is not valid. As soon as the third phase (gas) enters the porous medium, a significant change occurs in capillary, and gravity forces. To reach a new equilibrium (balance) between active forces, connate water begins to mobilize and to achieve a new saturation distribution. Therefore, in gas/oil gravity drainage process in addition to oil there is some kind of displacement in connate water.

2- In those experiments with a mixed-wettability system i.e. Experiments: 3 and 17 (Table 4.2-4), parts of the pores and throats surfaces are oil-wet, while the rest are water-wet. Movement of both oil and water in one pore as wetting phase was recognized and by this arrangement the oil was observed to be mobile most of the pores. This implies that recovery of oil at a given level of water cut could be higher in mixed-wet system than in completely water-wet system.

3- Our observation indicates that no matter how slow the gas is moved, there will not be a stable horizontal gas oil contact moving down in a piston like displacement (even in small cross section area of the micromodel).

4- When gas breaks through the bottom of micromodel, several big clusters of oil are still present throughout the model, all being by-passed by loops of gas. After the gas breakthrough gas leaves the model intermittently. As soon as the gas pressure overcomes the threshold pressure of the oil saturated throats at the exit, it rushes out of the micromodel. The oil recovery in this period is mainly by film flow process and gas continuous to flow intermittently.

5- In tertiary recovery, we observed that individual oil blobs, were displaced and joined each other to create larger clusters of oil. Due to small vertical length of micromodel

these clusters of oil in various parts of the model, however, did not grow large enough to form an oil bank ahead of gas front. In the case of positive spreading coefficient, most part of the residual oil was drained through its own film that was spread over the water surface.

6- The displacement efficiency and ultimate recovery were significantly lower for the case of layered network. Due to entrapment of oil in low permeability layers, the overall performance of the layered system is much poorer than that in a single homogeneous layer.

7- When the spreading coefficient is negative the volume of trapped oil blobs remains almost constant for a long time after they have been invaded by gas i.e. no significant oil drainage takes place by film flow process. For the case of positive spreading coefficient, decrease in oil volume of one cluster and at the same time an increase in the oil volume of another separate nearby oil cluster is observed. This event indicates that there is a good communication between different individual oil clusters via a continuous oil film for positive spreading coefficient.

4.3.1 Pore Level Investigation of Flow Mechanism in Secondary Recovery Mode

All the four secondary-recovery gravity-drainage experiments (Nos. 1, 2, 3, and 18 in Table 4.2-4) were carried out with the same test fluids (methane, distilled water, and decane). The third experiment was performed in a mixed-wet micromodel. Photograph of a typical oil and water saturation distribution before starting the gas injection is shown in Figure 4.3-1. It took more than four hours before the break through of gas, to observe the recovery process until the ultimate recovery, experiments were run for 48 hours after break through time. Following is a more detailed description of the flow phenomena observed while performing experiments.

Gas flow mechanism, in secondary process

The pattern of advance of the gas front is highly sensitive to the heterogeneity of the micromodel and distribution of other phases (i.e. oil and connate water). Initially, for the case in which micromodel is saturated with only a single phase (oil), gas preferably enters the model through the largest pore. However, when connate water is present as third immiscible phase, gas will not always enter through the largest pores. Let us compare a large pore that further down the model is connected to a small throat occupied by water, with a medium size pore that is connected to a larger throat. In most cases, due to less pressure difference which is required, gas prefers to enter the latter. The gas flow process, which is governed by the complex combination of pore geometry and fluid distribution, creates a completely irregular pattern and sometimes unexpected movement of the gas front in different direction within the model is observed. In general, however, the gas penetrates those throats that need smaller entry pressure. The main mechanism of gas flow is as follows (Figures 4.3-2 and 4.3-3):

1- Gas invades an oil saturated pore, from the center of the entrance and pushes oil toward other connected throats. Residual oil remains as a film over the surface of connate water in presence of gas.

2- The connate water saturation distribution changes due to gas invasion into the model.

3- In the case of positive spreading coefficient, a film of oil is formed between gas and water phases.

4- The entrance of gas into a small oil-filled pore is delayed until the capillary entrance pressure is overcome by differences in the flowing gas and oil pressure gradients.

5- When enough driving force builds up behind the gas front, because of differences in the flowing pressure gradients between oil and gas, the gas can finger through the smaller pore opening.

6- Since the capillary pressure in the pore body is less than that in the throat (due to larger radius), snap-off phenomenon usually causes, disconnection of gas front inside the pore from the main gas body. The conditions that must be met for snap-off to occur in a flow channel are for the leading film of a bubble to advance into pore bodies considerably larger than the throats; i.e., a favourable pore-body-to-throat ratio must exist. In the homogeneous models, leading films are constrained by matrix grains on the downstream side before the curvature can expand enough to cause snap-off at the upstream pore neck.

7- Qualitative estimate of the oil recovery, based on visual examination of photographs, indicates that roughly 70-80% of original oil in place could be recovered at breakthrough time.

Figures 4.3-2 and 4.3-3 are examples illustrating the status of three sections of a heterogeneous model before and after gas injection in a secondary recovery process.

In these figures oil is shown by red colour, water by blue and gas by light coloured spaces surrounded by dark edges. These are actual photographs taken from the video recorded experiments. Comparison of figures reveal the above mentioned facts.

Oil flow mechanism in secondary recovery process

Prior to and during the secondary oil recovery process, the oil phase is hydraulically continuous throughout the micromodel. It is generally displaced by leaky piston type mechanism which after breakthrough, gradually shifts to film flow mechanism. Due to positive spreading coefficient most of the trapped oil (even those residing inside blind alleys or dead end pores) are drained by film flow process in gas invaded parts of the micromodel. The following phenomena have been observed during the displacing period.

1-Oil was drained by two processes:

a- If the oil is connected to the main body of the oil phase, then the displacement is of the leaky piston type.

b- If the oil is disconnected from the main oil body, and is trapped in a dead-end pore,

or it is isolated by a narrow throat filled with water, the drainage would be by film flow over the water surface in the case of positive spreading coefficient (Figure 4.3-4).

2- Local decrease in gas pressure would cause increases in oil volume, which is trapped between gas tip and water. In this case oil is fed from the main oil phase till equilibrium conditions are satisfied (Figure 4.3-5).

3- Due to balance of interfacial forces, always gas and water phases are separated by a thin layer or a disk of oil (Figure 4.3-6).

4- The resistance to flow in throats i.e. $2\sigma/r_t$, is much greater than that in pore bodies i.e. $2\sigma/r_p$. When gas tip crosses a pore throat, the spontaneous movement of gas tip into pore body causes some reduction in local gas pressure, which due to that a backward movement of gas tip in nearby throats have been observed. The upward movement of gas front during its journey, is an indication that displacement is completely gravity stable.

5- The residual oil at gas breakthrough in not evenly distributed in the model, but it is in form of individual clusters of different size.

6- The oil displacement consists of advancement of menisci and rupture of oil connections. The disconnection process is strongly influenced by the local pressure field near the front.

7- As is demonstrated in Figure 4.3-7, although the opening of pore 1 is larger than pore 2 the water blockage, below pore 1 prevents the gas entry into this pore and the gas prefers to enter via the smaller pores 2, 3 and push the oil through pores 4 and 5. The advancement further down the model resembles a gas fingering process, whereas in fact the gas flow rate is low enough for the displacement to be entirely gravity stable. The gas advancement continues until a conduit more restrictive than pore 1 is encountered; in which case gas will enter pores 1, 6 and the like, and the flow pattern will change.

4.3.2 Pore Level Investigation of Flow Mechanism in Tertiary Recovery by Gas Injection

Fourteen gravity stable gas injection experiments were carried out in water flooded models (Figure 4.3-8 shows the fluid distribution after water flooding and prior to start of gas injection. The aim of the first four i.e. Experiments 4, 5, 6, and 7 (Table 4.2-4), was to study the displacement mechanism in water wet models (as a base case). The effect of different physical properties of test fluids was studied in the next five experiments. Then two experiments were performed to study the recovery process in layered porous media (heterogeneous micromodel). The layered micromodel which consists of horizontal homogeneous layers with different aspect ratios, co-ordinate numbers and pore sizes, were used in Experiments 13 and 14. To observe the effect of spreading coefficient, another set of two Experiments 15 and 16 were carried out.

The Experiment 17 was performed to study the effect of wettability on draining process. In most of the experiments gas flow through the model continued for several days after gas breakthrough to investigate the oil recovery by film flow process.

Gas flow process in tertiary recovery

1- A good communication is established between different gas fingers during the displacing period. When one finger invades a pore and causes a small pressure drop (due to small increase in gas volume), in other throats, gas retreats and the wetting phase imbibes back, through its own film, to accumulate in the throats (see Figure 4.3-10).

2- The flow mechanism through porous media, is the same for both gas and oil phases, compared to water (in water-wet model). They both act as non-wetting fluids, and prefer to invade larger pore throats from their center. For this reason in most cases gas front follows the same route as the moving oil cluster ahead of it.

3- In many cases as the gas tip crosses a narrow throat, which is connected to large pore, a small bubble of gas breaks away (snaps off) from the gas front and jumps to occupy a

larger pore (Figure 4.3-9). As the gas pressure in the main gas body increases enough to overcome the prevailing capillary force, again a gas finger is formed and advances to joint the disconnected bubble.

4- Oil drainage occurs both, in front of the gas phase and in the gas invaded zone. As the gas front moves deeper in the model the pressure difference between the gas and oil phases in the gas invaded part increases. Therefore pressure difference between gas and oil phases in upper parts of the model increases to required value for entering into the smaller pore openings (drainage of oil).

5- When oil ganglia is surrounded by water filled pores/throats, the displacing phase (i.e. gas) must be able to penetrate into those water filled pores/throats before the oil ganglia could be displaced. The gas can displace residual oil only if it can enter all water filled pores that surround the isolated ganglia of oil.

6- When two fingers of gas approach each other by drainage of liquid phase, liquid lamella between the two tips vanish quickly. But for the case of two oil fingers, in most cases a water lamella stays between the two tips for a long period of time and moves with the bulk of oil (Figure 4.3-10). This phenomenon is due to larger interfacial tension between oil/water compared to that of gas/oil. When oil-water interfacial tension is higher than that of gas-oil there is less tendency for rupturing the liquid lamella.

7- Snap-off phenomena occurs many times, during the flow process. Due to smaller threshold pressure of pore, compared to connecting throats, the oil displacement from the large pore takes place very quickly. The subsequent increase in gas volume, and resulting local decrease in its pressure, affects the gas front inside the neighbouring pores, that causes the snap-off of gas and isolation of it as bubbles inside the pore.

8- As the gas front penetrates an oil slug, part of the oil spreads over the water surface as a thick film, which later thins out by draining gradually toward the main oil cluster through the film.

9- Layered micromodel, consists of several layers with different pore geometry, aspect ratio, co-ordination number and pore sizes, while each layer itself contains fairly regular and homogeneous pattern. When a highly permeable layer is placed at the bottom of a less permeable layer, the overall recovery of the system is much less than the sum of the recoveries of the individual layers, when they drain separately. In other words, averaging of transmissibility of layers, do not reflect the vertical displacement of the two immiscible phases through layered porous media correctly. As soon as the tip of the longest gas finger touches the high permeability zone, gas front propagates in that bed laterally. This event causes a reduction in oil relative permeability in front of the oil bank, so the recovery from the top layer decreases sharply.

10- At breakthrough time, several large clusters of oil are formed throughout the model, all being by-passed by loops of gas. After the gas breakthrough from the outlet of the model gas leaves the model intermittently. Visual observations during these events showed that they were caused by periodic invasion and blockage of the gas flow path by liquid. A temporary blockage of the gas flow path caused the upstream gas pressure to increase. As soon as the gas pressure overcomes the threshold pressure of the oil saturated throats at the exit, it rushes out of the micromodel. Due to the large volume of the outlet gap, its pressure is rapidly decreased and the gas body is ruptured by the snap-off process. There will be a time delay before gas phase is locally repressurised for another cycle of discharge. The oil recovery by film flow process and gas intermittent flow are demonstrated in Figure 4.3-11.

Oil flow process in tertiary recovery

Before gas injection, the oil distributed in the micromodel is mainly in the form of individual ganglia and slugs which are located in the center of large pores, with water film around them. As the gas front progresses into the micromodel a cluster of oil is formed ahead of each gas branch. After some time the oil cluster is by-passed by a gas finger and

this process is repeated several times during each tertiary gravity drainage process. Following are the main observations made of oil flow during the tertiary process;

1- As soon as the moving oil ahead of the gas front touches a new trapped oil blob, it coagulates with it.

2- While oil is displaced by gas a small portion of it is left behind at the entrance of each throat and is trapped there.

3- Due to light reflection it is not possible to distinguish a very thin film of water on the pore surface and a thin film of oil which is between gas and water phases. However, there are many features pointing to the existence of such films. They act as conduits for flow of oil and water.

4- Oil is drained by two ways:

a- If there is no obstruction ahead of the oil body it is mostly displaced in the form of a leaky piston leaving a film of oil between gas and water phases.

b- If there is some obstruction (e.g. a dead end pore or a small pore throats) ahead of the oil it is displaced by counter current flow of oil through its own film.

6- Movement of the gas front, causes local displacement of residual oil and reconnection of individual oil blobs to form large clusters of oil in different parts of the micromodel. The volume of these slugs change during the displacement process depending on the variation of pressure. This indicates the existence of an oil film between the gas and water phases throughout the gas invaded zone of the micromodel. While gas is advancing, the oil slug shrinks in size, but when the local gas pressure is decreasing the process is reversed, i.e. gas is retracted and oil flows through its film and fills the space evacuated by the gas (Figure 4.3-12a).

5- When a gas finger approaches, the entrance of the gas filled pore, the oil volume ahead of gas finger shrinks and it spreads over the water surface inside the pore (Figure 4.3-12b).

7- When a blob of water is confined within two oil fingers from two sides, it shrinks and is squeezed out by a film flow process to form a thick water bridge. The water bridge is subsequently squeezed further to form a very thin lamella between the two oil tips. The water lamella will remain there for long time. But when two gas fingers approach each other, the liquid between them (oil or water) is drained to a lamella and is quickly ruptured (Figure 4.3-12c).

8- The local and short time reduction in gas pressure takes place following a gradual pressure build-up and immediately after overcoming a local capillary threshold.

9- Continual backward and forward movement of gas front reduces the volume of oil blob ahead of it by spreading the oil on the water surface. The rhythmic movements of oil-water contact and gas-oil contact in different throats and pore bodies show good hydraulic continuity inside each phase.

10- As soon as the pressure of gas phase overcomes the threshold pressure of the oil filled cluster of pores, it penetrates and pushes oil out of the cluster.

11- In gas invaded zone a number of large clusters of oil are formed, which are surrounded by the other gas and/or water phases.

12- Movement of gas front while displacing an oil slug ahead of it, through several pores and throats, indicates that under suitable conditions the water flood residual oil could be displaced by gas for a long distance. When oil cluster reaches an obstruction, it may be penetrated by the gas finger behind it.

13- In the case of layered micromodel, the displacement efficiency of each layer depends on the location of that layer. There would be a sharp reduction in drainage rate, if the transmissibility of lower layer is higher.

14- Before the start of displacement, oil resides, in the form of blobs, mainly in the large pores. During the gas injection, a cluster of oil forms ahead of each gas branch and moves with it, but it does not take long before it is by-passed by a gas finger.

15- As is demonstrated in Figure 4.3-12b, a quick advancement of gas into a large pore (marked by 1) increases the gas volume. This causes some decrease in the local gas pressure which forces the gas to retreat from other locations (marked by 2 and 3). The film flow movement of water is observed in location 4.

16- When the spreading coefficient is negative (Table 4.2-6) the volume of trapped oil blobs remains constant for a long time after they have been invaded by gas i.e. no drainage takes place by film flow process (Figures 4.3-13 a, b). For the case of positive spreading coefficient, decrease in oil volume of one cluster and at the same time an increase in the oil volume of another separate nearby oil cluster is observed. This event indicates that there is a good communication between different individual oil clusters via a continuous oil film at gas/water interface (Figure 4.3-14 a, b, c, d). The connection between the oil ganglia inside the micromodel, and the exit of the model is via the oil film layer at the interface of water and gas phases, which determines the drainage process (Figure 4.3-15). It should be remembered that in real reservoirs the spreading coefficient is generally positive because of low value of gas-oil interfacial tension.

4.3.3 Propagation of Gas Finger in Porous Media

The manner in which one fluid i.e. gas displaces another i.e. oil, depends on the ratio of their mobilities $M = (k_g/\mu_g)/(k_o/\mu_o)$, where suffix g denotes the displacing gas, and suffix o denotes the reservoir oil. End point mobilities are used for segregated flow, and for the diffuse flow, gas and oil mobilities are replaced by the mobilities evaluated at the Buckley-Leverett shock-front saturation. In tertiary stable gas injection, the mobility ratio between an oil bank and the displacing fluids may then be taken as; $M = (k_g/\mu_g + k_w/\mu_w)/(k_o/\mu_o + k_w/\mu_w)$, and the mobilities being evaluated at the appropriate average saturations. If $M<1$, oil is capable of moving faster than gas, for a given pressure

differential; fingering will be suppressed, and a sharp flood front is possible. This gives a favourable displacement. If $M>1$, fingers will develop and propagate leading to early gas breakthrough.

As soon as the capillary threshold pressure at the interface of the gas phase and the wetting-phase is overcome, gas will penetrate the micromodel and continues to move until it is stopped by an obstruction (Figure 4.3-16). Fingers can be triggered by gradients in composition, density, viscosity of fluids, and/or permeability of the model. The spectral distribution of the finger size, shape, and spacing depends on these factors as well as on the flow rates and flow history. Although the gas front moves in different directions in the majority of cases it stops at a depth lower than the starting position. As the gas tip moves further down the model, due to increase in buoyancy force the gas finger begins to propagate laterally. Once formed, fingers tend to grow both laterally and longitudinally through viscous and dispersive forces. As the fingers grow, they spread transversely at their tips and split there into smaller fingers. Most of the fingers that were formed as a result of tip-spreading and splitting did not grow, but were prevented from growth by larger fingers. Gas finger will move sideways, upstream, and downstream toward the outlet of the model. In all experiments, there existed only two or three main fingers at breakthrough time.

4.3.4 Experiments to Determine the Spreading Coefficients

The purpose of this study was to see whether the dyes had significant effect on spreading phenomena. The absolute values of *IFT*'s are different in micromodel experiments from those measured under laboratory conditions. However, it was assumed that if the dyes did not change the value of S under laboratory conditions it would be unlikely that they would change S at micromodel conditions. The micromodel pressure was about 500 psi and the

temperature about 23 °C compare with laboratory atmospheric pressure and temperature of about 23 ± 1 °C (in 12 hrs).

Nine experiments were conducted by adding a droplet of decane (undyed and dyed red) on the surface of water (undyed distilled-brine, and dyed in blue), and observing the behaviour of spreading process. The results are summarized in Table 4-3.1.

The first two experiments (pure decane on distilled water and brine) indicated that the initial spreading coefficient must have been negative and tended to reduce even further and resulted in small lenses of 0.5 and 0.2 cm in diameter after 40 minutes. The third experiment (using pure decane on methyl blue water) resulted in a relatively stable lens of 2.5 cm in diameter. In Experiments 3,5,7, and 8 decane seemed to evaporate (and/or dissolve) and disappear, when observation was made after 12 hours. Test 9 (Sudan red decane on methyl water) indicated a near zero spreading coefficient by spreading to 7 cm and staying rather stable.

For the micromodel conditions of pressure and temperature the values of interfacial tensions for gas/oil were calculated using parachor method. For water hydrocarbon systems after conducting compositional calculations, to determine the composition of the three phases (assuming equilibrium at 500 psig and 23°C), Firoozabadi/Ramey correlation was used. The compositions of the test fluids are given in Table 4.3-1:

Table 4.3-1 Composition of $C_1/C_{10}/H_2o$ at 500 psig and 23° C.

Component	Mole Fraction		
	Gas	Oil	Water
C1	0.99888	0.00079	0.13974
C_{10}	0.00018	0.00000	0.85947
H_2O	0.00094	0.99921	0.00078
Density (g/cc)	0.02402	0.70053	0.95020
Density difference (g/cc)	$\Delta\rho_{wg} = 0.92619$	$\Delta\rho_{wo} = 0.24963$	$\Delta\rho_{og} = 0.67651$
Interfacial tension, mN/m	$\sigma_{wg} = 56.19$	$\sigma_{wo} = 42.80$*	$\sigma_{og} = 14.51$**

* (Figure 9, Firoozabadi/ Ramey's paper), ** (Weinang and Katz Parachor Method)

Parachors used: $Pr\text{-}_{C1} = 77$, $Pr\text{-}_{C10} = 415$, and $Pr\text{-}_{H2o} = 49.52$

Table 4.2-6 presents the value of *IFT* and spreading coefficients at initial and test conditions.

4.4 CONCLUSIONS AND RECOMMENDATIONS

4.4.1 Conclusions

An investigation in the microscopic displacement processes can be used to improve our understanding the microscopic as well as macroscopic behaviour of displacement which would in turn help in modelling the flow mechanism in large scales. The micromodel experiments have provided, a significant insight and much better understanding of the underlying physical principles involved in gas/oil/water displacement processes in porous media. Different phenomena such as the spreading, snap-off, and coalescence of thin films were magnified, observed, investigated and studied in detail. The results of the micromodel observations can be used in conjunction with core flow experiments and network model simulations. Following are the highlights of the most interesting observations made of the experimental results.

Secondary recovery

The following results were obtained when gas was injected, at very low rates, in a micromodel that was saturated with oil in presence of connate water.

1- The connate water in the rock is generally considered immobile when gas injection studies are conducted using reservoir simulators. Our experiments revealed that this is an incorrect assumption. The injected gas changes the balance between gravity and capillary forces and can result in mobilization of water and redistribution of all phases. The film flow of water is an important phenomena in the fluid flow process under gas injection.

2- No matter how low the displacement rate is, the front will never advance with a horizontally descending gas-oil contact within the pore structure. Gas will find the least

resistance path to move forward. It appears that initially the buoyancy effects are overshadowed by capillary forces.

3- The current practice of using simple two-phase and three-phase relative permeabilities, with constant immobile water saturation is not adequate to describe the physical process of oil recovery by gas injection accurately. With positive, or near zero spreading coefficient, which is generally the case for most reservoir oils and waters, oil spreads over water and forms a film between gas and water phases. This oil film provides an efficient conduit for flow of oil between various pores under the combined effect of gravity and capillary forces. Viscous forces are negligible under low flow rates, used in the majority of gravity stable gas injection operation.

4- The displacement efficiency and ultimate recovery decrease significantly for the case of layered network. Due to entrapment of oil in low permeability layers, the overall performance of the layered system is much poorer than the performance of a single combined layer with average properties of the constituent layers.

5- Oil drainage occurs both, ahead of the gas phase and behind it in the gas invaded zone. As the gas front moves deeper in the model the pressure difference between the gas and oil phases in the gas invaded part increases. Therefore, gas can overcome higher values of capillary pressure and enter smaller pore openings and cause further drainage of oil. A temporary blockage of the gas flow path caused the upstream gas pressure to increase. Visual observation while this happened showed that all gas flowed through a critical path.

Tertiary recovery

The observations stated here are the results of gravity stable gas injection into micromodels that had been initially water flooded and their oil saturation had been reduced to residual values.

1- The residual oil remaining in the pore space, after water flooding, can be re-mobilized by injection of gas. The oil blobs are generally invaded by gas phase and form a film of

oil between gas and water phases. This process facilitates the flow of oil through its own film between the pores.

2- Depending on the balance of forces the oil and water could flow concurrently or counter-currently with gas, when they flow through their own films.

3- When two fingers of gas approach each other by drainage of liquid phase, liquid lamella between the two gas tips vanish quickly. But for the case of two oil fingers approaching each other in most cases a water lamella between the two oil tips remains there for a long time and moves with the bulk of the oil.

4- The capillary pressure largely dictates the residual phase saturation during the displacement process. It also provides the driving force for some of the liquid lamella rupture and coalescence events that occur between adjacent non-wetting (gas and/or oil) tips.

5- Although some large oil blobs or clusters were formed in the model, they were often by-passed by gas. The general view that oil bank is formed and pushed ahead to be recovered was not observed in our experiments. The start of oil production occurred together with gas breakthrough and thereafter by the film flow process. This might be the artefact of the small size of the micromodel and its two dimensional nature.

4.4.2 Recommendations

Based on the gravity stable gas injection experiments reported in this chapter, it is recommended that:

1- More micromodel experiments should be performed using the realistic rock and fluid properties. These should include:

. a rough texture within the model to resemble real rocks

. using mixed wet micromodels

. using micromodels with different pore size (and depth) distribution

. using actual reservoir fluid at reservoir pressure and temperature, to simulate surface forces more accurately

. using different patterns of heterogeneity and layering.

2- Perform mechanistic modelling and network modelling of the flow processes in the porous media. The observations made in physical micromodel experiments should be honoured by such mathematical modelling. The modelling should be formulated to handle flow of three fluid phases in three dimensional space and be capable of simulating the micromodel experiments in two-dimensional models.

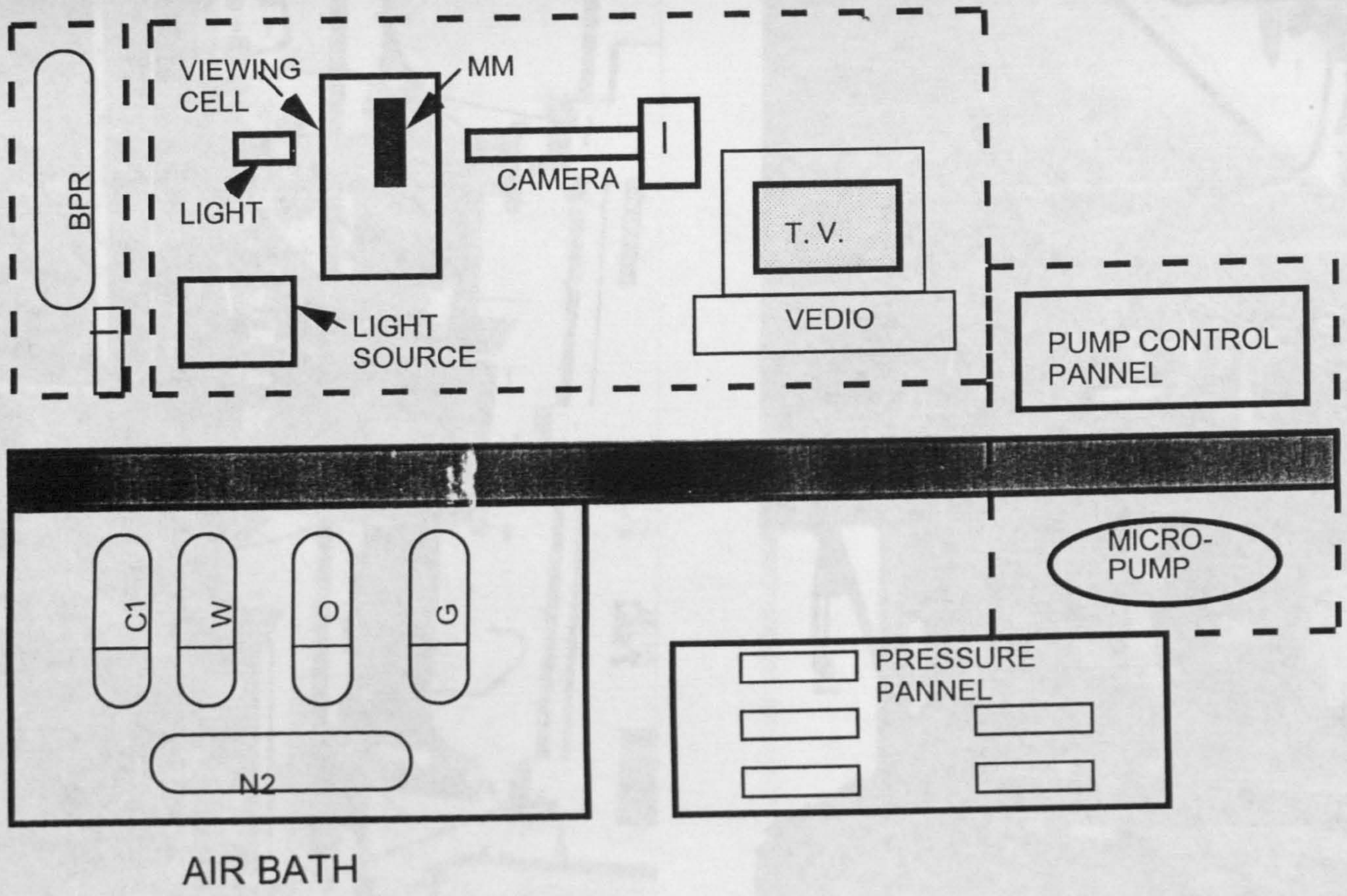

Figure 4.2-1 Micromodel Flow Diagram.

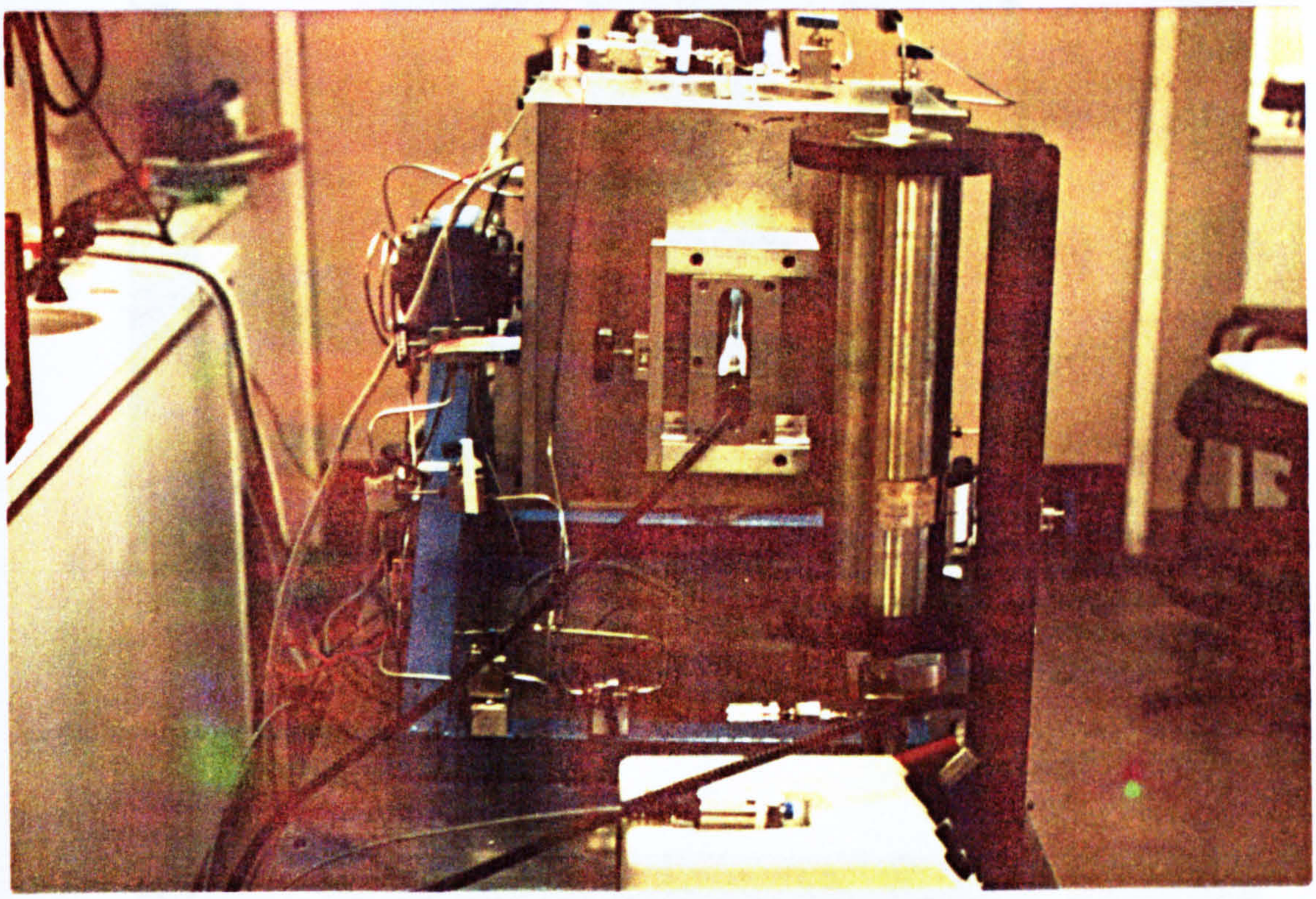

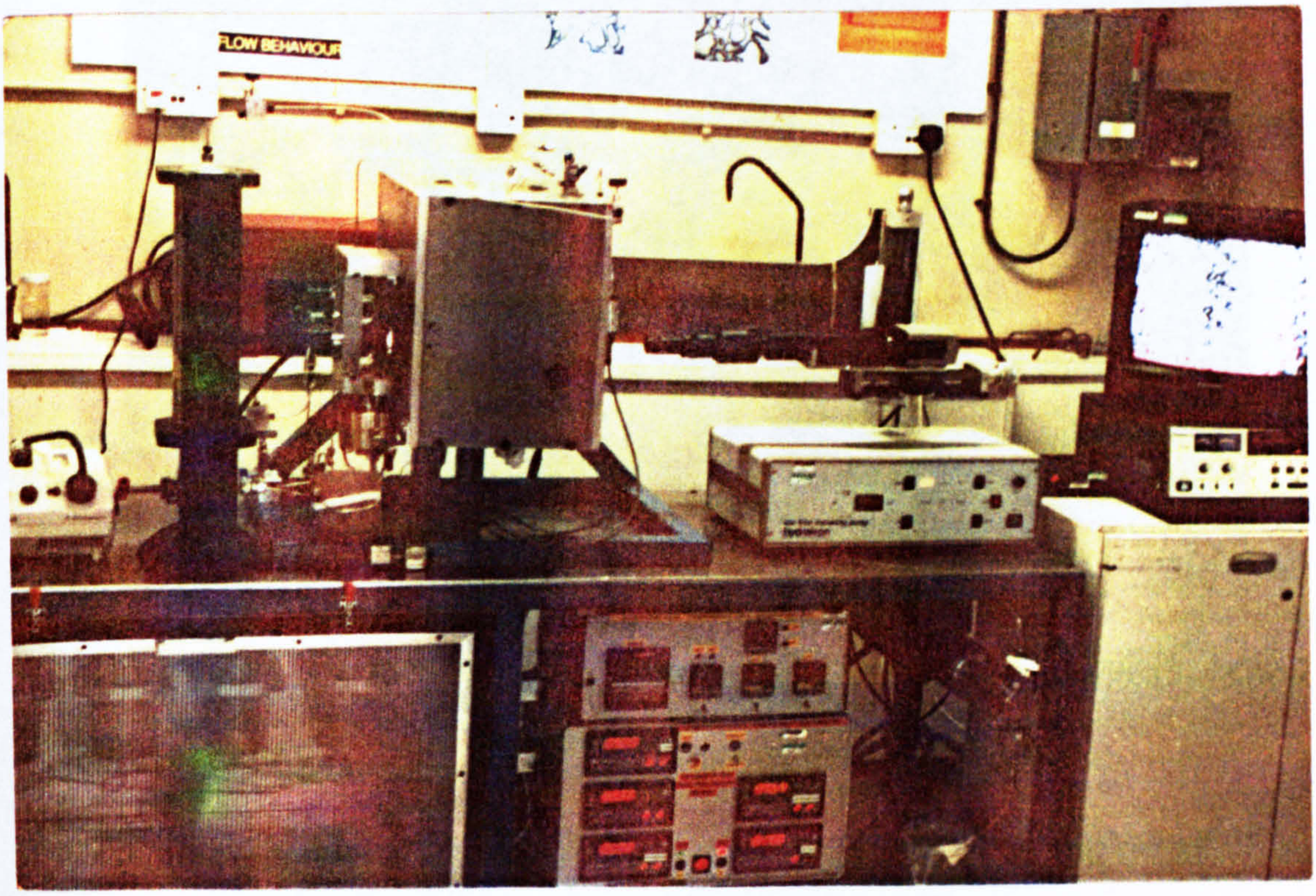

Figure 4.2-2 Arrangement of Apparatus .

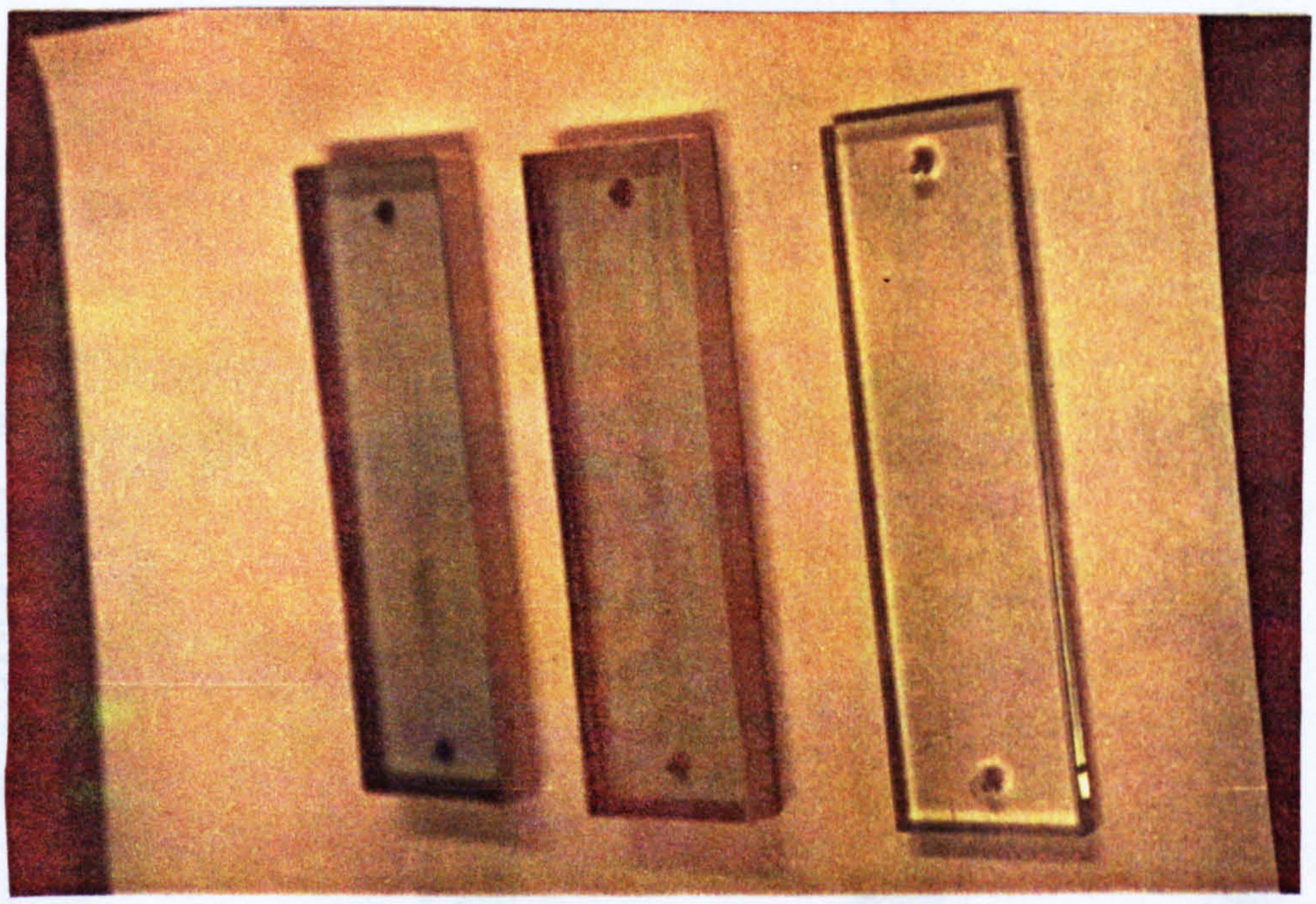

a: Micromodel glass plates.

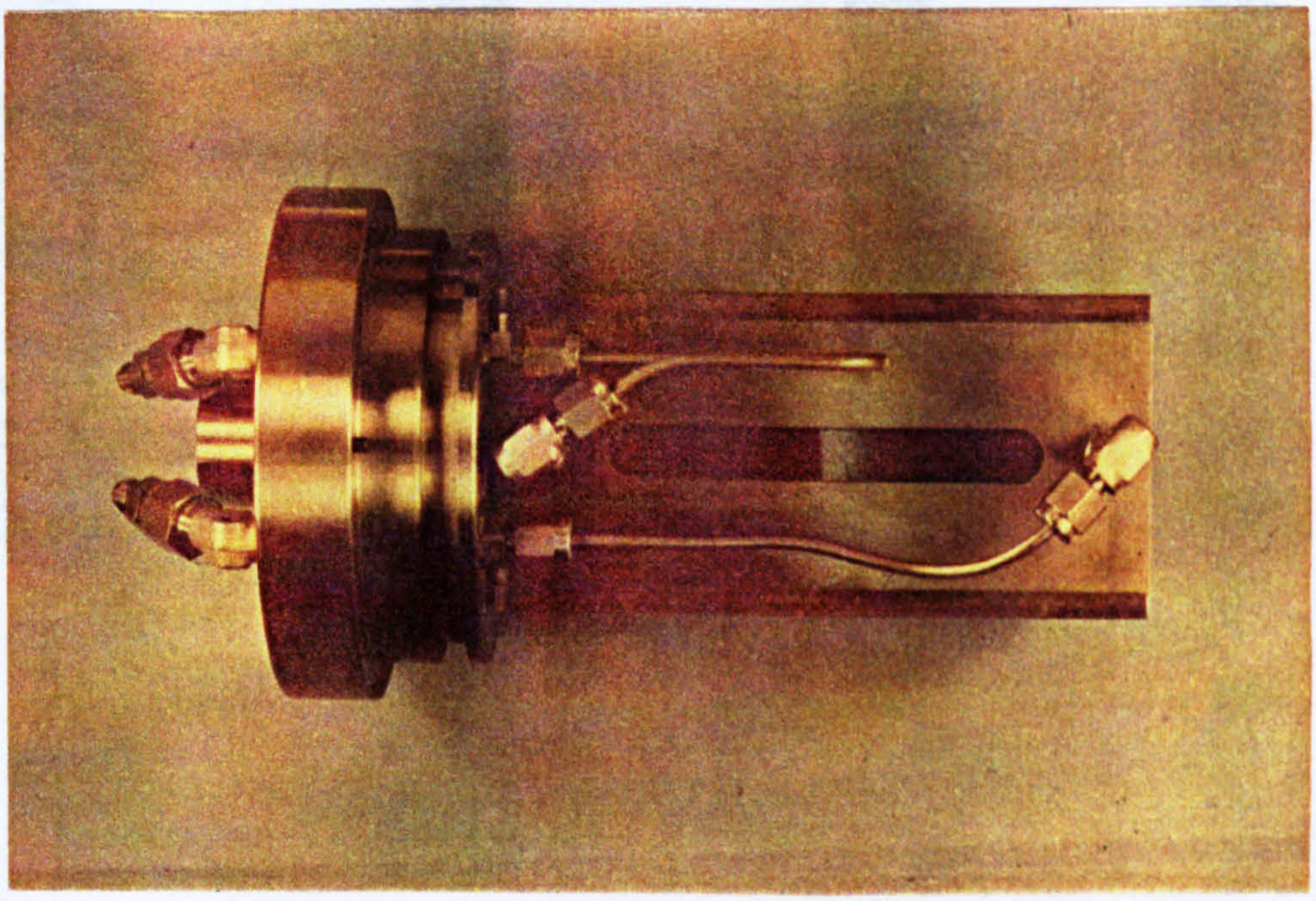

b: Micromodel clamp.

Figure 4.2-3 Photographs of micromodel glass plates and clamp.

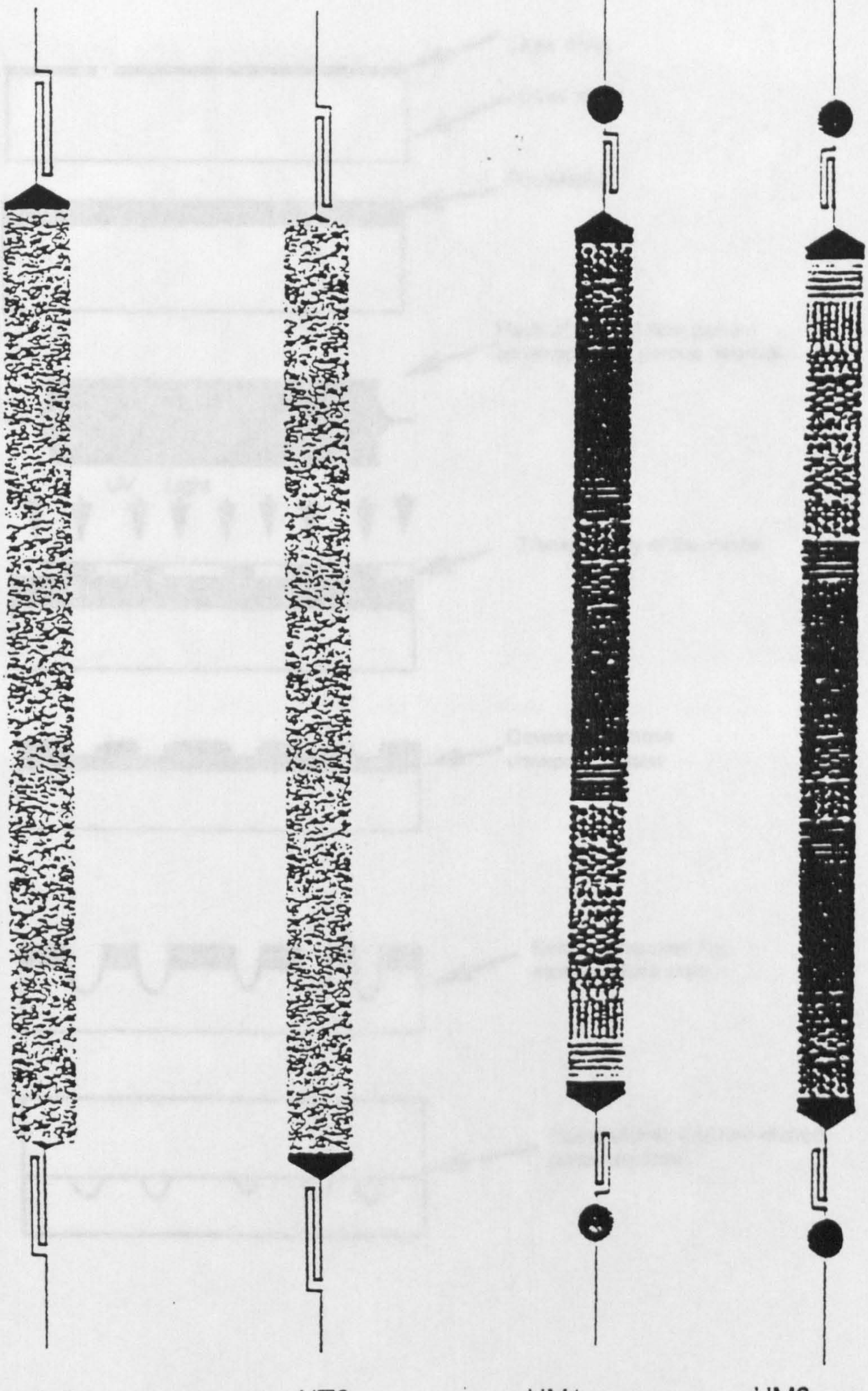

Figure 4.2-4 Pore network configuration of the micromodel.

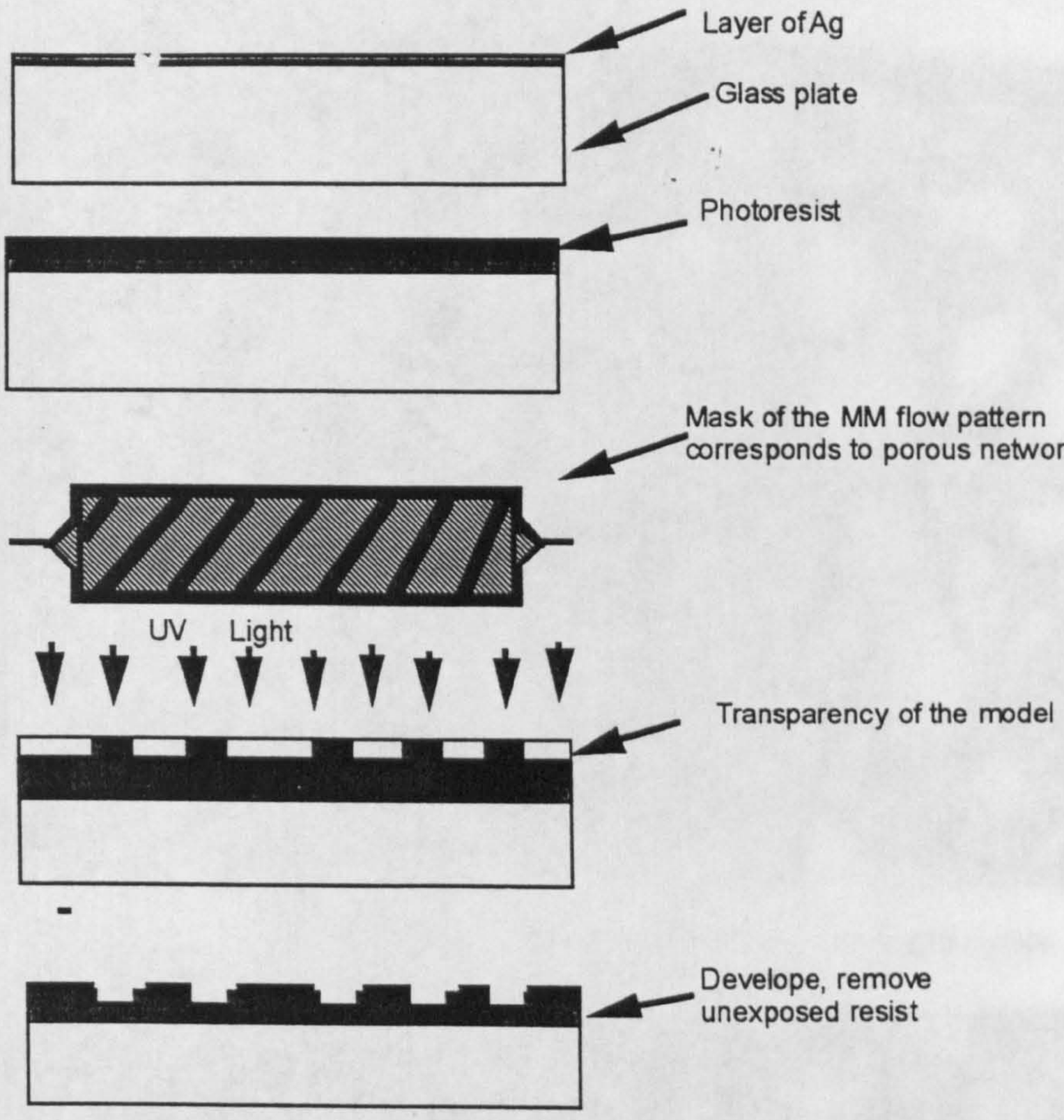

Figure 4.2-5 Fabrication of etched glass micromodel.

a- Initial oil in place in presence of connate water.

b- Initial oil in place is a discontinuous phase.

Figure 4.2-6 Photographs of oil-water distribution before gravity stable gas injection.

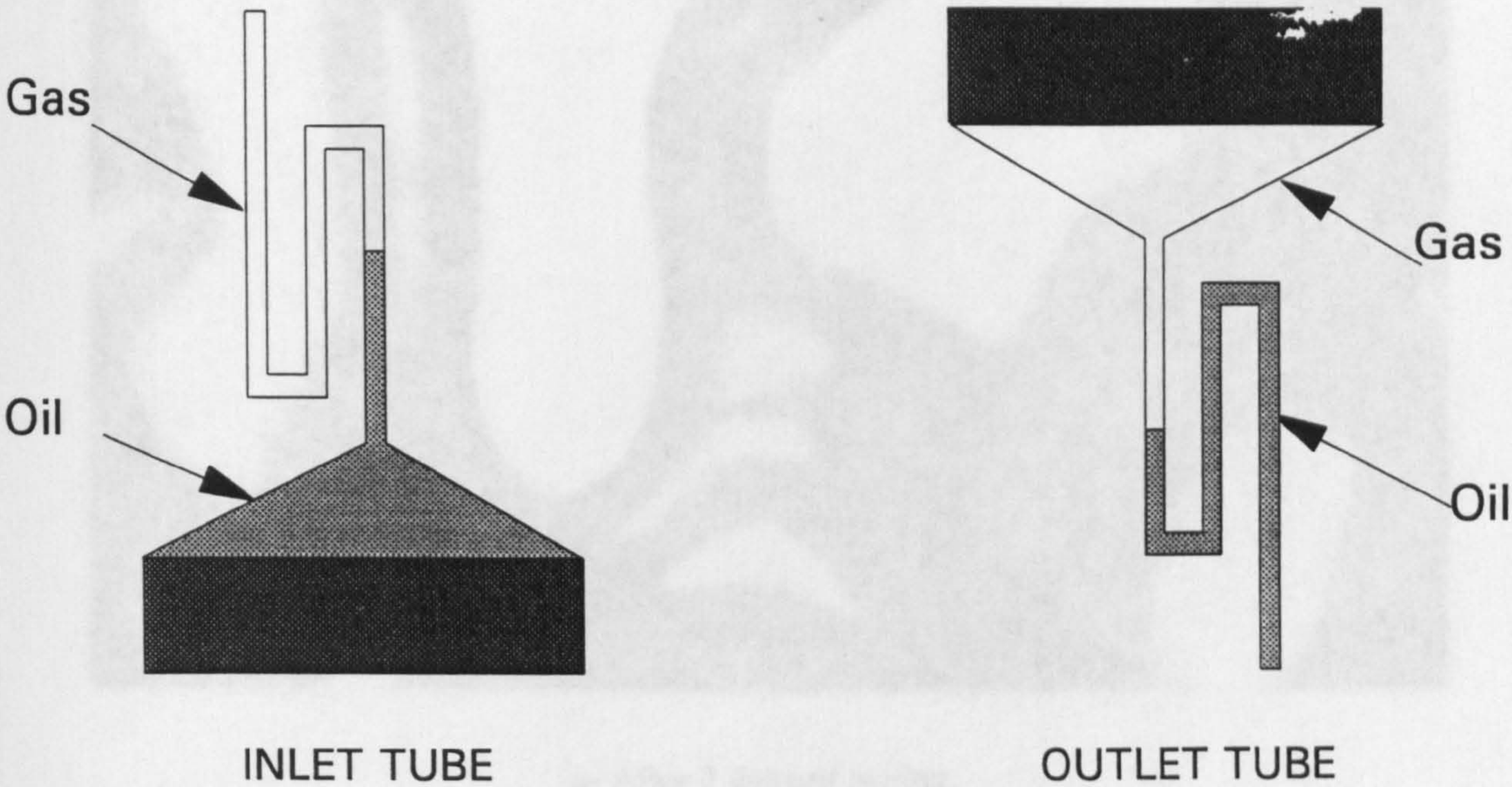

Figure 4.2-7 Flow measurement using the "U" tubes.

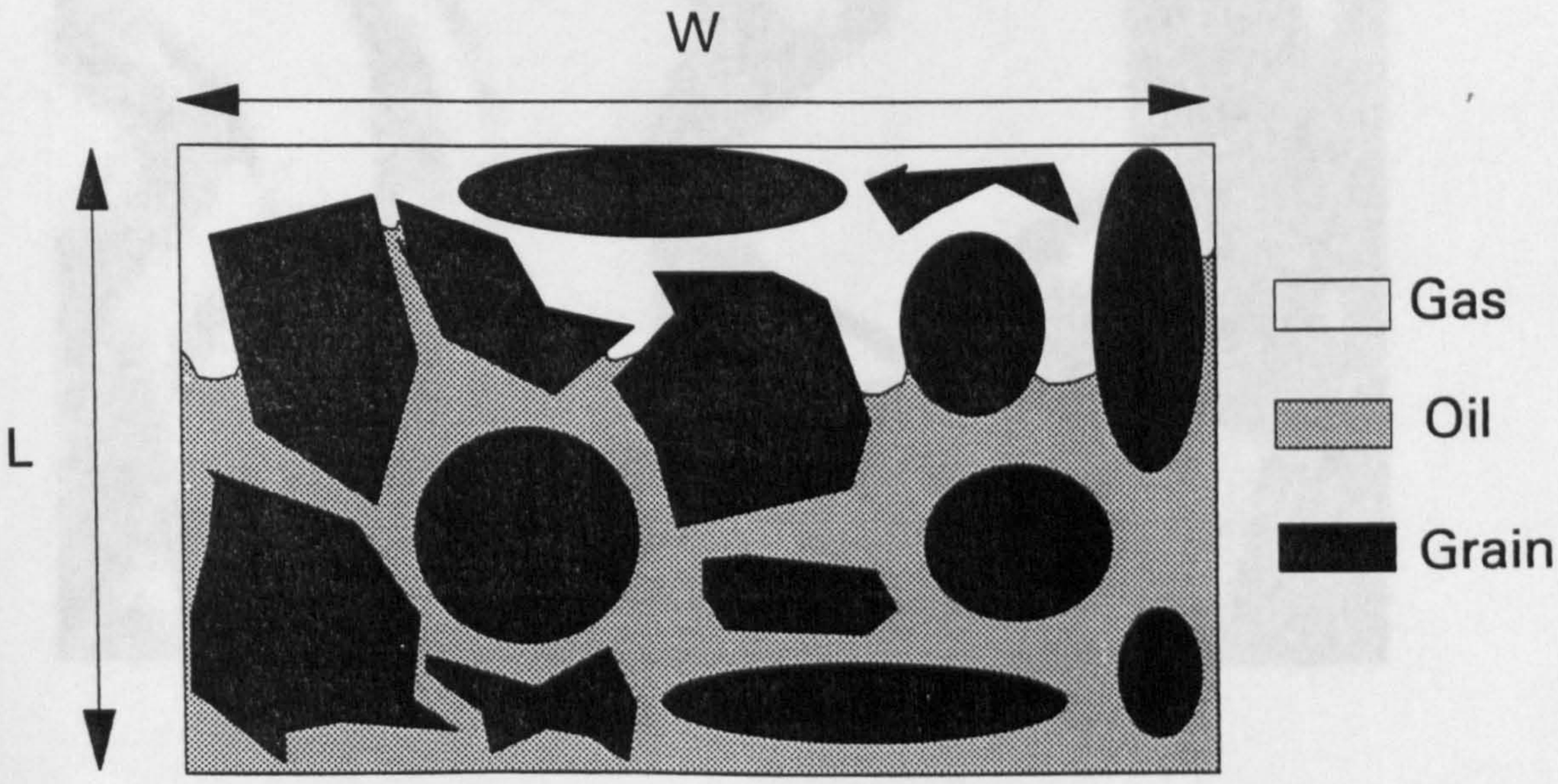

Figure 4.2-8 Flow measurement using a section of the Model.

a- After 2 days of ageing.

b- After 22 days of ageing.

Figure 4.2-9 Photographs illustrating the wettability alteration sequence for specific portion of the model.

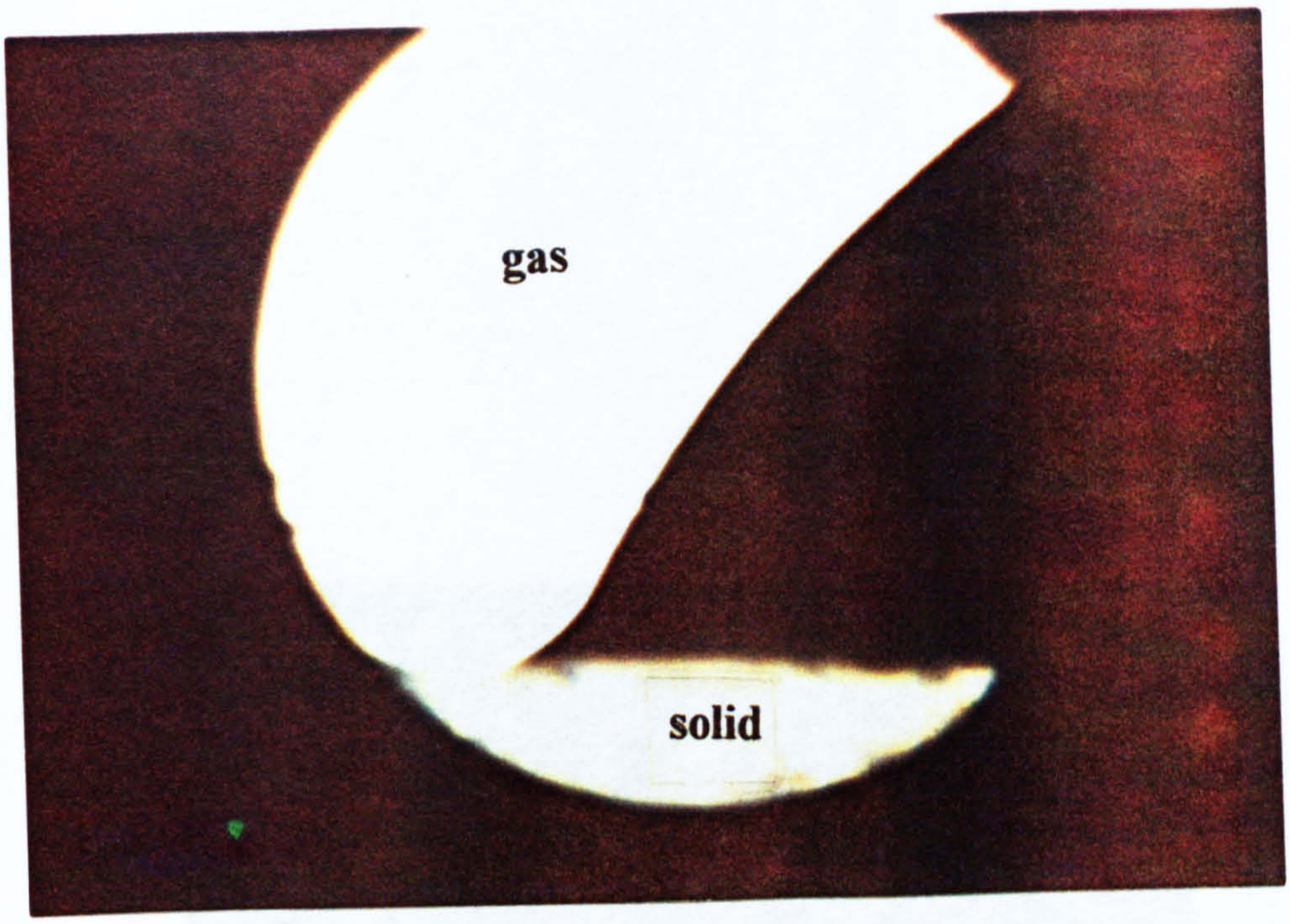

a- After 6 days of ageing .

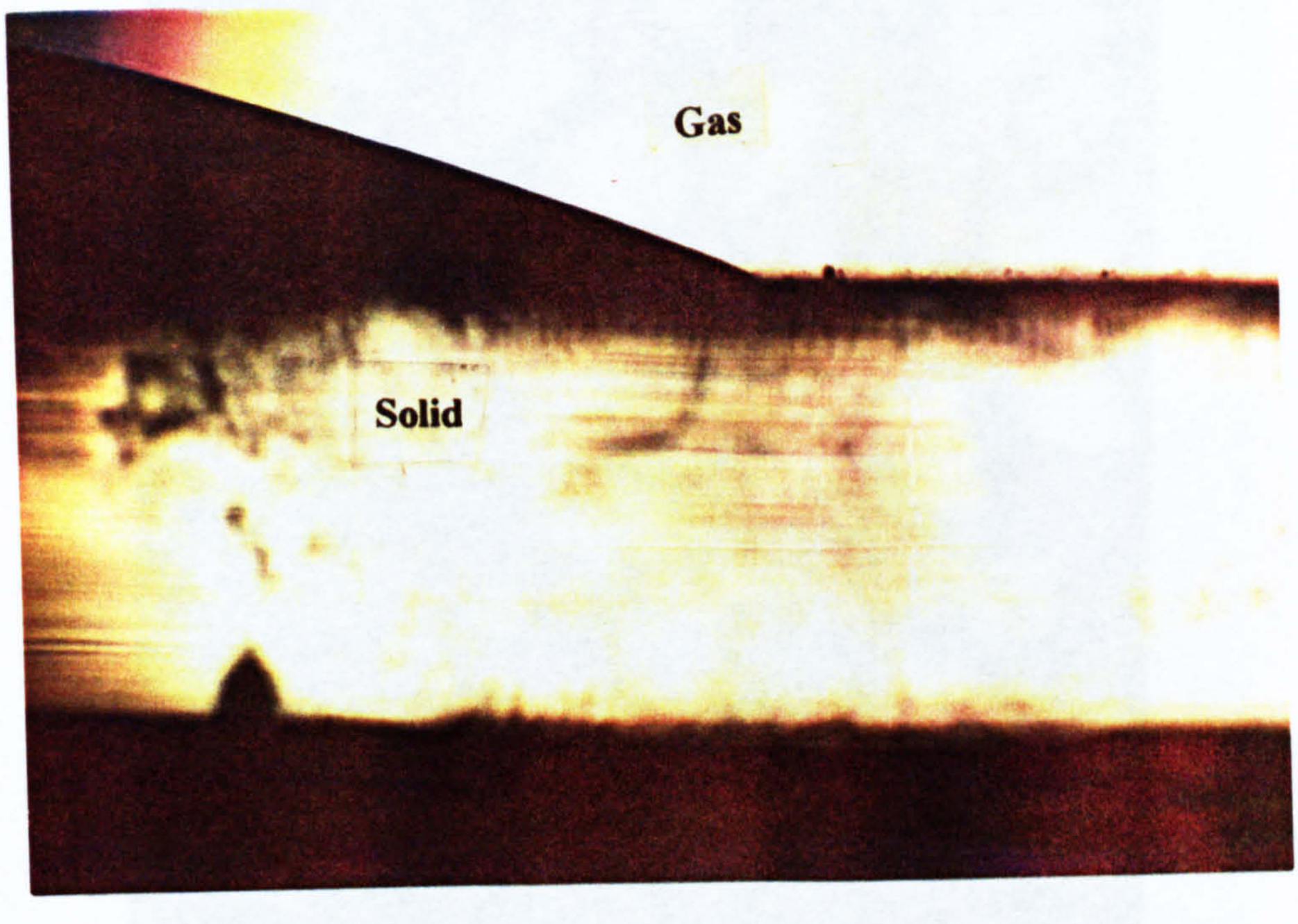

b- After 18 days of ageing .

Figure 4.2-10 Photographs illustrating the change in contact angle on smooth glass plate .

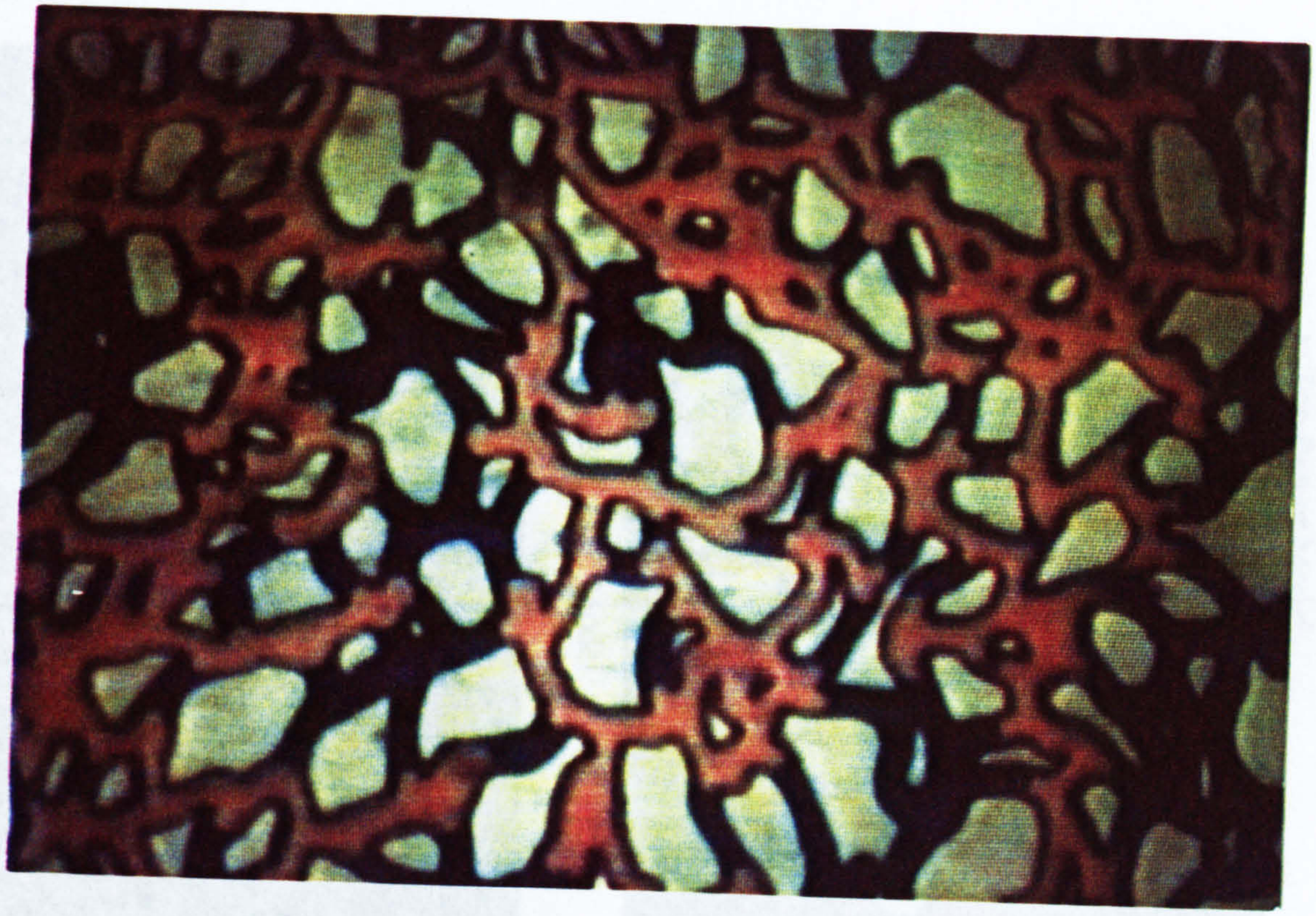

Figure 4.3-1 Photograph of oil and water distribution for water-wet conditions (oil in red, water in blue).

2.5 mm

a: Top Part of Model

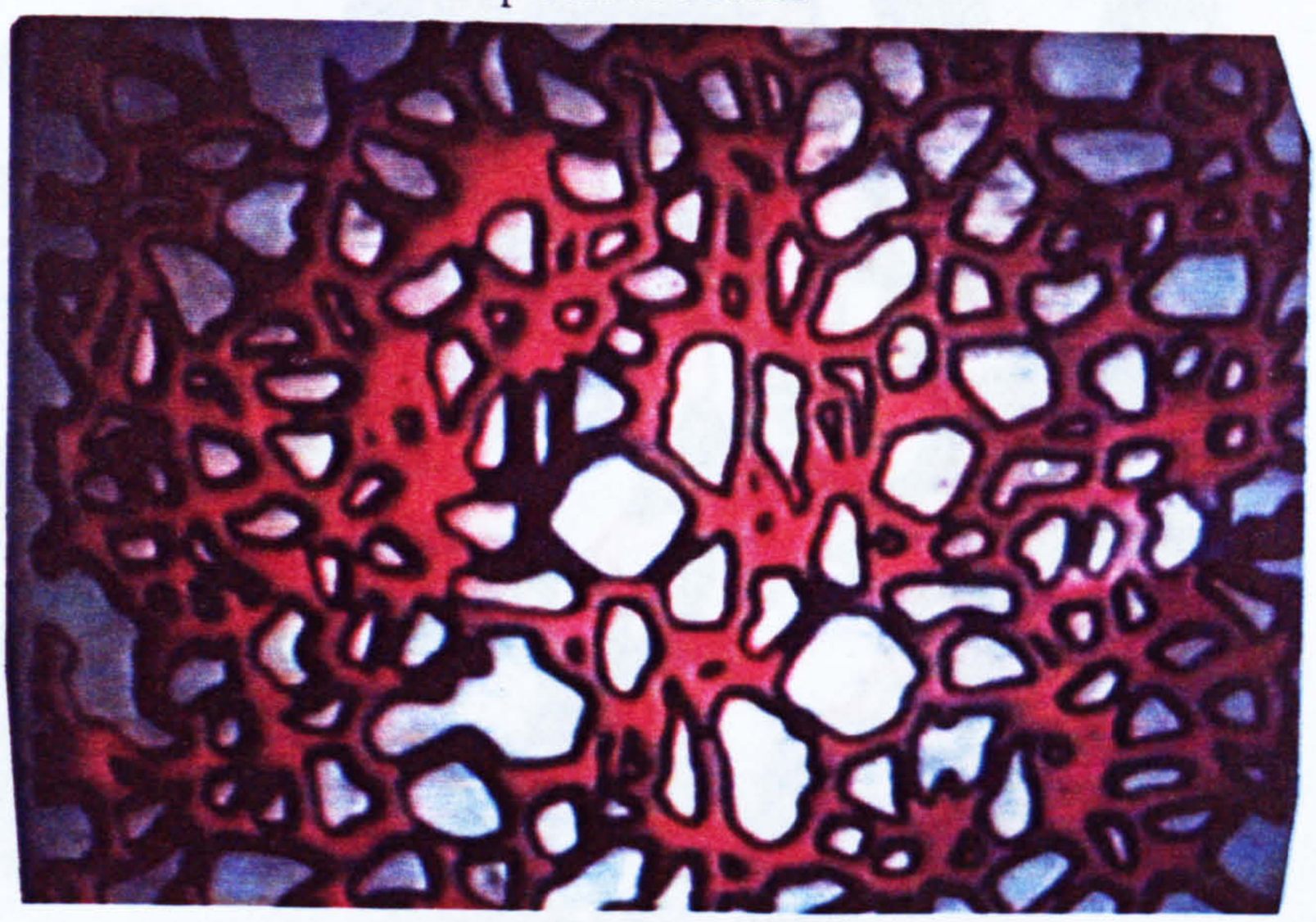

b: Middle Part of Model

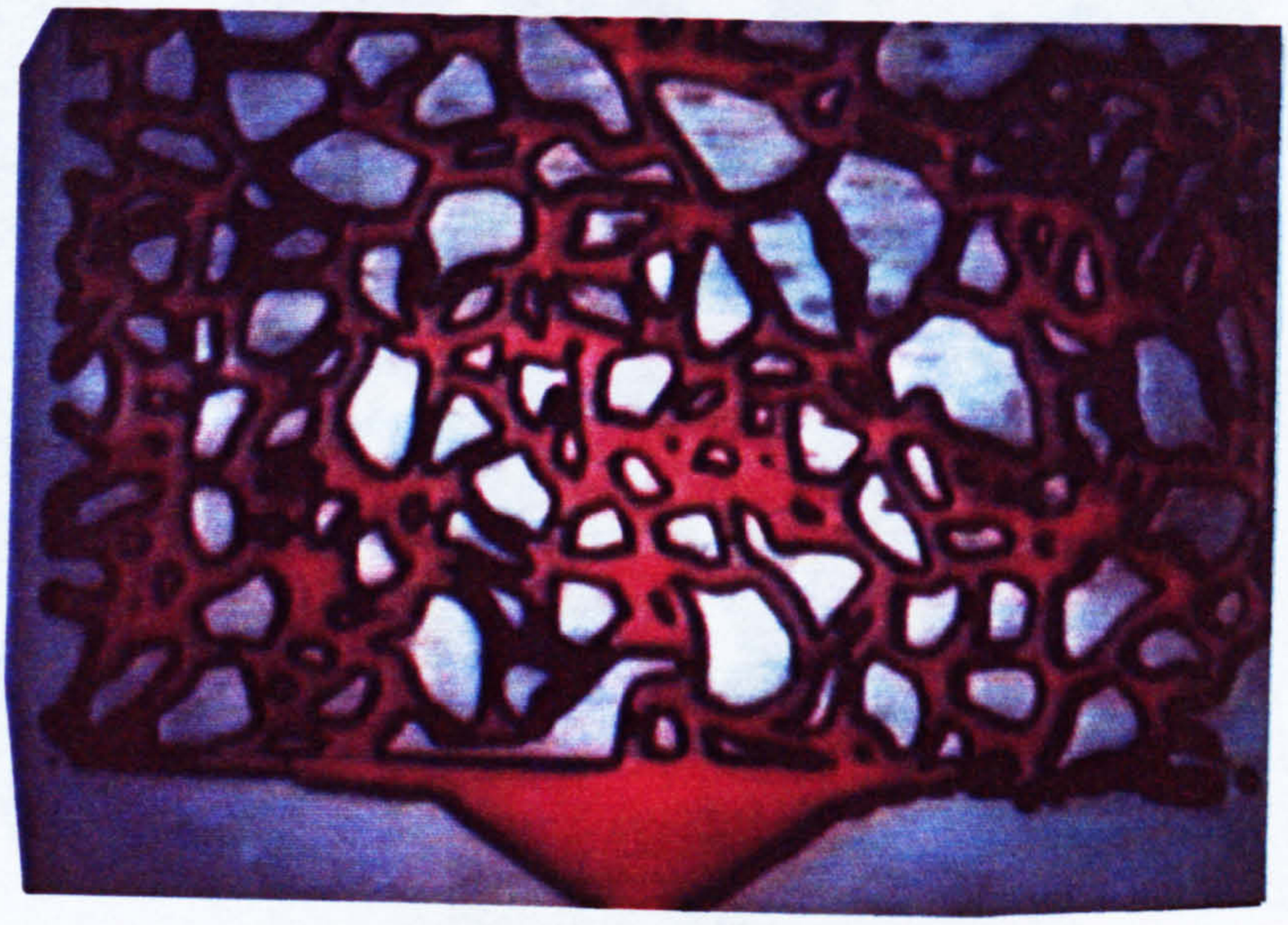

c: Bottom of Model

Figure 4.3-2 Photographs of oil-water distribution before gas injection.

2.5 mm

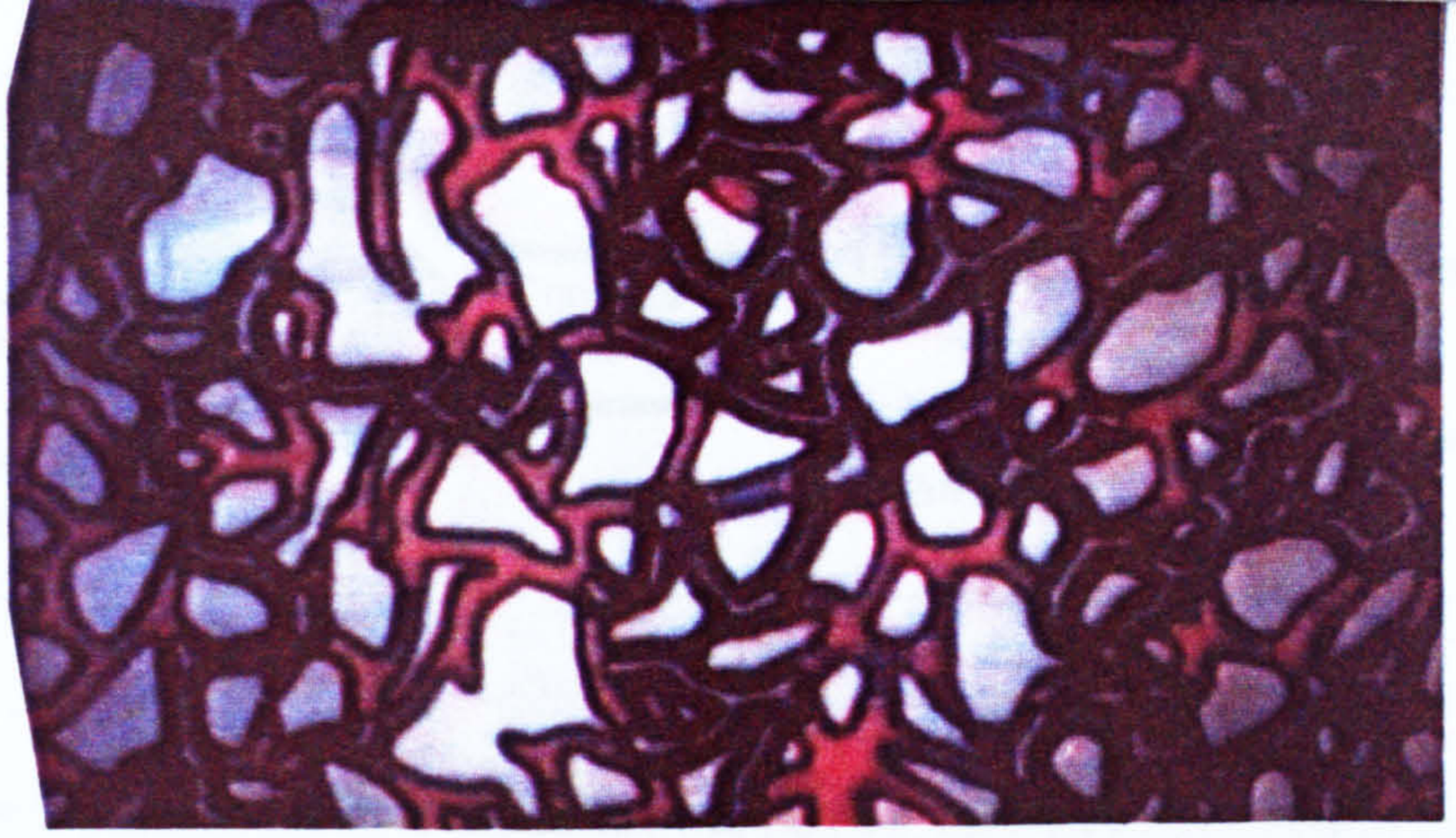

a: Top Part of Model

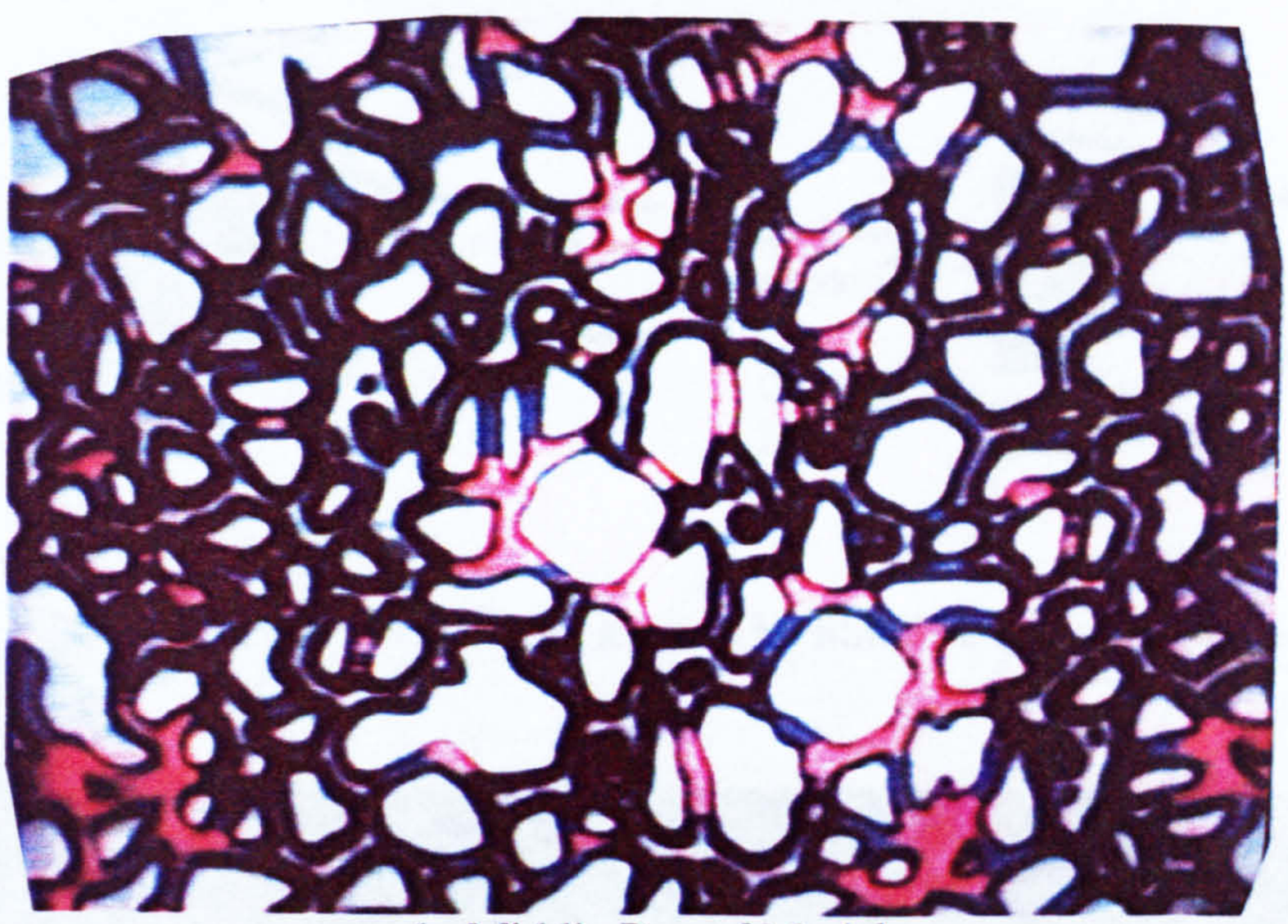

b: Middle Part of Model

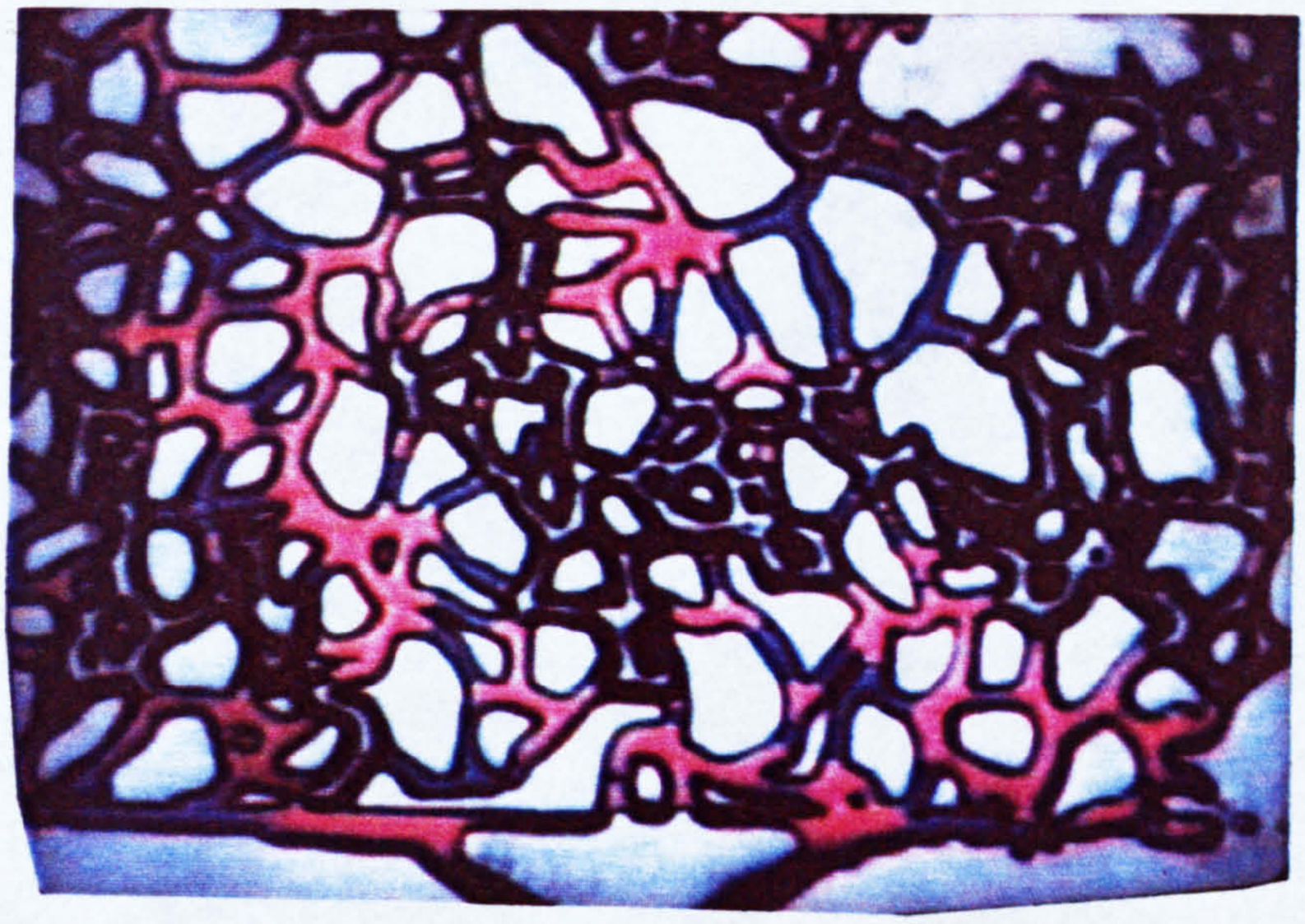

c: Bottom of Model

Figure 4.3-3 Photographs of oil-water distribution after gas injection,

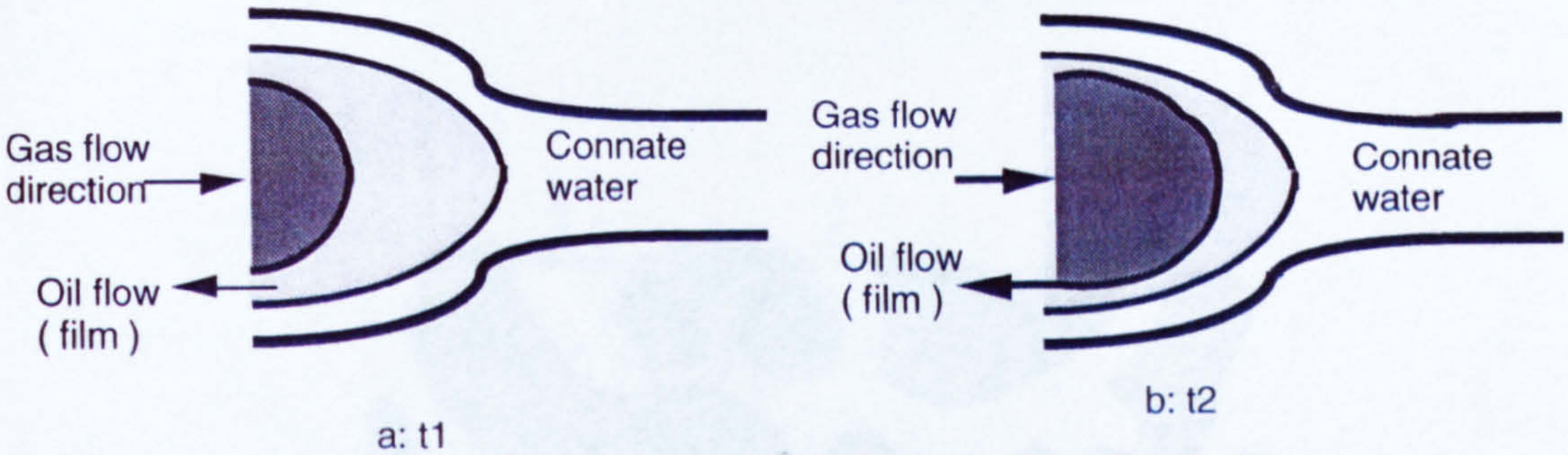

Figure 4.3-4 Gas advances into the trapped oil, oil flows out through its own film (Time $t_2 > t_1$).

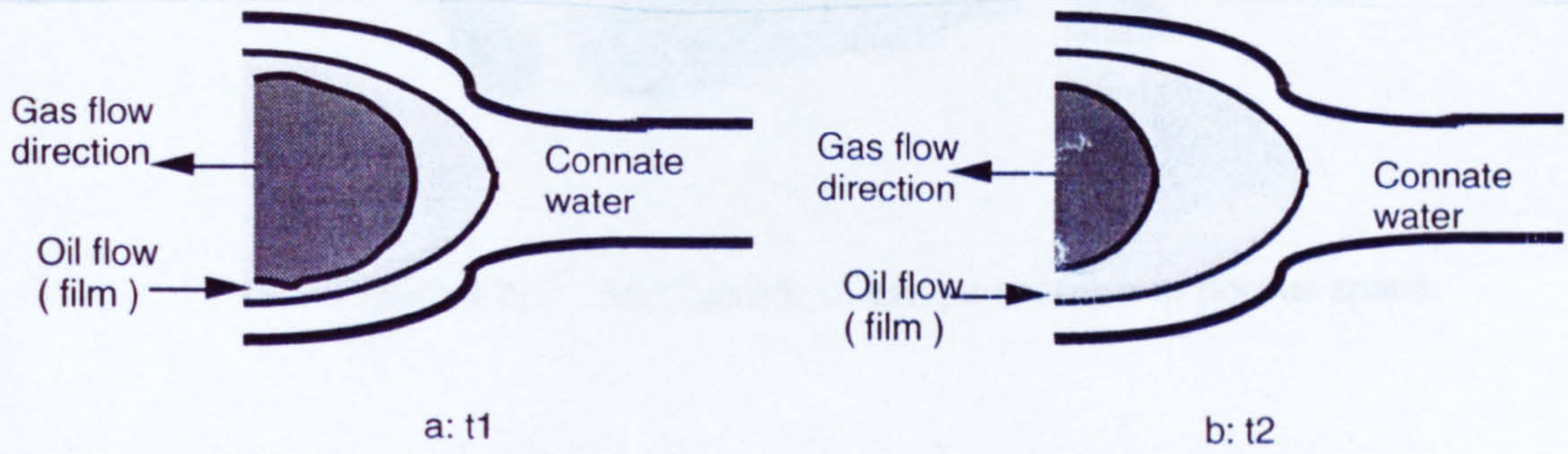

Figure 4.3-5 Oil volume growth by film flow process (Time $t_2 > t_1$).

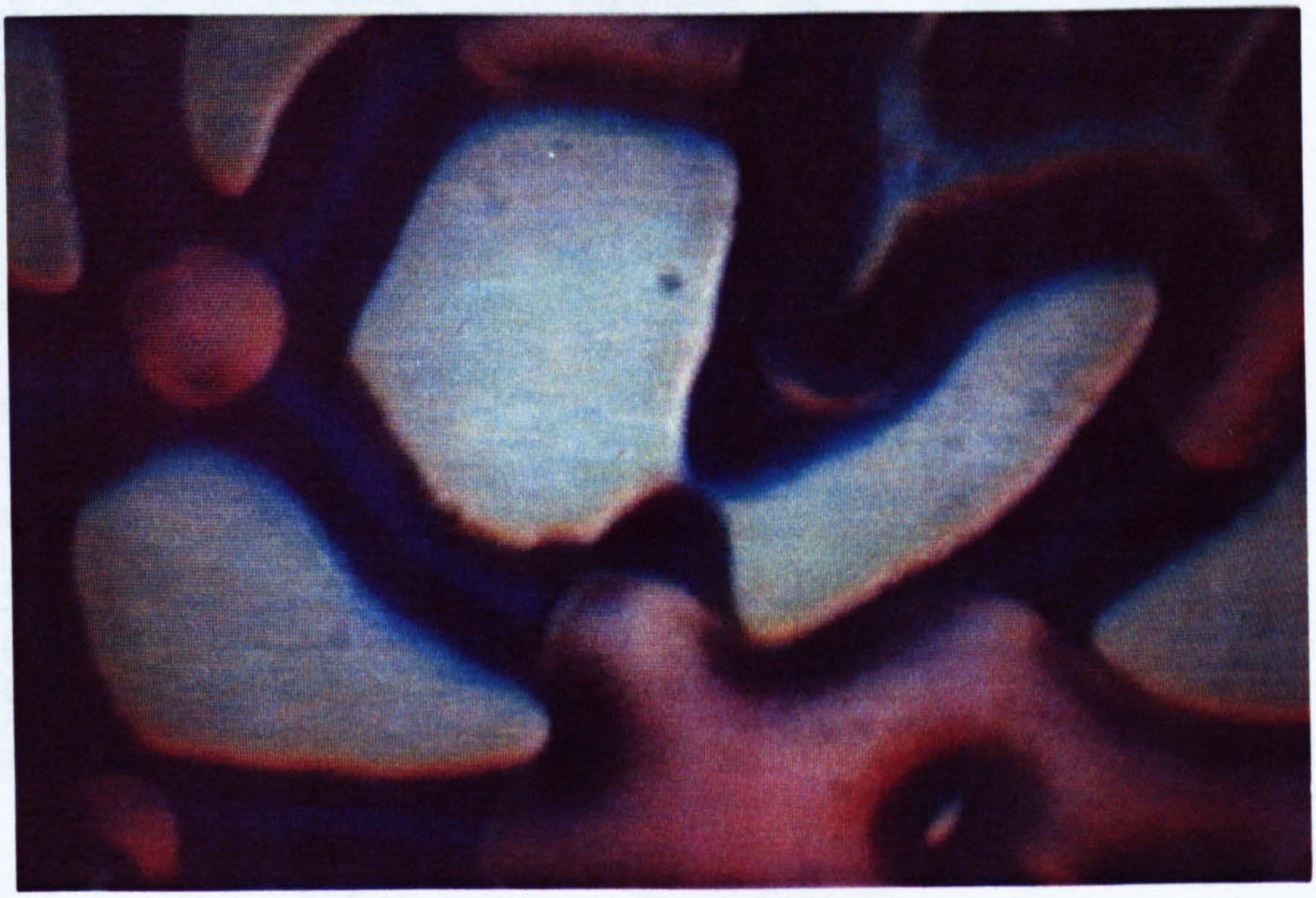

Figure 4.3-6 Thin layer of oil at the interface of gas and water.

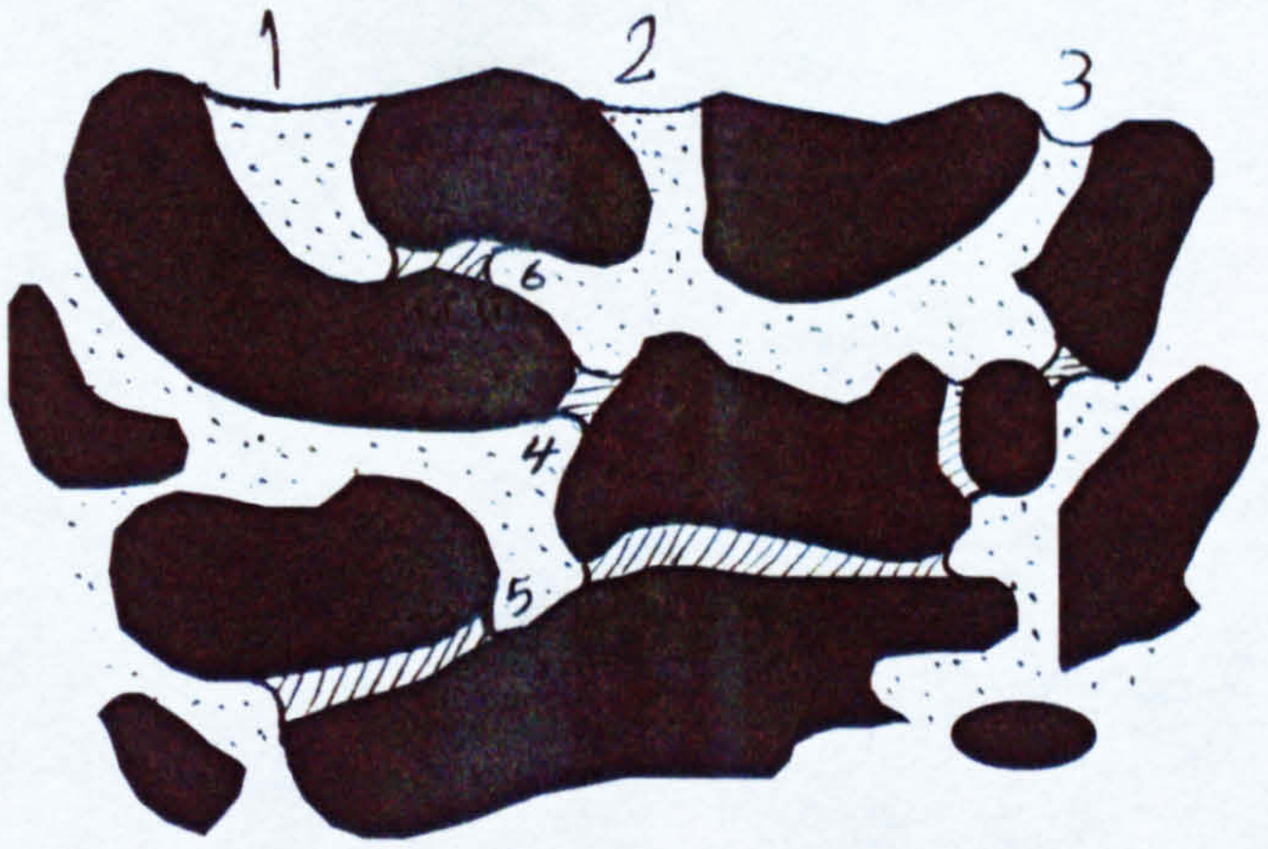

Figure 4.3-7 Mechanism of gas penetration in porous space.

Figure 4.3-8 Photograph of oil-water distribution after water flooding (oil in red, and water in blue).

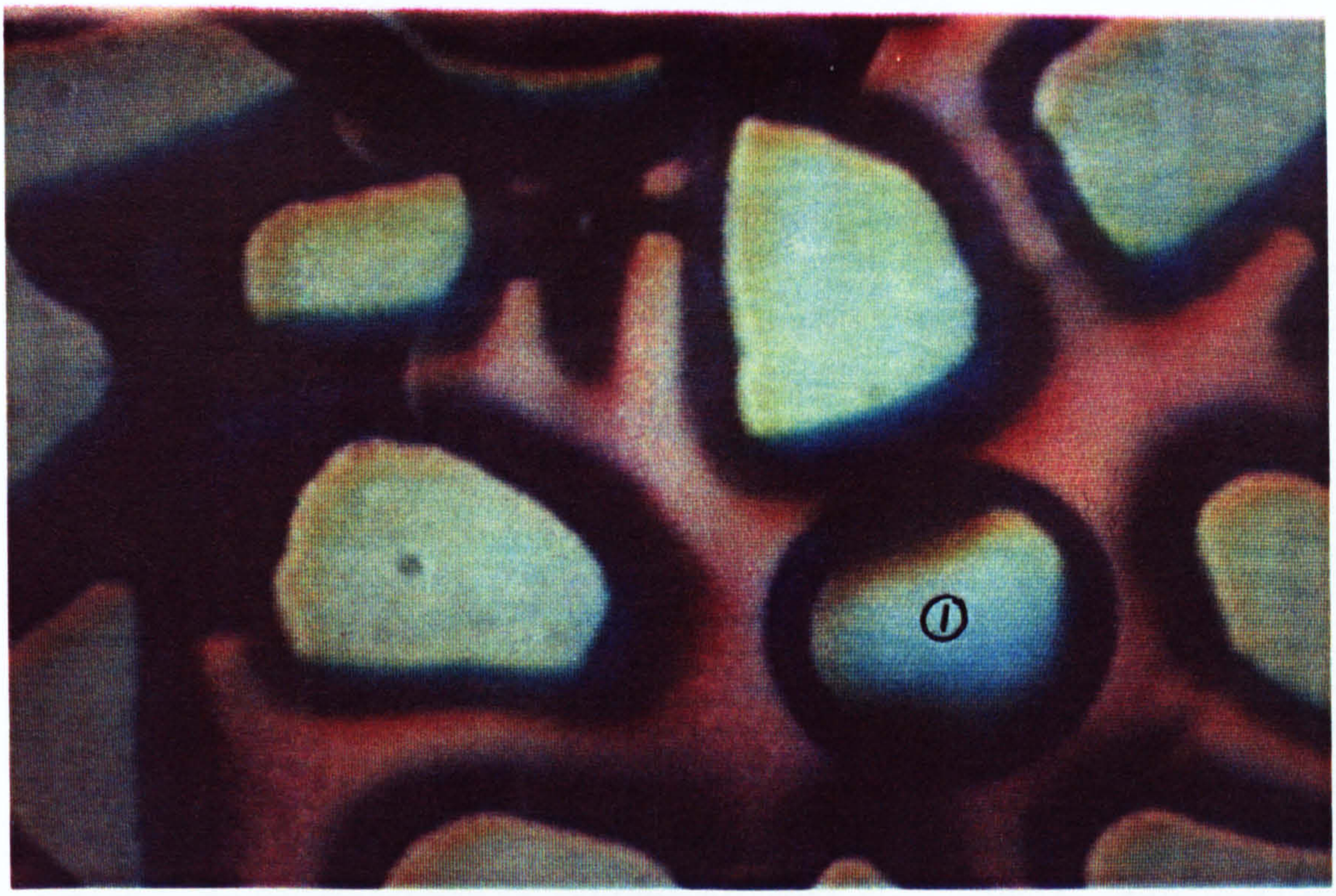

Figure 4.3-9 Trapping of gas bubble due to Snap-off event.

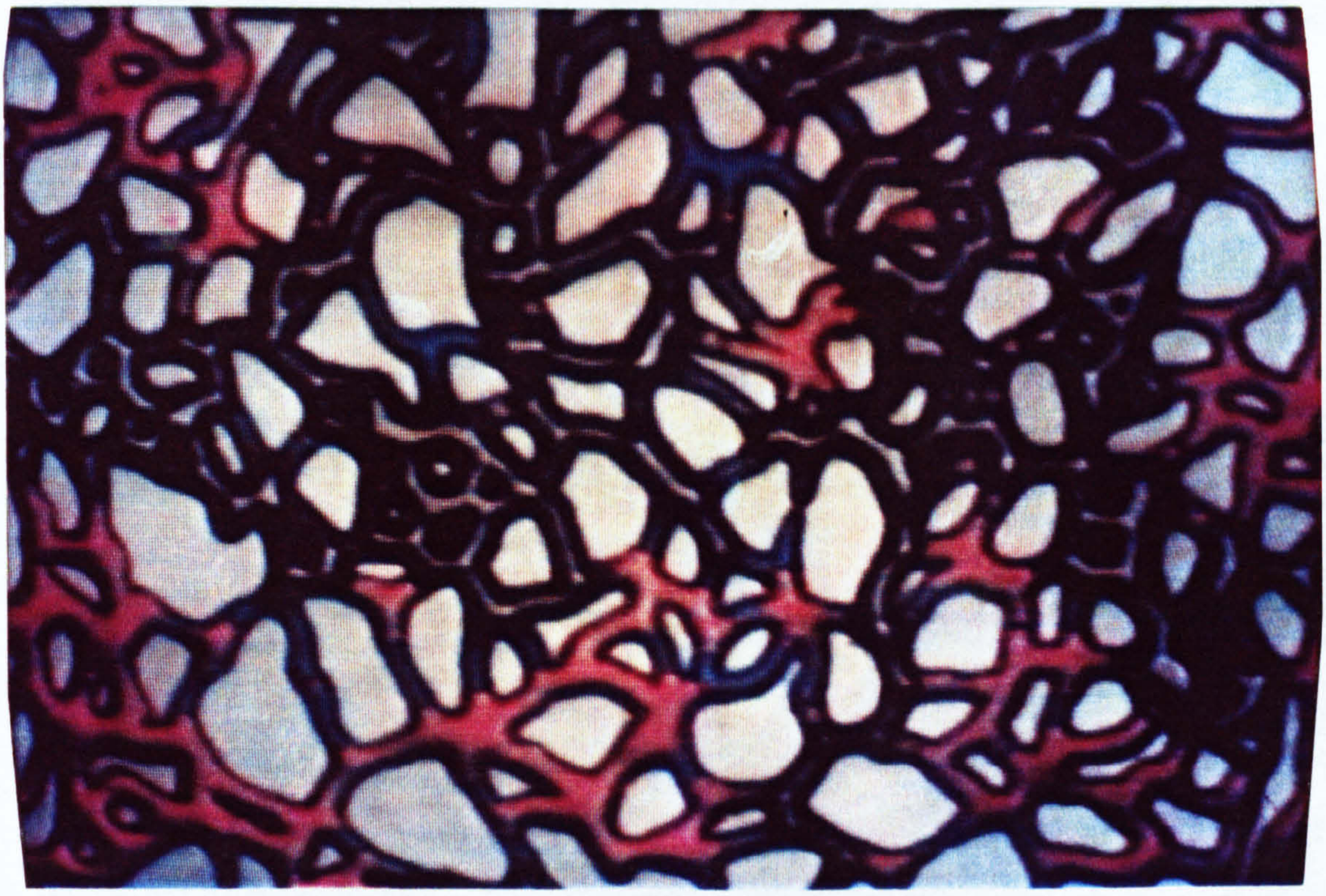

Figure 4.3-10 Coalescence of small gas fingers from top "1" and left "2" of the model, leaving no oil or water at the point of coalescence.

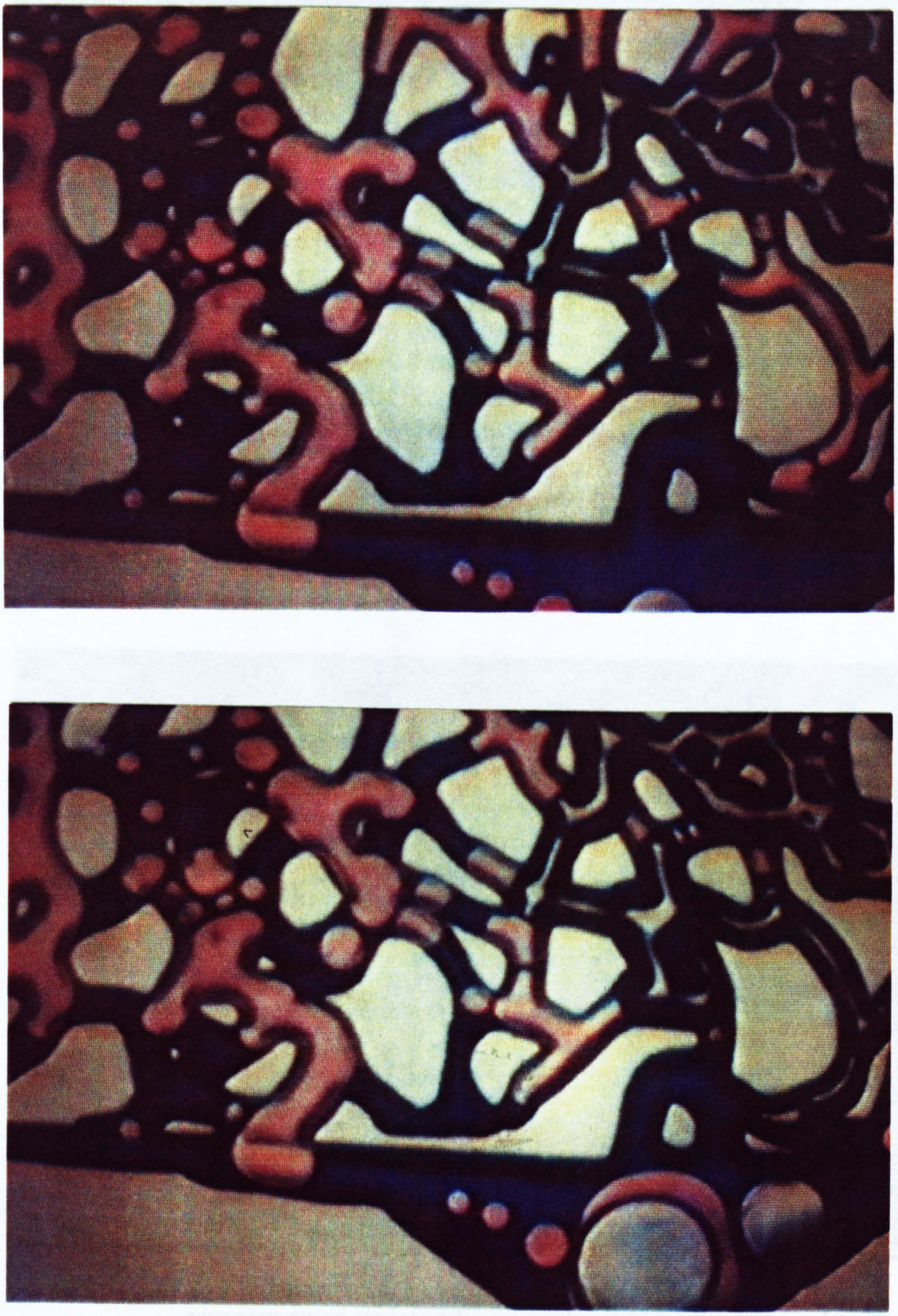

Figure 4.3-11 Photographs of oil film flow and gas intermittent flow out of the model.

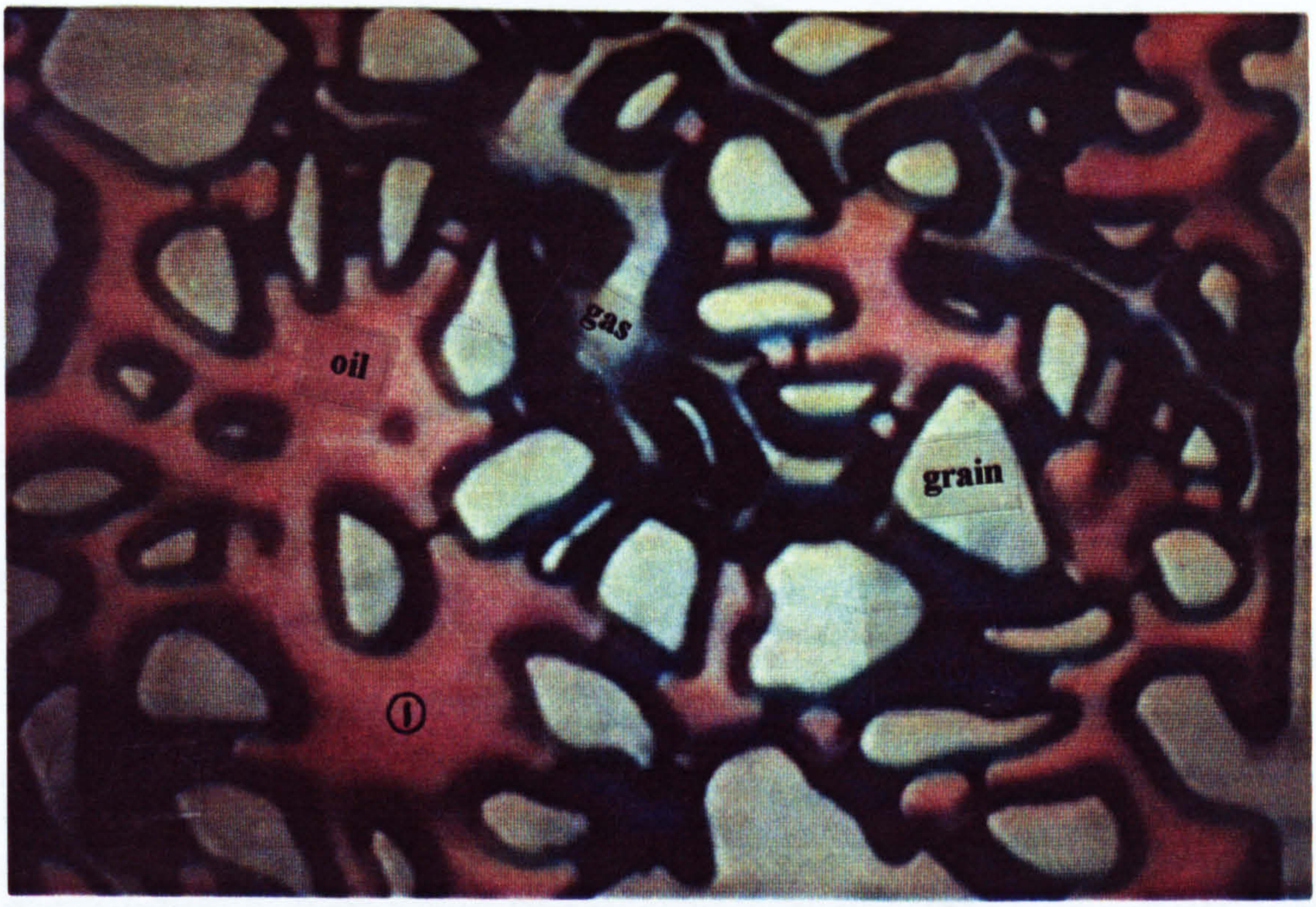

Figure 4.3-12a Gas invasion; Gas starts to invade the oil filled pore through the largest connecting throat.

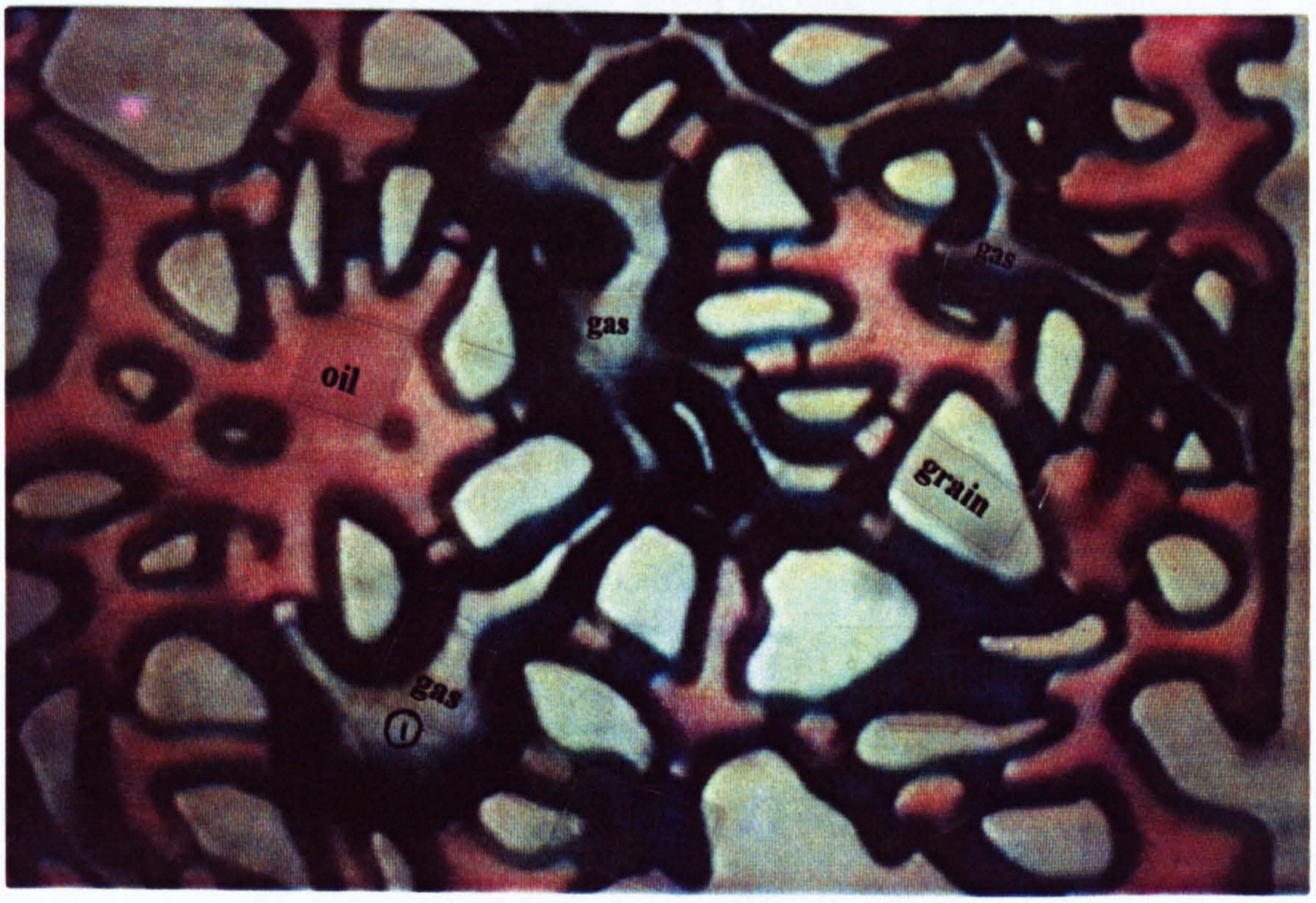

Figure 4.3-12b Gas advancement into a large pore (compare Figures a and b); A quick advancement of gas into a large pore (marked by 1) increases the gas volume thereby decreasing its pressure causing the gas to retreat in other locations (marked by 2, 3). Note the movement of water (by film flow process) at location 4.

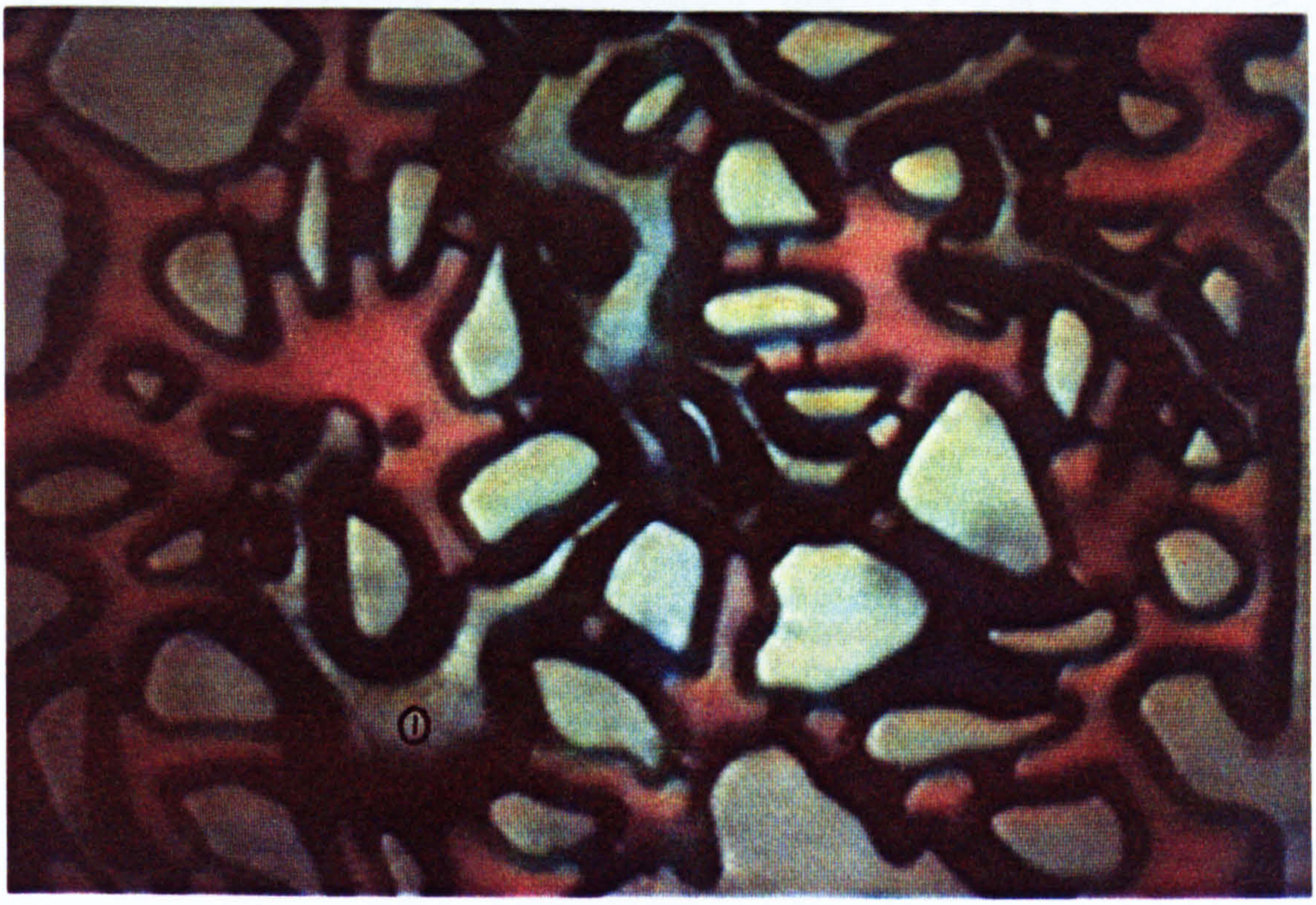

Figure 4.3-12c Upward movement of gas front; There is a thin layer of oil at the interface of gas and water due to the positive spreading coefficient of the system (compare a, b, and c).

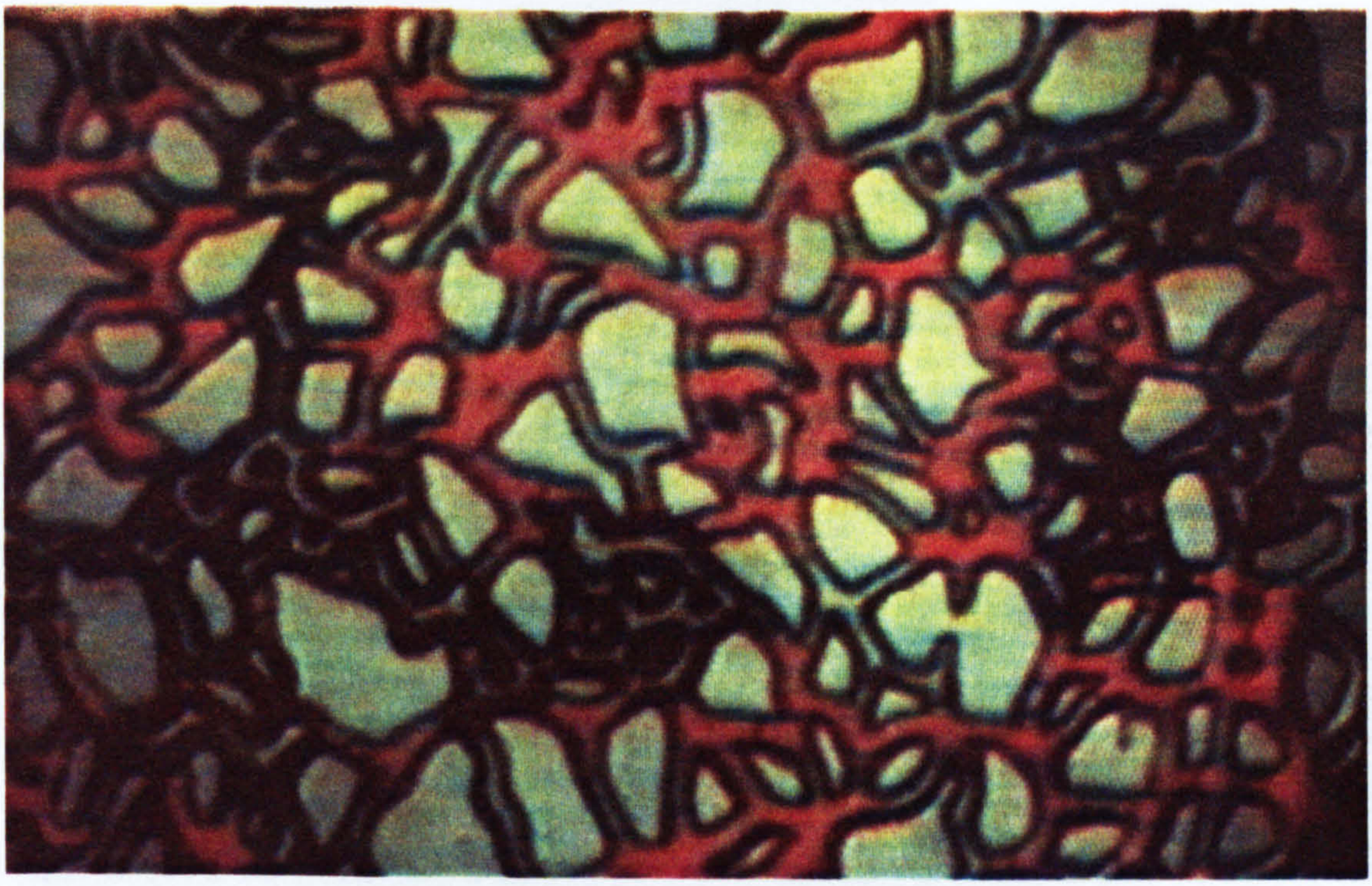

a: Gas, oil and water distribution at gas breakthrough time.

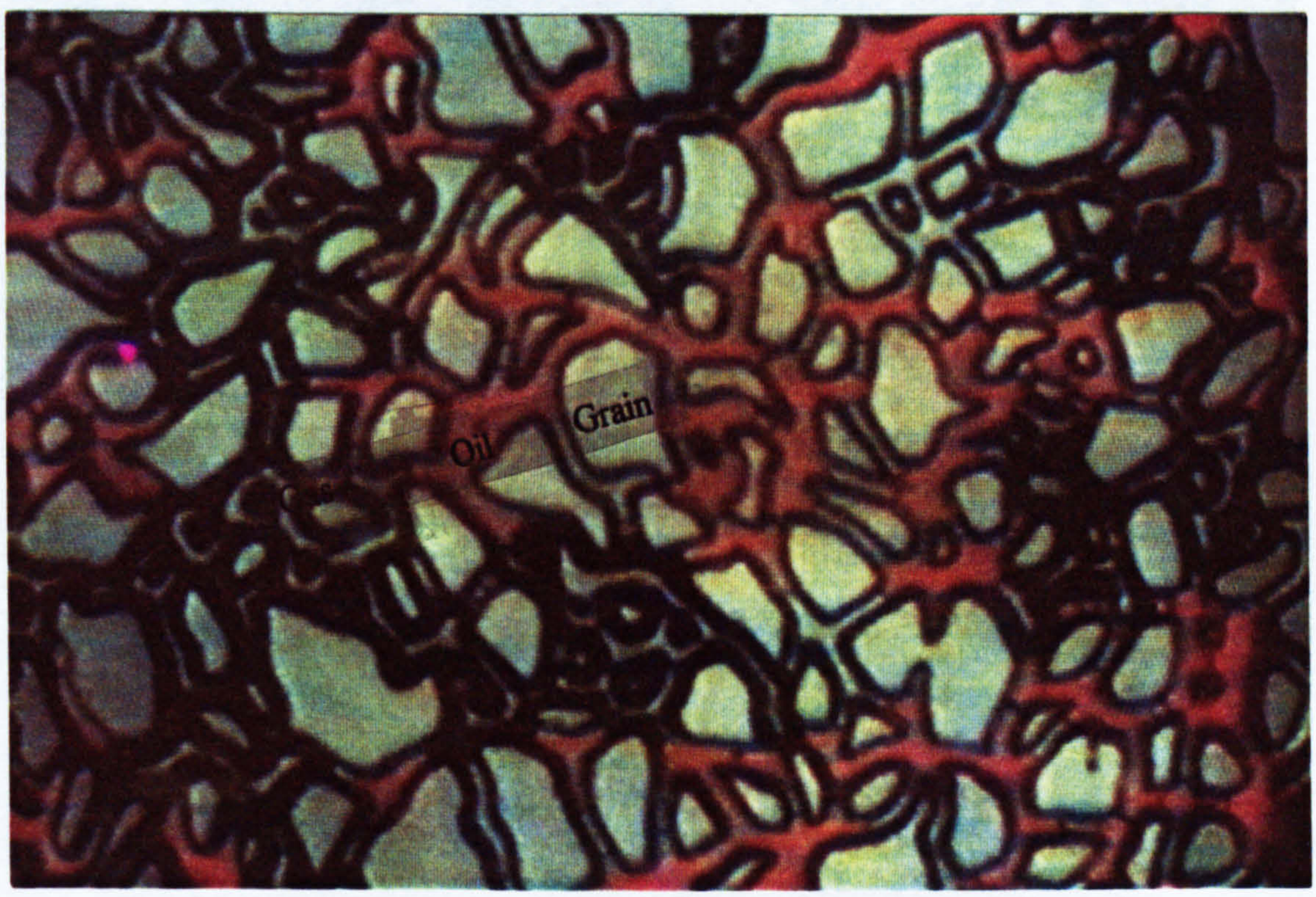

b: Gas, oil and water distribution, 48 hours after gas breakthrough time.

Figure 4.3-13 Photographs of experiment no. 16, negative spreading coefficient, no decrease in oil volume of oil slug at the upper part of RHS of the model.

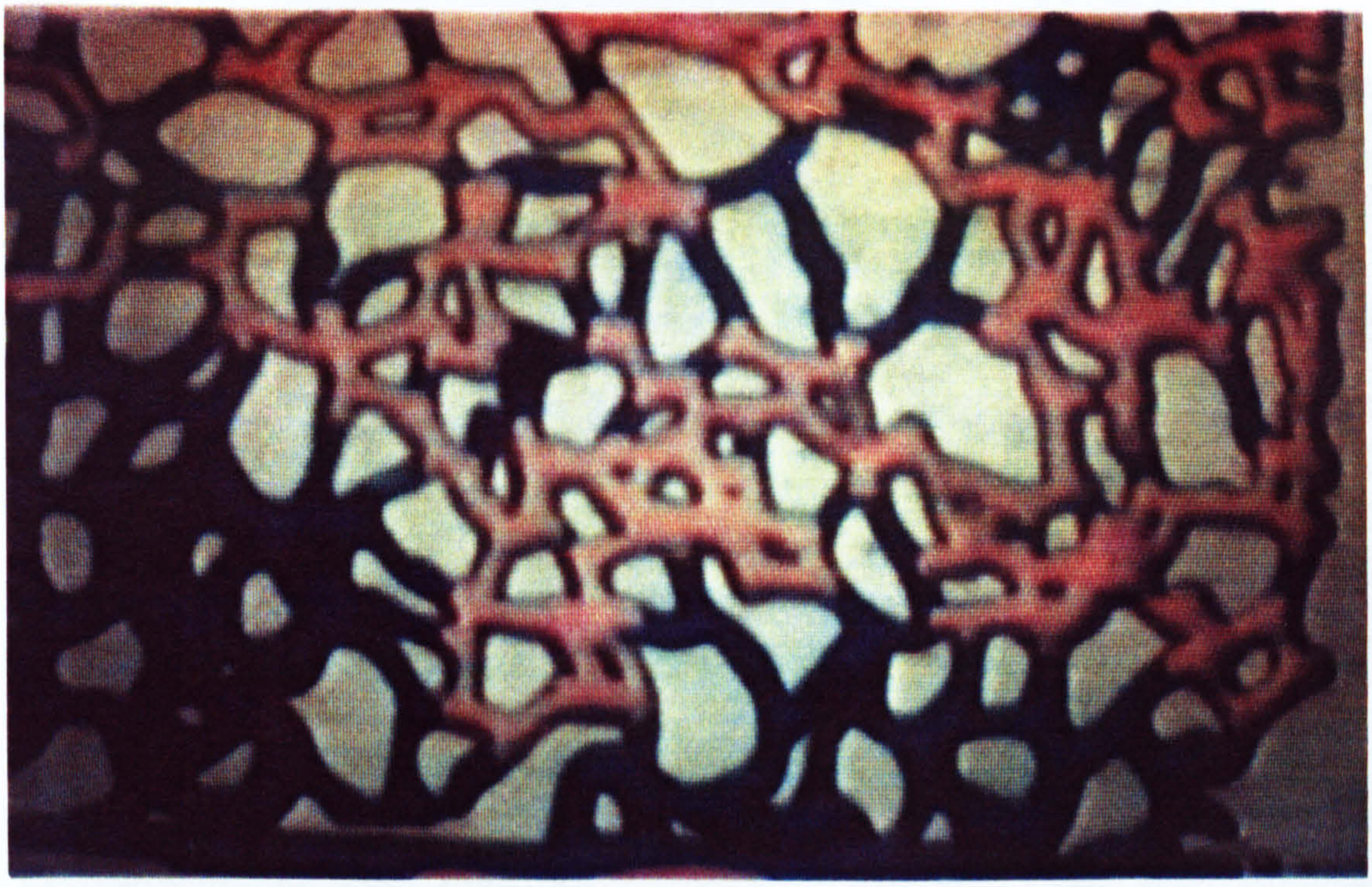

a: Gas, oil and water distribution at gas breakthrough time.

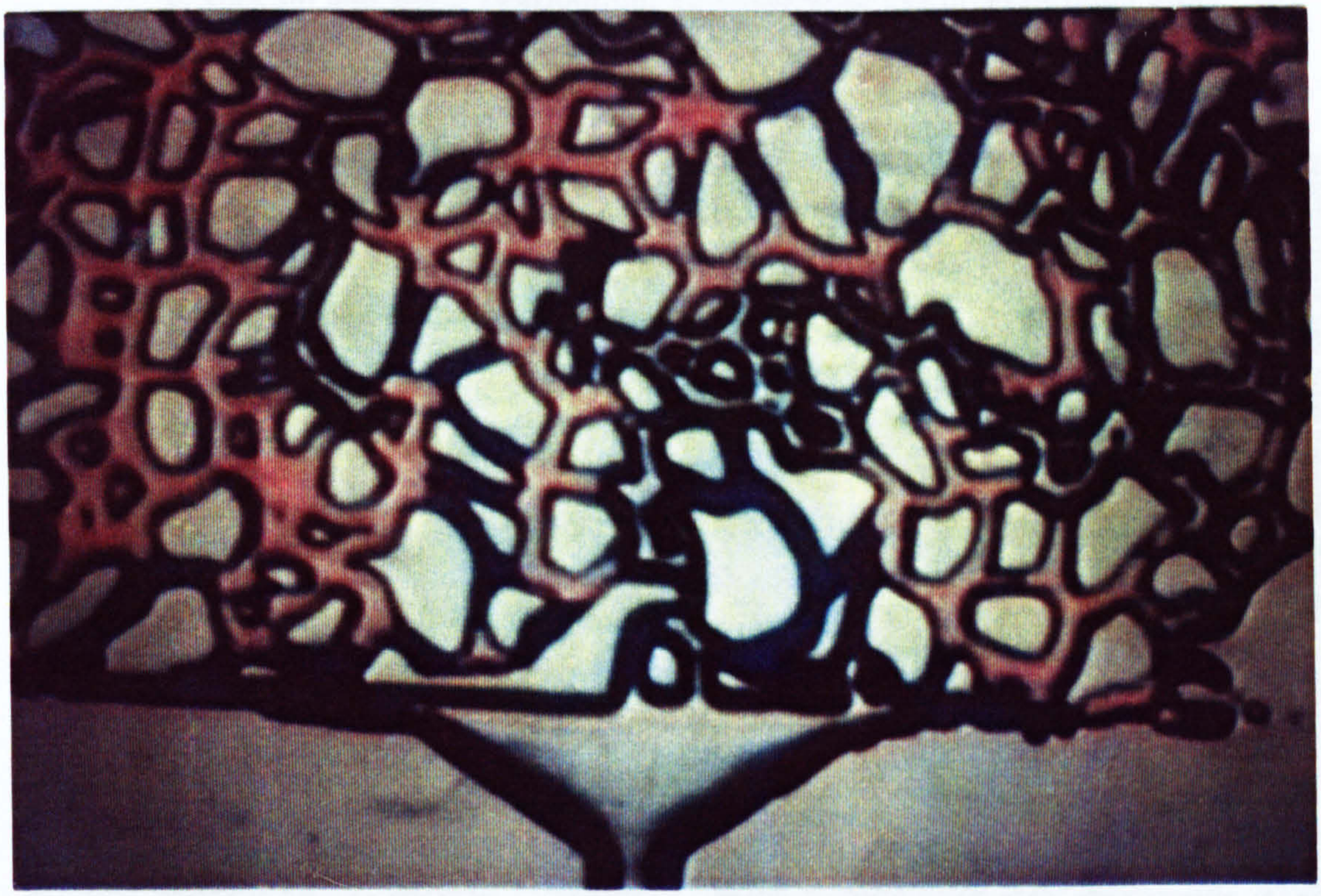

b: Gas, oil and water distribution, 1 hours after gas breakthrough time.

Figure 4.3-14 Photographs of experiment no. 4, positive spreading coefficient, reduction in oil volume of those slugs in contact with gas is due to film flow mechanism.

c: Gas, oil and water distribution, 12 hours after gas breakthrough time.

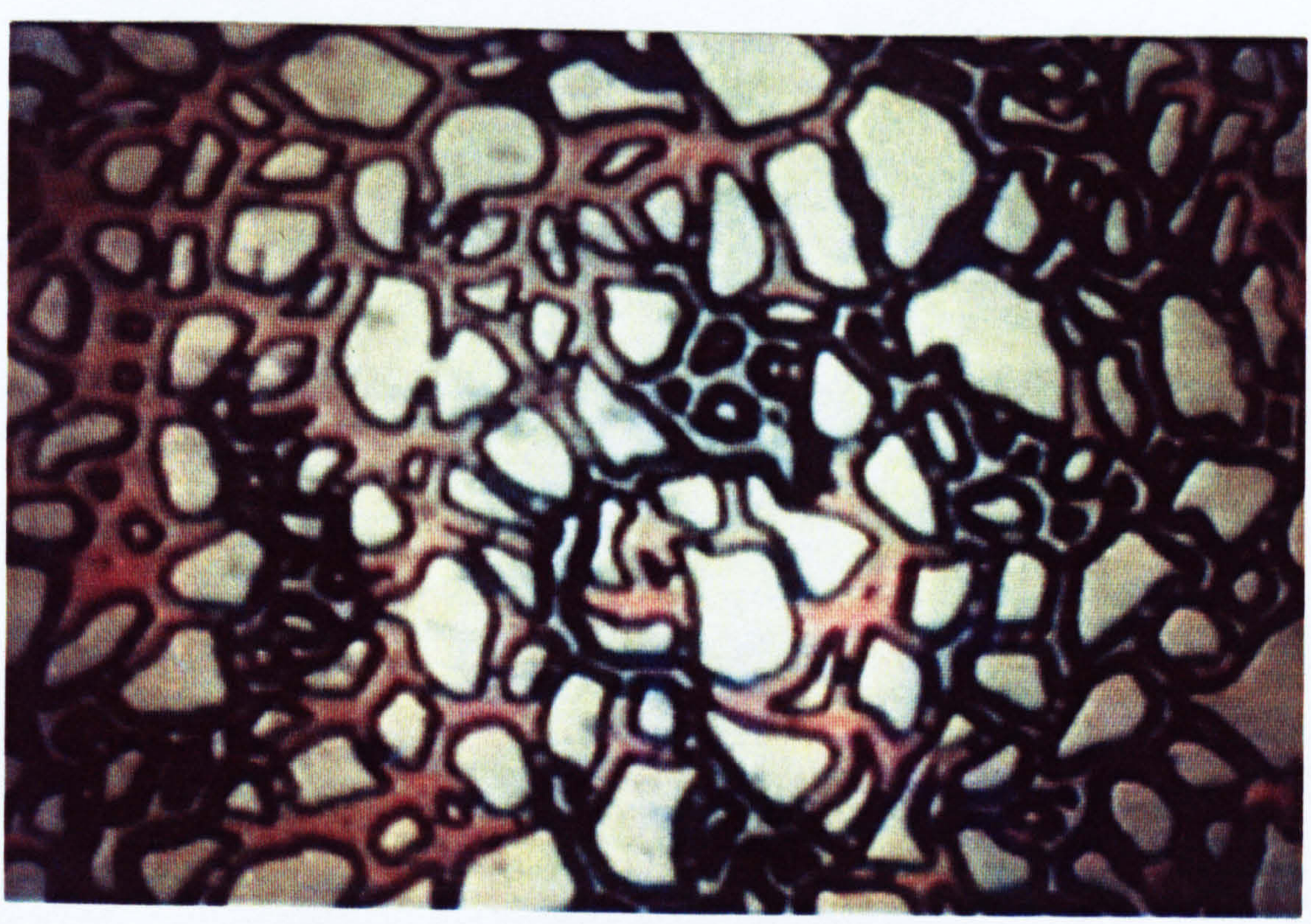

d: Gas, oil and water distribution, 18 hours after gas breakthrough time.

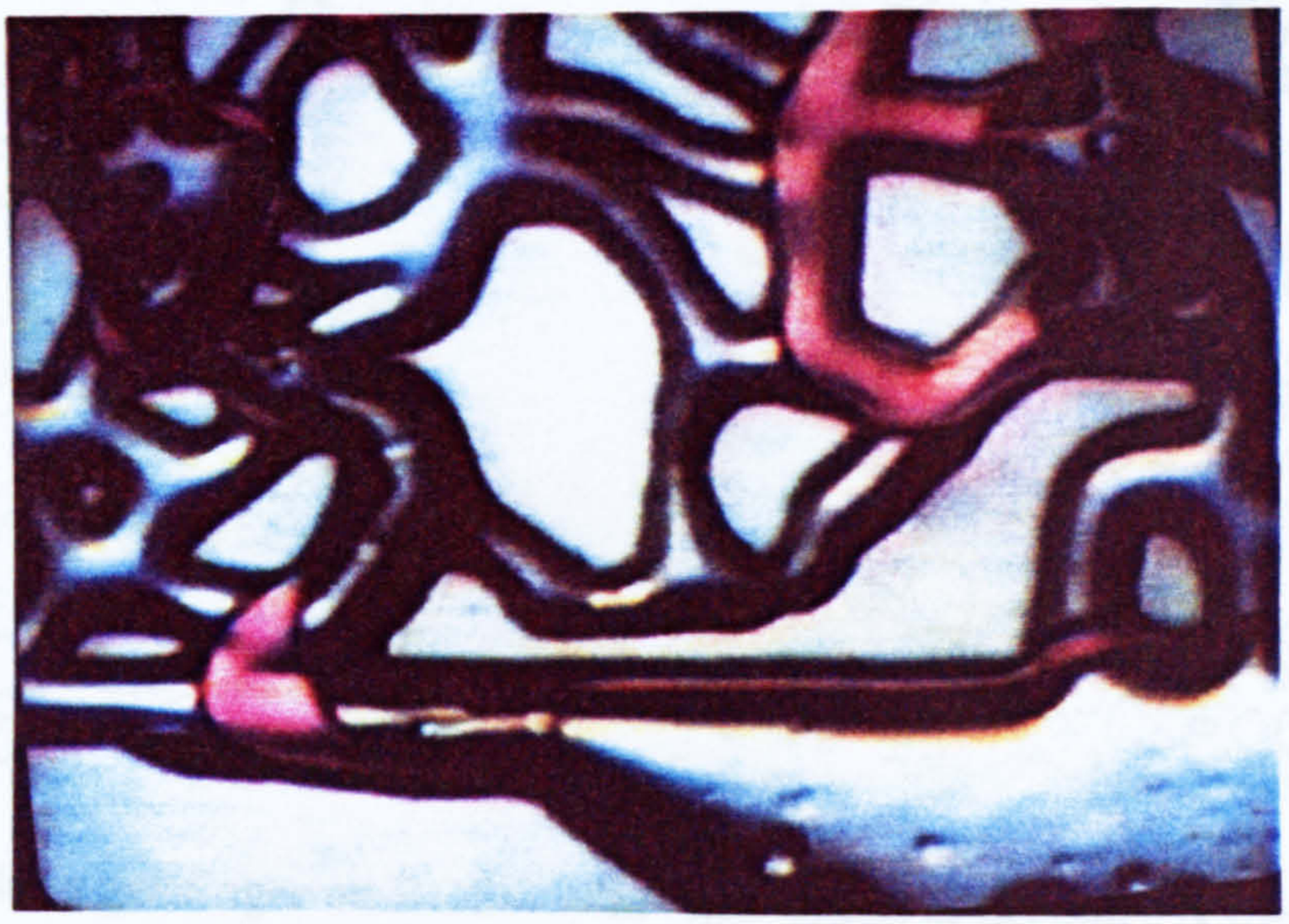

Figure 4.3-15 Oil drainage mechanism under film flow process

a: Progress of the long gas finger on RHS.

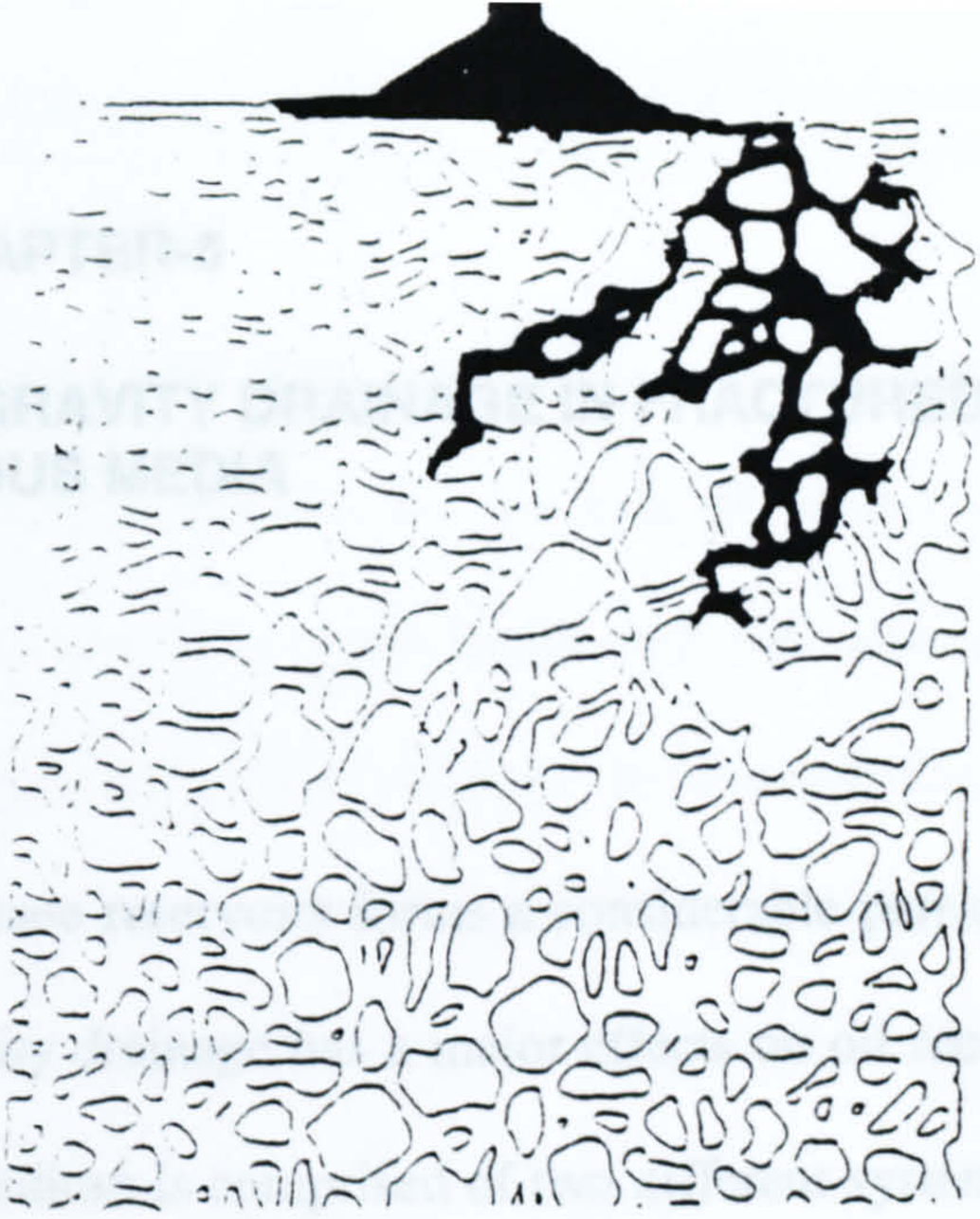

b: Increment of pressure is such that gas pressure on upper part of finger has overcome the capillary pressure of throats.

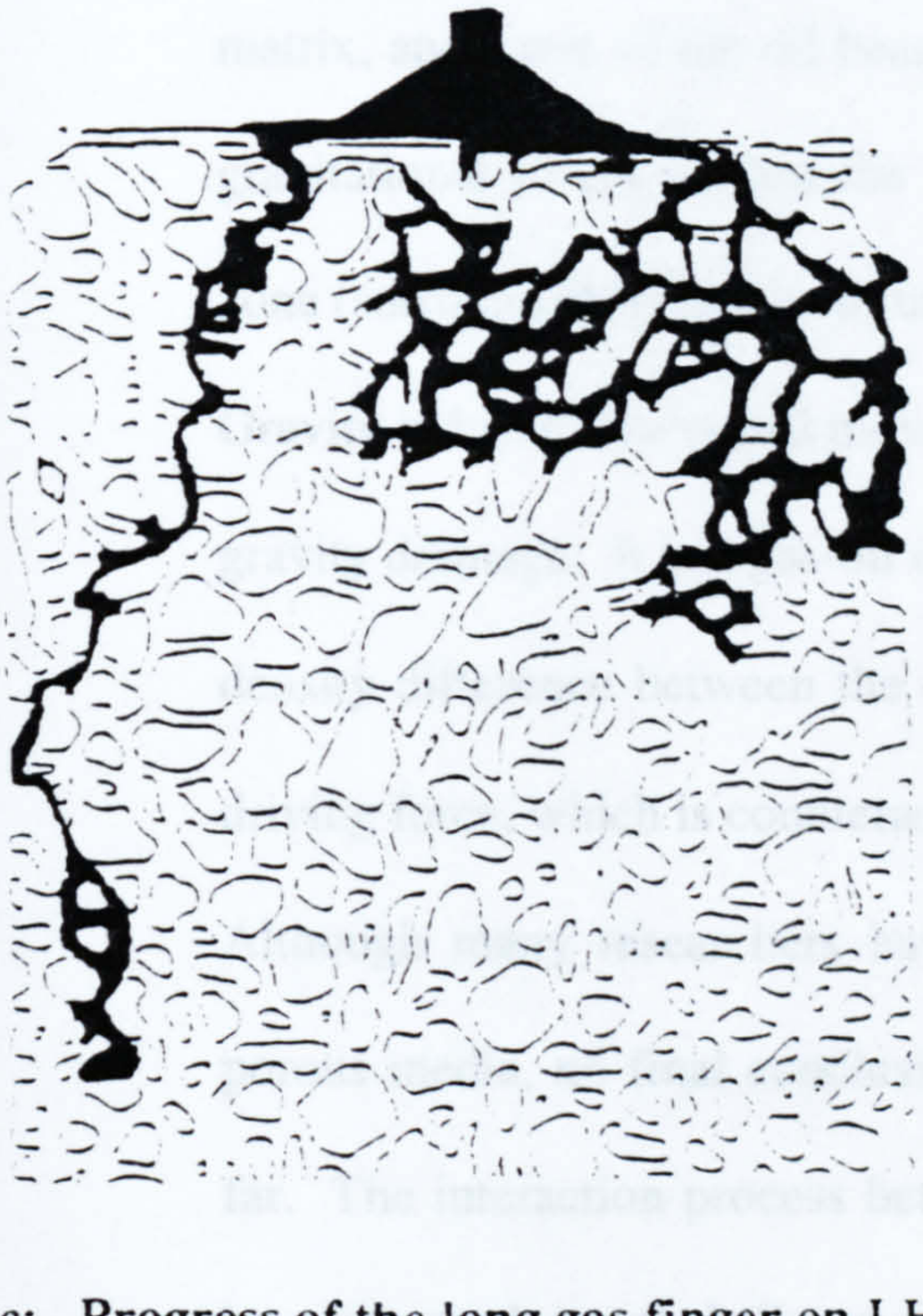

c: Progress of the long gas finger on LHS.

d: Increment of pressure is such that gas pressure has overcome capillary pressure of throats both on top and bottom of gas finger.

Figure 4.3-16 Gas progress mechanisms due to capillary and buoyancy forces.

CHAPTER-5

EXPERIMENTAL STUDIES OF GRAVITY DRAINAGE IN FRACTURED POROUS MEDIA

5.1 INTRODUCTION

Oil production from well fractured carbonate reservoirs forms a considerable part of the total oil production in the world and gravity drainage has a major effects on oil recovery in these reservoirs. A fractured porous medium is comprised of two different systems: 1- matrix porous media with high porosity and low permeability, and 2- fracture network with high permeability and low porosity. In a fractured reservoir, as production begins and reservoir pressure drops, the gas oil contact in the fracture descends below that in the matrix, and some of the oil bearing matrix blocks become surrounded by gas. When the gravitational forces exceed the capillary forces, those matrix blocks in the gas-invaded zone (surrounded by gas), will undergo a gravity drainage process.

Gravity induced downward movement of oil in the presence of gas has been referred to as gravity drainage. It is a gas-oil displacement in which gravity forces are dominating. The density difference between the oil in the matrix and the gas in the fracture is the main driving force, which is counteracted by the matrix capillary pressure.

Although many researchers have studied the process of gravity drainage in fractured porous media, no final conclusions have been reached on the physics of this process so far. The interaction process between blocks, and the role of fracture in gravity drainage have imposed a real challenge to researchers during the last thirty years.

The main issue in understanding the flow behaviour in fractured porous media is the block-to-block interaction, that is capillary continuity and infiltration. This chapter reports the results of the experiments in physical models and in core to investigate gravity drainage processes in fractured porous media.

5.1.1 Capillary Continuity

When blocks in a stack are completely isolated from each other, each of them will ultimately have its own capillary threshold height, but for the case of some capillary continuity, their ultimate recovery is like that of a single block with the same height. Although in real reservoirs, horizontal fractures are not frequent, most researchers have focused their attentions to such fractures. Based on the results of their simulation of fractured reservoirs Gilman and Kazemi (1988), mentioned that horizontal fractures would reduce recovery and cause capillary discontinuity between matrix blocks. Stones et al. (1992-A and 1992-B) argued that, since the permeability of the fracture has been shown to be much greater than that of the matrix, flow across the fracture probably does not limit the eventual recovery. They concluded, since observed liquid recoveries form fractured porous media are lower than those of comparable fully consolidated sands, fractures must change some fundamental aspects of flow. They also suggested that no general agreement had been reached on the actual physical processes involved and little experimental work had been presented.

In their simulation work, Quandalle et al. (1987) assumed zero fracture capillary pressure. However Firoozabadi (1992-A) emphasized that the Young-Laplace equation, $P_c = 2\sigma/b$ could be the framework for fracture capillary pressure. In 1993, he demonstrated that the capillary pressure contrast between the matrix medium and fracture medium had a pronounced adverse effect on the recovery performance. Since then, several other researchers have used the same concept, or some modified form of it, to represent the fracture capillary pressure. The weak point is that the Young-Laplace capillary pressure equation in the form of $P_c = 2\sigma/b$, is only applicable to the fluid flow parallel to the fracture surface. It is not valid for free gravity drainage where the flow is mostly perpendicular to the fracture surface.

The first attempt to identify the required conditions for establishing stable liquid bridges across a fracture, was done by Saidi (1987). He concluded that, if the fracture aperture is about 50 μm or more, capillary continuity between a stack of blocks can not be realized. Stones et al. (1992-A and 1992-B), illustrated that at some experimental conditions bridging did not appear to be a major factor in the eventual recovery. In 1994-C, Firoozabadi and his co-workers suggested that, if more fluid bridging were to occur across a horizontal fracture, one would expect more total flow to occur through the fracture. Therefore more ultimate recovery from a fracture set of rock having intergranular porosity is expected. Sajjadian et al. (1998-B) based on the results of their experimental work, concluded that there exists a critical fracture thickness for each set of physical conditions of the fracture system. When the fracture aperture is more than this critical value, there would be capillary discontinuity between blocks and the drainage takes place by formation and detachment drop process. In this case the pressure difference between gas and oil in a horizontal fracture (the fracture capillary pressure) is governed by the radius of curvature of the hanging drop.

When the fracture aperture is less than its critical value, the enlarging drops deform to liquid bridges connecting the upper and the lower blocks. For this case, the fracture capillary pressure can be calculated from the equation, "$P_{cf} = \Delta\rho.g.h$", in which h is the elevation of the horizontal fracture from the level of zero capillary pressure. They also emphasized that there exists a maximum capillary pressure for the liquid bridge, i.e. $P_{cl\text{-}max}$. When during descending of *GOC* in vertical fracture, the capillary pressure of the horizontal fracture exceeds $P_{cl\text{-}max}$, the liquid bridges will disintegrate and capillary continuity will shift to discontinuity.

5.1.2 Infiltration

In gas invaded zone, the oil leaving the upper block of a stack can penetrate through the top and side boundaries of the lower block (infiltration), thus delaying the drainage process of the lower block and/or causing resaturation when the lower block has already undergo some drainage process.

In 1979, Saidi et al. observed that when oil was trickledto a fully saturated block with a height of less than the capillary pressure rise, the oil preferred to travel through the matrix block instead of passing along the surface. Coats et al. (1989) have discussed the subject of infiltration by using fine grid simulation. In their study, the fractures between a stack of six blocks were assumed to be horizontal for one case, and in the later case, they were given an angle of 11 degrees with the horizontal plane. With sloped fractures between the matrix blocks, Coats' calculations show no infiltration. The results of our experimental work on infiltration processes (see Section 5.5) show that the infiltration is still active in a stack with an angle of 40 degrees with the horizontal plane.

Infiltration of the drained liquid from the upper block(s) to the lower block(s) is a key process which is often neglected (Firoozabadi 1994-A, B). As will be shown in Section 5.5, the main mechanism in the infiltration process is that the draining fluid develops an oil film over the block surfaces, which is surrounded by gas. Since the oil pressure is lower than the gas pressure by the amount of the capillary pressure, the oil film is imbibed into matrix rather than flowing through the vertical/inclined fracture.

In this chapter, some of the uncertainties about the block-to-block interaction, i.e. *capillary continuity* and *infiltration* will be discussed. In this work, four series of gravity drainage experiments were carried out to detailed the followings:

a- the flow pattern inside a matrix block, b- the effect of the horizontal fracture, c- the capillary continuity, d- the infiltration phenomenon.

The combination of experimental results revealed the physics of gravity drainage in a stack of blocks. The experiments were performed in a simple, but fully characterized systems. The main features of these tests are as follows:

1- Single and/or stack of two homogeneous blocks, 2- Artificially constructed porous and non-porous spacers, 3- Utilizing synthetic oil and air as test fluids, 4- Free gravity drainage at controlled room conditions.

5.2 PHYSICAL PROPERTIES

5.2.1 Physical Models

Gravity drainage experiments were conducted in sandstone cores, sand pack models, and glass beads pack models which are specified by '*L*', '*TS*', and '*G*'/'*GL*' respectively. The physical properties of different specimens are given in Tables 5.2-1, 5.2-2, and 5.2-3.

Table 5.2-1 Physical properties of cylindrical models.

Models	radius, cm	length, cm	Porosity %	Perm. (D)	t*-min	q* -cc/min calculated	Fluids
G-1 **	1.250	29.50	33.90	42.376	29.75	1.65	Oil 2/Air
G-4 **	1.250	29.50	33.5	42.635	29.22	1.66	Oil 2/Air
G-5 **	1.250	29.50	35.20	42.812	30.52	1.67	Oil 2/Air
GL-1**	2.000	20.00	35.56	19.278	46.52	1.92	Oil 2/Air
GL-2**	2.000	20.00	35.52	20.153	44.59	2.00	Oil 2/Air
G-6 **	2.170	58.090	32.40	26.562	241.48	1.15	Oil 1/Air
G-7 **	2.170	58.012	32.48	26.104	246.68	1.13	Oil 1/Air
TS	2.500	200.00	41.76	20.002	20.002	47.73	Water/Air

** Transparent models

Table 5.2-2 Physical properties of rectangular sandstone models.

Models	X -cm	Y - cm	Z -cm	Porosity, %	Perm. (mD)	t*-hrs	q* -cc/hr calculated	Fluids
L-3	3.311	2.953	33.5	22.12	741	22.29	3.450	Oil 2/Air
L-6	3.329	2.950	38.2	22.25	762	23.52	3.466	Oil 2/Air
L-13	3.925	2.377	33.5	22.60	753	21.197	3.345	Oil 2/Air
L-15	3.918	2.511	34.5	22.49	759	21.74	3.555	Oil 2/Air

To study the flow pattern inside a single block, the measurement should not disturb the flow of fluid and minimize the end effect. This requires that the system to be long enough, and with enough sampling points along its length. Sand pack model were packed with clean sand, while it was in vertical position and was shaken in the horizontal direction.

Packing of the glass-bead models were accomplished in the following manner: first, the model was set at an inclined position, and then, glass beads were introduced via the filling port. In order to ensure that the pack was tight and uniform as possible, the model-assembly was gently hammered during packing. Due to homogeneity and high permeability of the glass pack and sand pack models, the gravity drainage flow rate is rather fast, which reduces the gravity drainage experiments period. The sandstone models were cut from a homogeneous outcrop of rocks in rectangular shape. The results of the permeability measurement at different directions and locations by a minipermeameter indicated that the rock was isotropic.

To investigate the production behaviour from porous media, the introduction of reduced dimensionless quantities are very convenient. In gravity-drainage experiments the characteristic flow rate can be taken as the maximum initial flow rate (q^*) of a vertical block with open top and bottom faces and without capillary retention of the oil.

$$q^* = \Delta\rho_{og}.g.\,\mathrm{k}.\,\mathrm{A} \,/\, \mu_o \qquad (5.2\text{-}1)$$

where $\Delta\rho_{og}$, g, k, A, and μ_o are the density difference, the acceleration of gravity, the permeability, the cross-sectional area, and the oil viscosity, respectively.

The characteristic time (t^*), is defined as the required time to produce all initial oil in place with the maximum drainage rate.

$$t^* = \frac{\mu_o\ \phi\,(1-S_{wc})L}{k.\Delta\rho_{og}.g} \qquad (5.2\text{-}2)$$

A dimensionless time scale (t_D) is defined by dividing the actual time to the characteristic time as:

$$t_D = \frac{t}{t^*} \qquad (5.2\text{-}3)$$

where t^*, t_D, ϕ, S_{wc}, and L are the characteristic time, the dimensionless time, the porosity, the connate water saturation, and the length of the model, respectively.

5.2.2 Test Fluids

Although two immiscible liquid phases (oil and water) are present in reservoir, only a single liquid is used in any one of the experiments reported here. The liquids used were water and two synthetic i.e., oil-1 and oil-2. These liquids served as analogues for oil in a reservoir during displacement by air, which was used as gaseous phase. The physical properties of test fluids are given in Table 5.2-4. In transparent models, oil was identified by a red color (dyed by Sudun). Liquid viscosities and densities were determined with a Brookfield viscometer and a 'PAAR DMA 45' Digital Density meter, respectively.

5.2.3 Physical Properties of Models

The porosity of models was measured by the saturation method. A Ruska air permeameter and the Darcy's set up were used to measure the permeability of the sandstone samples and the packed models, respectively. These values were corrected to an absolute permeability by using the Klinkenberg correction. After the air permeablity measurements were completed, a vacuum was applied to the top of the core holder for a period of about 24 hours. Then oil was allowed to enter the model through the bottom port. The capillary pressure of sandstone samples (Figure 5.2-1) were measured by the mercury injection method. The oil relative permeabilities (Figure 5.2-2), were measured

experimentally by the unsteady state process. The capillary pressure and relative permeabilities of the pack models (glass beads and sand pack) were tuned by matching the recovery of free gravity drainage experimental data with the output of the simulation model. The results are shown in Table 5.2-5.

Table 5.2-3 Lithology specification of sandstone model.

Grain size	Medium sand, 0.1-0.5 mm
Cementation	Lose cemented
Type of cementation	Calcite, fair
Lithology	80-90%, Quartz + Chert
Sorting	Well sorting

Table 5.2-4 Physical properties of test fluids

Test Fluid	Density, gr/cc	Interfacial Tension, mN/m	Viscosity, cp
Air	$1.2*10^{-3}$	-------	0.018
Oil-1	0.857	36.00	17.00
Oil-2	0.842	30.50	6.20
Water	0.998	72.78	1.002

Table 5.2-5 Pseudo's relative permeability and capillary pressure of physical models, generated by matching the recovery data.

a- *Glass pack, block G1*

S_g	P_c *(atm)*	S_o	k_{ro}
0.000	0.0000	0.00	0.0000
0.126	0.0144	0.10	0.0000
0.252	0.1024	0.20	0.0001
0.378	0.3024	0.25	0.0016
0.504	0.5144	0.30	0.0081
0.630	0.5500	0.40	0.0250
0.720	0.6459	0.50	0.062
0.810	0.7144	0.60	0.1300
0.900	0.8019	0.70	0.2400
1.000	0.1597	0.80	0.4100
		0.90	0.6600
		1.00	1.0000

b- Sand pack model

S_g	P_c *(atm)*	S_o	k_{ro}
0.000	0.002	0.00	0.000
0.126	0.003	0.25	0.000
0.252	0.004	0.33	0.003
0.378	0.005	0.40	0.018
0.504	0.010	0.48	0.050
0.63	0.020	0.55	0.100
		0.63	0.180
		0.70	0.280
		0.78	0.410
		0.85	0.570
		0.93	0.770
		1.00	1.00

c- Glass pack, block GL2

S_g	P_c *(atm)*	S_o	k_{ro}
0.00	0.0107	0.00	0.0000
0.09	0.0120	0.10	0.0000
0.18	0.0126	0.19	0.00001
0.27	0.0154	0.28	0.00032
0.36	0.0178	0.37	0.00240
0.45	0.0223	0.46	0.01000
0.54	0.0267	0.55	0.03100
0.63	0.0407	0.64	0.08000
0.72	0.0437	0.73	0.17000
0.81	0.0467	0.82	0.33000
0.90	0.0707	0.91	0.59000
1.0	0.1597	1.00	1.00000

5.3 FLOW PATTERN INSIDE A SINGLE-BLOCK

5.3.1 Introduction

Immiscible displacement experiments have been performed by many researchers to study the two phase flow process and flow pattern under external viscous forces. Buckley and Leverett (1942) presented a theoretical analysis of immiscible liquid displacement based on the equation of continuity and the Darcy equation for viscous flow of each fluid. The theory applies to a linear displacement process involving two immiscible fluids with no mass transfer, taking place between them. The theory suggests that the fractional flow of each phase is solely a function of saturation. Terwilliger et al. (1951), obtained good agreement between the theory and the experimental data for the constant rate displacement of water by gas in a long vertical sand column. Rapoport et al. (1953) studied the immiscible displacement in the laboratory and showed that the recovery is related to a 'scaling factor' which included the product of length of the system, velocity of the fluid, and viscosity of the fluid. In 1954, Levine performed a series of experiments in a large core. He concluded that the calculated breakthrough recoveries using Buckley-Leverett fractional flow equation gave reasonable agreement with experimental values, if the capillary pressure and gravity terms were kept constant.

In order to obtain data for recognizing the displacement process inside a single block under free gravity drainage process, it was necessary to measure saturation distribution at successive time steps. A series of four experiments with the same initial conditions, but different duration, were performed (9, 32, 124, and 192 minutes). Saturation was measured by taking samples at different locations at the end of each experiment.

5.3.2 Experimental Set-up

A major difficulty with core studies is that capillary transition zones may be a foot to several feet in extent and it is difficult to obtain continuous core long enough to measure gravity drainage rates above the region of the transition zone. A schematic diagram of the flow system that was used in these experiments is shown in Figure 5.3-1. A cylindrical stainless steel core-holder, 200 cm long and 5 cm in inside diameter, was packed with clean sand (50-200 μm), while it was in a vertical position and was shaking horizontally.

Nine sampling points, about 6 mm in radius, were machined along the core holder at different heights (at 20, 34, 60, 79, 119.5, 141, 160, 186, and 195 cm from bottom). All sample points were closed by a screwing-cap, such that after fastening, the internal surface of the core holder was perfectly smooth. The location of each sample point had a 120° deviation from the previous point. By this pattern, sampling points were distributed in both the lateral and vertical directions. A cylindrical sampler with an outside radius of 0.5 cm and a length of 4 cm was used to collect sand samples through sampling locations. At the end of each run, the porous medium would be cleaned by pumping methylene chloride and acetone into the model. Finally, residual solvent, if any, would be removed by blowing nitrogen gas through the porous medium.

Four gravity drainage experiments were performed. The experiments were discontinued at 9, 32, 124 and 192 minutes, respectively. Nine sand samples (about 3.1 cc each), were taken from the sampling points, at the end of each experiment.

To measure the liquid volume, the difference between sample weight before and after cleaning, was divided by the liquid density. Then, the grain volume was calculated by dividing the weight of the cleaned grains by the grain density. In this series of experiments water and air (see Table 5.2-4) were used as oil and gas phases, respectively.

Also, for each run, a graduated cylinder on a digital balance (± 0.01mg precision) was used to collect the water draining from the model as a function of time. After each run, the sand was removed from the core holder and was cleaned, before it was put back and saturated for the next run.

Table 5.3 -1 Block specification for saturation distribution study.

Experiment no.	5.3-1	5.3-2	5.3-3	5.3-4
Duration of experiment	9-min.	32-min.	124-min.	192-min.
Type of model	Sand-packed			
Density of sand grain	2.60 gr/cc			
Block dimensions	L=200, D=5 cm			
Porosity	41.76 %			
Permeability	20.07 D			

Table 5.3-2 Oil saturation at specified time and location.

	Oil saturation %								
Sampling location (cm)	200.0	186.0	160.0	141.0	119.5	79.0	60.0	34.0	20.0
9-minute	33.5	43.0	49.0	50.4	100.0	100.0	100.0	100.0	100.0
32-min.	33.0	37.0	38.0	40.0	42.37	100.0	100.0	100.0	100.0
124-min.	32.5	34.4			38.6	40.0	44.0	100.0	100.0
192-min.	32.0	33.9			34.36	37.0	37.5		100.0

5.3.3 Analytical Solution

Hagoort (1980) introduced a complete mathematical model with exact boundary conditions which could predict the flow from a draining matrix with good accuracy. Even though drawbacks existed in experimental data and simplified assumptions in theory (Saidi 1987), the match between the experimental data and theory was shown to be reliable.

Let $k_o = k.S^n$, then, the variation of saturation with time and the recovery rate are given by:

$$\left(\frac{\Delta z_d}{\Delta t}\right)=\frac{\rho.\mathrm{g}}{\mu.\varphi}.\frac{\left[k\left(1-\frac{h_t}{L-z_d}\right)-k_d\right]}{\left(1-S_d\right)} \qquad (5.3\text{-}1)$$

$$R=\frac{z_d}{L}\left[\left(1-\frac{S_{or}.B_{or}}{S_{oi}.B_o}\right)-\frac{B_{oi}}{S_{oi}}\left(\frac{1-S_{or}}{B_o}\right).\left(\frac{n-1}{n}\right).\left(\frac{\mu.\varphi}{n.\rho.\mathrm{g}.k}\frac{z_d}{t}\right)^{\frac{1}{n-1}}\right] \qquad (5.3\text{-}2)$$

where $k_d=k.S_d{}^n$, $S_d=f^{-1}\left(\frac{z.\mu.\varphi}{\rho.\mathrm{g}.t}\right)$, z_d = the position of the demarcation (the boundary between the unsaturated and saturated regions), L = the column length, h_t = the minimum height to which the wetting phase (at 100 pct saturation) will drain, S_d = the saturation an infinitesimal distance above the demarcation, k = the permeability of the medium to the fluid at 100 pct saturation, B = oil formation volume factor and k_d = the permeability at the saturation just an infinitesimal distance above the demarcation.

For our test conditions ($B_o = B_{or} = 1$, and $S_{oi} = 1$), therefore, Equation (5.3-2) can be simplified as:

$$R=\frac{z_d}{L}(1-S_{or})\left[1-.\left(\frac{n-1}{n}\right).\left(\frac{\mu.\varphi}{n.\rho.\mathrm{g}.k}\frac{z_d}{t}\right)^{\frac{1}{n-1}}\right] \qquad (5.3\text{-}3)$$

5.3.4 Results

The maximum gravity drainage rate and the characteristic time for the process were calculated as 0.381 cc/sec, and 48.11 minutes, respectively. The oil saturation data at different locations and different times are given in Table 5.3-2. The results are compared with predictions based on presented theory. Results of the last experiment (t =192 minutes) are plotted on Figures 5.3-2*a* and 5.3-2*b*. The production data for the other three experiments perfectly coincide with the same curve, which indicates a good reproducibility of the experiments.

Figure 5.3-3 illustrates schematically the changing liquid distributions from a time $t = 0$ when the core is 100% liquid saturated to times $t = 9$, 32, 124 and 192 minutes. Liquid is

moving out through the base of the model by free gravity drainage while air was entering the top of the model. Air preferentially enters the larger conducting pathways as liquid drains and a liquid saturation gradient is established, which eventually becomes an equilibrium capillary transition zone when no more liquid can drain. This is shown schematically at time t = 192 in Figure 5.3-3 (the curves are drawn through the data points). The shape of the front movement at different stages of gravity drainage depend on parameters such as the densities, viscosities and surface tension of the fluids, the pore size distribution in the core and the wettability of the core. The comparison between calculated gravity drainage and the location of demarcation height (based on Equations 5.3-1, 5.3-2 and tuned value of n), with experimental data from sand pack model are shown in Figures 5.3-4 and 5.3-5.

5.3.5 Discussion

Two types of drainage processes are recognized; 1- gravity drainage of the main body of oil (movement of main gas-oil interface) where gravity acts as the main driving force, 2- gravity drainage of oil film. The final saturation profile in a porous medium under free gravity drainage process is governed by capillary/gravity equilibrium. At each point, the capillary pressure is balanced by gravity pressure at that point. At higher level S_w is less and radii of curvature, R_1 and R_2 are smaller than their values at lower levels. The mechanism of front movement as illustrated in Figure 5.3-3, indicates that generally the displacement process is the 'Buckley-Leverett' type. At the time of 124 minutes, the gas front is reached to the threshold pressure height of the model (20 cm), then, the drainage process is mainly governed by the film-flow process. The oil transmissibility through oil-film will decrease to such an extent that the production of remaining oil will take an extremely long time. The approximate agreement of theory and experiment shows that

gravity drainage velocities for the region above the transition zone can be estimated from vertical permeabilities and fluid properties as given by Equation 5.3-1. This is important because, whereas vertical permeability is a relatively easy property to measure experimentally, gravity drainage rates in the region above the transition zone require experiments in very long cores which generally are difficult to obtained or are unavailable.

5.4 EFFECT OF HORIZONTAL FRACTURE ON GRAVITY DRAINAGE

In this section, the effect of horizontal fracture on gravity drainage processes is examined. In this work, the fracture capillary pressure is discussed in detail, and a new concept about the fracture capillary pressure is presented. The experiments were performed in a pair of blocks separated vertically from each other by a horizontal fracture.

Several papers related to fracture capillary pressure have been published over the last two decades. Kazemi (1976), and Gilman et al. (1988), in their simulation work assumed P_{cf} $=0$. This assumption is appropriate, only if, the matrix block of a fractured petroleum reservoirs is assumed as discontinuous blocks. Other researchers, emphasized that the Young-Laplace capillary equation in the form of P_c as a function of σ/b, (where σ, and b are the interfacial tension, and fracture aperture, respectively), could be the frame work for fracture capillary pressure (Firoozabadi, 1994-B).

Once a hanging drop touches the top surface of the lower block, it will be deformed to a liquid bridge. Therefore, the critical value of fracture aperture (b_{cf}), may be defined as the maximum value of the fracture aperture that retains a stable liquid bridge. It is controlled by physical properties of fracture and fluids such as roughness, density difference of fluid phases and interfacial tension between gas and oil. In literature, there are some theoretical

and empirical expressions for estimating the maximum drop size. A drop which is a body of revolution about a vertical axis cannot be heavier than W_m (Freundlich, 1930), where,

$$W_m = 19\,\sigma^{1.5}\,(g.\Delta\rho_{gl})^{-0.5} \qquad (5.4\text{-}1)$$

W_m is expressed in N, σ in mN/m and $\Delta\rho_{gl}$ in gr/cc are weight of drop, the interfacial tension and density difference between liquid and gas, respectively. A drop does not fall, because its weight is too great for the interfacial tension to support it, it falls because the 'neck' becomes too long and narrow contracts to one or several drops. If *IFT* is low, the neck narrows faster. The number of secondary drops which follow the main drop depends on the size of the exposed pores and the magnitude of the interfacial tension. The formation of secondary small droplets (Figure 5.4-5) reflects the dynamic effects of surface, gravity and viscous forces.

To concentrate on the effect of horizontal fracture on free gravity drainage from top block, it is necessary to eliminate the influence of lower block. The results of our experimental work (see Section 5.7), show that when there is an interaction between two blocks, the capillary pressure of horizontal fracture is controlled by the height of the continuous oil path inside the lower block. To eliminate the block-to-block interaction effect in the following experimental work, a non-porous block and an oil filled container were used in case *1*, in case *2, respectively.* At the end of each run, the porous medium would be cleaned by pumping methylene chloride and acetone into the model. Finally, residual solvent, if any, would be removed by blowing nitrogen gas through the porous medium.

The details of experimental set-up and results are as follows:

5.4.1 Case-1, Block G1

Experimental Set-up

Cylindrical perspex core holder, have been constructed in which cylindrical blocks can be placed. The model can hold a stack of two blocks. The blocks are separated from the perspex walls of the model by means of pieces of metal wire in such a way as to create a fracture annulus of about 0.4 mm. A circuit for the fluids allowed the produced oil to be automatically replaced by the corresponding amount of gas. The production as a function of time could be detected both by volume and weight measurements. Four types of free gravity drainage (*FGD*) experiments were carried out with block *G1*, i.e. 1- Spacers in the fracture space between the blocks (Experiments 5.4-1a and 5.4-1b), 2- Fully open fracture (Experiment 5.4-2), 3- Direct contact between two blocks (Experiment 5.4-3), and 4- Direct contact between top block and the free oil surface (Experiment 5.4-4). The goal was to identify the effect of horizontal fracture on recovery from the upper block. The top block (*G1*) is a glass pack cylindrical model with high permeability (42 D) and high porosity (33.9 %), see Table 5.2-1. This model allowed taking photographs of the flow of fluid by using different colors for different fluids.

This medium is very homogeneous, and the high permeability gives a rather fast gravity drainage process. Due to narrow distribution of grain size (210-280 μm), the plateau of the gas front is flat. To eliminate the effect of the lower block, a non-porous metal block was used with the same dimension of the upper block. With fluids system which were used, the threshold pressure corresponded to a 7.20 cm height of liquid column. The block *G1* and the lower medium (impermeable block/oil container) were placed in a transparent cylindrical core holder filled with oil which had the boundary diameter which was 5-mm larger than the block *G1*.

Experiments started after draining all external oil from the fractures and dead volume inside the core-holder. The amount of drained oil collected in a graduated cylinder positioned below the core-holder on top of a high precession balance was recorded as a function of time to a precision of 0.001 gr. A schematic view of the experiment is shown in Figures 5.4-1 and 5.4-2, details of experiments are given in Table 5.4-1. To established the same initial condition after each experiment, the model was taken apart and was treated in such a way that the wettability became the same for all experiments and then the block was saturated with oil-1, (see Table 5.2-4). The maximum gravity drainage rate of the model was calculated to be equal to 1.64 cc/min.

Experiments 5.4-1*a* and *b*, were conducted by using four porous spacers (2 * 2 mm), each with a thickness of 2 mm, between two blocks, which provided a horizontal fracture with a 2 mm aperture. Experiment 5.4-1*b* is a duplicate of Experiment 5.4-1*a*, the reason for performing two experiments exactly at the same conditions was to investigate the repeatability of experiments, and to see the influence of experimental error on the recovery curve (see Figures 5.4-3*a* and *b*). The small difference between the recovery for these two duplicate experiments (i.e. 0.001 pv) shows the amount of uncertainty of the experimental results.

To provide a fully open fracture in the Experiment 5.4-2, the upper block was suspended by a hanger just 3 mm above the top surface of the lower block. In Experiment 5.4-3, block *G-1* was placed directly at the top of the non-porous block, and to ensure full contact, a heavy weight was put on the top of the upper block (see Figure 5.4-1 for apparatus schematic). In the last experiment (5.4-4) the gravity drainage was run with block *G1*, while its bottom surface touched the free oil surface in the container. The schematic diagram of experimental set-up is shown in Figure 5.4-2.

Table 5.4-1 List of experiments for Case-1 (Block-*G1*).

Experiments no.	Ultimate recovery (pv)	Fracture/Spacers	Duration (min)
5.4-1*a*	0.644	Four porous spacers (2 * 2 *2 mm)	2465
5.4-1*b*	0.643	Four porous spacers (2 * 2 *2 mm)	2465
5.4-2	0.637	Open fracture (3 mm)	2465
5.4-3	0.634	Direct contact with lower block	2480
5.4-4	0.631	Direct contact with liquid surface	2475

Results

The specifications and results of experiments are given in Table 5.4-1. To compare the different experiments, the oil production (fraction of pore volume) as a function of the dimensionless time (t_D) is plotted for each case (see Figures 5.4-4 *a* and *b*).

When four 2 mm thick spacers used between the blocks (Experiments 5.4-1 *a* and *b*), the produced oil volume and the drainage rate have their maximum values. While, when there is full contact between the upper block with the liquid surface (Experiment 5.4-4), the oil production and the flow rate have the minimum amounts. For the case of open fracture (Experiment 5.4-2), the amount of oil production is between these two extremes i.e., Experiments 5.4-1 and 5.4-4. These differences could be explained as follows:

1- Due to the existence of porous spacers, the fracture aperture is added to the effective block height which results in the highest value in oil recovery for Experiments 5.4-1*a* and 5.4-1*b*.

2- For the cases of direct contact (Experiment 5.4-4) the fracture capillary pressure may be assumed equal to zero. In this case the oil recovery is only controlled by the physical properties of the matrix block without any boundary effect from the fracture side.

3- When there are liquid bridges inside the horizontal fracture, some small pressure difference across the interface of liquid bridge (fracture capillary pressure) are present.

Although the capillary pressure inside the fracture is close to zero, but more probably it has positive capillary pressure at the bottom face of the block. This positive capillary pressure at the bottom surface acts as external force and results in some additional oil drainage from the upper block. In this case, the capillary pressure of the fracture, causes some reduction in the threshold height of the upper block.

The reduction in threshold height of the block with 2 mm porous spacers is equivalent to an external pressure equal to $\Delta\rho.g.b$ = 172 dyn/cm^2 or 0.0024 psi (b is fracture aperture). Since the drainage rate and the recovered oil volume for the 3 mm open fracture (liquid bridges inside the fracture) is less than those of 2 mm porous spacers, this indicates that the liquid bridges introduce some positive capillary pressure at the bottom face of the block is, which is less than 0.0024 psi.

5.4.2 Case-2, Block G4

Experimental set-up and results

To check the repeatability of the results from case 1, two gravity drainage Experiments 5.4-5 and 5.4-6 were carried out. The same kind of assembly and procedure as described earlier for Experiments 5.4-2, and 5.4-4 were used, but with block *G4* which is similar to block *G1* (see Table 5.2-1). In Experiment 5.4-5 block *G4* was initially saturated with oil-1, then it was suspended by a hanger such that a 3 mm open horizontal fracture formed between block *G4* and the liquid surface. To have a full contact (no horizontal fracture), an oil container was placed under the block, such that the bottom of block *G4* touched the free surface of the oil.

Table 5.4-2 List of experiments for Case-2 (Block-*G4*).

Experiments, no.	Ultimate recovery, (pv)	Fracture	Duration, (min.)
5.4-5	0.638	Open fracture (3 mm)	2938
5.4-6	0.634	Direct contact	2963

Results

The maximum drainage rate was calculated to be equal to 1.65 cc/min. The specifications of the experiments are given in Table 5.4-2. The production volume and the flow rate are plotted versus the dimensionless time in Figures 5.4-6*a* and *b*, respectively. From these figures, it can be concluded that the existence of a horizontal fracture has small effect on drainage performance of the upper block.

5.4.3 Theory

When there is a horizontal fracture at the bottom of the block, the experimental results show a small increase in ultimate recovery compared to the case of direct contact due to the fracture capillary pressure. That is, when the capillary pressure of fracture introduces a positive capillary pressure at the bottom face of the block, it acts as an external force and causes extra drainage of oil. Based on the fracture aperture, in the following two cases, an estimation of fracture capillary pressure are presented.

a- For the case that the fracture aperture is more than the critical value, $b > b_c$, the drainage is mostly by the formation and detachment of droplet. The fracture capillary pressure is equal to the capillary pressure of the liquid drop. Photographs of the initial formation of the drop and its later detachment are shown in Figures 5.4-5*a* and 5.4-5*b*, respectively. Assuming that the oil drop is part of a sphere, its capillary pressure is equal to:

$$P_{cf} = (P_c)_d = \frac{-2\sigma}{r} = -\Delta\rho \,.\, g.\, (r+d) \qquad (5.4\text{-}2)$$

where d is the distance between drop center and the bottom of the block (Figure 5.4-7), which varies between 0 to b_c-r. For a typical model, when $d \cong 2r$, the radius of curvature for the configuration shown in the Figure 5.4-7 can be calculated as:

$$r = \left(\frac{2\sigma}{3.\ \Delta\rho \,.\, g}\right)^{\frac{1}{2}} \qquad (5.4\text{-}3)$$

By assumption that the critical fracture aperture is twice the radius of the droplet, it is calculated as:

$$b_c = 2r = \left(\frac{8\sigma}{3\,\Delta\rho.\ g}\right)^{\frac{1}{2}} \qquad (5.4\text{-}4)$$

b- When $b < b_c$, the drained oil is transferred through liquid bridges. In this case by applying the Young-Laplace equation, the fracture capillary pressure is equal to:

$$P_c = \sigma\left(\frac{1}{r_1}+\frac{1}{r_2}\right) \qquad (5.4\text{-}5)$$

where r_1 and r_2 have opposite directions (sign). Considering that most probably, when $r_1 \cong -r_2$, the liquid bridge has some sharp curvatures, and at the same time P_{cf} is close to zero. In this situation the absolute value of the fracture capillary pressure (pressure difference between gas and oil) is less than the maximum value of the capillary pressure of the drop (just before detaching). Therefore, the absolute value of the fracture capillary pressure, without considering the influence of the lower block, is less than the capillary pressure of a stable hanging drop.

In actual reservoirs, when the fracture aperture is more than b_c, the effect of fracture capillary pressure on gravity drainage process from the upper block is negligible, and may be ignored. Therefore, for the case of hanging drop, most probably the amount of fracture

capillary pressure would be adjusted, such that the value of capillary pressure at the bottom of the block becomes close to zero (see Figure 5.4-8). When liquid bridge is present, the capillary pressure at the bottom of the block has a small positive amount which acts as an external pressure, and may causes a small amount of extra drainage, at the best.

5.4.4 Discussion

When oil is draining from a block into an open fracture, it tends to fill up the irregularly shaped and rough surfaces by spreading around the exit points. Then, initially, a relatively even oil film will be formed over the bottom surface of the block. For the case of a completely horizontal surface by accumulation of draining oil, the oil film becomes thicker, and later unstable, until it deforms at several points, and the excess oil is transferred through liquid bridges or by formation and detachment of droplets.

If the fracture is very narrow, the surface of lower block will easily make contact with this oil drop, before its detachment, and a liquid bridge between the two blocks is formed. This will provide a path for continuous flow of liquid from the top block into the lower one.

The absolute value of capillary pressure of the liquid bridge, which may be a positive or a negative value is much smaller than the capillary pressure of the oil drop, which is always a negative value. The radii of the curvature, have opposite signs and negative signs for liquid bridges and oil droplets, respectively. In both cases, the fracture capillary pressure at reservoir conditions is extremely low. For droplets with a radius of 0.16 cm (1/16 inch), and interfacial tension equal to 50 mN/m (50 dynes/cm), the capillary pressure might be in the range of 60 Pa (0.009 psi). In general the amount of fracture capillary

pressure has a negligible effect on the capillary pressure at the bottom face of the upper block. Therefore, when the lower block(s) is dead, although some capillary pressure are present across the gas/oil interface inside the fracture (fracture capillary pressure), its effect on the drainage of the upper block is negligible.

5.5 INFILTRATION IN FRACTURED POROUS MEDIA

The oil contained within the matrix of the gas invaded zone begins to drain down into the fracture system and into the lower matrix blocks, due to the force of gravity. Some of the oil that is drained out of the upper matrix blocks can infiltrate into the lower matrix block(s) from the top or side surfaces and can flow down through the areas of contact between block(s).

In the case of no infiltration (complete segregation in the fracture system), the gravity drainage rate for a column of N blocks approaches N times the single block rate. For full infiltration case, the gravity drainage rate approaches the flow rate of a single block whose height would be equal to the height of the column of all blocks above the fracture gas-oil contact, i.e. oil from top block would travel through all the blocks. In practice, the matrix blocks of the fractured reservoir are not all horizontal and are not isolated from each other. The contact areas between the blocks and the inclination of the blocks result in a different flow performance to that of a single block or a single column of isolated blocks. When oil is trickled at the top face or at the upper part of the side boundary of a desaturated block, this oil is imbibed into that block at a rate comparable with the maximum gravity drainage rate. Blocks in a stack that show this kind of interference will have a drainage performance as a function of time that differs considerably from that of a stack of isolated blocks. Generally all or part of the draining oil from the upper block(s)

infiltrate into the lower block(s) which causes a time delay in the recovery process. Once the oil saturation increases to the required value for steady state flow, the oil will pass through the block without any change in oil saturation, Sajjadian (1999).

In actual reservoirs, if the flow rate from the top blocks changes, the infiltration rate will also change, and it is unlikely that stabilized oil saturation and distribution will reach.

Literature Review

The scarcity of experimental data and difficulty encountered in obtaining such data, have made the theoretical approach to this process attractive. Although, much of the literature on infiltration is devoted to developing enhancement for modelling, still, no final conclusions have been reached on the physics of this process so far. Lefebvre du Prey (1978), in his study of drainage process across a stack of matrix blocks using a one dimensional numerical model, assumed that oil drained from an upper block is imbibed by the block underneath. Result of simulation across a stack of eight blocks (which were initially fully saturated) showed a considerable delay in production. Saidi (1979), studied the process of block to block flow within a column of matrix blocks that were not in contact with each other. They concluded that the recovery rate under this system was much slower than that of a group of independent single blocks. Saidi (1987), speculated that the infiltrated oil prefers to pass through the saturated block without displacing the original oil. Coats (1989), studied the subject of infiltration by using fine grid numerical simulation. The fractures between a stack of six matrix blocks were assumed to be horizontal for one case, and were given an angle of 11°, with the horizontal plane in another case. With sloped fractures between the matrix blocks, Coats calculations show no infiltration. Fung (1991), used new approach to incorporate infiltration in a dual-

porosity model. His mass balance equation included term(s) to represent the contribution of infiltration. In his calculation, the infiltration rate was controlled through a parameter "β", called fractional infiltration parameter. This parameter was apparently assumed to be independent of the fluid saturation within the blocks.

Theory

An estimate of the film thickness and volumetric flow rate of a draining film over the vertical surface of the lower block under influence of gravity is necessary for calculating the transmissibility of the vertical fracture. By assuming that oil film drainage is viscous, unidirectional (i.e. vertical), steady state, and ignoring the influenced of the infiltration process, the Navier-Stokes equations reduce to:

$$\frac{\partial}{\partial x}\left[\frac{\mu_o.\partial v}{\partial x}\right]=(\rho_o-\rho_g)(g) \qquad (5.5\text{-}1)$$

where ρ_o and ρ_g are oil and gas density, respectively.

For the boundary condition, $\partial v/\partial x = 0$ at $x = t_f$ (the film thickness), Equation 5.5-1 can be integrated to give Equation 5.5-2 for the point velocity in which the constant of integration is zero, $v = 0$ at $x = 0$.

$$v=\frac{\Delta\rho.g}{\mu}\left[\frac{x^2}{2}-x.t_f\right] \qquad (5.5\text{-}2)$$

The film thickness (t_f) in terms of the average velocity ($\bar{v}$), and volumetric flow rate per unit width of the film (q) can be obtained by integrating Equation 5.5-2:

$$t_f=\left(\frac{3\mu.\bar{v}}{\Delta\rho.g}\right)^{1/2} \qquad (5.5\text{-}3)$$

$$q=\frac{\Delta\rho.g.\,t_f^3}{3\mu} \qquad (5.5\text{-}4)$$

5.5.1 Experimental Work

Apparatus

The experiments were performed using a simple but well characterized system. Infiltration tests, by using synthetic oil and air as test fluids, were conducted at controlled room conditions. Peripheral accessory equipment consisted of a vacuum pump, saturation system, a low-rate syringe micro-pump (*SAGA* model 341*1B* syringe pump) which was used to inject oil, and a digital high precision (0.001 gr) balance interfaced to a computer for recording oil production. The models were placed in a transparent core holder. The amount of drained and trickled oil were recorded as a function of time. To have the same initial condition after each experiment, the model was taken apart and was treated in such a way that the wettability should be the same for all experiments. A schematic view of the experimental set up and block(s) position in infiltration experiments are shown in Figures 5.5.1*a*, and 5.5.1*b*, respectively.

Rock Properties

Three outcrop sandstone cores (identified here by *L6, L13*, and *L15*), and a glassbeads pack model (*G1*) were used as rock models in this study. The porosity of the models was measured by the saturation method. A Ruska air permeameter and the Darcy's set up were used to measure the permeability of the sandstone samples and the packed model, respectively. These values were corrected to an absolute permeability, using the Klinkenberg correction. The mercury injection method was applied to measure the capillary pressure of the sandstone models (see Figure 5.5-1), and their relative permeabilities were measured experimentally, by the unsteady state process (see Figure 5.5-2). The block (*G1*) is a cylindrical model with high permeability (42 D) and high porosity (33.9 %). Due to narrow distribution of grain size (210-280 μm), this medium is

very homogeneous. Physical properties of models, their characteristic time (T^*), and characteristic rate (q^*) are given in Tables 5.2-1 and 5.2-2.

Test Fluids

A Synthetic oil i.e. oil-2, was employed as oil (wetting phase), in all experiments. The physical properties of test fluids are given in Table 5.2-4. The trickled oil was identified by a red colour (dyed in Sudan red).

Experimental Set-up

Infiltration experiments were carried out with the following five types of the block(s) arrengment: 1-Saturated glass pack model (*G5*) in vertical position, 2- Desaturated sandstone model (*L6*) in vertical position, 3- Desaturated sandstone block (*L6*) tilted an angle of 40°, 4- Two saturated side-by-side sandstone blocks (*L13, L15*) with a vertical fracture between them, 5- Two saturated side-by-side sandstone blocks (*L13, L15*) tilted an angle of 20° with a fracture between them. The experiments were repeated three times and the average rates of the three runs were used to obtain the data for the graphs. Also, comparison between the results of the three runs shows a good repeatability of the experiments. The details of experiments are given in Table 5.5-1. At the end of each run, the porous medium would be cleaned by pumping methylene chloride and acetone into the model. Finally, residual solvent, if any, would be removed by blowing nitrogen gas through the porous medium.

Table 5.5-1 Specification of infiltration experiments.

Exp.	Block(s)	Initial sat, %	Position, (Tilt angle; degrees)	Trickled flow rate	Entry location
5.5-1	(G5)	100	Vertical, (0)	1.65 cc/min	Top surface of block
5.5-2	(L6)	94.08	Vertical, (0)	3.46 cc/hr	Top surface of block
5.5-3	(L6)	94.86	Inclined, (40)	2.7 (t < 322 min), 4.1 (t > 322 min) ;cc/hr	Top corner of block
5.5-4	(L13/L15)	100	Vertical, (0)	6.9 cc/hr	Top of vertical fracture
5.5-5	(L13/L15)	100	Side by side, (20)	6.9 cc/hr	Top of inclined fracture

5.5.2 Results

Case 1, Fully saturated block in vertical position

The infiltration test (Experiment 5.5-1) was performed on sample *G5*, while it was saturated with the colorless oil and in a vertical position. The red oil was trickled on its top surface at rate of 1.65 cc/min. Since the trickled rate was slightly less than the characteristic drainage rate of the block (q^* = 1.67 cc/min), a small portion of the top corner of the block had been desaturated. As shown in Figure 5.5-2, the cumulative drainage curve is slightly above the infiltration curve. At any time the cumulative desaturation volume is equal to the difference between total produced oil and total infiltrated oil. The drainage, infiltration and desaturation rates are plotted in Figure 5.5-3, which indicate that the infiltrating and draining oil have followed the same trend. There was no indication of trickled red-oil in the producing-oil before draining 93.5% of the initial oil in place from the block. The high amount of recovery of initial oil before breakthrough time revealed that the displacement mechanism in the infiltration process was mainly piston-type.

Case 2, Desaturated block in vertical position

In this case, after the block *L6* had been allowed to drain by gravity drainage process to an oil saturation equal to 94.08% with the flow of oil being stopped, oil was trickled on its top surface at a rate of 3.45 cc/hr (the characteristic gravity drainage rate was 3.45 cc/hr), while the block was in a vertical position. Drainage, infiltration, and accumulation/desaturation are the main oil flow processes, which concern infiltration into a desaturated block. Due to some hysteresis and redistribution of the fluids, it took almost four minutes, before the drainage began. Accumulation of the oil inside the block started from time zero with the highest rate equal to the trickled rate and then by starting drainage (with increasing rate) the accumulation rate decreased. Four periods can be identified from the graph of drainage and accumulation rate versus time (see Figures 5.5-4, and 5.5-5). In the first period (0-4 min) the accumulation rate is almost equal to the supplying rate, that is, all infiltrated oil is accumulated to increase the oil saturation to the required amount for starting drainage. In the second period (4-6 min) there is a sharp decrease in the accumulation rate due to a sharp increase in the drainage rate. In the next period (6-1336 min) the accumulation rate decreases gently. In the last period (after 1336 min), the accumulation rate decreases sharply to its minimum value while the drainage rate increases with the same slope to its maximum value.

Case 3, Inclined, desaturated block

The block *L6* was tilted (40°), and allowed to drain by free gravity drainage process to the oil saturation equal to 94.86 %. The oil was trickled at two different rates, less and more than the characteristic drainage rate of the block. During the first 278 minutes oil was trickled on the top edge of the block at a flow rate equal to 2.5 cc/hr, then the oil supply rate was increased to 4.1 cc/hr. In the second period of the experiment, the surplus oil

was drained as an oil film over the lower boundary (which was observed by reflection of light). The reported amount of drainage volume and rate includes the total oil production both by film flow over the boundary surface and drainage from inside the block (infiltration rate = 3.45 cc/hr, film flow rate over the block boundaries = 0.55 cc/hr). The gap between the oil drainage and oil infiltration curves (see Figure 5.5-6) is equal to the volume of accumulation oil inside the block. At the beginning of the infiltration process the oil saturation inside the block becomes unstable, and as time goes on, the oil accumulation rate decreases while the oil drainage rate increases (see Figure 5.5-7). As soon as the drainage rate becomes equal to the infiltration rate, there will be no further oil accumulation and the system becomes stable.

Case 4, Two side by side saturated blocks, in vertical position

In this set up, two saturated sandstone blocks (*L13* and *L15*) with a vertical fracture (1-mm aperture) between them were used. Red-oil was trickled directly on the top of the vertical fracture at a flow rate equal to 6.9 cc/hr, compared with the characteristic drainage rates of 3.345 and 3.555 cc/hr for blocks *L13* and *L15*, respectively. All of the inserting oil was infiltrated into the blocks and oil production was from the bottom surface of the two blocks. In spite of the high transmissibility of the vertical fracture compared to that of matrix block, since the pressure of oil inside the block is less than that of the oil in the surrounding fracture, trickled oil prefers to move through the matrix instead of the fracture. During the first 300 minutes, small amount of trickled oil was used for creating oil film and liquid bridges inside the fracture, which results a gap between the infiltration rate and the drainage rate. From time 300 minutes on, a steady state condition (i.e. drainage rate equal to infiltration rate) was achieved. Once the system

became stabilized, there was no significant change in the infiltration and the drainage process (see Figures 5.5-8 and 5.5-9, respectively).

Case 5, Two side by side inclined, saturated blocks

In this experiment, the set up was the same as that in the case 4, except that the whole system was rotated to make an inclination angle of 20 degrees from the vertical direction. The produced oil (colorless) from the bottom portion of the lower block was mainly from the initial oil in the block which was displaced by the trickled-oil (red color). In the first period of the test (0-100 min), small part of the trickled oil was used to create an oil film and liquid bridges inside the fracture (see Figures 5.5-10 and 5.5-11). Visual observation showed some desaturation in top corner of the upper block during first 100 minutes. The steady state condition was achieved after 100 minutes when the production and infiltration rates became equal.

5.5.3 Discussion

The required condition for the infiltration process is that the contact point of draining oil must be above the capillary hold-up zone. When geological conditions (along-dip and cross-dip barriers, flat and open fractures) are such that the wetted region is below the threshold height, since all pores are filled by wetting phase, there will be no capillary force for the infiltration process.

When the trickled-oil rate exceeds the characteristic drainage rate the difference will be flow downward over the block boundaries through the fracture system. Saidi (1987) speculated that the infiltrated oil prefers to pass through the saturated block without displacing the original oil. However, in all the experiments that were performed in this

work, it was observed that the initial oil is almost displaced by the supplying oil in a piston type process.

When oil is trickled at the top of a desaturated block, the saturation changes at the top, and oil is penetrated by film and/or bulk flow downward, and gradually the oil saturation, relative permeability, and drainage rate will increase. As long as the trickled oil rate is less than the characteristic drainage rate, after a transitional period, stabilized oil saturation and distribution is observed, again. In other words, the drainage rate will be equal to the infiltration rate i.e. steady state condition. The oil saturation in the block will increase only when the flow rate of the trickledoil is more than the drainage rate at that particular saturation. When the flow rate of trickled oil is equal to or more than the characteristic drainage rate, after some transitional period the block's saturation will reach to its maximum value i.e. $1\text{-}S_{gc}$.

The results obtained in cases 4 and 5, indicate that, if an oil film flows along the sides of the matrix block, the capillary pressure reduces to zero at the surface. Since the capillary pressure at the bottom of the block is also close to zero, the oil potential gradient causes sucking of oil into the matrix block. In other words, oil pressure inside the oil film becomes equal to gas pressure which is more than the local oil pressure inside the block by an amount of local capillary pressure at that elevation.

The oil leaving the upper block of a stack can penetrate through the top and side boundaries of the lower block. The infiltration process depends on the flow rate of trickled oil, and the saturation of the block.

In inclined cases, similar to the vertical ones, the trickled oil preferred to move through the porous media rather than slipped over the fracture surfaces. The inclination will result a reduction in effective height of the block by the amount of $H_b\,(1\text{-}\sin\theta)$, where θ is the angle of inclination. When the width of the inclined blocks is large enough, the upper

corner of the top block may undergo some drainage process. Therefore the volume of drained oil will be more than the volume of oil by the amount of desaturation at upper corner of the top block.

5.6 EFFECT OF CONTACT AREA ON FLOW RATE AND RECOVERY

Fractures may be partly filled with impermeable material with only a limited contact between the two blocks formed by some permeable media. A constriction factor is defined as the ratio of the flow rates with and without the constriction area. The main goal of this section is to investigate the effect of the contact area of two neighboring blocks on the oil production by the gravity drainage.

5.6.1 Experimental Set-up

Two series of gravity drainage experiments were performed: 1- Five central-contact experiments with different contact areas, 2- One dispersed opening with 20% contact area. A stack of two glass pack models (*G6*, and *G7*), saturated with oil-1 were used (see Tables 5.2-1, and 5.2-4). The initial conditions of all six experiments were the same, except for the area and position of contact regions (see Table 5.6-1). Experiments were performed in the stack of two blocks with 10% (Experiment 5.6-1), 20% (Experiments 5.6-2*a*, 5.6-2*b*), 30% (Experiment 5.6-3), 50% (Experiment 5.6-4), and 100% (Experiment 5.6-5) contact area between blocks, respectively. To evaluate the effect of opening location on oil recovery, the Experiments 5.6-2*a*, 5.6-2*b* have the same physical conditions and experimental procedures, except for the opening locations. In Experiment 5.6-2*a* the opening was at the center, while in Experiment 5.6-2*b* the opening was divided into four equal circles.

After specifying the location and area of the opening on the top surface of the lower block, a sealing wax was rubbed on the part of the surface outside the opening. At the end of each run, the porous medium would be cleaned by pumping methylene chloride and acetone into the model. Finally, residual solvent, if any, would be removed by blowing nitrogen gas through the porous medium.

Figure 5.6-1, shows the geometry and assembly of the stack-block, and the two different types of opening (i.e. central, and dispersed) are illustrated in Figure 5.6-2.

Table 5.6-1 Effect of direct contact area on gravity drainage recovery using blocks *G6* and *G7*.

Experiments	Area of contact region, (%)	Opening Location	Recovery (pv) , after t*/2	t*	506 t*
5.6-1	10	Center	0.167	0.269	0.639
5.6-2*a*	20	Center	0.184	0.358	0.642
5.6-2*b*	20	Dispersed	0.186	0.361	0.642
5.6-3	30	Center	0.201	0.374	0.643
5.6-4	50	Center	0.238	0.383	0.644
5.6-5	100	Center	0.289	0.406	0.647

t* : Characteristic time (=244 minutes)

5.6.2 Results

In Figures 5.6-3*a* and 5.6-3*b* the oil recovery as a function of time is shown for different degrees of contact area. The ultimate recovery is the same for all four experiments with a delay in production at intermediate period (during 0.1 t* - 10 t*), which increases by decreasing the contact area between the two blocks.

A comparison between the two recovery curves of Figures 5.6-4*a* and *b* indicates that for a 20% opening, flow restriction for the case of four openings is slightly less than that of a single (central) opening with the same total contact area. In general, from ultimate recovery point of view, even for very limited contact between matrix blocks (e.g. 10%),

the blocks behave like a single unit. As a consequence, in real reservoir conditions the effective block heights may be much larger than is predicted by geological evidences. Also, from the oil flow rate point of view, this indicates that the magnitude of the contact area is more important compared to its distribution or shape.

5.6.3 Discussion

For the free-fall gravity drainage rate of a dipping formation which is restricted at the bottom face, Dykstra (1978) suggested that the flow rate is less than the case were the entire face is open to flow. He defined the constriction coefficient as:

$$C = q_c/q_u \qquad (5.6\text{-}1)$$

where q_c, q_u, and C are the flow rate through the constricted block, the flow rate through the unconstricted block, and the constriction coefficient, respectively.

The above definition could not be applied in free gravity process from a porous medium, since the *FGD* flow rate of rock is a function of oil saturation. As the drainage is going on, the unconstricted block saturation decreases more sharply, and the ratio of two flow rates will change as a function of time. Therefore, based on the above definition, C may not be considered as a constant value for the entire period of gravity drainage. In addition, we could not match our experimental results with any constant value based on the above relationship between constricted and unconstricted cases. Further more, the existence of restriction had no effect on the ultimate recovery of the porous medium.

Since the main effect of constriction is to introduce some delaying time in production, it is recommended that the constriction coefficient to be defined as:

$$C = t_c/t_u \qquad (5.6\text{-}2)$$

where C, t_c, and t_u are a constant factor, the drainage duration of the constricted, and unconstricted cases, respectively. By fine tuning of C, it is possible to match the

production data of a restricted block from the data of the unrestricted case. A good match is observed between the experimental free gravity drainage data for both the restricted and unrestricted conditions, when the time scale of the latter case is multiplied by the constricted coefficient base on the Equation 5.6-2 (see Figure 5.6-5). To match the measured drainage rate of a stack with different contact areas, the time scale of drainage rate of full contact stack can be multiplied by the corresponding constriction coefficient.

The results of the first series of experiments illustrate that even for a limited contact area, the blocks behave like a continuous system (capillary continuity). For the conditions investigated so far only a slight influence of the constriction was observed on the ultimate recovery of the stack-block, due to the contact restriction, while there was a significant progressive delay in recovery as the contact area decreased. The gravity drainage rate is significantly influenced by the magnitude of the direct contact area between the two sandstone blocks (at least for our experimental conditions). The effect of capillary contacts across a natural fracture can be taken into account by modifying the matrix permeability. The results of the second series of experiments (Figures 5.6-4*a* and *b*) illustrate that oil recovery for the disperse contact is slightly more than the concentric contact. The difference is due to the fact that multiple contacts (for the case of 20 % opening) give rise to less flow restriction than a single contact with the same overall opening. In other words, less deviation of flow stream lines in the disperse case are present. Generally, the dispersed openings impose less restriction to flow compared to that of one opening with the same total contact area (opening).

5.7 CAPILLARY CONTINUITY

In a stack of oil saturated blocks which is surrounded by gas, the oil drained from the upper block(s) travels through all blocks under it by infiltration process and/or via the contact area. When there is capillary continuity, the ultimate recovery of a stack of *N* interacting blocks is like that of a single block with the same height. The presence of porous and/or liquid spacers between two blocks and oil film around the non-porous spacer results in the capillary continuity between the blocks. Because of the capillary continuity, the capillary hold up zone in the upper block will drain into the lower block until a new gravity/capillary equilibrium is achieved. Due to the capillary pressure gradients around the contact bridges, the contact region will form a preferential flow route for the oil. However the flow rate is reduced since the contact regions also acts as flow restrictions.

For the case of capillary discontinuity between blocks, each block will retains its own threshold oil zone, and the ultimate recovery of the system will be equal to the number of blocks times the ultimate recovery of a single block.

The goal of this section was to identify the main parameters that must be considered in capillary continuity between blocks.

5.7.1 Experimental Set-up

The main goal of performing these series of experiments was to identify the effect of type and thickness of spacers on capillary continuity between blocks and the gravity drainage performance. Scouting experiments were carried out on free gravity drainage of oil from stack block. In these experiments, the gas was in thermodynamic equilibrium with the oil inside the matrix. Cylindrical perspex core holder have been constructed in which

cylindrical blocks can be placed. The model can hold a stack of two blocks. The blocks are separated from the perspex walls of the model by means of pieces of metal wire in such a way that it creates a fracture annulus of about 0.4 mm. A circuit for the fluids allowed the produced oil to be automatically replaced by the corresponding amount of gas. Also the production as a function of time could be detected both by volume and weight measurements. The physical properties of the blocks and type of contact for each experiment are shown in Tables 5.2-2 and 5.7-1.

The stack-block experiments involved only two blocks. In the first set of experiments, two oil-saturated rectangular sandstone blocks (*L3 and L6*), one on top of the other, were used (Figure 5.7-1). In the second set of experiments, two transparent glass tubes filled with glass beads (*GL2 and GL1*) were used. The blocks were placed in a container of oil which had the boundary dimension which is 4-mm more than the stack-block (Figure 5.7-2). At the end of each run, the porous medium would be cleaned by pumping methylene chloride and acetone into the model. Finally, residual solvent, if any, would be removed by blowing nitrogen gas through the porous medium.

Table 5.7-1 Specifications of experiments for Case-1 (stack-block, *L3/L6*).

Exp.*	Ultimate recovery (pv)	Fracture/Spacers	Duration (min)
5.7-1	0.325	Direct full contact	31300
5.7-2	0.323	Four 2*2*0.5 mm, porous spacers	33201
5.7-3	0.322	Four 2*2*0.5 mm, metal spacers	33100
5.7-4	0.237	Four 2*2*2.6 mm, porous spacers	32130
5.7-5	0.225	Four 2*2*2.6 mm, metal spacers	32100

* stacked block *L3* and *L6*

Table 5.7-2 Specifications of experiments for Case-2, (*GL2/GL1*).

Experiments	Ultimate Recovery (pv)	Fracture/Spacers	Duration (min)
5.7-6	0.210	Two isolated blocks	12687
5.7-7	0.483	Direct full contact	6560
5.7-8	0.391	Four 2*2*5-mm porous spacers	10085

CASE 1, Stack of two sandstone blocks

A stack of two homogeneous cylindrical blocks (*L3 and L6*) with block heights equal to 33.5 cm and 38.2 cm were used. The sandstone rock used for these tests is from the outcrop, with medium permeability (0.75 D) and porosity (22%). The sandstone rock is homogeneous and the plateau of the capillary pressure curve (Figure 5.2-2) is approximately flat and ranges over a wide saturation zone. The threshold pressure at experimental conditions corresponds to a 30.35 cm height of oil column, which means a matrix block smaller than 30.35 cm does not give any recovery by gravity drainage. The average oil saturation behind the gas front (above the threshold height) is equal to 47.5%. The maximum gravity drainage rate of blocks was calculated as 3.46 cc/hr.

Five types of experiments were carried out: 1- Full direct contact between blocks; 2- Four 2*2 mm porous spacers, each with thickness 0.5 mm; 3- Four aluminium shims (2*2), each with a thickness of 0.5 mm; 4- Four 2*2 mm porous spacers, each with a thickness of 2.6 mm; 5- Four aluminium shims (2*2 mm), each with a thickness 2.6 mm; (Table 5.7-1). Initially both blocks were saturated with oil-2 (see Table 5.2-4 for properties of this oil), and all five tests were performed at room conditions. Fractures surrounding the matrix blocks were initially filled with oil, the rapid drainage of oil in vertical fractures left a thin layer of oil film over the vertical boundaries.

CASE 2: Stack of two glass-bead pack blocks

Three gravity drainage experiments were performed to study the influence of porous bridges on gravity drainage recovery. A stack of two homogeneous cylindrical blocks (*GL2 and GL1*), each block 20 cm height, were used. Two blocks used for this case were glass-pack, with a high permeability (20 D) and porosity (35.5%). The blocks were homogeneous, and the high permeability gave fast gravity drainage recovery. The plateau of equilibrium capillary pressure height was about 15 cm. The characteristic gravity drainage rate of blocks (neglecting the effect of threshold pressure) was calculated to be 2 cc/min. The transparent cylindrical boxes filled with glass beads, allows making photographs of the flow of fluid by giving the fluids different colors.

Three types of experiments were carried out; 1- Two isolated blocks, 2- Blocks in direct contact, 3- Four 2*2 mm porous spacers, each with a thickness 2.6 mm (Table 5.7-2). The ultimate oil recovery from direct contact, and two single blocks (twice of that from a single block) are two limits with full and without block-to-block interaction, respectively.

5.7.2 Results

CASE 1, Stack of two sandstone blocks

Experiment 5.7-1, Blocks in direct full contact

Figures 5.7-3 *a* and *b*, and 5.7-4 *a* and *b* show the cumulative oil production and flow rate data versus time respectively. During the time interval (0-30 min), the production rate is more than the calculated characteristic drainage rate (3.46 cc/hr). The film flow of the oil, which was initially over the boundary surfaces of the upper block, creates this difference. The rapid drainage of oil in vertical fractures prior to the test commencement left a thin layer of oil over the vertical boundaries of blocks. During the next time interval (30-300 min), the recovery rate decreased sharply from 4.01 to 0.37 cc/hr, indicating a transition

period from mainly the bulk flow to mainly film flow process. Finally, from time 300 min the slope of the flow rate curve with time becomes flatter, demonstrating that the front has reached to the threshold height and the drainage is mainly by film flow from the two phase region-transient period. At the end of the test (31300 min) the oil flow rate is 0.00175 cc/hr, and after this time, one can see that the production is still continuing by the film flow process. An increase of 0.02 gr was observed in the weight of receiver in the next 50 hours.

Experiment 5.7-2: Four 2*2 mm porous spacers, each with a thickness 0.5 mm

The ultimate recovery of this experiment is the same as that of Experiment 5.7-1. The results are shown in Figures 5.7-3 *a and b*, which shows that a good degree of capillary continuity between two blocks is present. The delay time in the production curve compared to that of full contact shows some restriction in oil transmissibility through the fracture. The reading of recovered oil was stopped at 960 hrs. Although it is not obvious on Figures 5.7-5*a* and *b*, the careful measurements showed that there was some flow of oil during time interval 537-960 hrs.

Experiment 5.7-3: Four aluminium shims (2*2 mm), each with a thickness 0.5 mm

The experimental procedure is the same as Experiment 5.7-2, but with non-porous spacers. There is a good match between the recovery curves of this experiment and Experiment 5.7-2 (see Figures 5.7-3*a* and *b*). Therefore, although the spacers are impermeable, the fracture aperture is small enough to form stable liquid bridges and capillary continuity. By the reduction in the overall transmissibility, the spacers will cause a delay time in production recovery compared to that of Experiment 5.7-2. However, oil transmissibility through the porous spacers has a smaller role in drainage process compared to that of liquid bridges.

Experiment 5.7-4: Four 2*2 mm porous spacers, each with a thickness 2.6 mm

The same set-up as Experiment 5.7-2 was used, while the thickness of the spacers was increased to 2.6-mm. The oil recovery severely slowed down as compared with Experiment 5.7-2 (see Figures 5.7-3*a* and *b*). The experiment was stopped arbitrarily at time 60.5 t* (i.e., after 9 days), at which the production was still going on at a small rate. The measured saturation at the end of the test indicated that for the lower block, the oil saturation was equal to the residual value, and due to negligible capillary continuity, the oil saturation in the upper block was only slightly less than its threshold value.

Experiment 5.7-5: Four aluminium shims (2*2 mm), each with a thickness 2.6 mm

The same assembly as Experiment 5.7-3 was used, but the thickness of spacers was changed from 0.5 to 2.6 mm. As expected the oil recovery of this experiment is the lowest compared to the other four tests of this series (see Figures 5.7-3*a* and *b*). Due to a high fracture aperture, liquid bridges can not be formed. The oil saturation of blocks, which is determined by balance between gravity and capillary forces in each block, at the end of the test is slightly less than the residual value. The experiment was stopped at time 150 t* (after 22.4 days), while oil was still flowing at a very small rate (0.007 cc/hr), see Figures 5.7-6*a* and *b*. The very small oil flow rate is attributed to the oil film around the metal spacers.

The oil film flow rate at the end of this test was about five times more than that of Experiment 5.7-3. This contrast was caused by the difference in the amount of oil saturation in the upper block. In this test, about 80% of the pore volume of the upper block was saturated by oil, and the only contact for oil flow from the upper block to the lower block was through the oil film around the spacers. However, at the end of Experiment 5.7-3, the oil saturation of the upper block was at its residual value.

CASE 2, Stack of two glass-bead pack blocks

The permeability and porosity of glass-bead pack models are considerably larger than those of the sandstone models. Therefore, the difference in recovery and flow rate of different runs can be distinguished in shorter times.

Experiment 5.7-6, Stack-block without block-to-block interaction

In the single block approach of gravity drainage, it is assumed that there is no interaction between blocks in a stack, and they act individually. For this hypothetical approach, which may be used only as a reference for comparison of more realistic conditions, the flow rate and ultimate recovery from a stack of *N* identical blocks is equal to *N* times the flow rate and recovery of one of the blocks. In actual cases, both in the field and laboratory, always there exists some block to block interaction (i.e., capillary continuity and/or infiltration). Therefore, it is impossible to simulate experimentally the condition of the no block-to-block effect by using a stack block. To get some idea about the performance of a stack of two blocks, based on the single block approach, the experiment was performed only by one block, then recovery and flow rate were multiplied by two. The data of produced oil and flow rate versus dimensionless time are shown in Figures 5.7-7*a* and *b*, and 5.7-8*a* and *b* with the ultimate recovery and film flow rate equal to 18.75 cc (0.210 pv), and 8E-5 cc/min, respectively. Therefore, for the stack of two blocks without block to block interaction the total expected oil recovery will be equal to 37.5 cc (0.210 pv).

Experiment 5.7-7, Blocks in direct full contact

The two blocks (*GL-1* and *GL-2*), were placed on top of one another. Due to the smooth surface of the blocks, there is a perfect contact everywhere between the blocks. In Figures 5.7-7*a* and *b*, and 5.7-9*a* and *b* the cumulative oil recovery and flow rate versus time are demonstrated. At time 127 t* the experiment was stopped, while production was still occurring (0.001 cc/min) due to the film flow process.

Experiment 5.7-8: Four 2mm * 2mm porous spacers, each with a thickness 2.6 mm

In this experiment, two blocks (*CL-1* and *GL-2*) are initially saturated with oil-1, and separated by four spacers (Table 5.7-2). In Figures 5.7-7*a* and *b*, the recovery as a function of time, for this experiment is compared with those of Experiments 5.7-6 and 5.7-7. The ultimate recovery of 5-mm porous spacers is more than that of the two blocks without block-to-block interaction (69.90 cc - 0.391 pv compared to 37.50 cc - 0.210 pv). While, its ultimate recovery is less than that of the full capillary continuity test (69.90 cc, 0.391 pv compared to 86.20 cc, 0.483 pv). Visual observation of the fracture space between the two blocks showed that, after 5 t* there was no stable liquid bridges between them. Therefore, the only conduit for oil drainage after that time were the four thick porous bridges. During the first 10 minutes, the gravity force is much more than the capillary force and there is no restriction from the fracture side on the drainage process (see Figures 5.7-10*a* and *b*). However as soon as the gas front in the top block reaches the height equal to its threshold height (15 cm), the difference in recovery process starts. In the full contact experiment (full capillary continuity), the stack of two blocks act as a single block with a height equal to that of the stack. The front continues to move down, until it reaches the threshold height of the lower block. There is a transition period from the time that the gas front reaches the threshold height of the lower block, until the equilibrium between capillary and gravity forces achieved.

For the case where the blocks are separated by thick porous spacers (i.e. more than 100 μm), the capillary continuity must be considered as ineffective. When the front reaches the threshold height of the upper block, the only available flow path for the draining oil is through the porous spacers. Therefore, the smaller the number and area of porous spacers, the smaller will be the transmissibility of the fracture and the flow rate. When

the contact area between blocks by porous spacers is small, it is more likely that the lower block undergoes drainage process, before the upper block is completely drained.

5.7.3 Discussion

When P_c and dP_c/dz are small, or when the effect of threshold height is negligible, the recovery curve versus time has a straight-line portion in the beginning. As soon as the effect of threshold pressure or fracture constriction becomes significant, the recovery curve changes its slope, and becomes steeper. In fact when compared to the block height, the threshold height is small, the end of the straight line corresponds to the time that the front reaches the bottom of the block. In cases that oil is draining from a stacked block, the recovery curve versus time shows an increasing ripple shape (Figure 5.7-10*b*). The starting time of each saddle illustrates the time that the next lower block starts to contribute in oil drainage process. Thus at any time, the number of shocks in the production curve is related to the number of blocks that were undergoing gravity drainage process.

The main parameter that must be considered in capillary continuity is the 'drainage duration'. By increasing the degree of capillary continuity between two blocks, the starting time of shifting from bulk-flow via the liquid and/or porous bridge, to film flow over and/or through the spacers will increase. In the case of two adjacent blocks having their outflow ends at the same level, side by side capillary contact has no effect on their drainage performance.

When oil is drained from a block into the open fracture, it tends to fill up the irregularly shaped surface and roughness by spreading around the exit point ($P_c = 0$). Then, a flat oil film is formed over the bottom surface of the block. For a completely horizontal surface, the accumulation of draining oil results in a thicker and unstable oil film which deforms at

several points. If the fracture is narrow, the surface of adjacent blocks will easily make contact with this oil film, and some stable liquid bridges between the two blocks are formed. From this time, the additional oil transfers mainly through the liquid bridges. For the case of wide fractures the draining oil will transfer by a formation and detachment of drop process and/or through unstable liquid bridges. As the oil production rate from the upper block decreases due to capillary retention and decrease in relative permeability, the average oil saturation within the fracture decreases which results in thinner film and/or a rupture in the unstable liquid bridges (for the case of thick fracture).

For the case of non-capillary contact between the blocks (wide fracture, water wet rock, and negative spreading coefficient), the total amount of ultimate recovery will be equal to the number of blocks times the ultimate recovery of a single block. For full capillary continuity between blocks, the performance of a stack block is similar to a single block with the same height.

In actual reservoir condition, the influence of overburden pressure, precipitation of asphaltene, and erosion between two neighboring blocks all may produce discontinuity between blocks. Therefore, experimental results by physical models, without considering geological conditions of the formations, can not be directly applied to the field conditions. As an example, Haft Kel field (IRAN) is a well fractured reservoir, with a formation thickness of about 900 ft and a gas invaded zone of 1000 ft. The past 70 years performance of this reservoir shows that oil gravity drainage from blocks of about 10 ft height is about 26% (which is dictated by capillary pressure of single block). In general, some degree of vertical continuity (i.e., ineffective) certainly exist in fractured reservoirs. But, if an effective capillary continuity in Haft Kel exists, a gas displacement efficiency of over 50% should have been considered during its depletion period (first 50 years).

5.8 CONCLUSION

The results of the experiments with sand pack physical models confirm that the displacement process is the Buckley-Leverett type. The theoretically derived gravity drainage equations by Hagoort (1980) for a single block matches very well with the experimental results, and can be successfully used in predicting gravity drainage performance in a single block.

The main goal of using a dead lower block in a stack of two blocks in Section 5.4 was to isolate the horizontal fracture. The experimental results reveals that there exists a critical fracture aperture (b_c) for each set of physical conditions of the fracture system. When the fracture aperture is more than b_c, the drainage takes place by the formation and detachment drop process. In this case the pressure difference between oil and gas in the horizontal fracture (the fracture capillary pressure) is governed by the radius of curvature of the hanging drop. The hanging drop has two effects on the drainage performance of the upper block, by its length and by its capillary pressure. The combination of these two effects, which have different signs, result to a very small capillary pressure value at the bottom surface of the upper block.

When the fracture aperture is less than its critical value, the enlarging drops deforms to some stable liquid bridges between upper and lower blocks. Since the lower block is dead, a continuous oil column inside the lower block does not exist, and the level of, P_c = 0, is at the top surface of the lower block. The capillary pressure of these liquid bridges can be calculated from radii of curvatures of liquid bridge and is expected to be close to zero. Existence of liquid bridges may induces some positive capillary pressure at the bottom surface of the upper block. Which may be considered as fracture capillary pressures that acts as an external force and has a positive effect on gravity drainage

performance from the upper matrix block. However, fracture capillary pressure, both for liquid bridge and hanging drop, are considered to be close to zero and or negligible.

The block-to-block interaction in a stack block consists of two phenomena, capillary continuity and infiltration. The infiltration process is active, when the wetted position is above the threshold height of the block. When oil is trickled at the top of a vertical/inclined fracture, initially, it extends as a film over the wall surface before being imbibed in the rock. The liquid film flows through the matrix rather than the open tilted or vertical fracture. The liquid infiltration into a block is due to the gas/oil pressure difference, and local capillary pressure. As long as, over the block boundary the liquid film is covered by the gas phase, it is forced to flow through the matrix block. The effect of saturation changes at the top of the block due to infiltration is extended by film and/or bulk flow to lower parts of the block, and gradually the oil saturation, relative permeability, and drainage rate of the lower block are increased. When the block is initially saturated, if the rate of the trickled oil is more than the maximum drainage rate of the block (i.e. $q_{o\text{-}max}$), the infiltration rate will be equal to $q_{o\text{-}max}$. The surplus will pass over the lower block via the fracture system and the block remains fully saturated. When the rate of trickled oil is less than $q_{o\text{-}max}$, all of it is infiltrate into the block, and the production from the block consists of the infiltrated oil from its top surface plus its own drainage. When the block has already been desaturated partly or totally, depending on the constant oil supply rate and the initial oil saturation of the block, there is a transition period, before achieving a pseudo steady state condition. During this transition period, the saturation and oil distribution inside the block will be adjusted until the system is stabilized. When the system is stabilized, there is no further changes in the oil saturation and the fluid distribution in the block remain constant, while the infiltration and drainage rate are equal. In all of the performed infiltration experiments, when the rate of the trickled oil

was less than that of $q_{o\text{-}max}$, the trickled oil preferred to move through the matrix due to the capillary force instead of flowing through highly transmissible fractures. In a stack of two blocks, when the gas front passes from the horizontal fracture, the supply oil from above block(s) toward horizontal fracture is smaller than infiltration in the downward direction. The liquid bridges between these blocks start to reduce in number and volume. By progressing of the process, the oil saturation inside the horizontal fracture decreases i.e., initially large liquid bridges gradually reduced in size and subsequently, the number of smaller bridges decreased.

At reservoir conditions, asphaltene precipitation, scale deposition and strong erosion are responsible for reduction in contact area (opening) between the two neighboring blocks to a fraction of available surface area. As long as the contact area is such that there is a capillary continuity between upper and lower blocks, the ultimate recovery is similar to a single block with the same total height, but with a delay time. There is a non-linear relationship between the gravity drainage rate and the contact area between the two blocks. To match the measured drainage rate of a stack with different contact areas, the time scale of drainage rate of full contact stack must be multiplied by a factor, inverse of this multiplier may be called the constriction factor. For each stack block system, there is a lower limit value for the contact area, beyond which the transmissibility of the oil will be so low that production takes an unacceptable long period.

There are three distinct periods in the gravity drainage from a block in a stack: 1- From the starting desaturation until the gas front reaches the threshold height, 2- A transition period during which the oil flow process inside the block changes from mainly bulk-flow to completely film-flow, 3- In the last period the drainage process is mainly film flow, and ends by gravity-capillary equilibrium.

The horizontal fracture has no effect on the amount of the draining oil during the first period of drainage, and gravity force will determine the oil recovery. The only effect of capillary continuity on the drainage process in the first period is on the duration of the bulk flow rate which gradually decreases to zero at the gravity-capillary equilibrium. Also, at the end of gravity drainage process, the oil saturation inside the upper block for the capillary continuity case is less than that of the capillary discontinuity. Therefore, the main effect of capillary continuity is on drainage of the oil which could be retained in the upper block due to the capillary discontinuity.

As long as the geological and petrophysical information is limited, it is difficult to estimate some overall degree of block-to-block interaction for an actual reservoir. If an out-flow face of top block and the adjacent face of the lower block is open to flow (no asphaltene and scale deposition over them, and no strong erosion), always some degree of capillary continuity between blocks exists. This capillary continuity help to drain the oil from the threshold zone of the upper block, but the rate of drainage depends on the transmissibility of the contact points, porous and liquid bridges, and oil film around the solid spacers.

In actual reservoirs, when the area of contact of porous spacers are small, due to a high over burden pressure, not only the spacers, but also the region around each spacer may undergo extreme reduction in permeability. Therefore, the local transmissibility of drainage oil toward solid spacer becomes negligible.

When the fracture aperture is high, the oil will drain mainly by film flow process. The film flow process over the non-porous spacers cannot provide adequate liquid transmissibility for flow across the fracture between the matrix blocks. The oil transmissibility by film flow is so small that production of oil from threshold zone of the upper block takes an extremely long time. Since the drainage flow rate by film flow is

very small, it is recommended that this kind of capillary continuity to be considered as non-effective. When the fracture aperture is small enough for existence of stable liquid bridges, the draining oil flows through the liquid bridges by the bulk flow process. Based on the high transmissibility of liquid bridge/bridges, this could be considered as effective continuity. There are still some delay time between the recovery performance of a stack block with the effective capillary continuity compared to that of a single block with the same height.

When the lower block is porous and permeable, if oil drop during its enlargement process attaches to the upper surface of the lower block, the pressure difference between oil and gas changes suddenly. The two radii of curvature of the liquid bridge are adjusted such that they represent a capillary pressure which is a function of density difference between oil and gas, and height of the fracture from level of zero capillary pressure. Therefore, when the continuity between matrix blocks are through the stable liquid bridges, as long as the fracture aperture is less than its critical value, the capillary pressure of horizontal fracture has no relation with the amount of the fracture aperture.

For the case of capillary continuity, the ultimate recovery of the stack block is equal to that of a single block with a height equal to that of stack block. The capillary pressure of each horizontal fracture plays the same role as porous medium at that elevation. Although different degrees of capillary continuity have the same effect from ultimate recovery point of view, but their transmissibility are not the same. The weakest degree of capillary continuity, i.e. capillary continuity through oil film over the boundary of solid spacers, results in the smallest transmissibility. When the fracture aperture is small, the transmissibility of a stack block, at the best condition, due to a larger number of liquid bridges will be such that its flow rate is close to that of a single block with the same height.

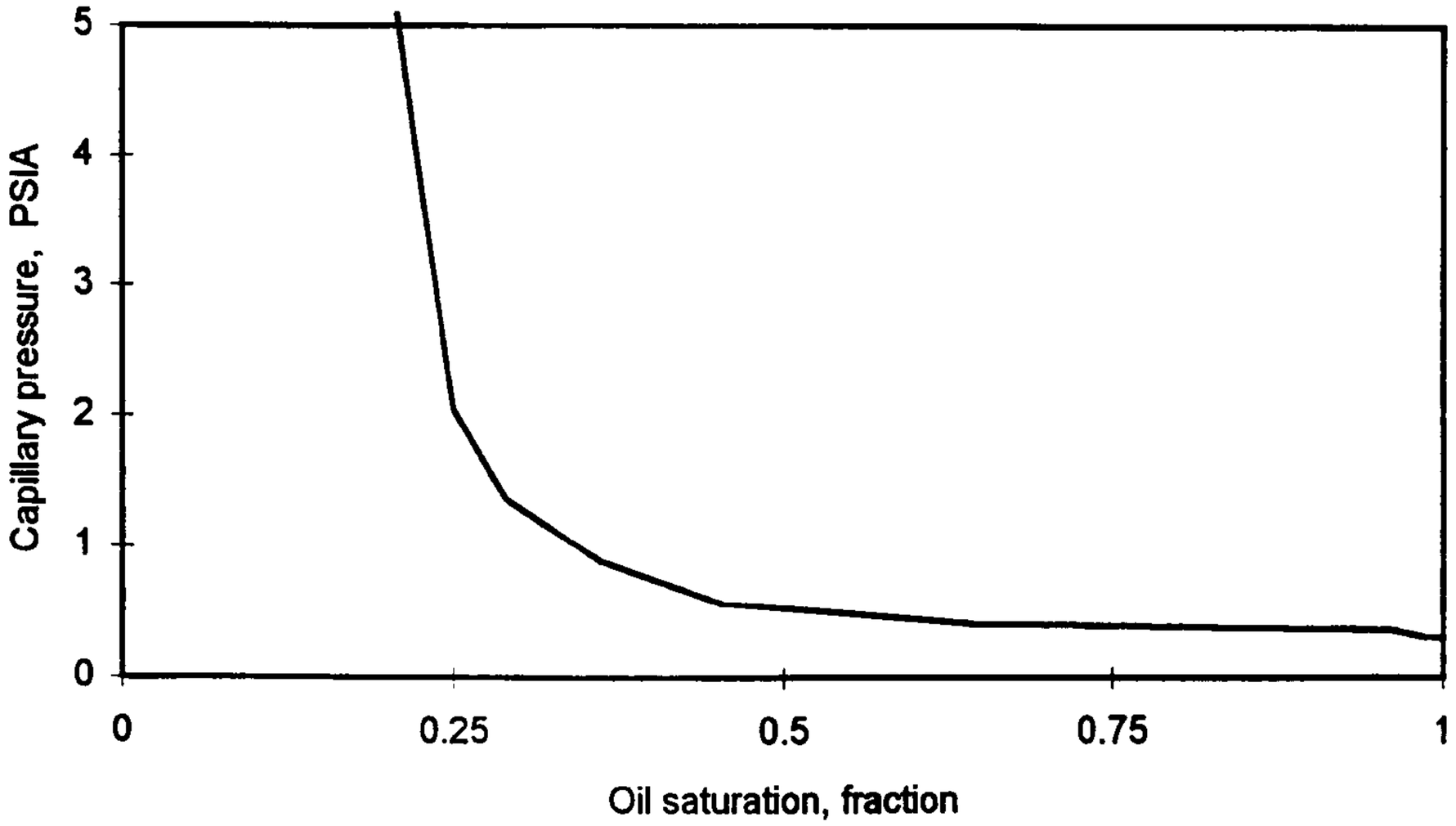

Figure 5.2-1 Capillary pressure of sandstone model.

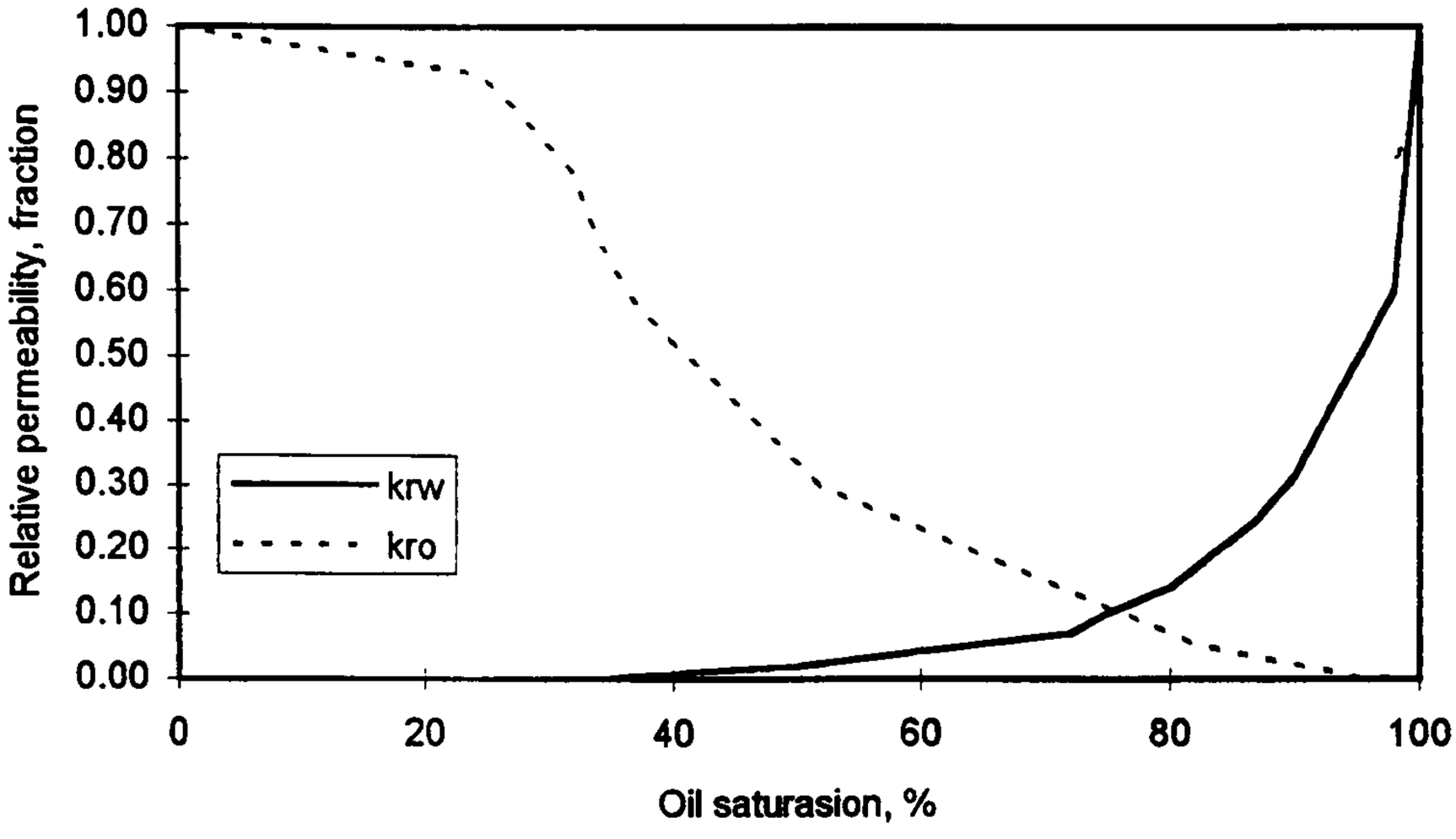

Figure 5.2-2 Relative permeability of sandstone model.

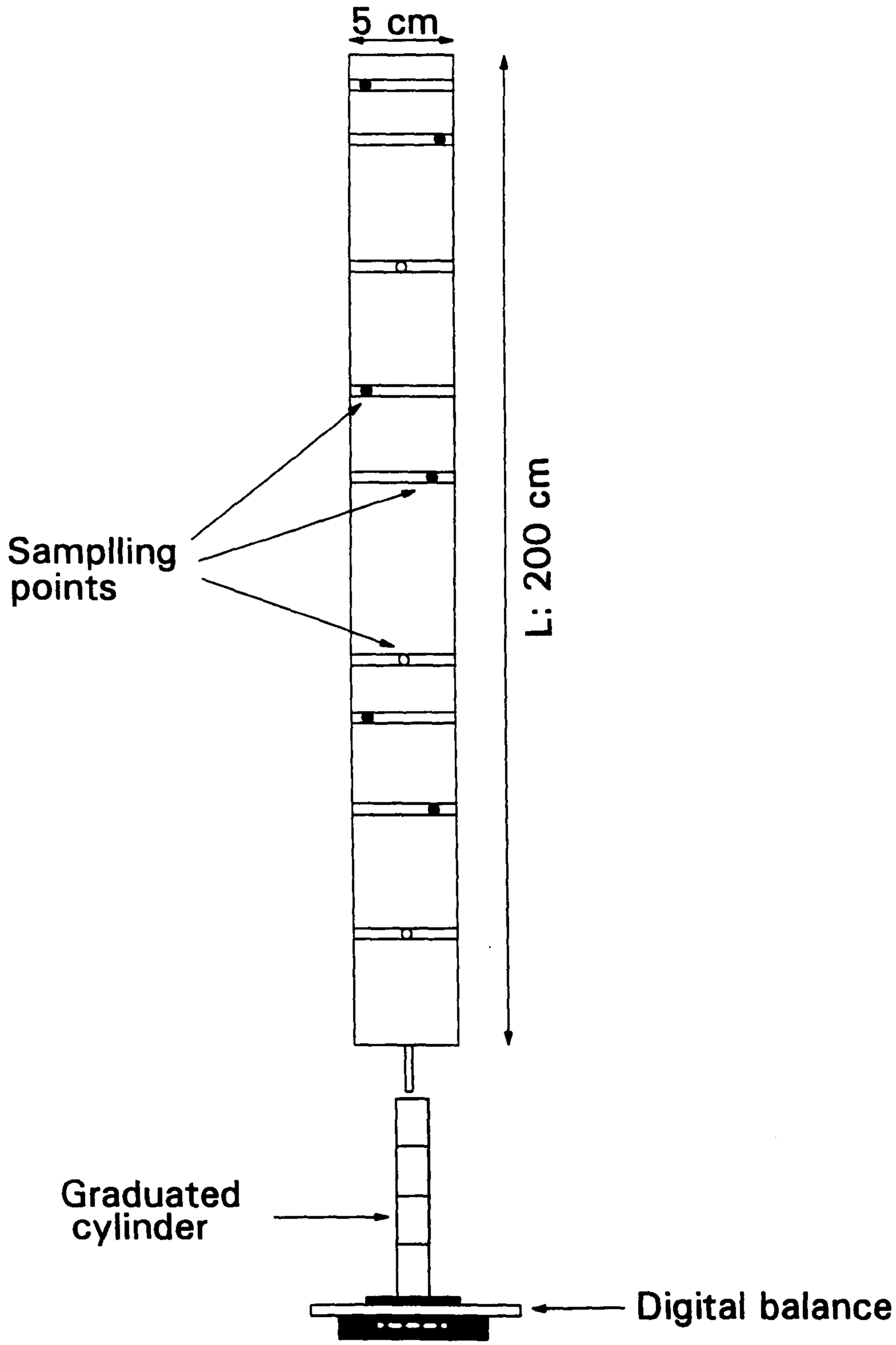

Figure 5.3-1 Schematic diagram of core-holder and experimental set-up.

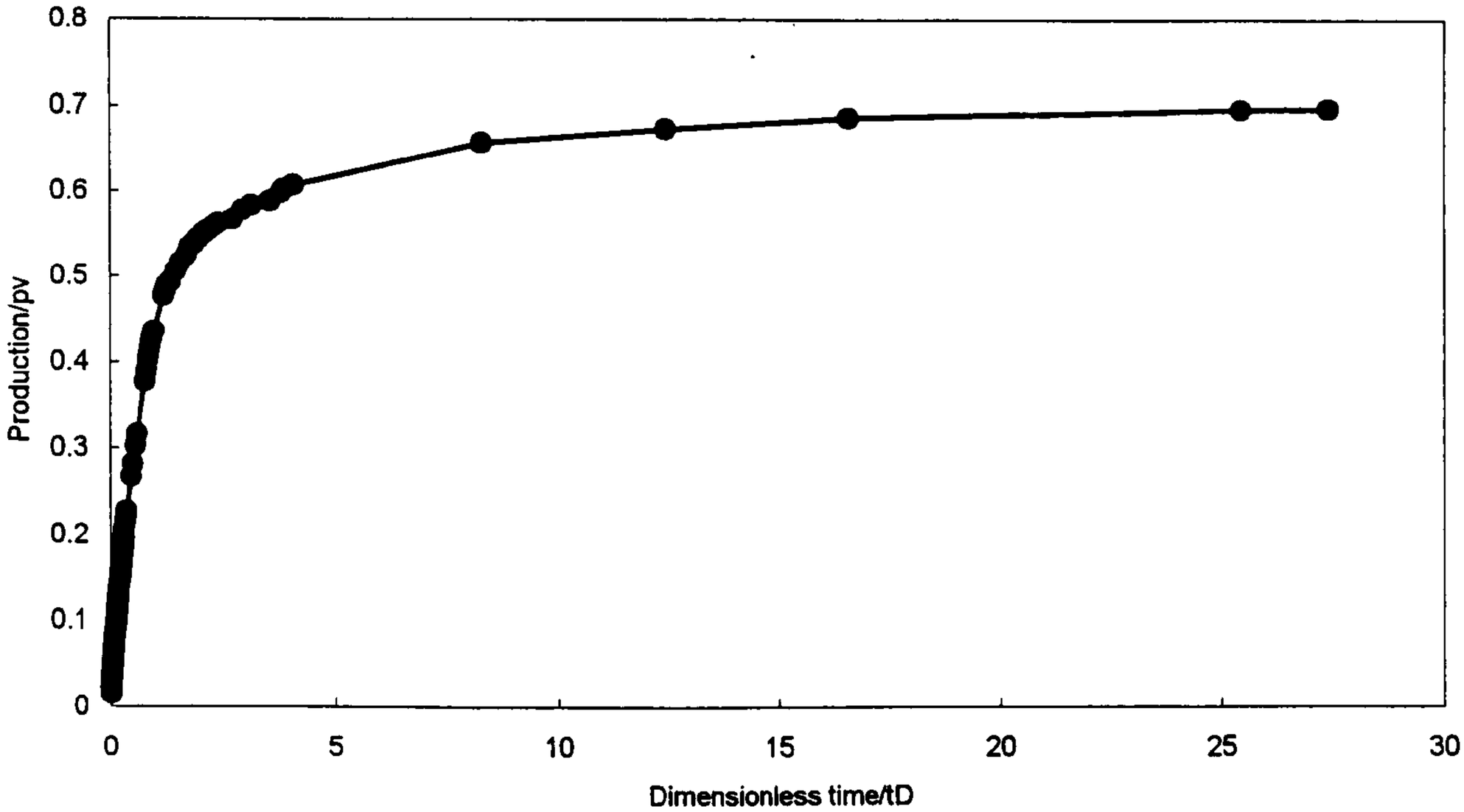

Figure 5.3-2a Production data vs. time (linear scale) for Experiment 5.3-4.

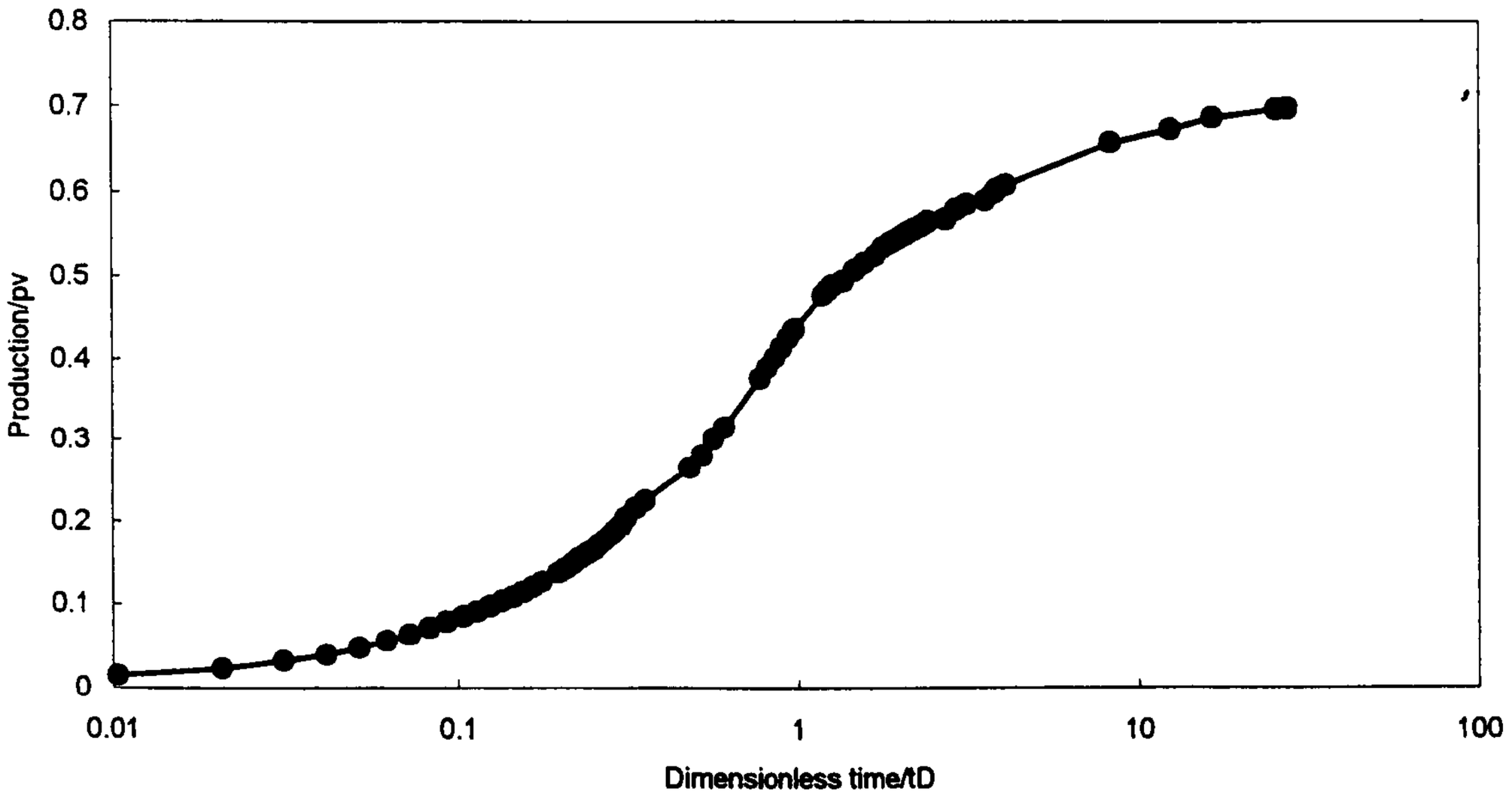

Figure 5.3-2b Production data vs. time (log scale) for Experiment 5.3-4.

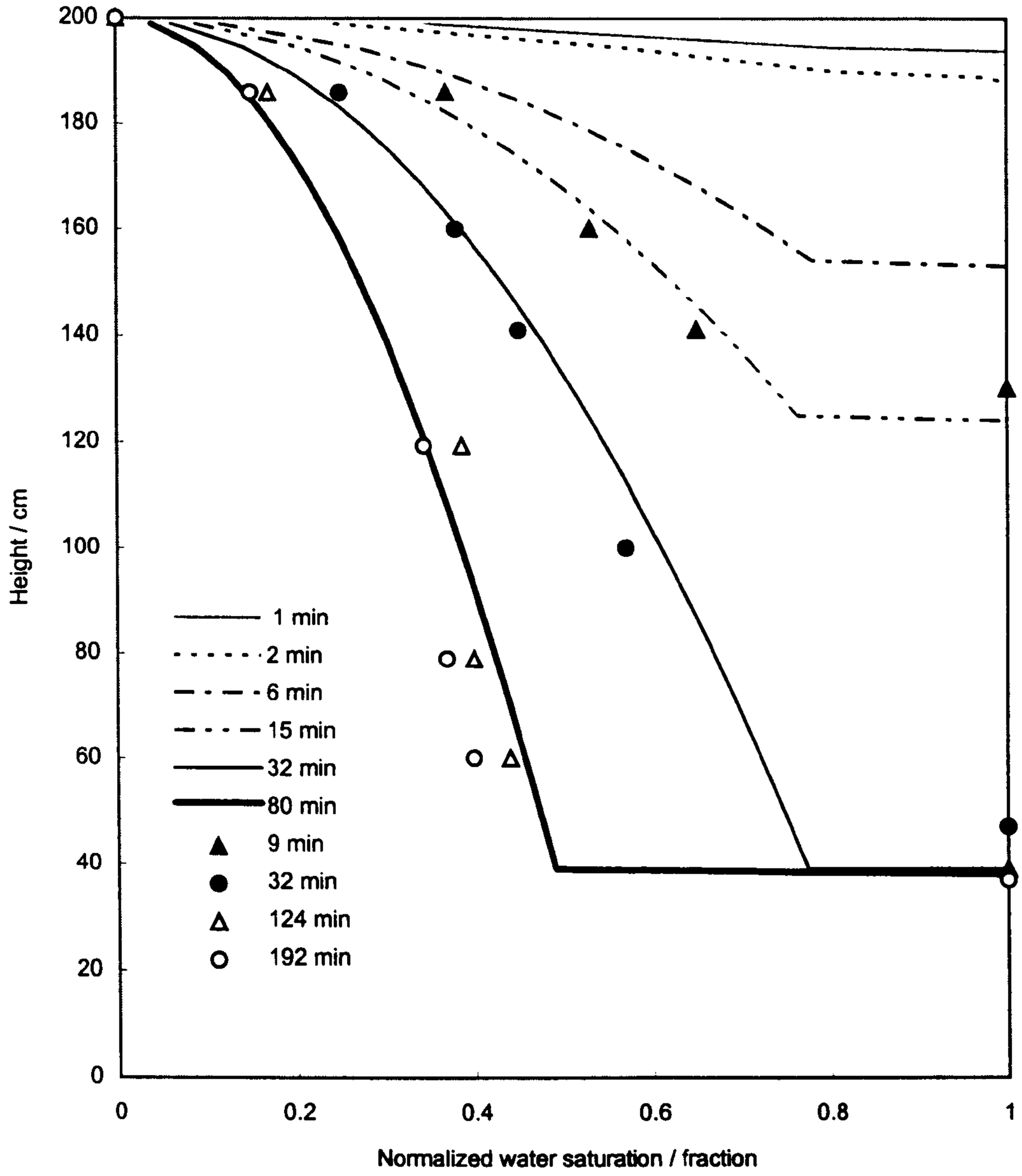

Figure 5.3-3 Measured and calculated saturation distribution at different drainage time for Experimen 5.3-4.

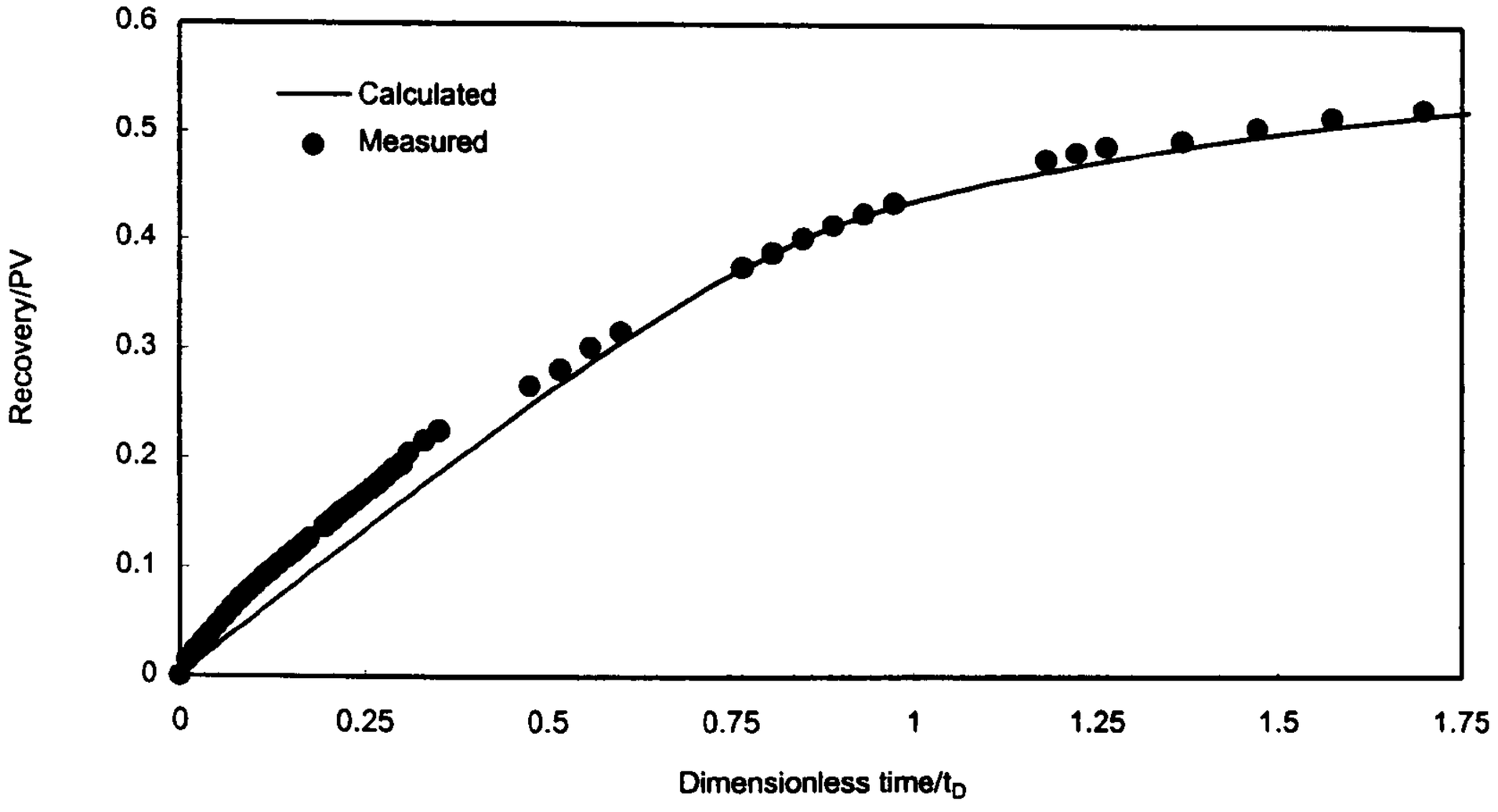

Figure 5.3-4 Comparison of calculated recovery with gravity drainage of sandpack experimental data.

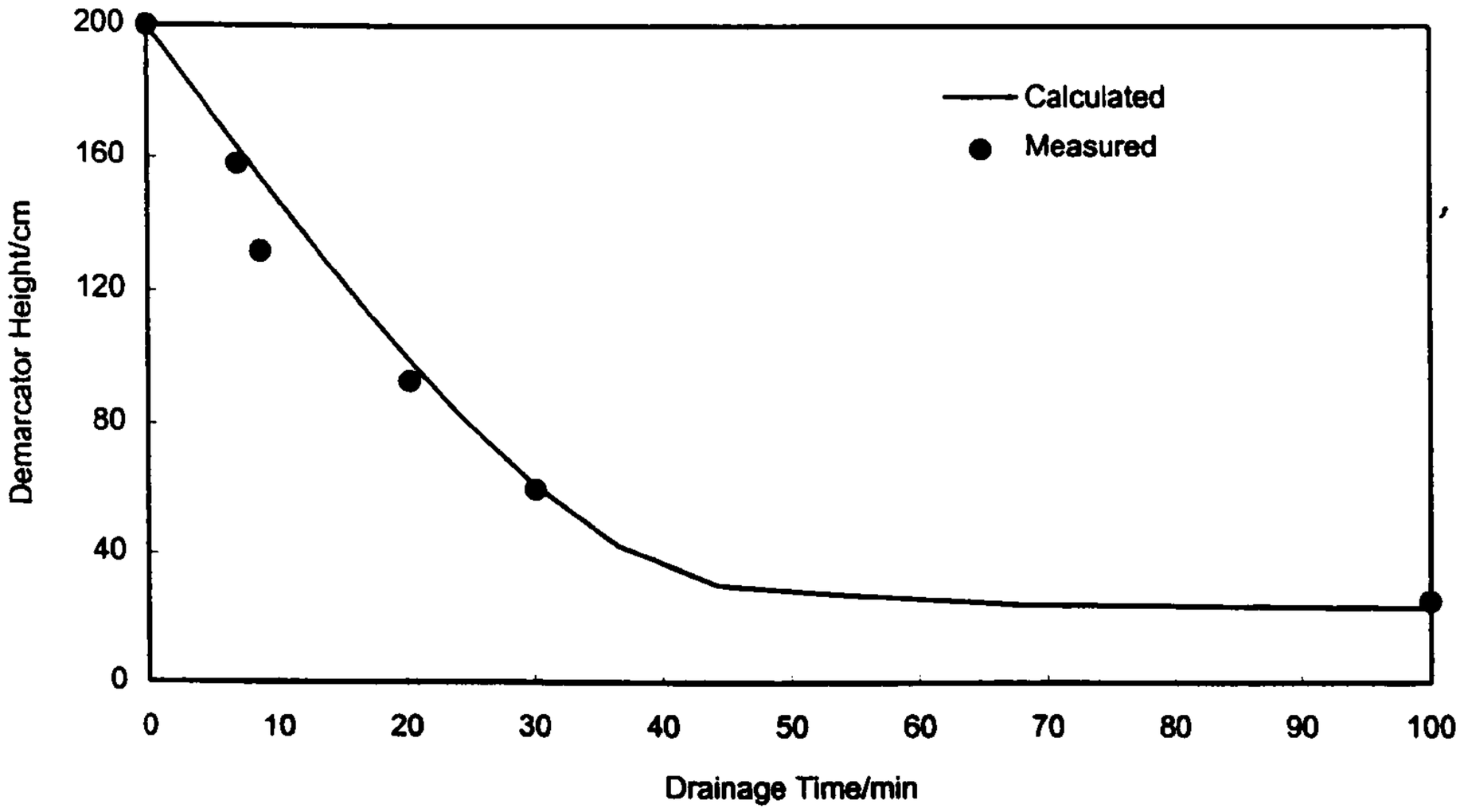

Figure 5.3-5 Demarcator height at various times for gravity drainage process of sandpack model, equilibrium threshold height equals 20 cm.

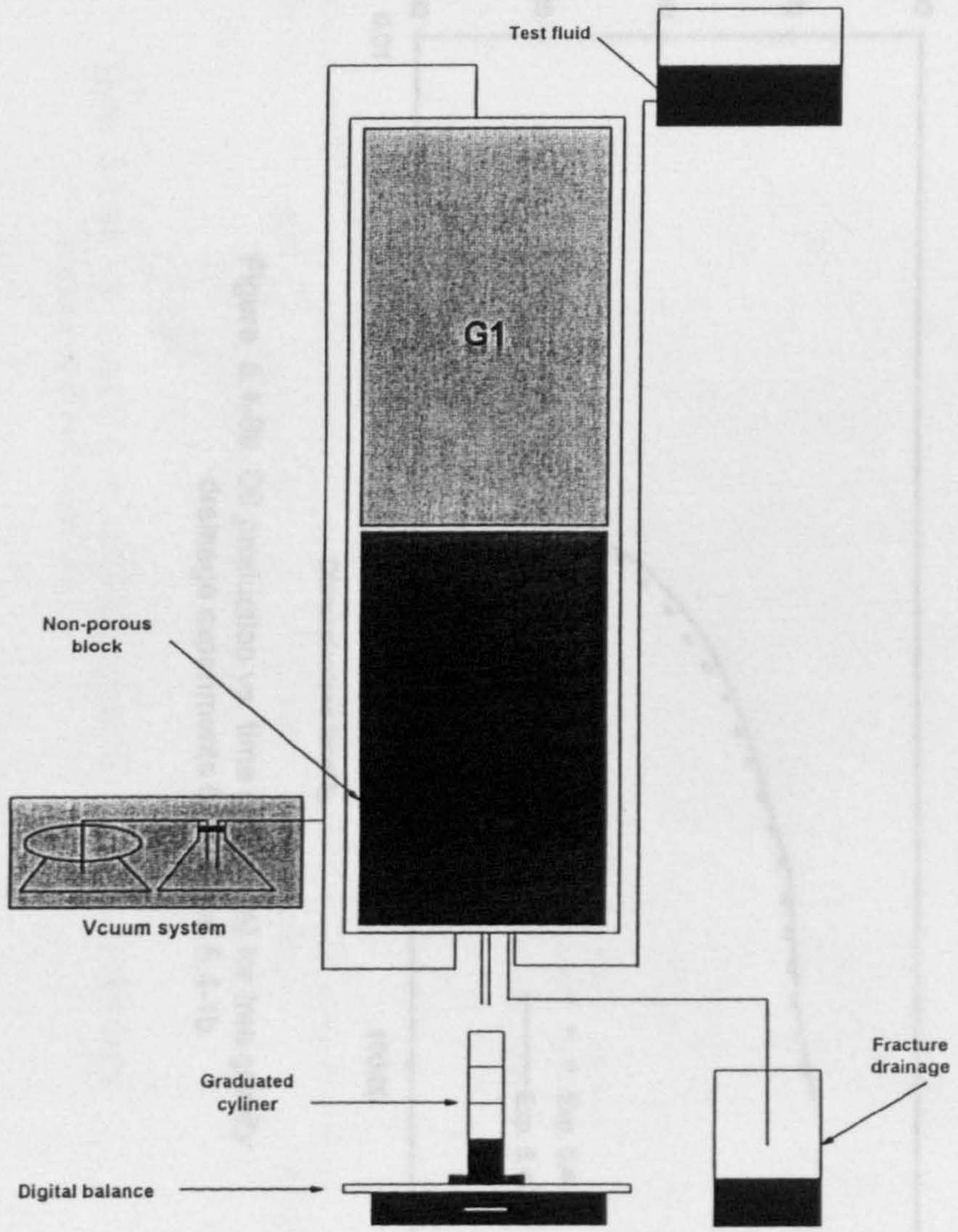

Figure 5.4-1 Apparatus schematic of Experiments 5.4-1, 5.4-2 and 5.4-3.

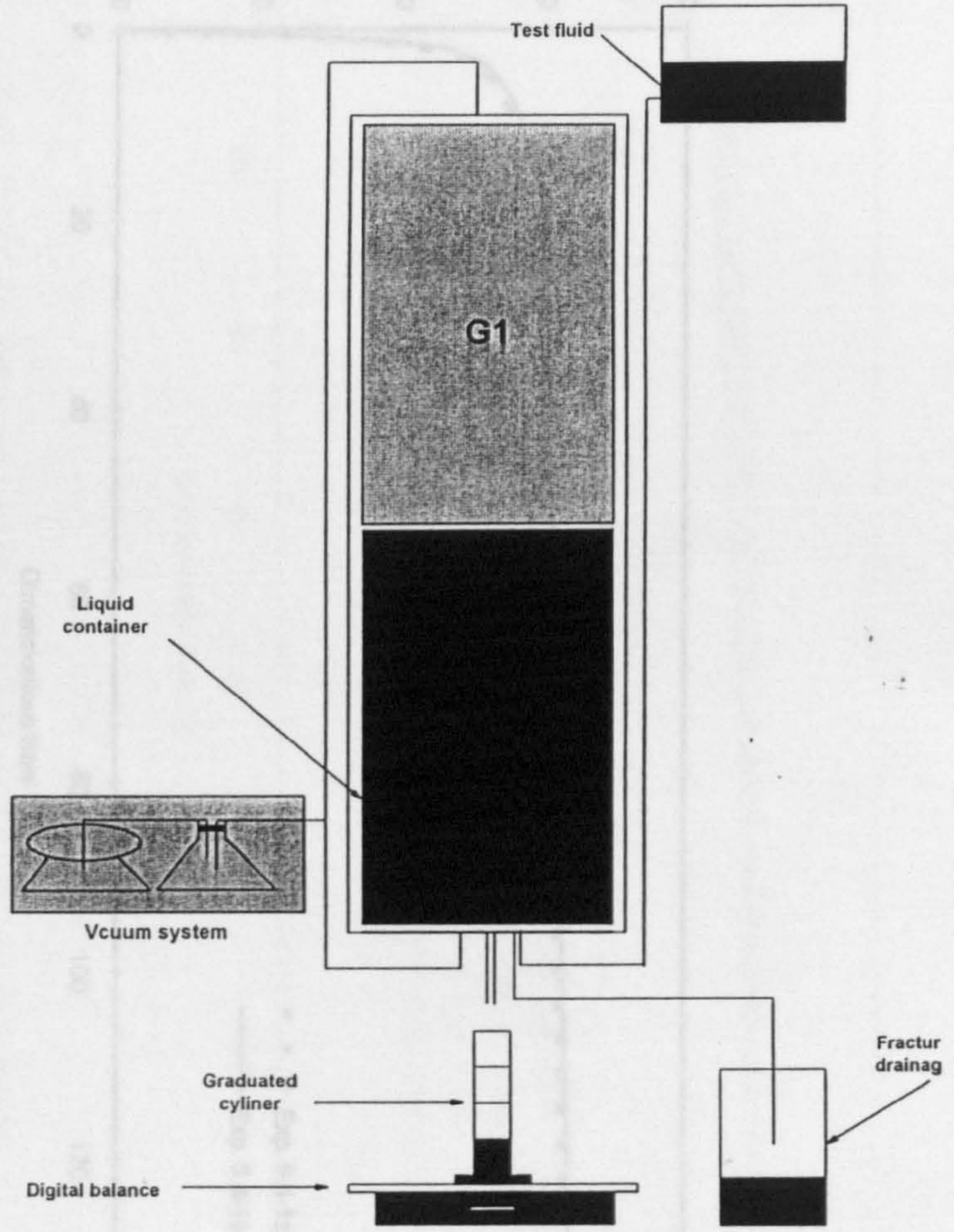

Figure 5.4-2 Apparatus schematic of Experiment 5.4-4

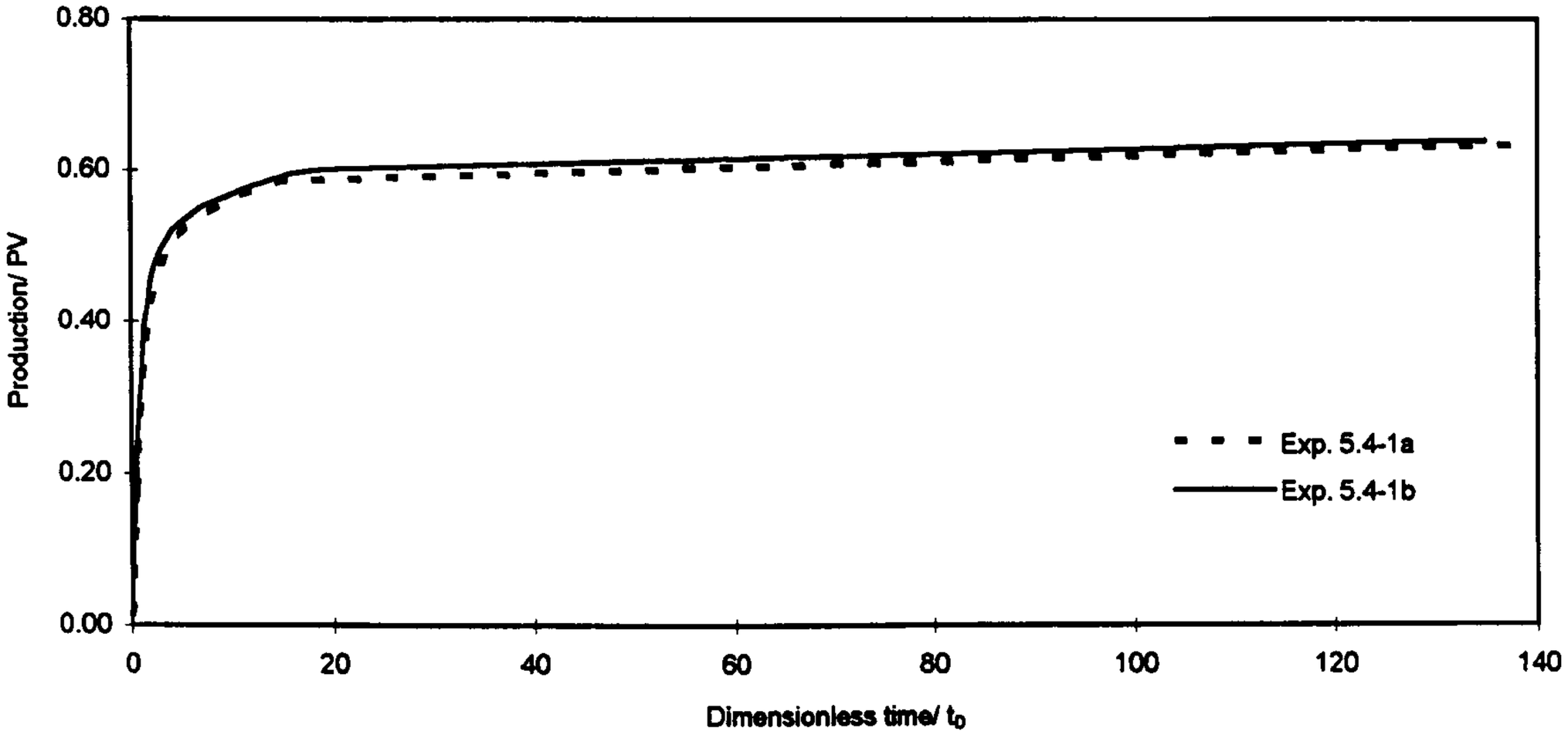

Figure 5.4-3a Oil production vs. time (linear scale) for free gravity drainage experiments 5.4-1a and 5.4-1b.

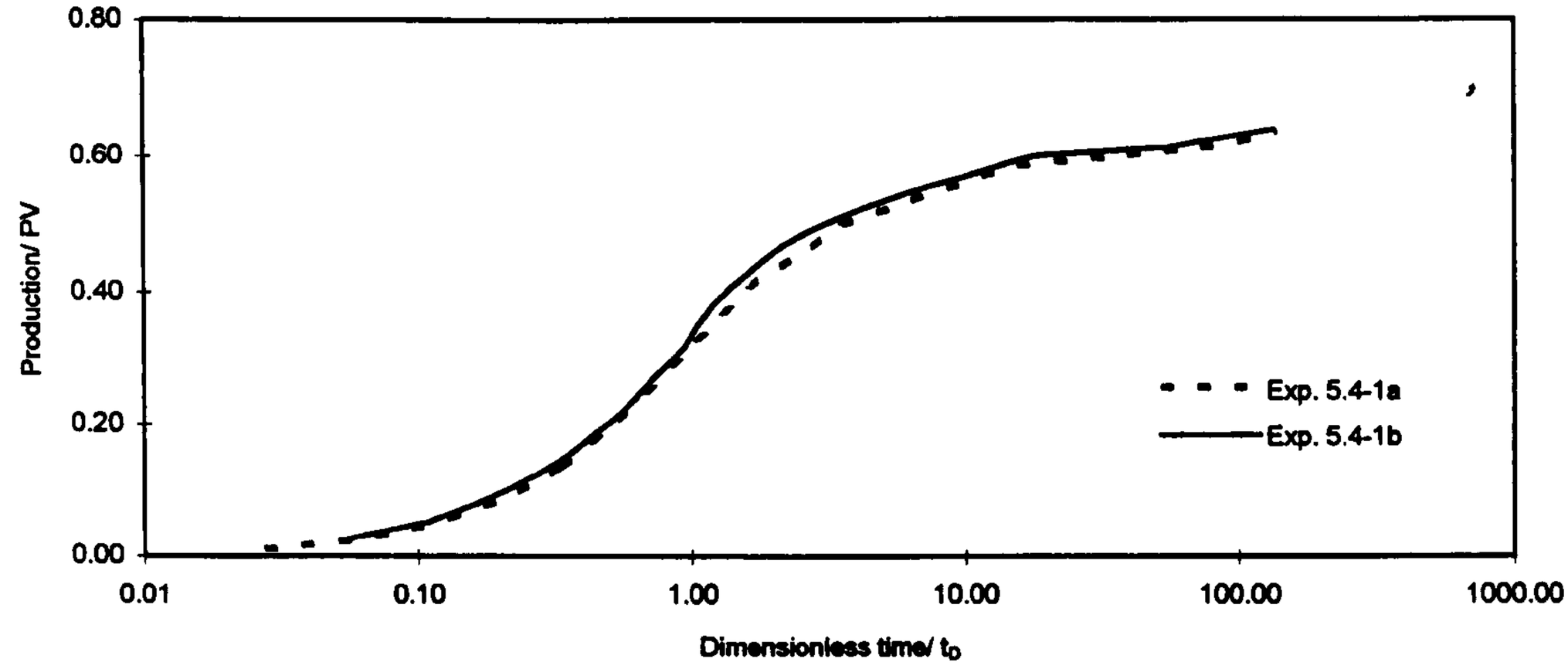

Figure 5.4-3b Oil production vs. time (log scale) for free gravity drainage experiments 5.4-1a and 5.4-1b.

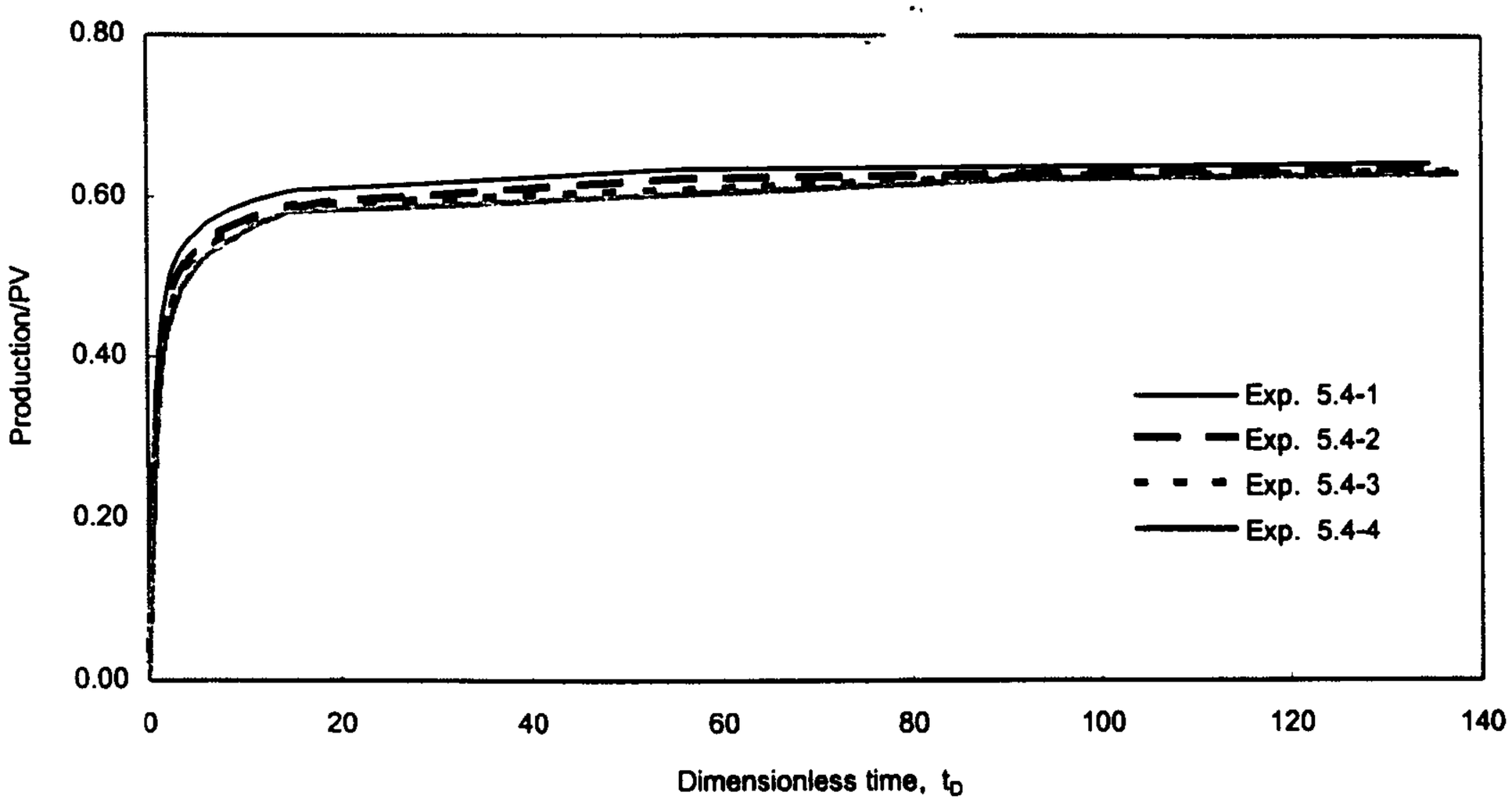

Figure 5.4-4a Oil production vs. time (linear scale) for free gravity drainage experiments of block G1.

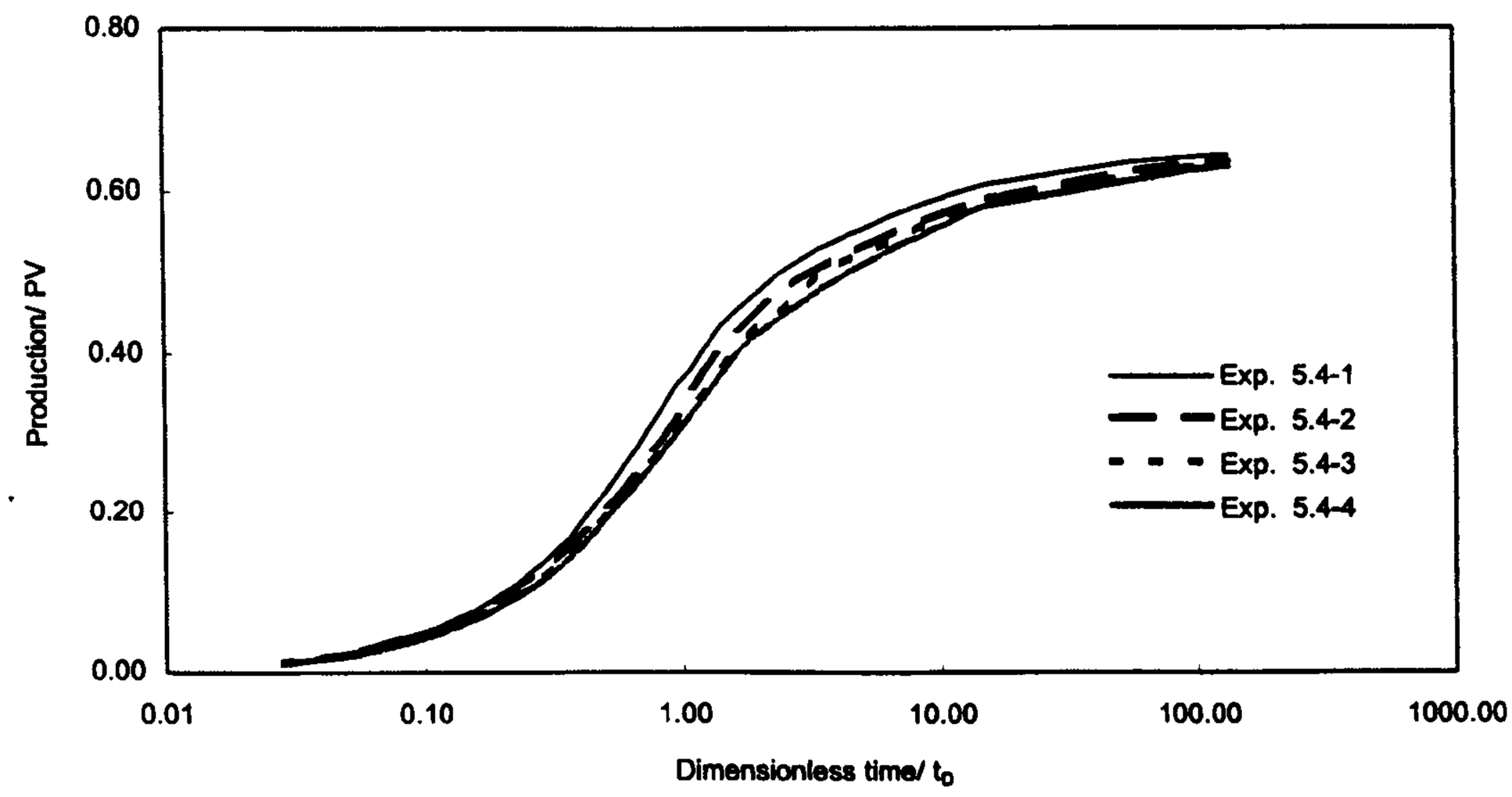

Figure 5.4-4b Oil production vs. time (log scale) for free gravity drainage experiments of block G1.

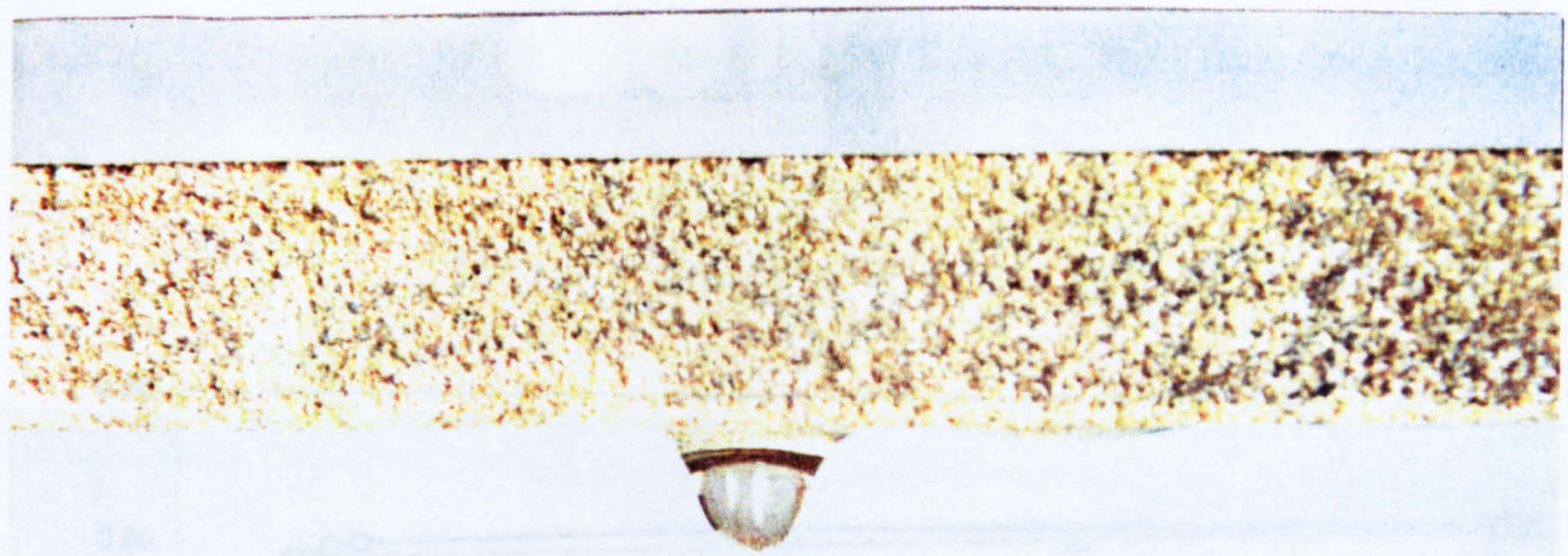

a: Drop enlargement process, due to free gravity drainage.

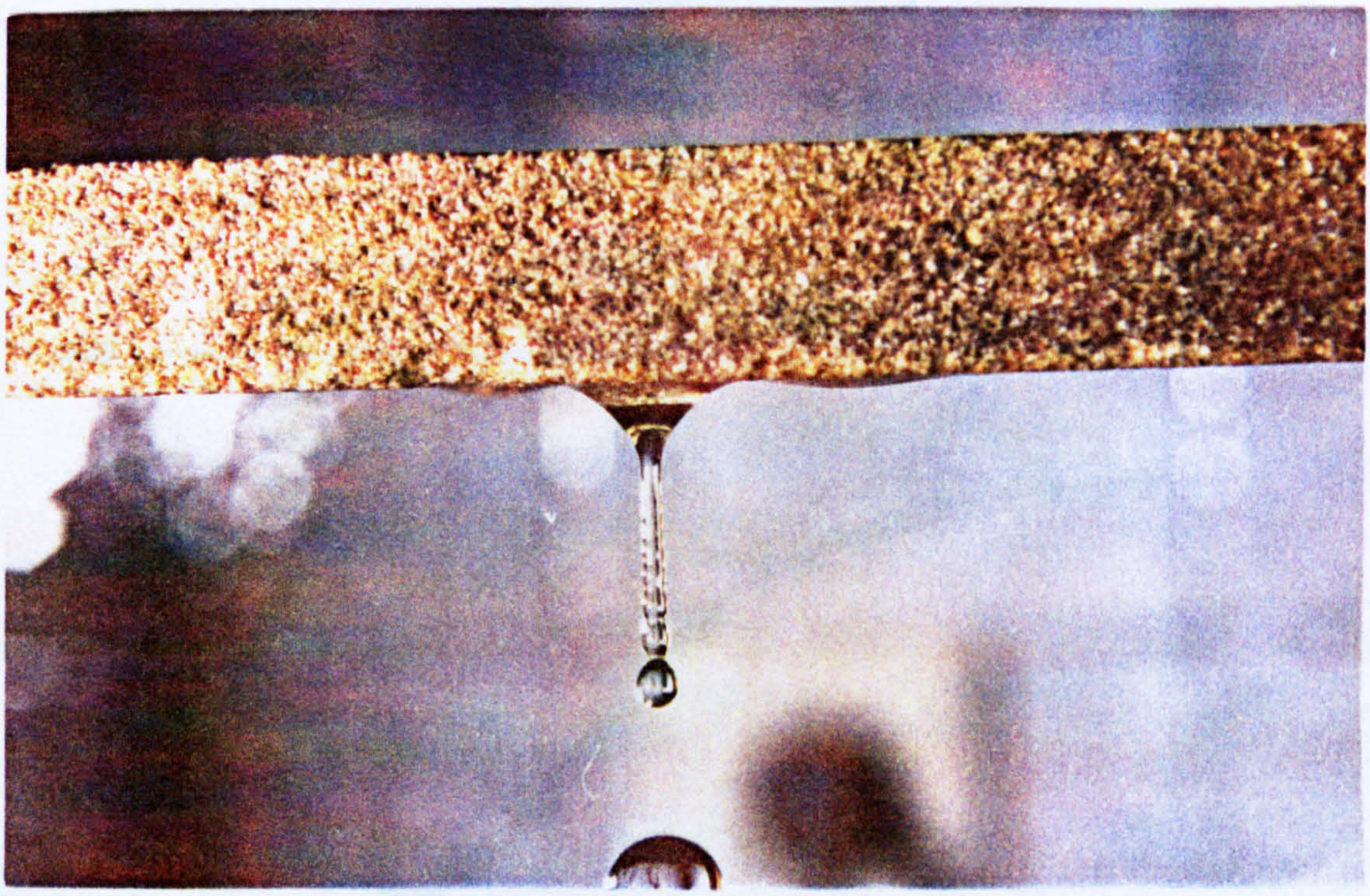

b: After the break down of the neck.

Figure 5.4-5 Photograph of a falling drop. Notice the secondary drop following the main drop.

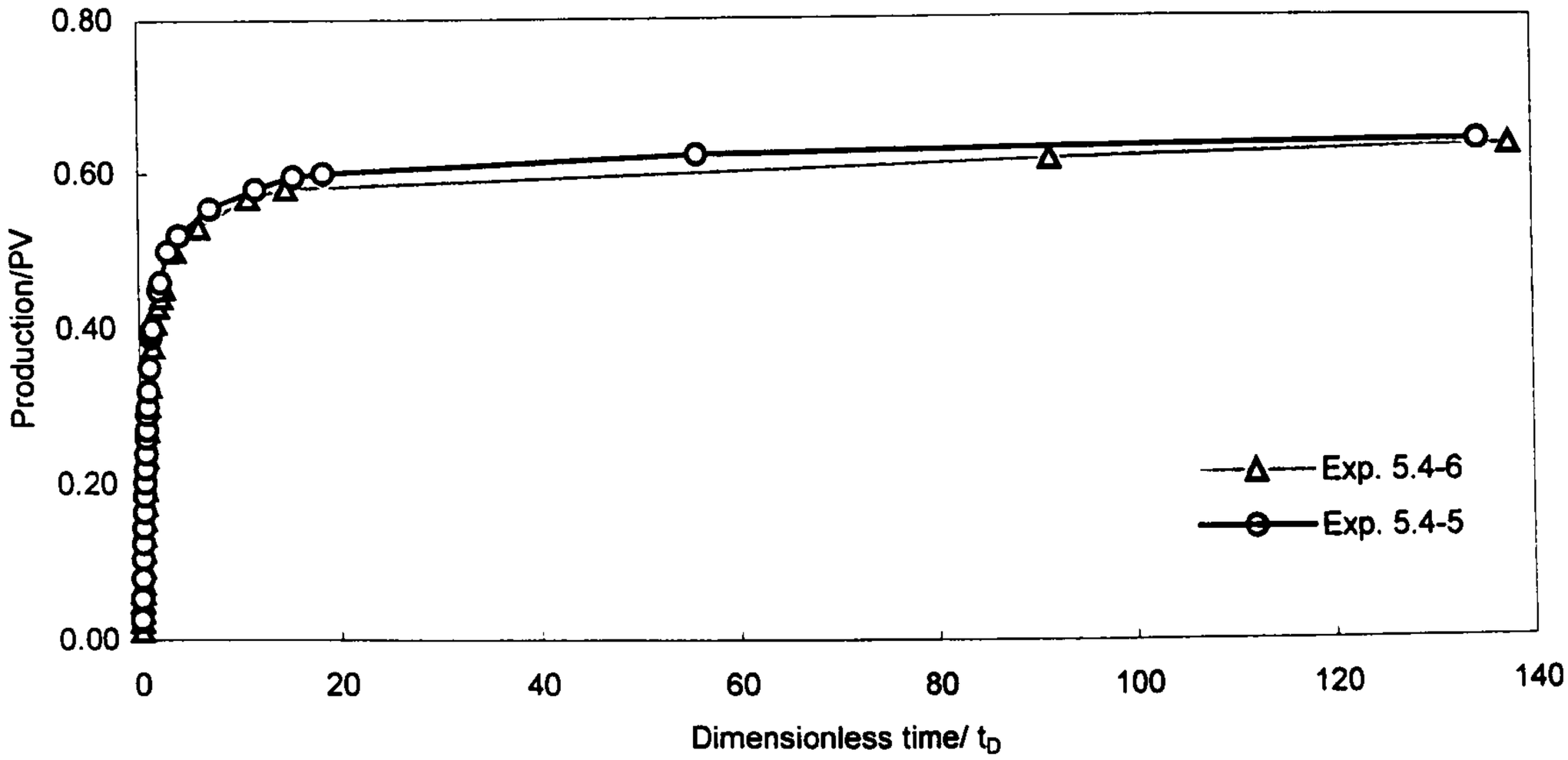

Figure 5.4-6a Oil production vs. time (linear scale) for free gravity drainage experiments of block G4.

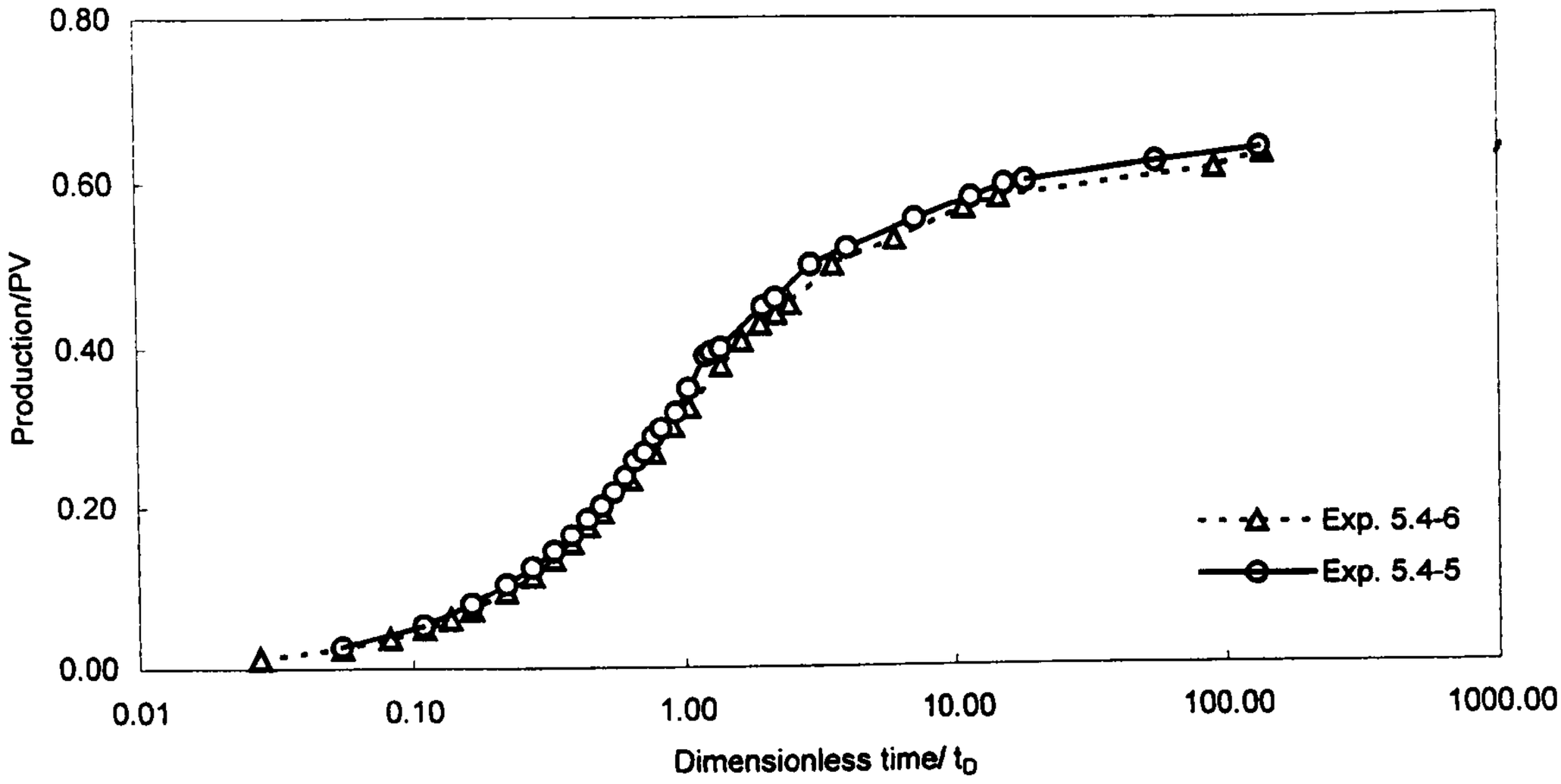

Figure 5.4-6b Oil production vs. time (log scale) for free gravity drainage experiments of block G4.

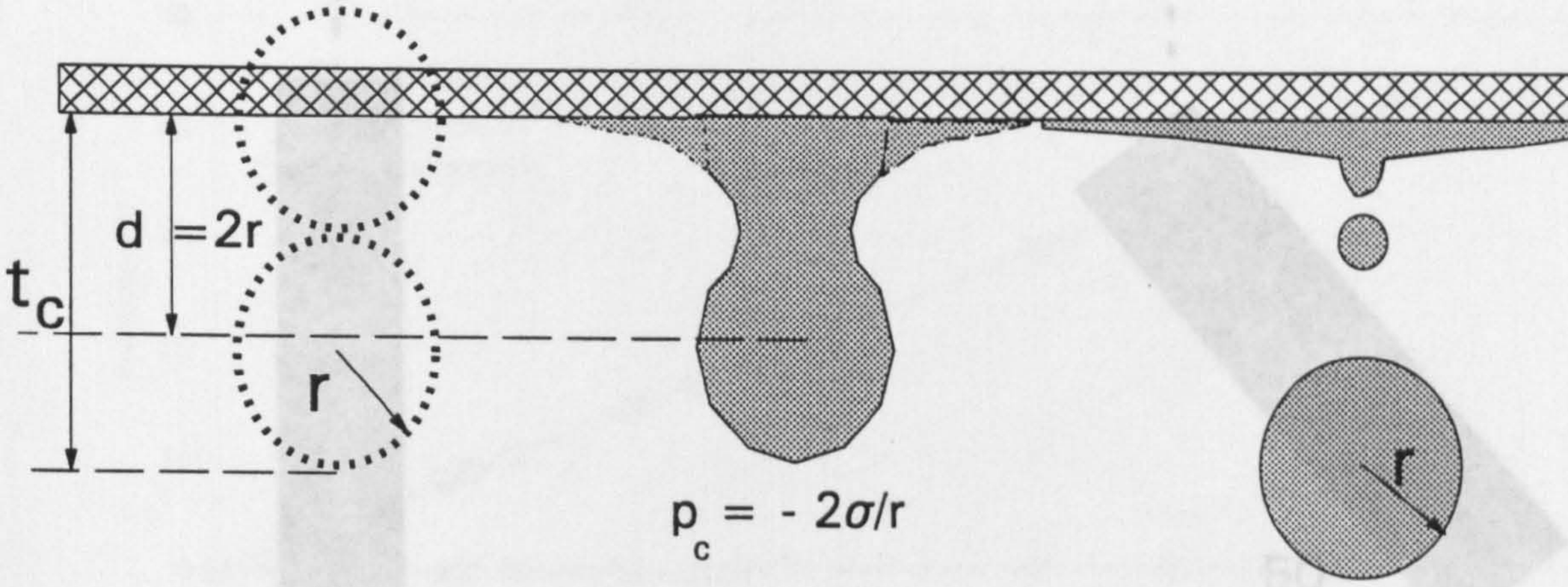

Figure 5.4-7 Scheme of a falling drop simulation.

$r_1 = -r_2$
$p_c = 0$

$r_1 = -r_2$
$p_c = 0$

$r_2 = \infty$,
$p_c \neq 0$

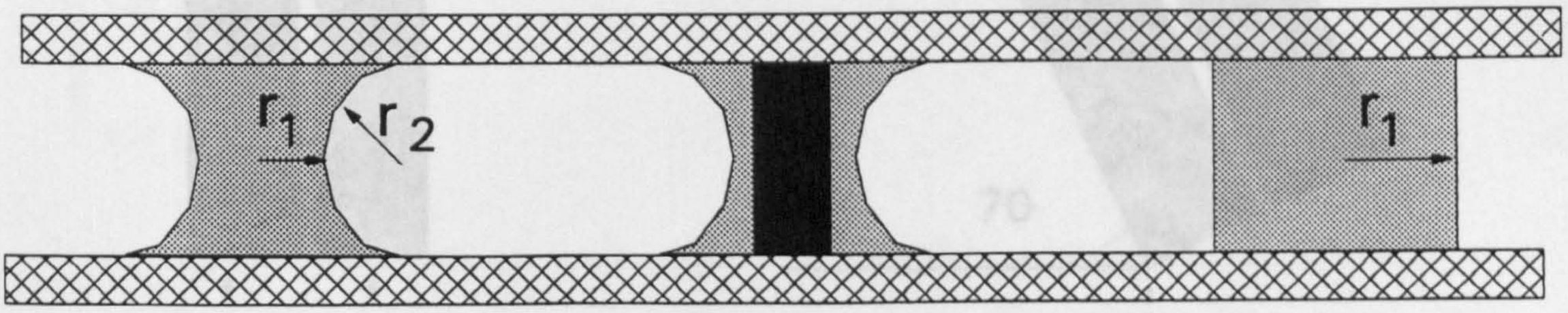

Figure 5.4-8 Local capillary pressure at the gas/oil interface, around the liquid and solid spacer.

Case 1-(G5), and Case 2-(L6)

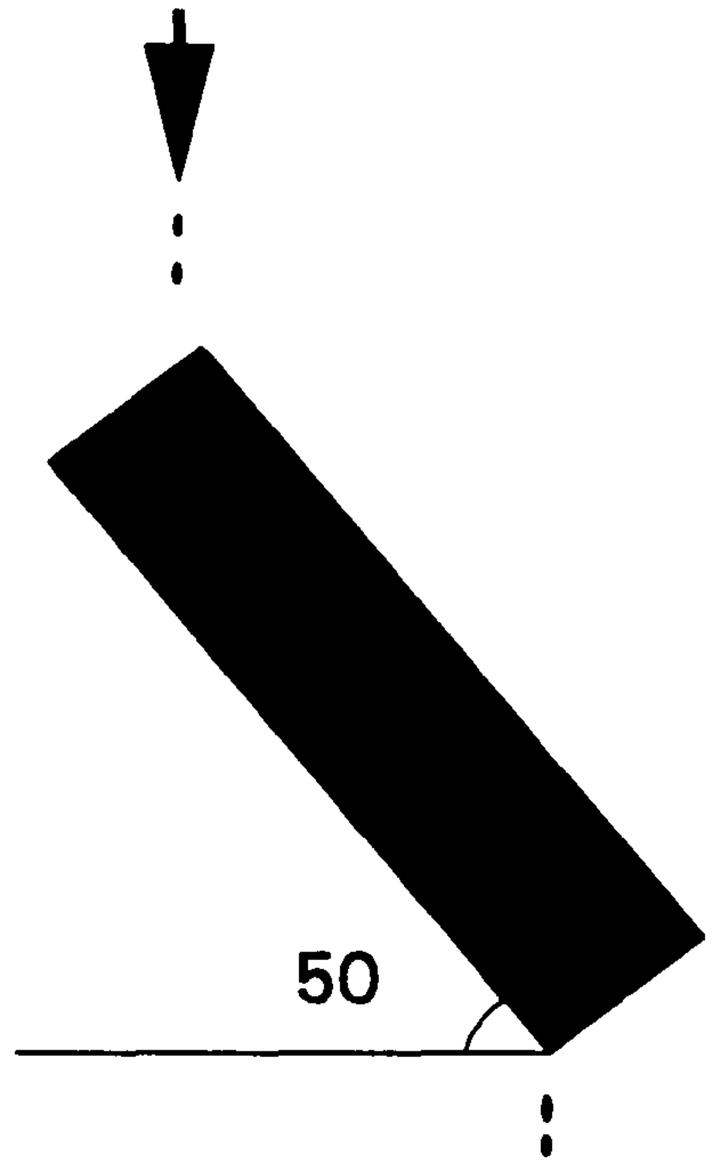

Case 3-(L6)

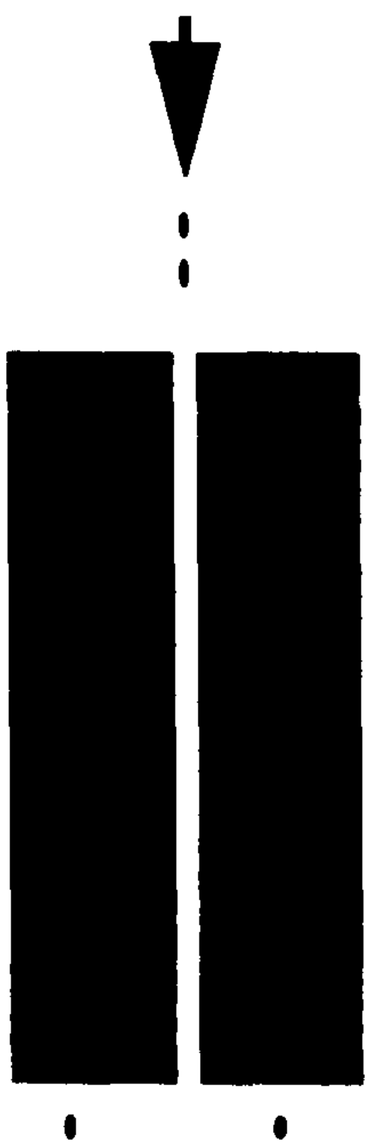

Case 4-(L13/L15)

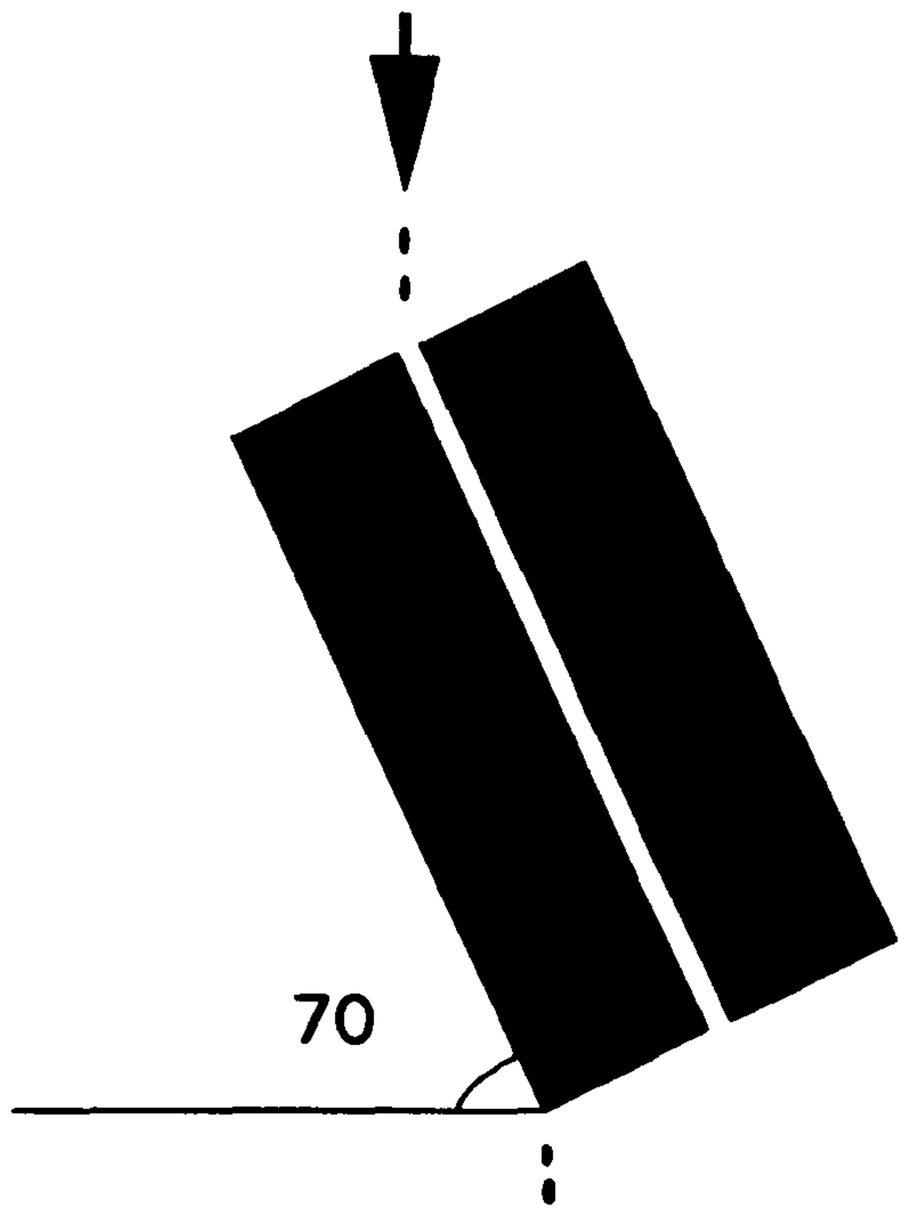

Case 5-(L13/L15)

Figure 5.5-1 Block/block assembly for reinfiltration experiments.

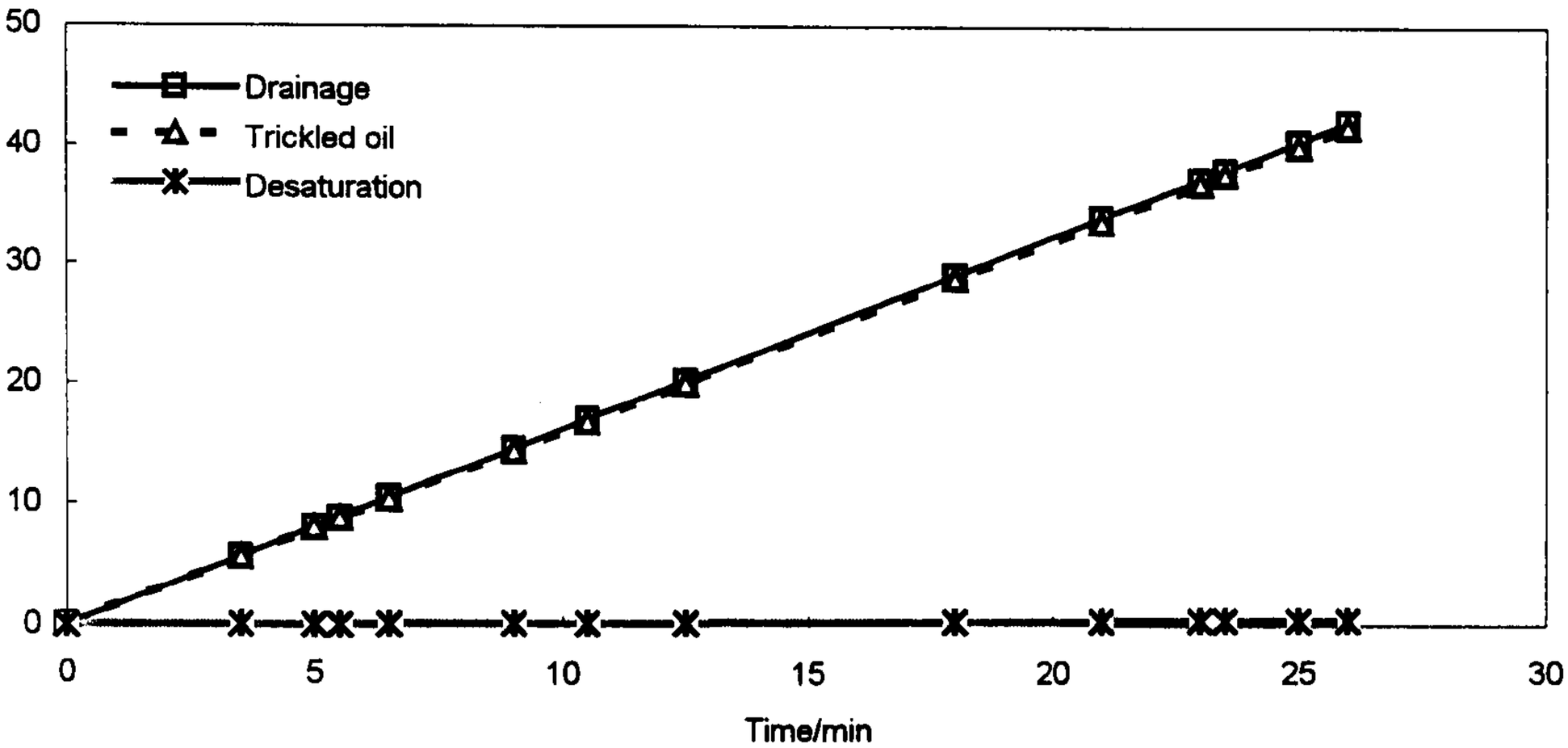

Figure 5.5-2 Drainage, trickled oil and desaturation vs. time (linear scale) for Case1.

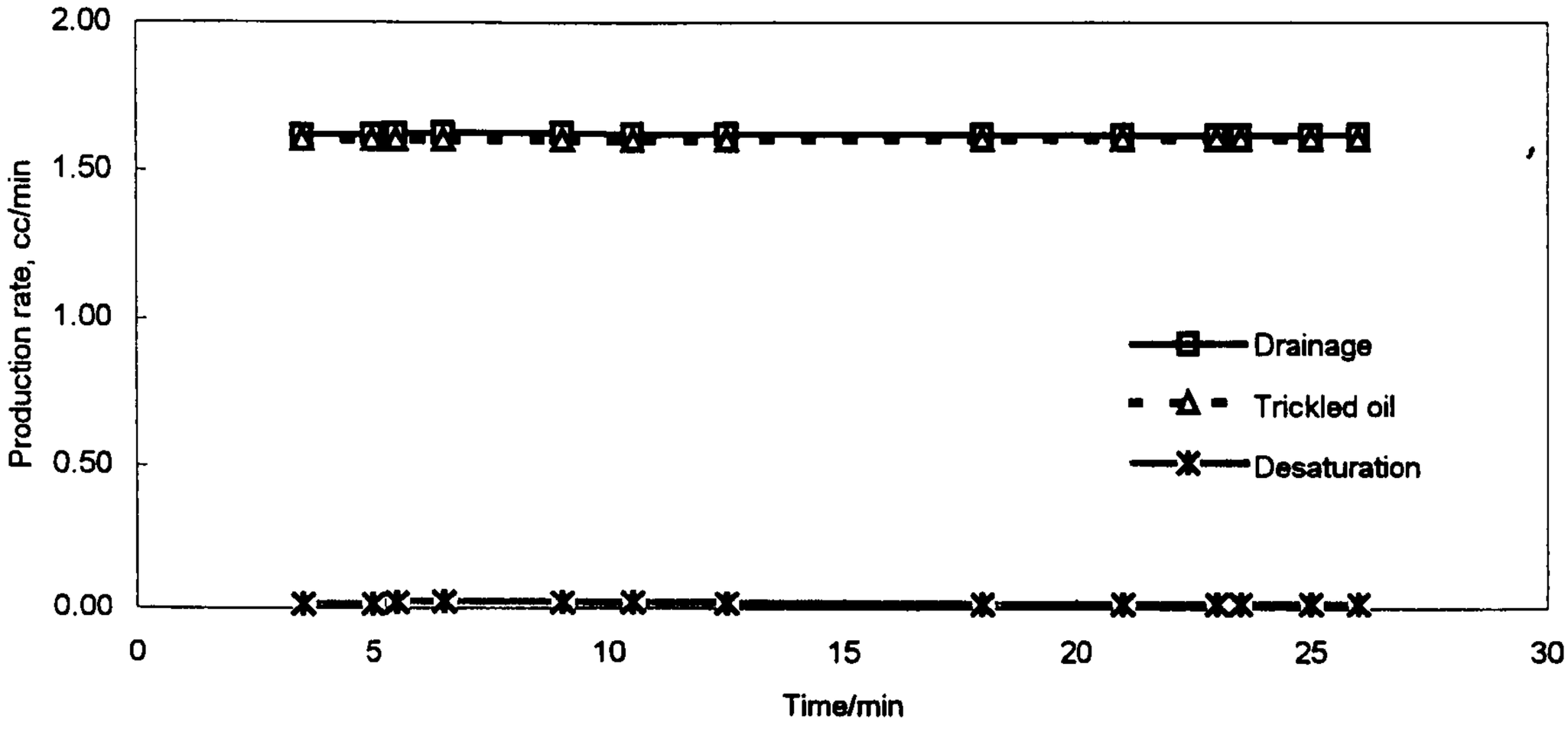

Figure 5.5-3 Production, trickled oil and desaturation rate vs. time (log scale) for Case1.

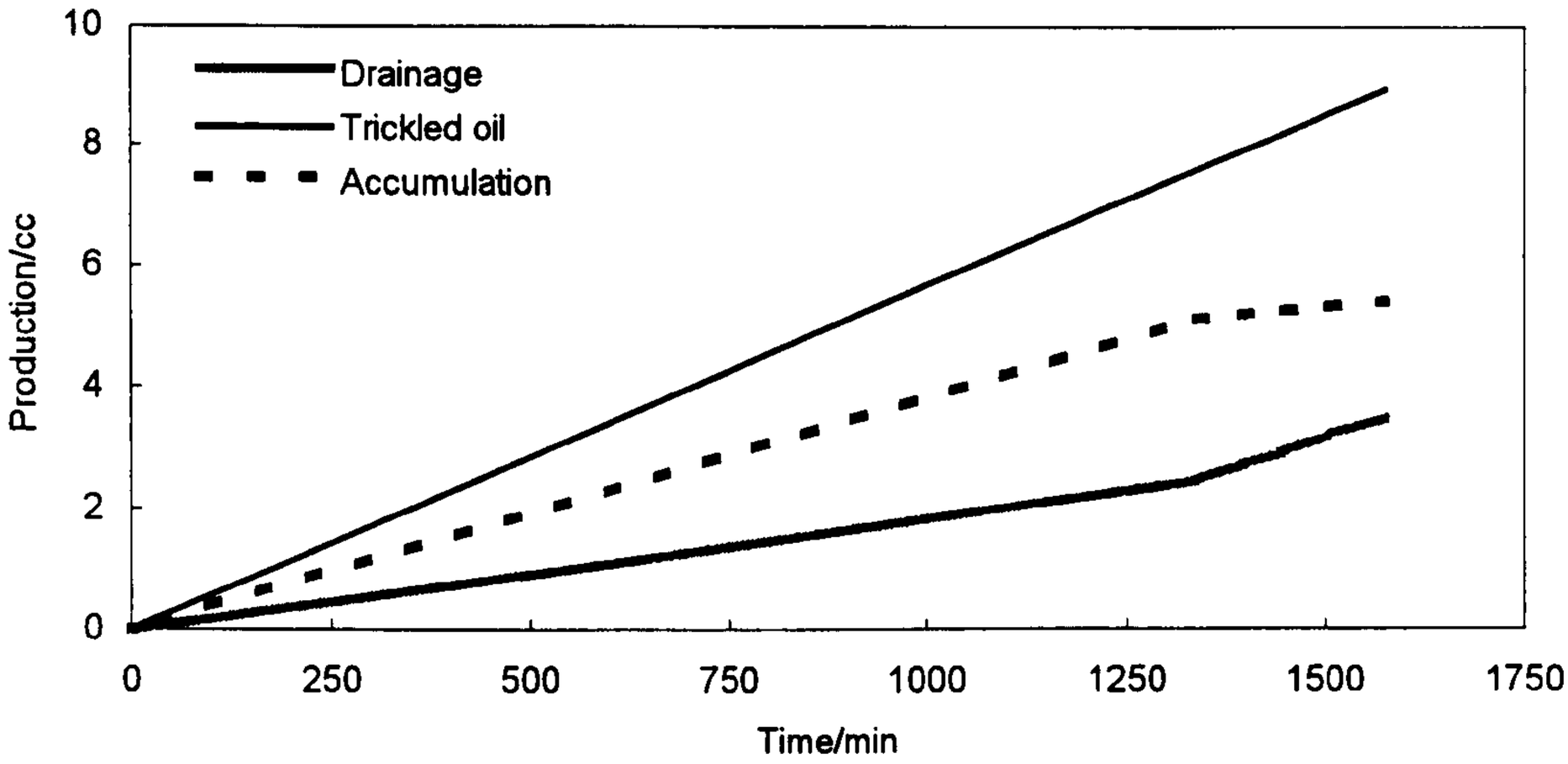

Figure 5.5-4 Drainage, reinfiltration and accumulation vs. time for Case 2.

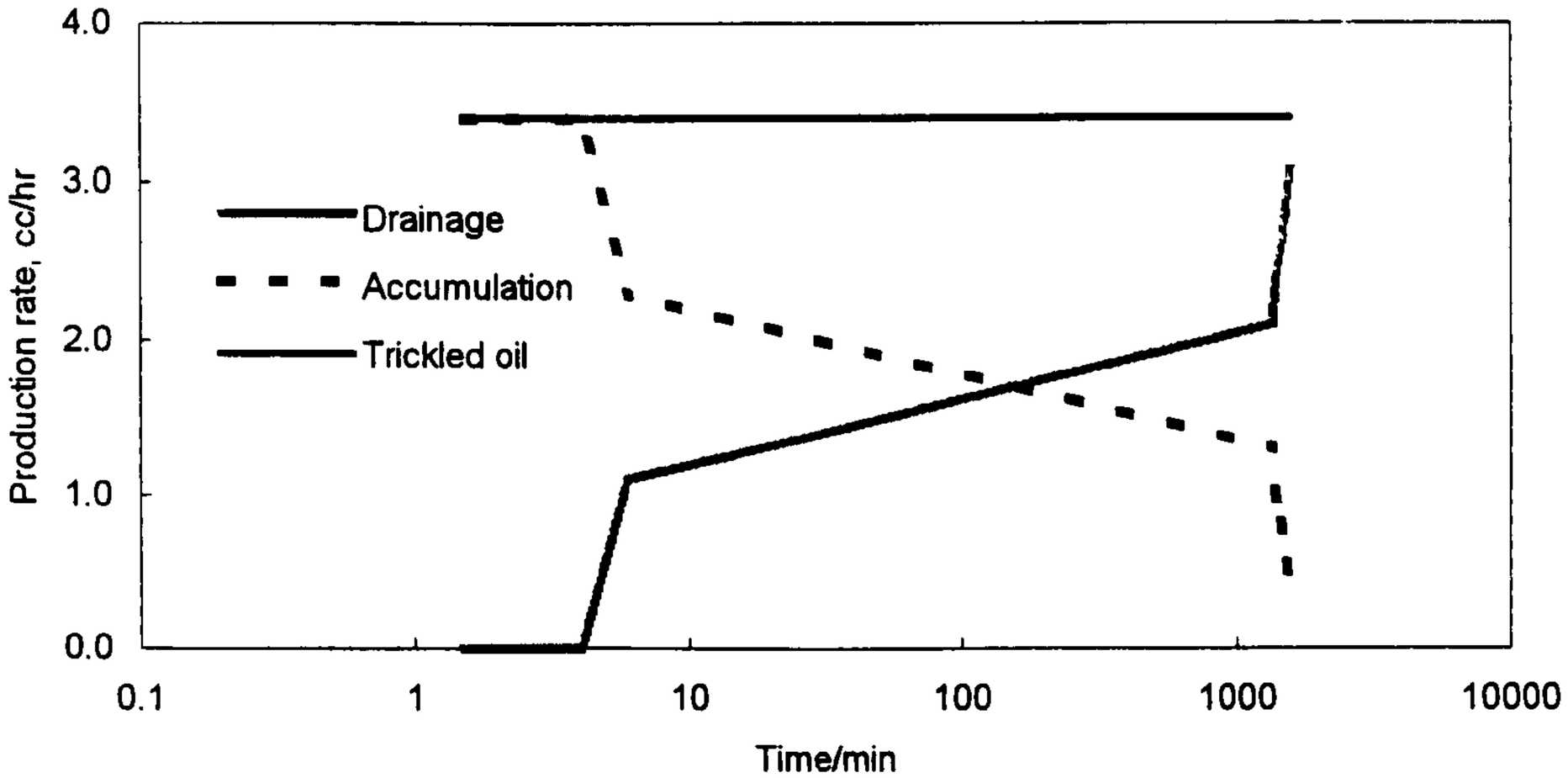

Figure 5.5-5 Drainage, accumulation and reinfiltration rate (log scale) vs. time for Case 2.

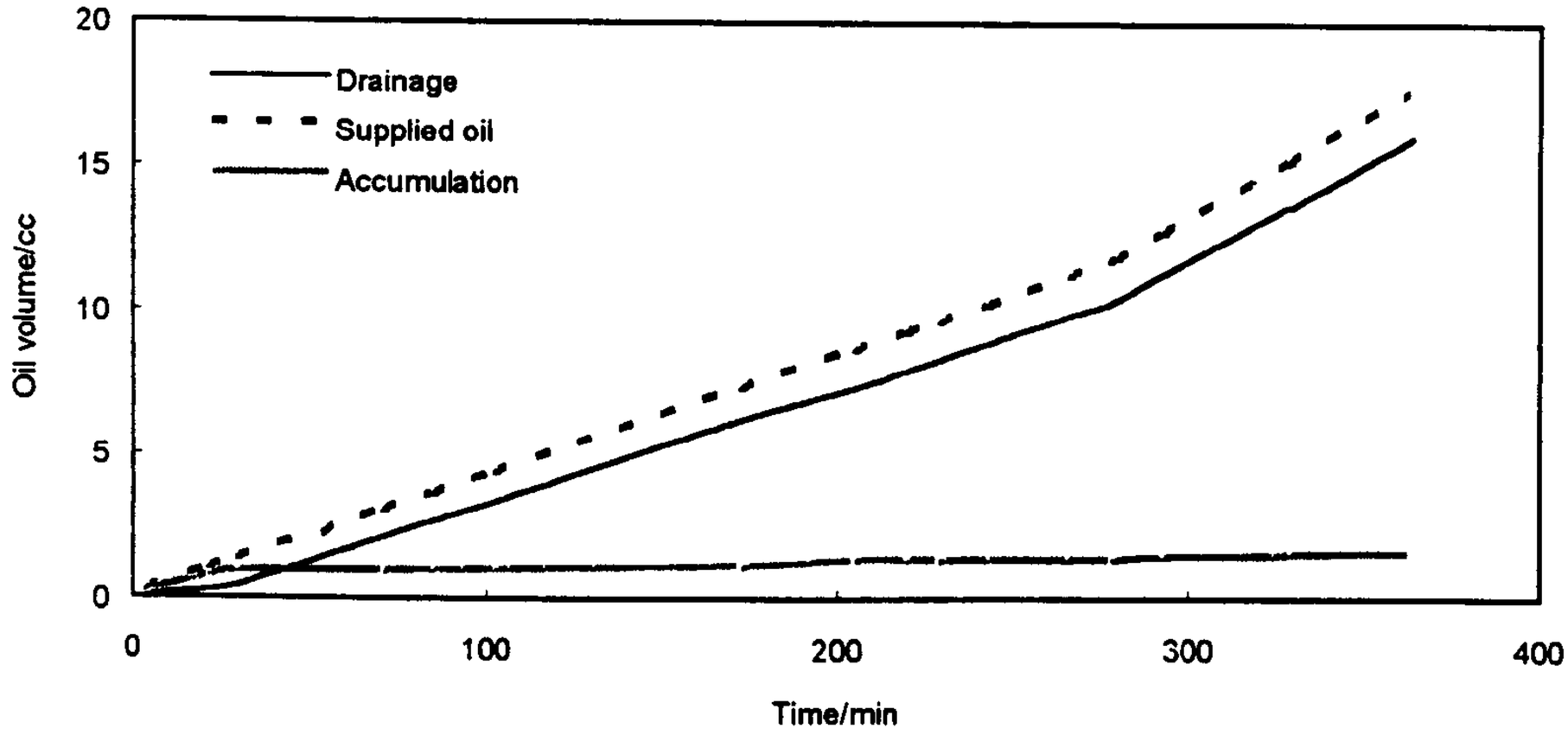

Figure 5.5-6 Drainage, supplied oil and accumulation vs. time (linear scale) for Case 3.

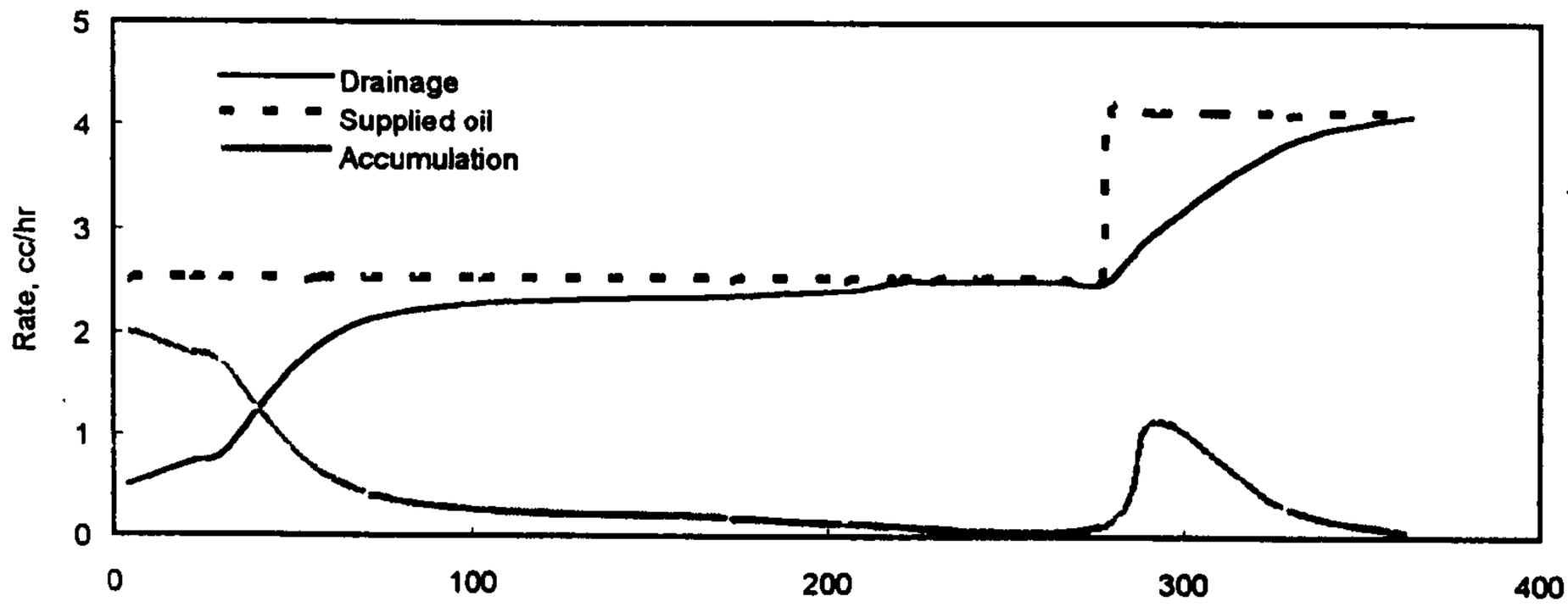

Figure 5.5-7 Drainage, supplied oil and accumulation rate vs. time (linear scale) for Case 3.

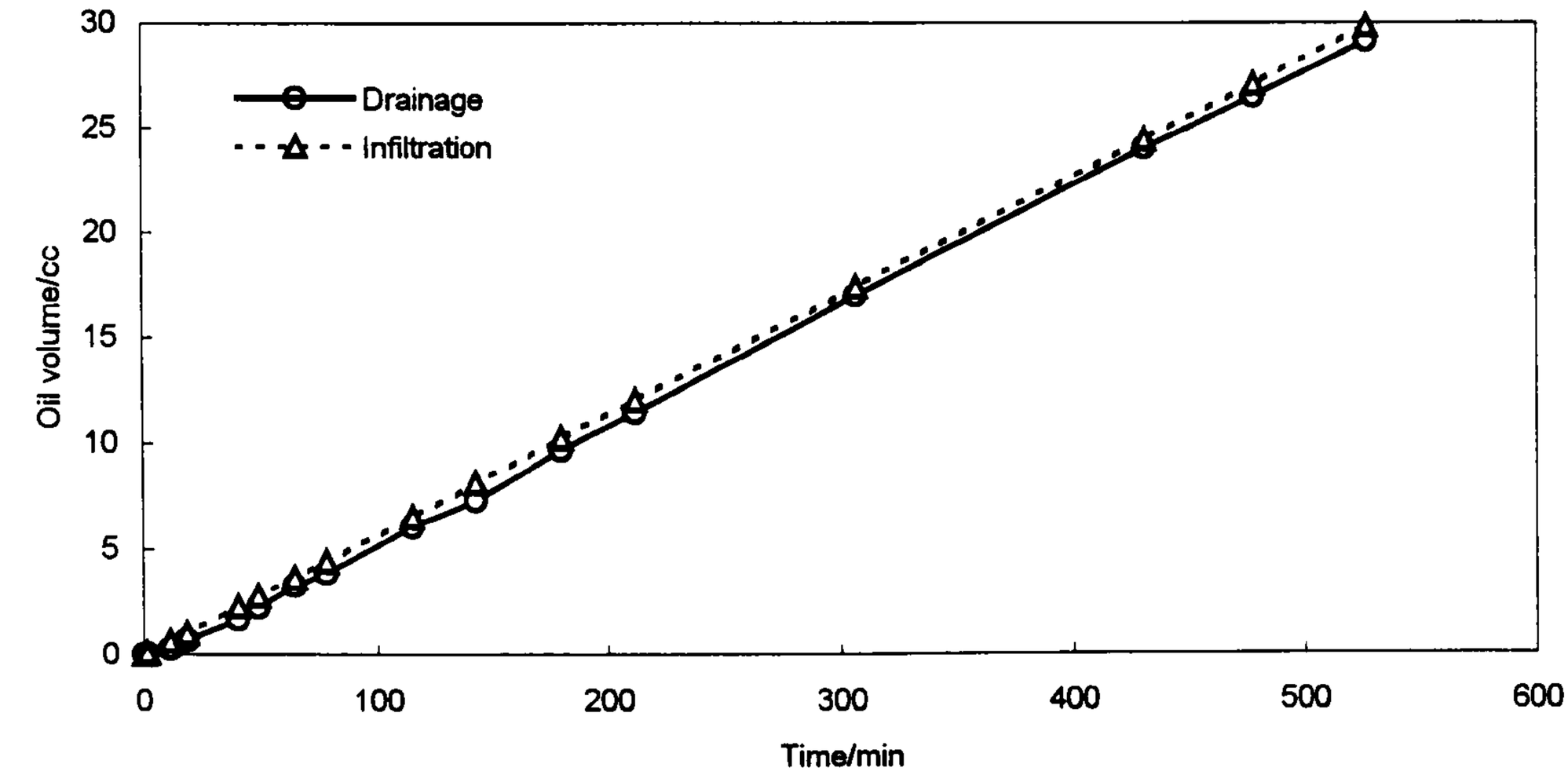

Figure 5.5-8 Drainage and infiltration vs. time for Case4.

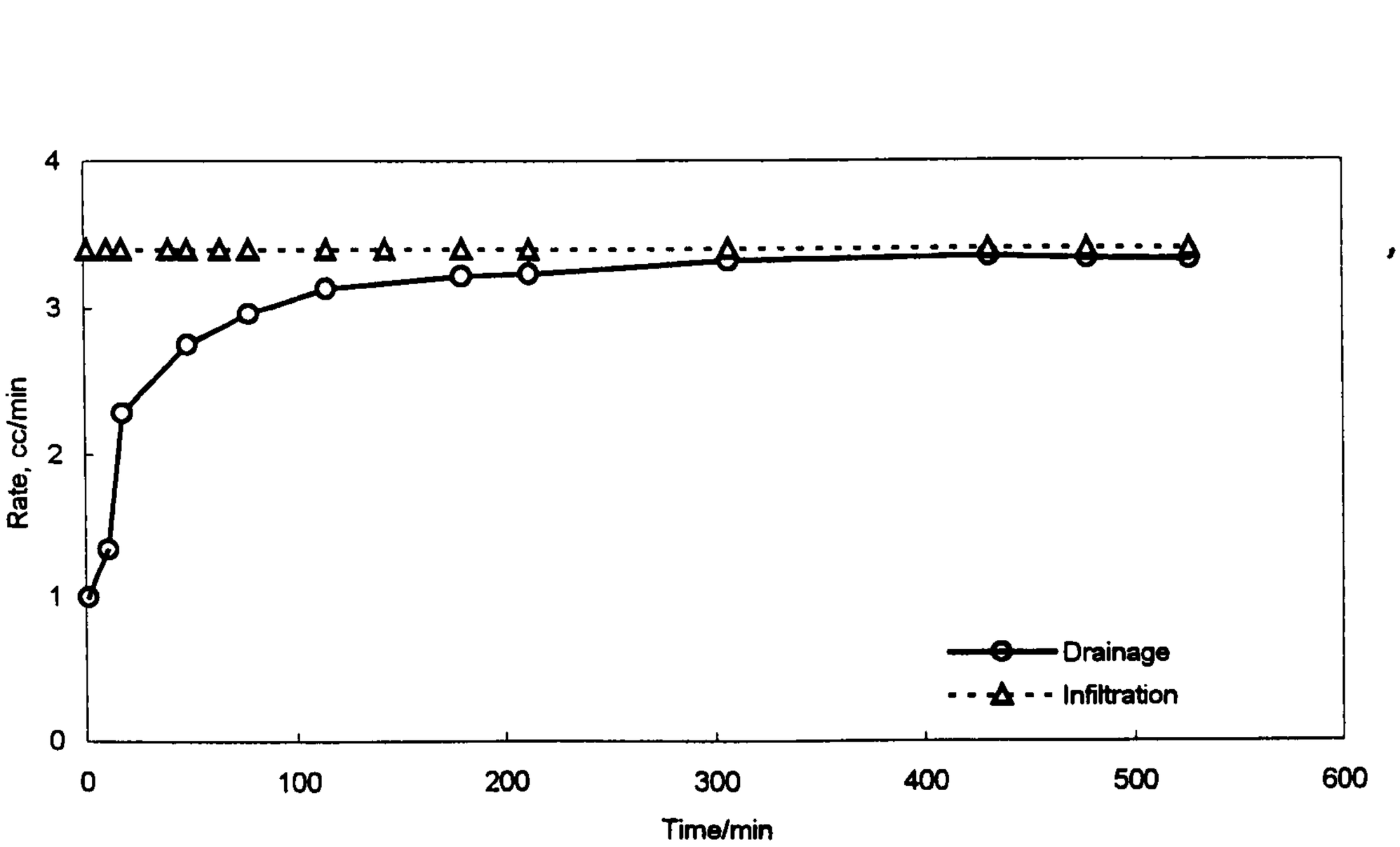

Figure 5.5-9 Drainage and infiltration rate vs. time for Case4.

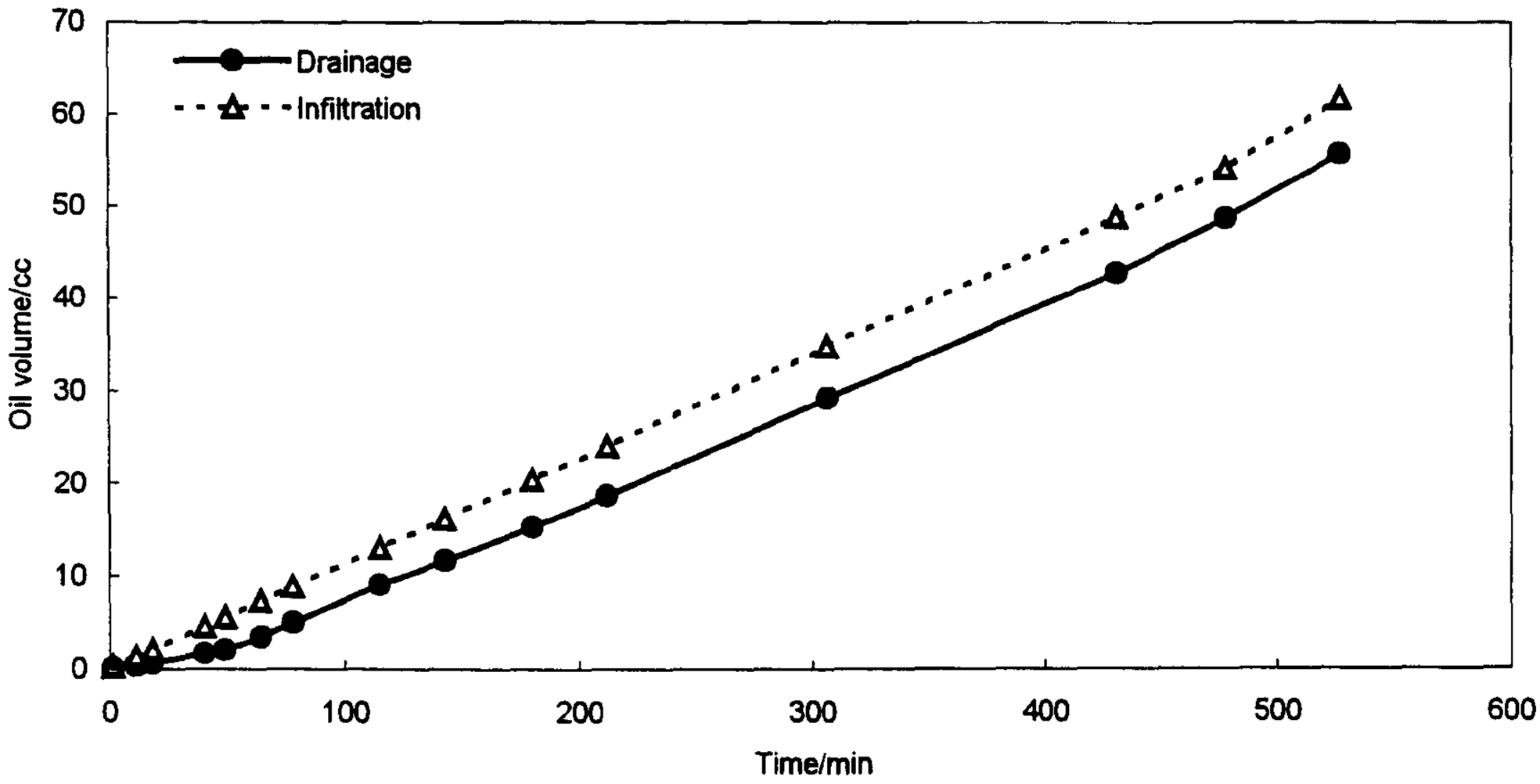

Figure 5.5-10 Drainage and infiltration versus time for Case 5.

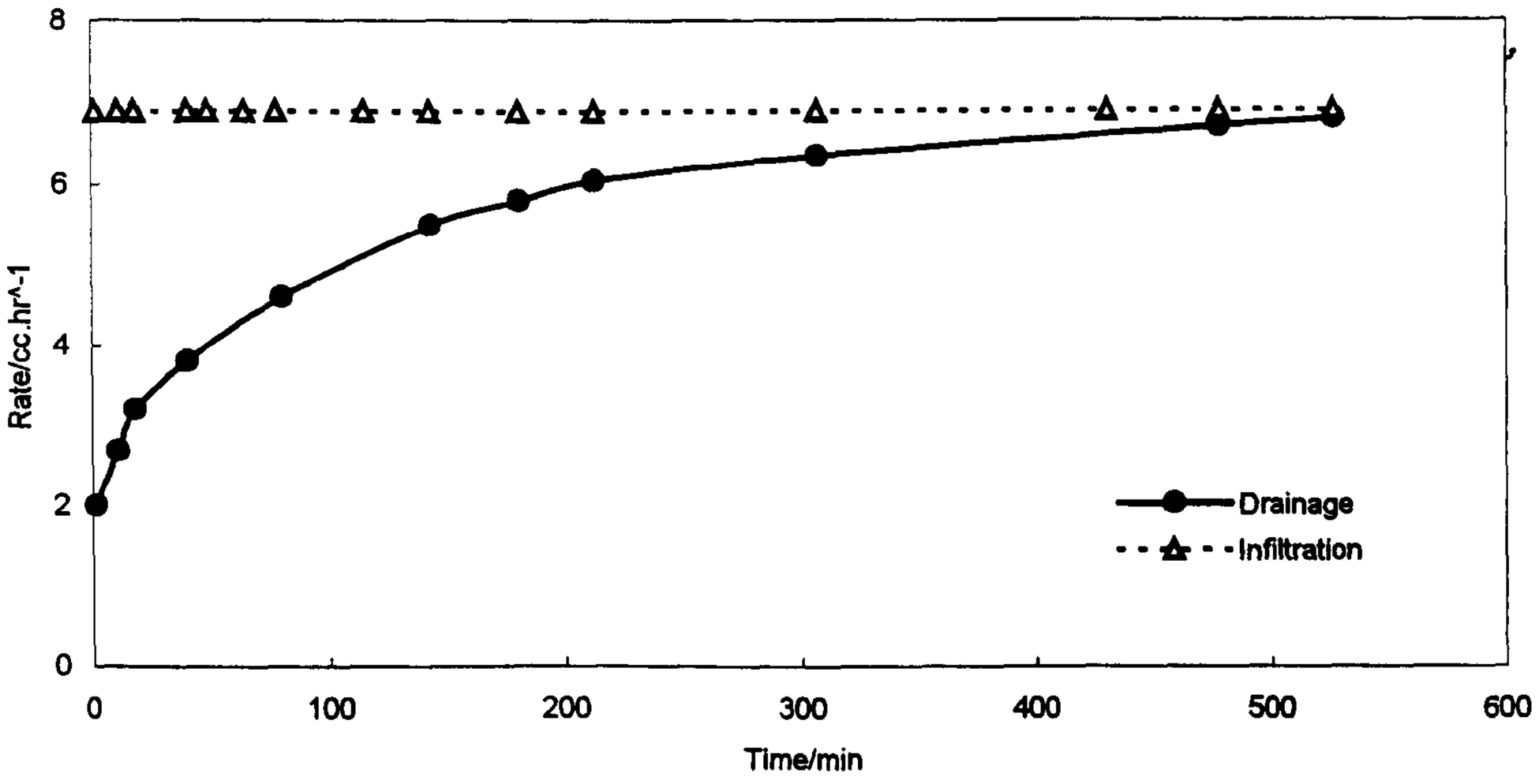

Figure 5.5-11 Drainage and infiltration rate versus time for Case 5.

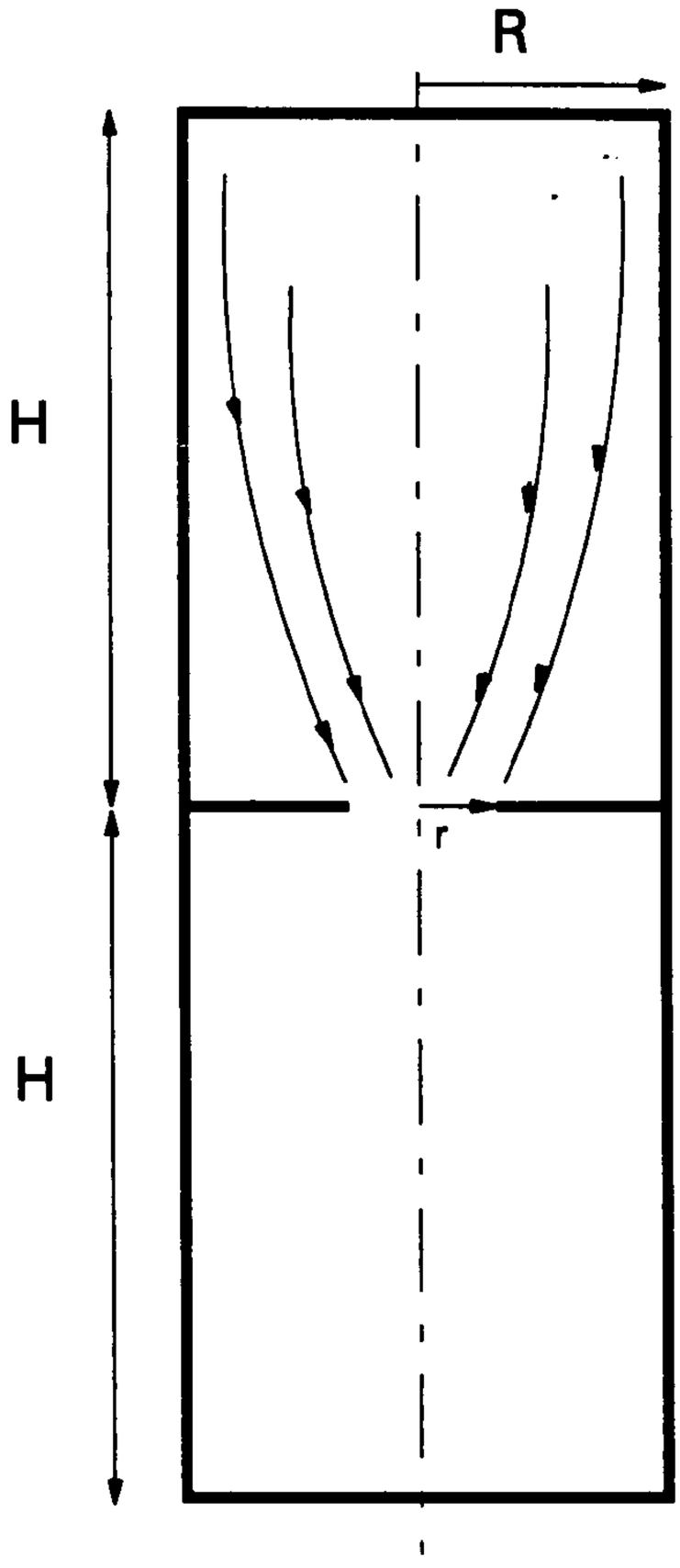

Figure 5.6-1 Geometry used in the two-block assembly for direct contact experiments.

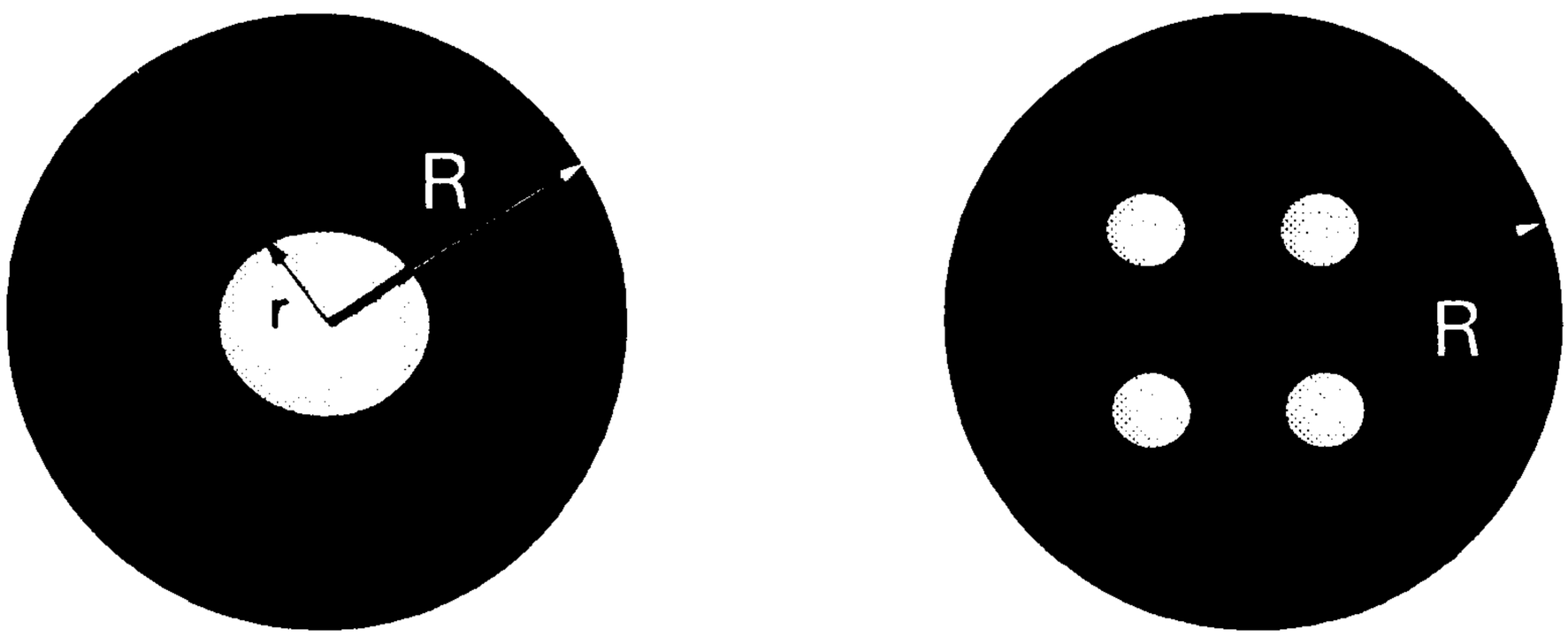

a: Concentrated

b: Dispersed

Figure 5.6-2 Geometry used in concentrated and dispersed contact-point for 20% contact area.

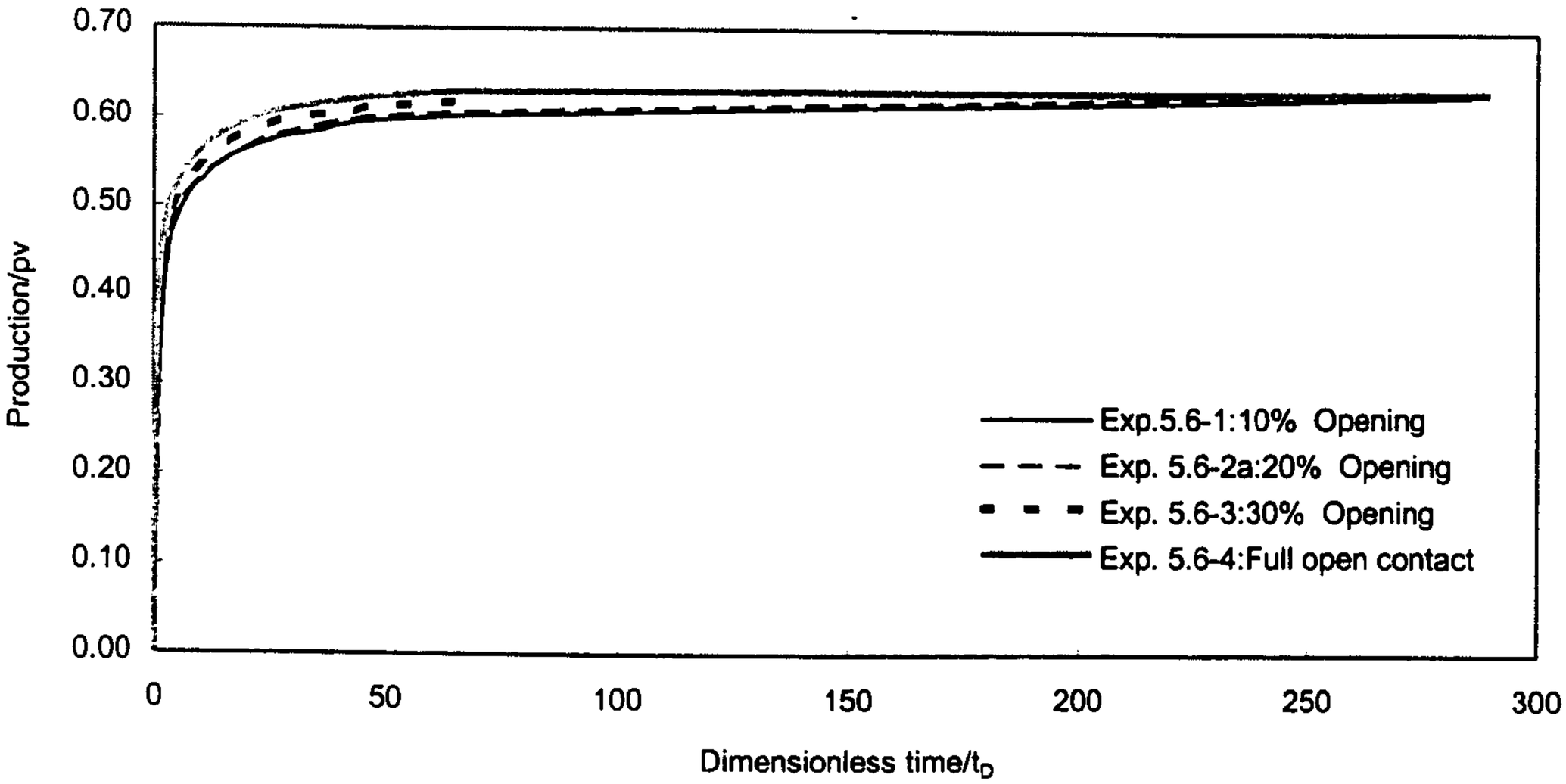

Figure 5.6-3a Production data vs. time (linear scale) for different value of contact area.

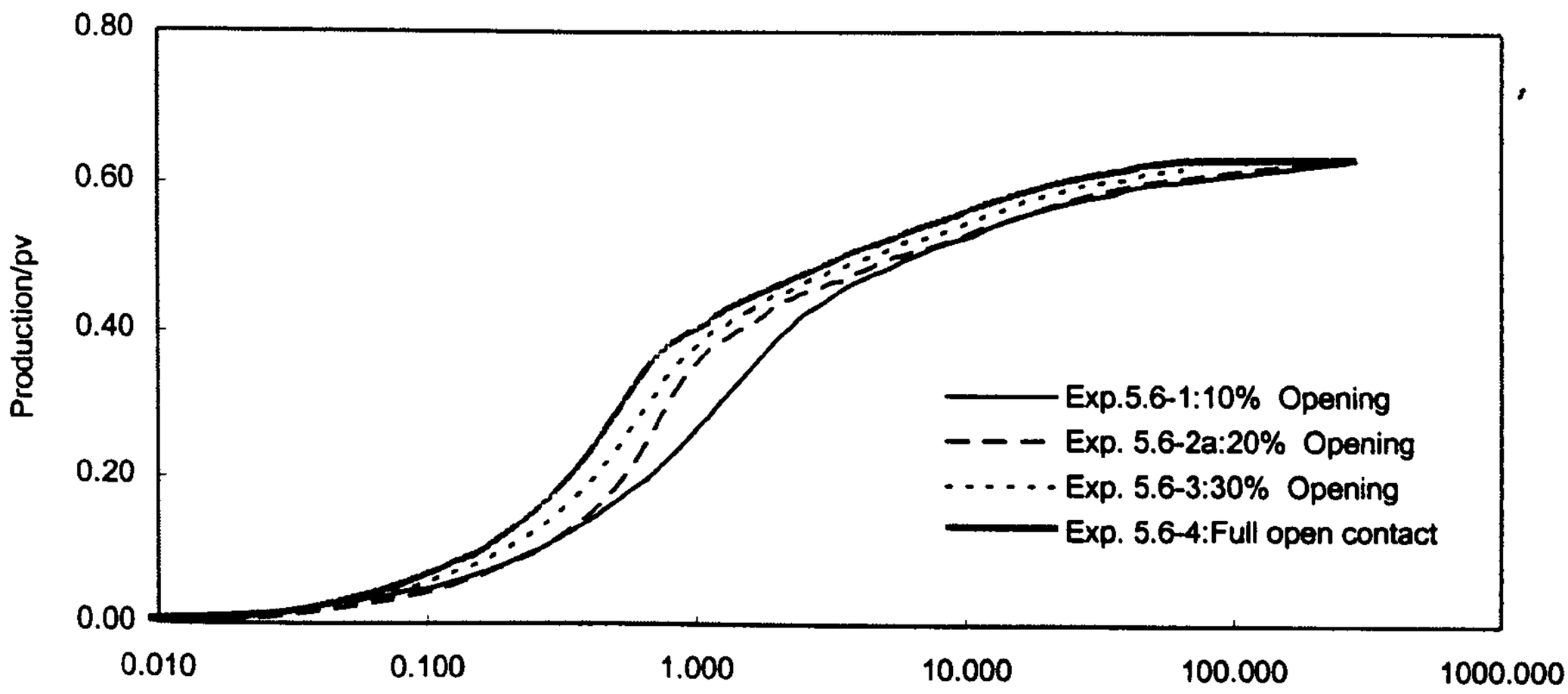

Figure 5.6-3b Production data vs. time (log scale) for different value of contact area.

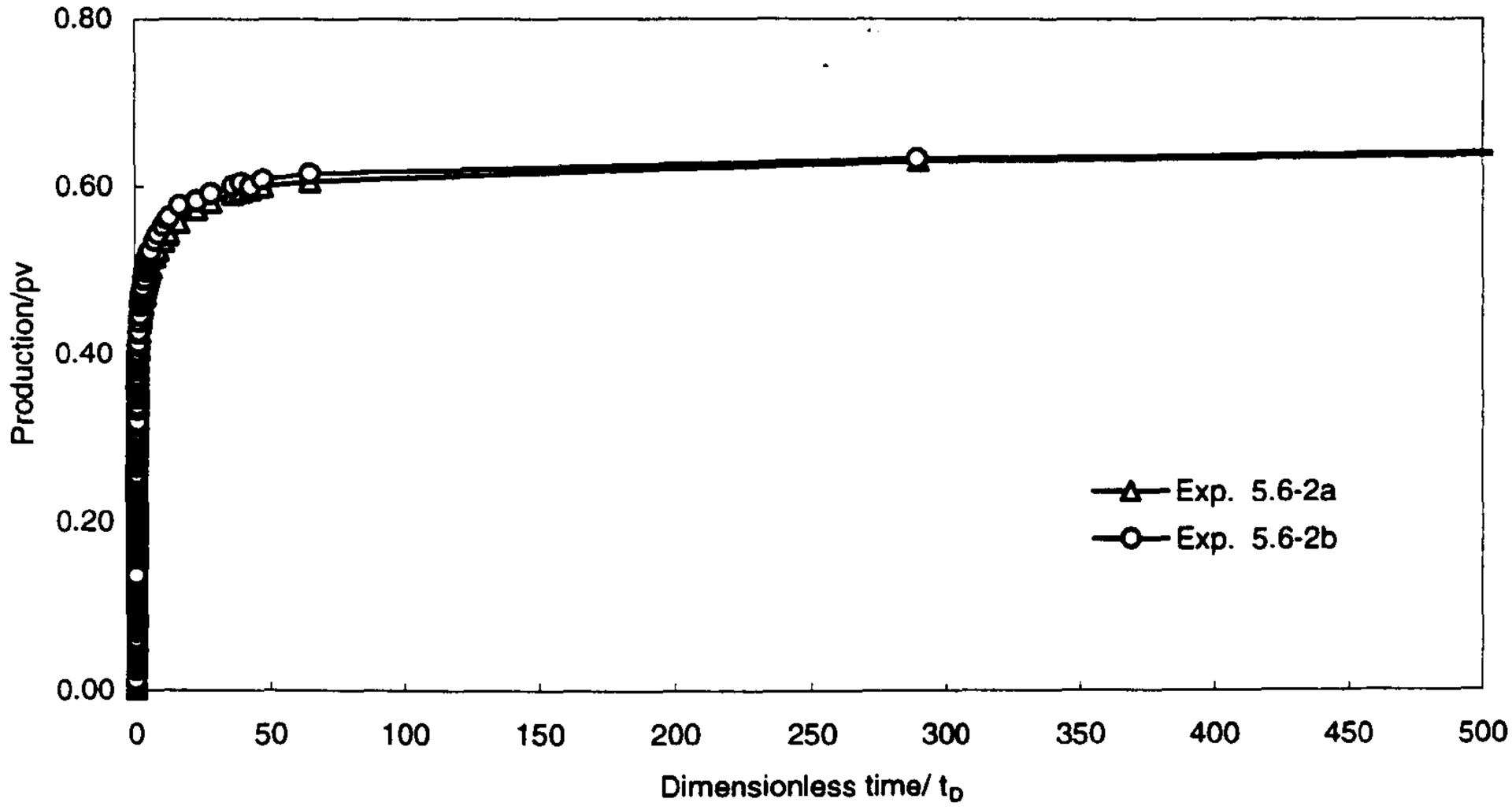

Figure 5.6-4a Comparison between recovery data vs. time (linear scale) through one central opening and four dispersed points (for 20% contact area).

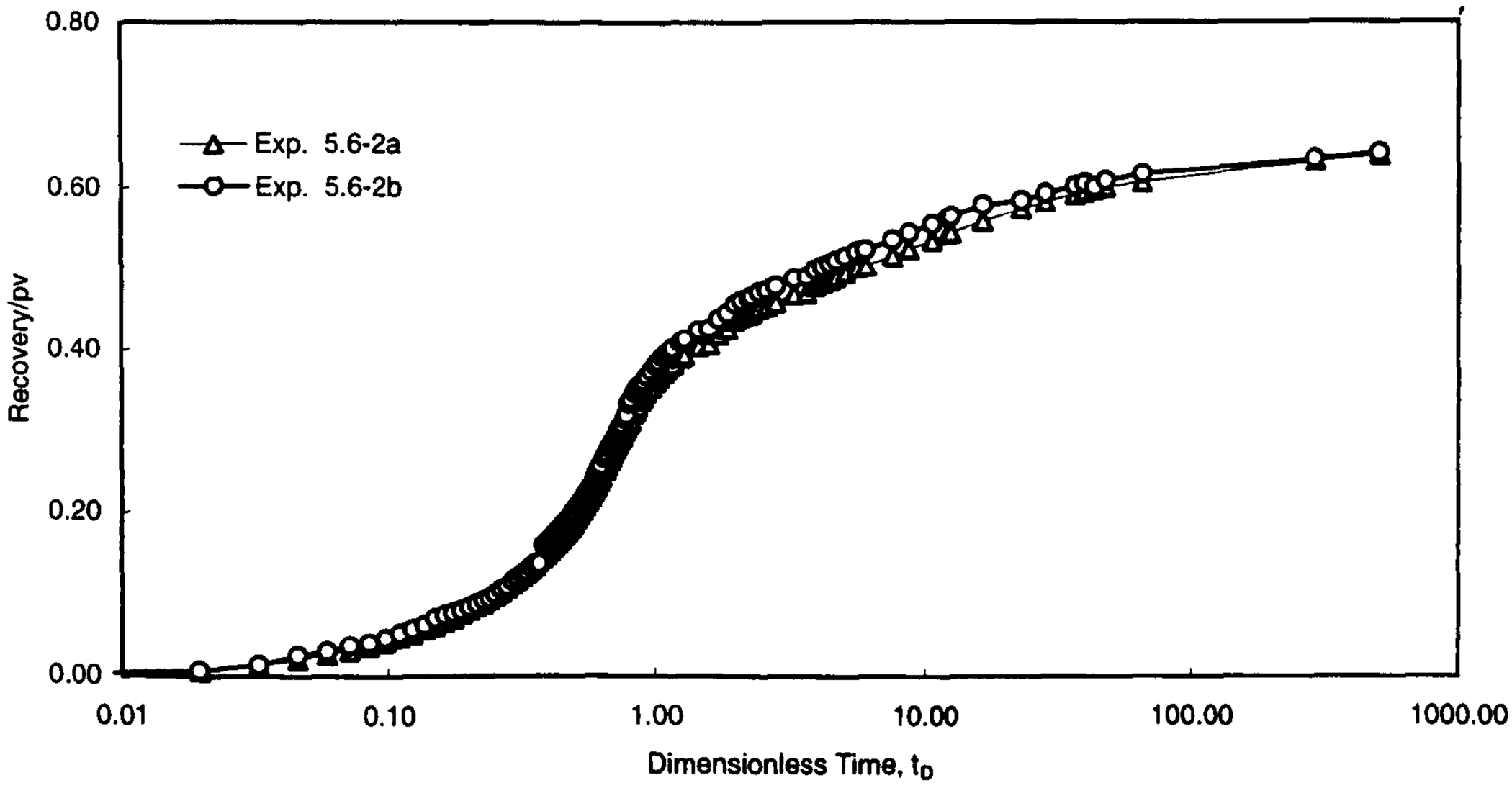

Figure 5.6-4b Comparison between recovery data vs. time (log scale) through one central opening and four dispersed points (for 20% contact area).

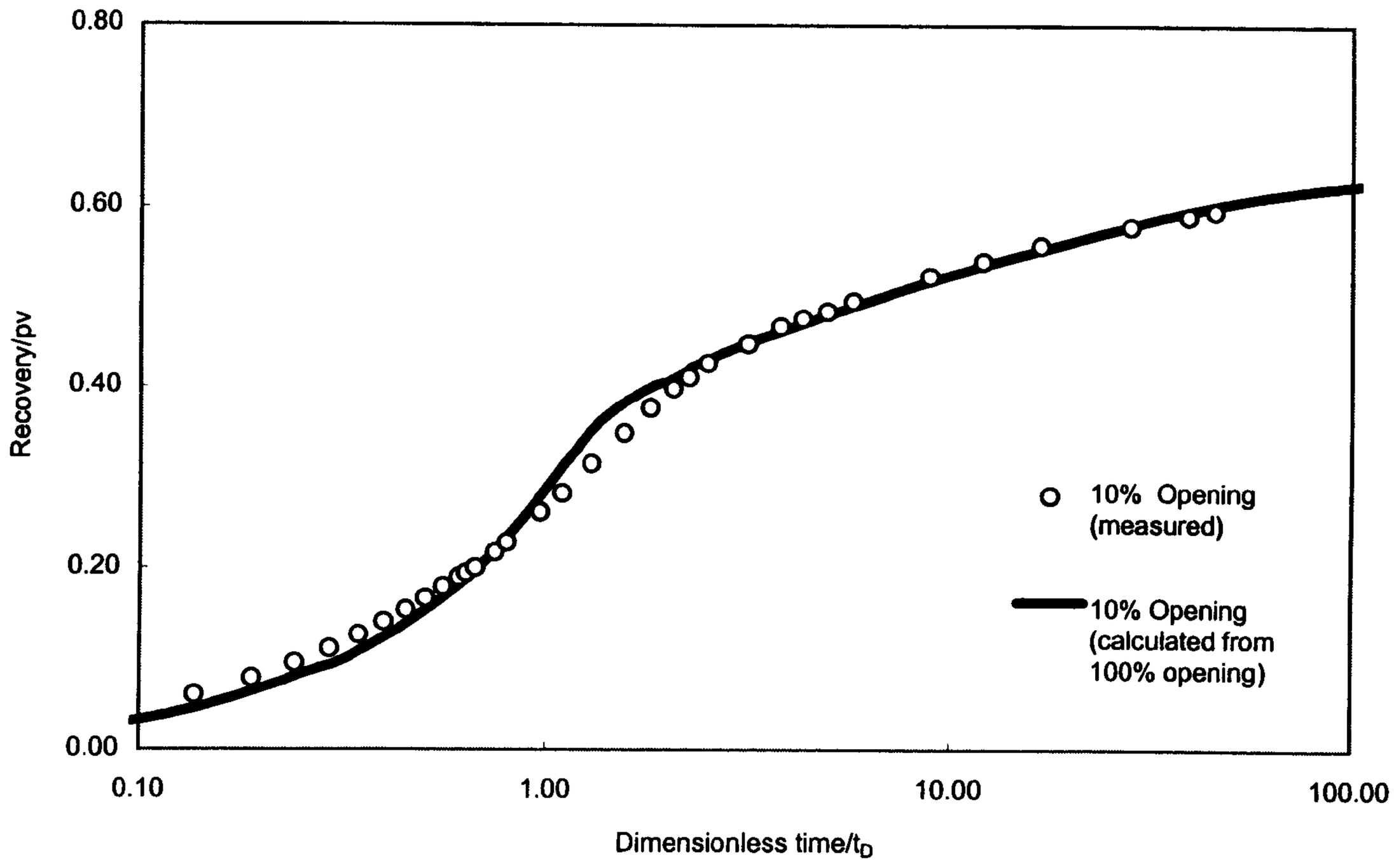

Figure 5.6-5 Comparison between measured and calculated oil recovery for Experiment 5.6-1.

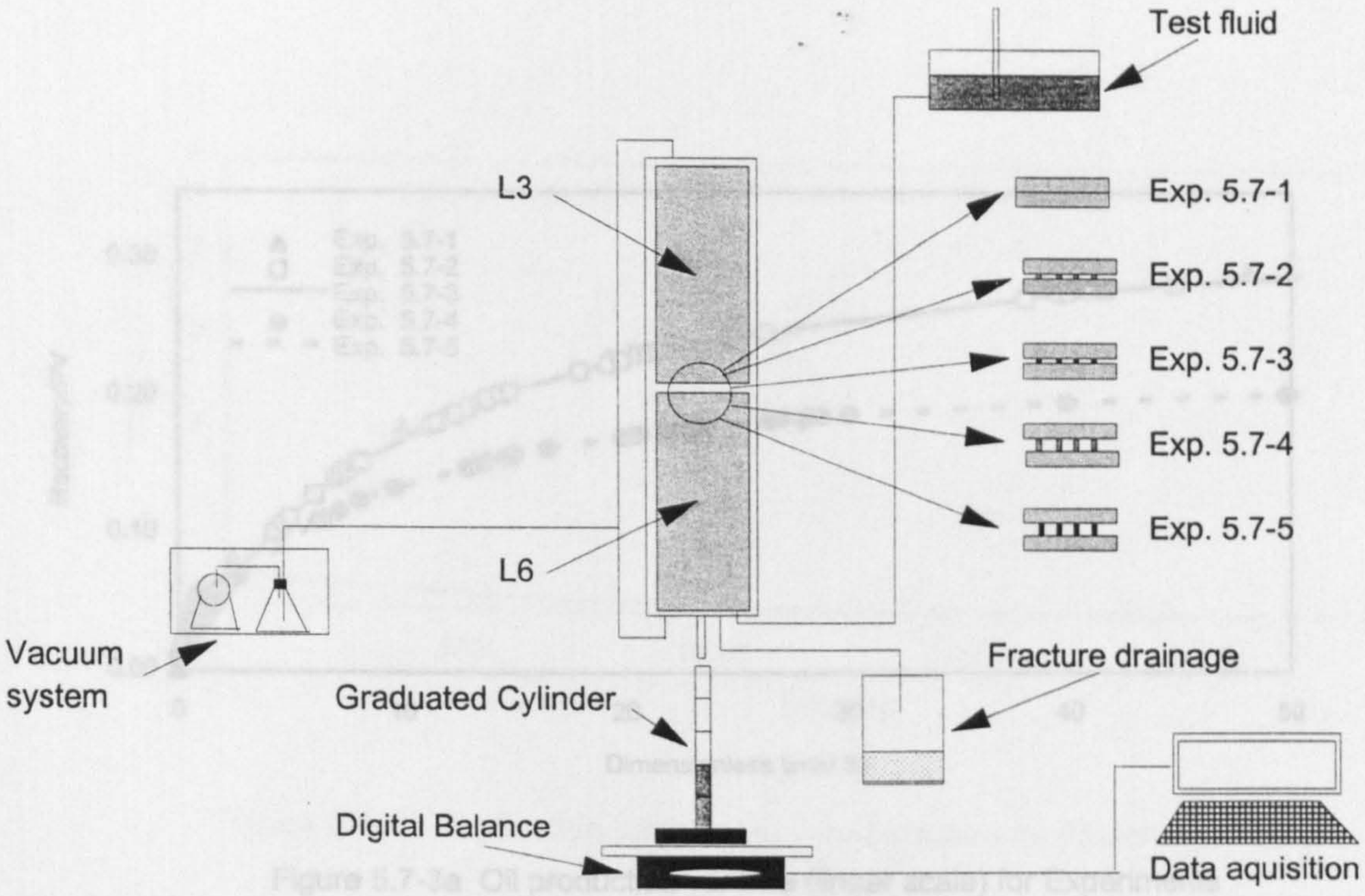

Figure 5.7-1 Apparatus schematic for Case1.

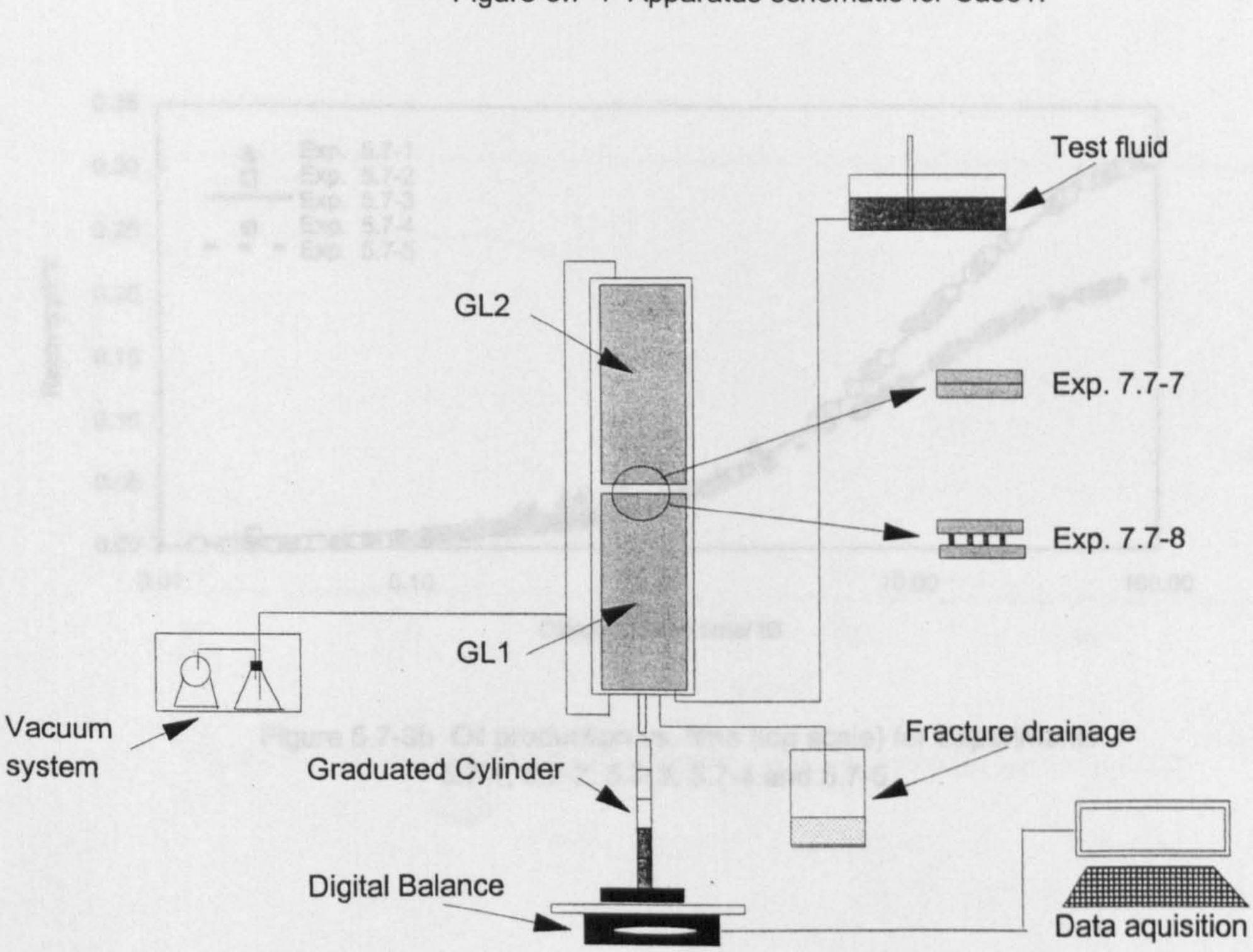

Figure 5.7-2 Apparatus schematic for Case2.

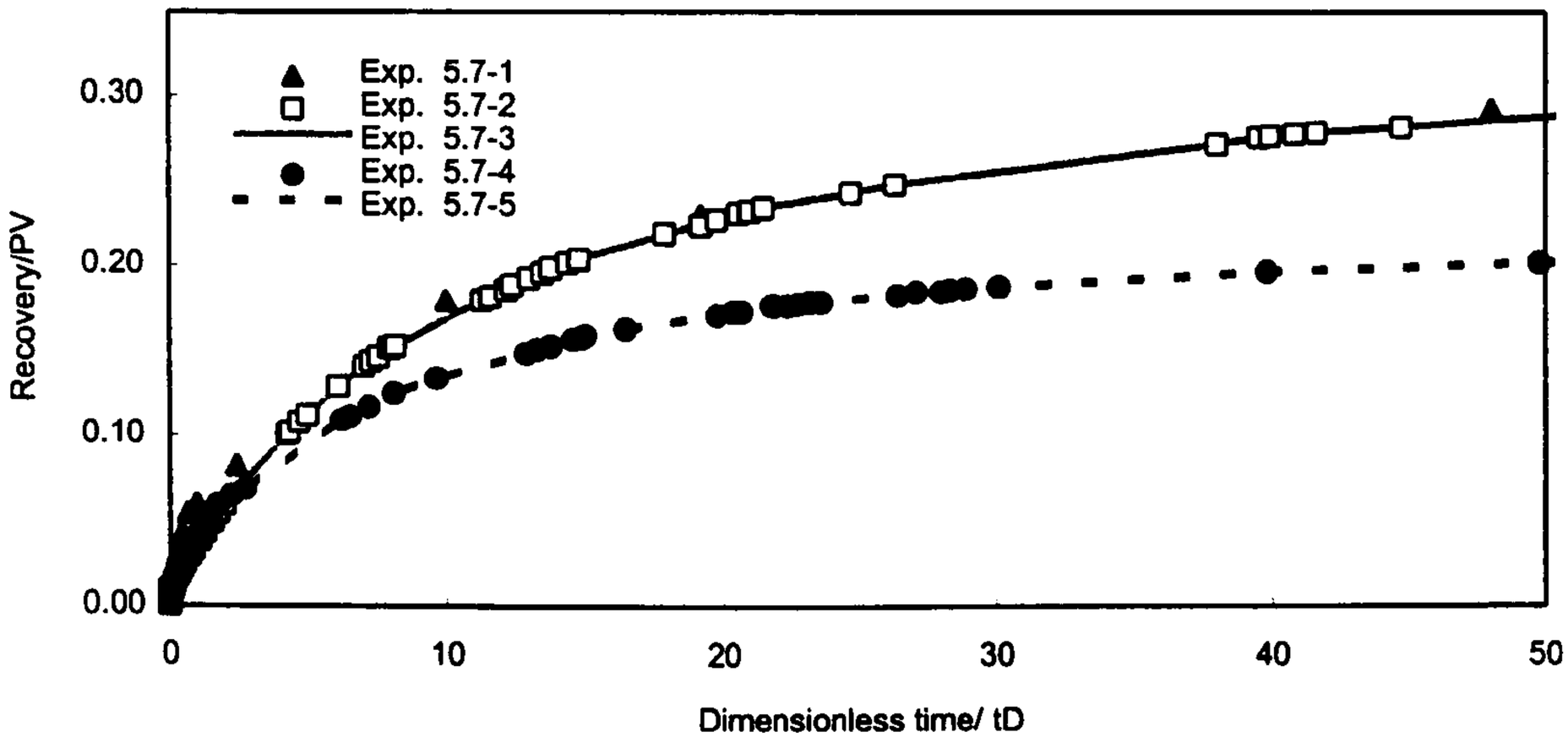

Figure 5.7-3a Oil production vs. time (linear scale) for Experiments 5.7-1, 5.7-2, 5.7-3, 5.7-4 and 5.7-5.

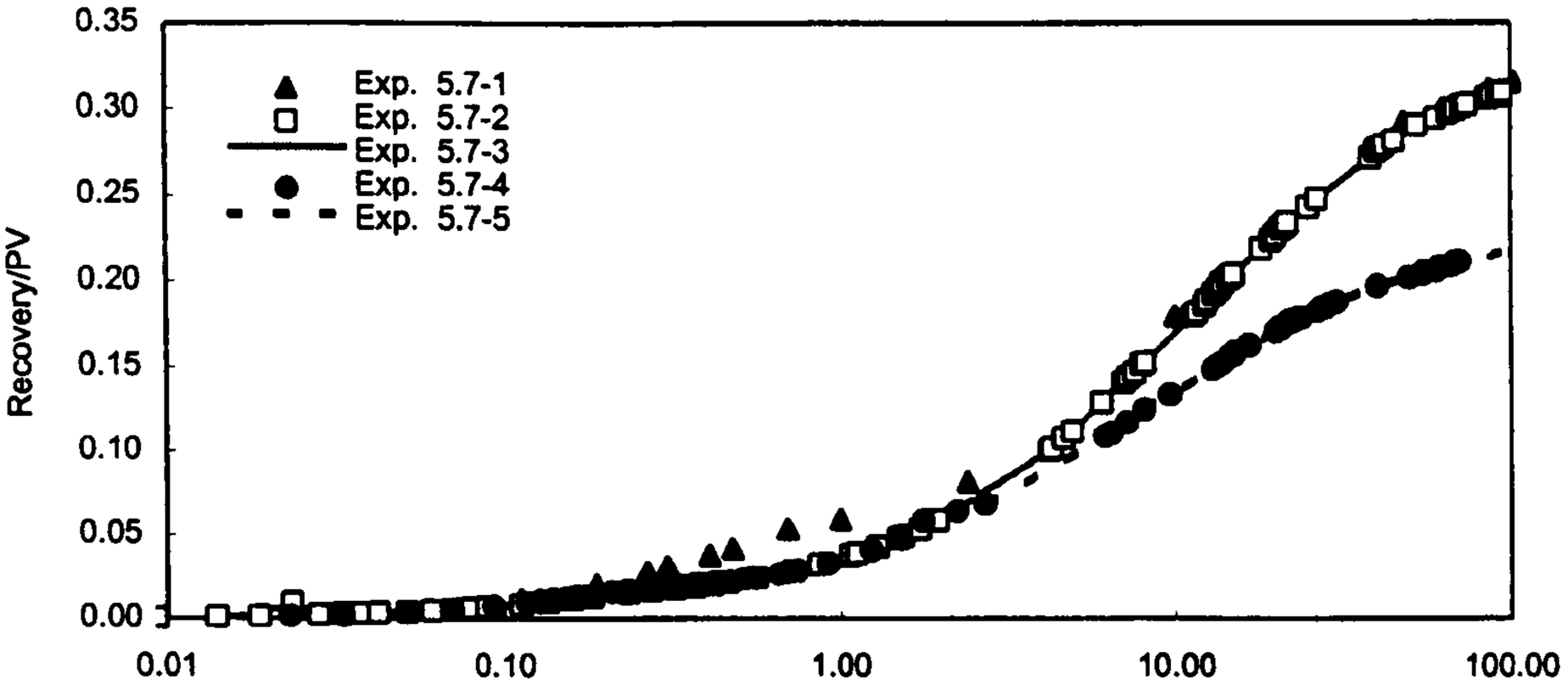

Figure 5.7-3b Oil production vs. time (log scale) for Experiments 5.7-1, 5.7-2, 5.7-3, 5.7-4 and 5.7-5.

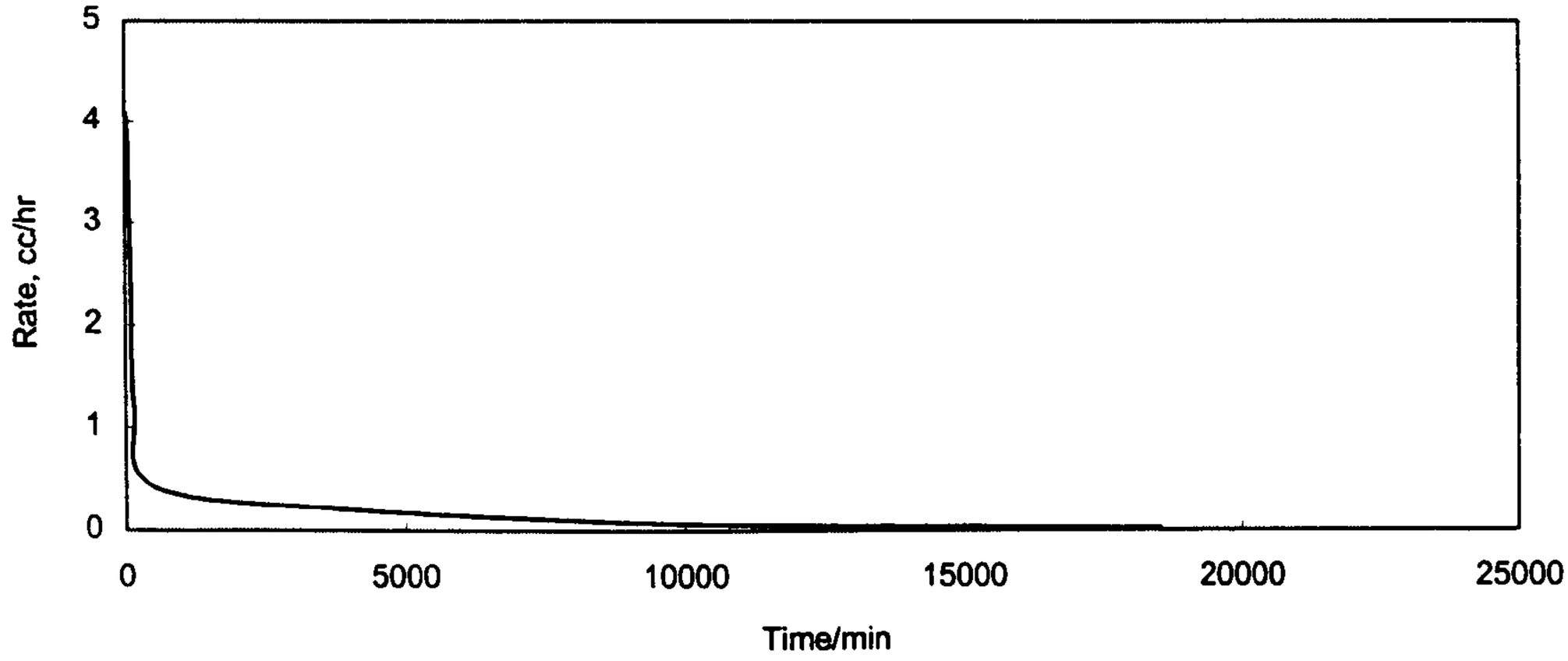

Figure 5.7-4a Production rate vs. time (linear scale) for Experiment 5.7-1.

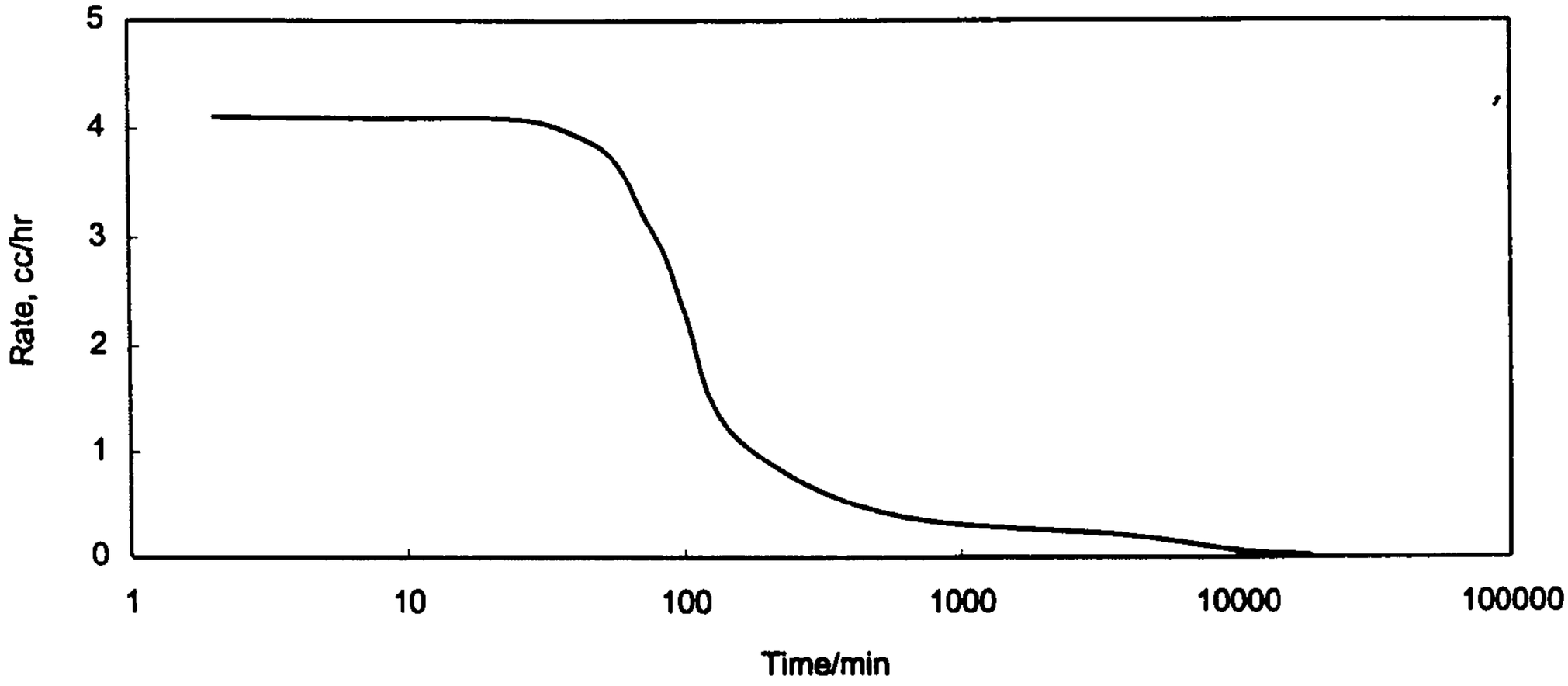

Figure 5.7-4b Production rate vs. time (log scale) form Experiment 5.7-1.

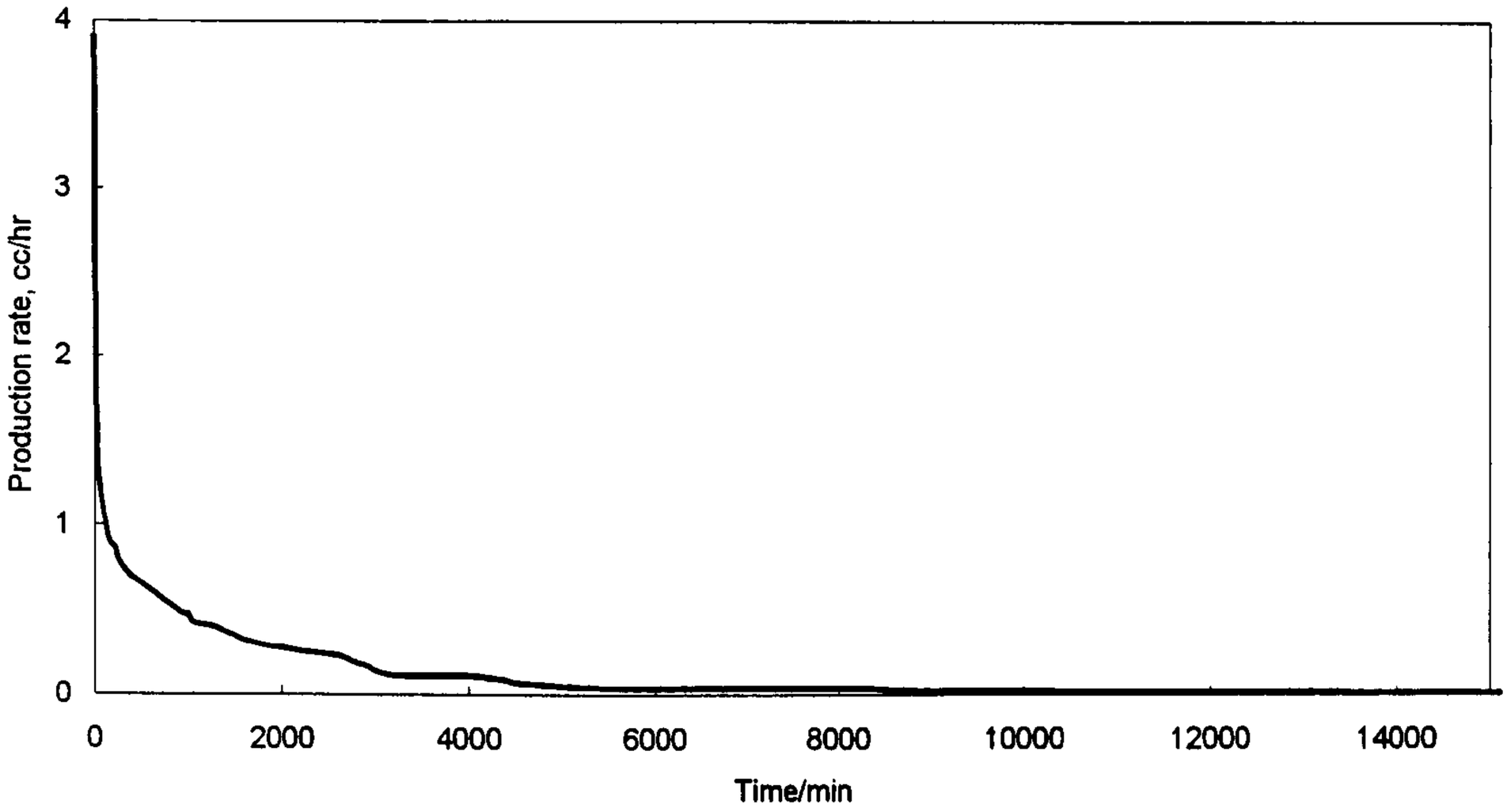

Figure 5.7-5a Production rate vs. time (linear scale) for Experiment 5.7-2.

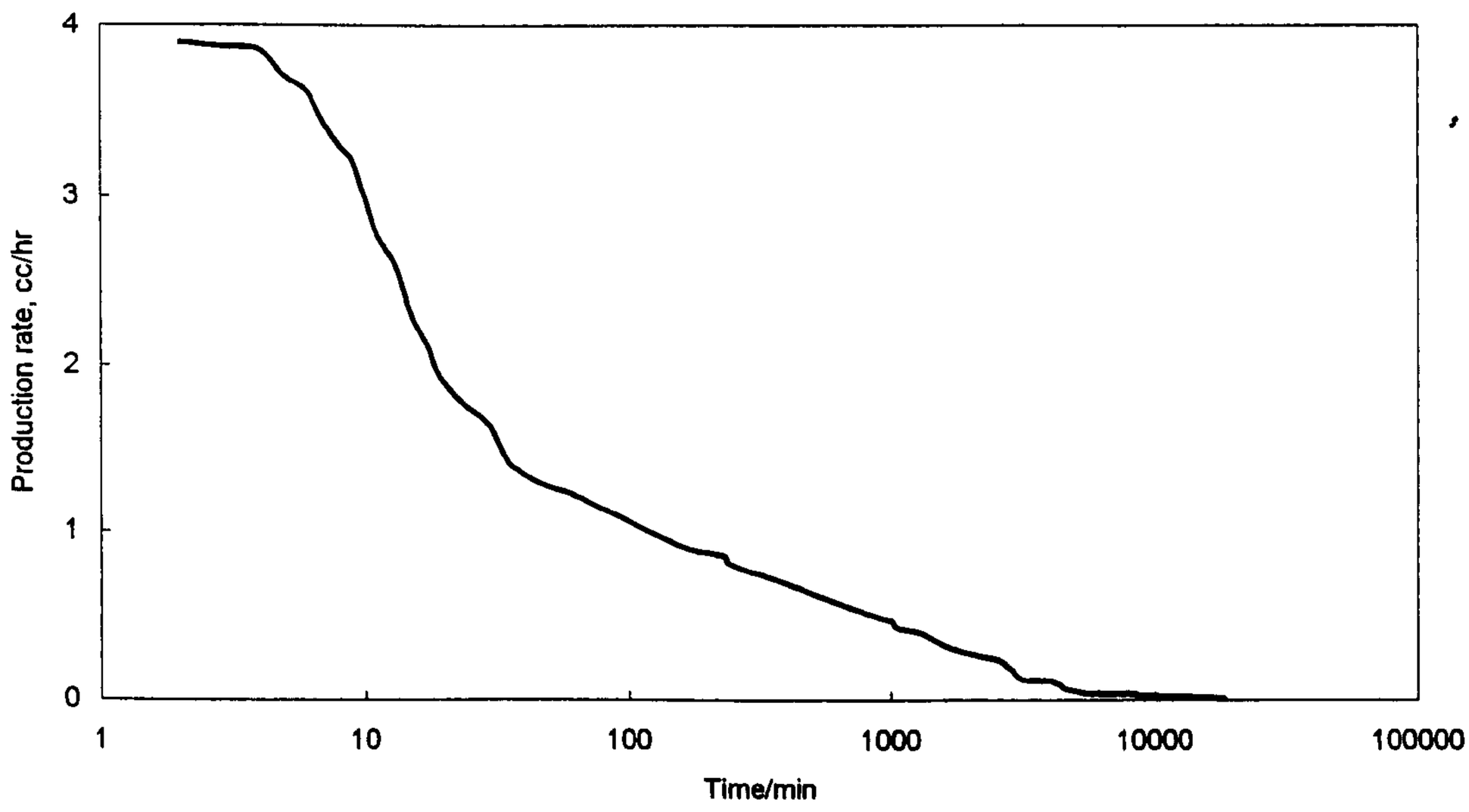

Figure 5.7-5b Production rate vs. time (log scale) for Experiment 5.7-2.

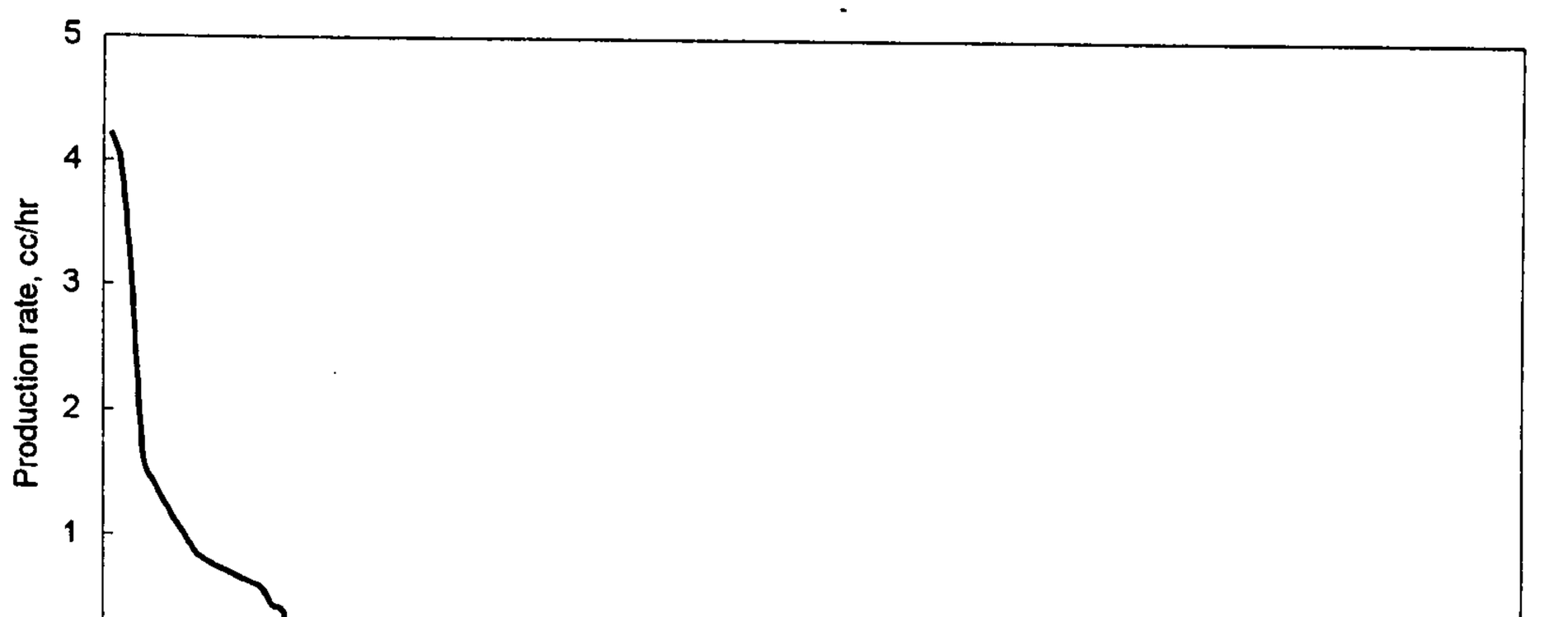

Figure 5.7-6a Production rate vs. time (linear scale) for Experiment 5.7-5.

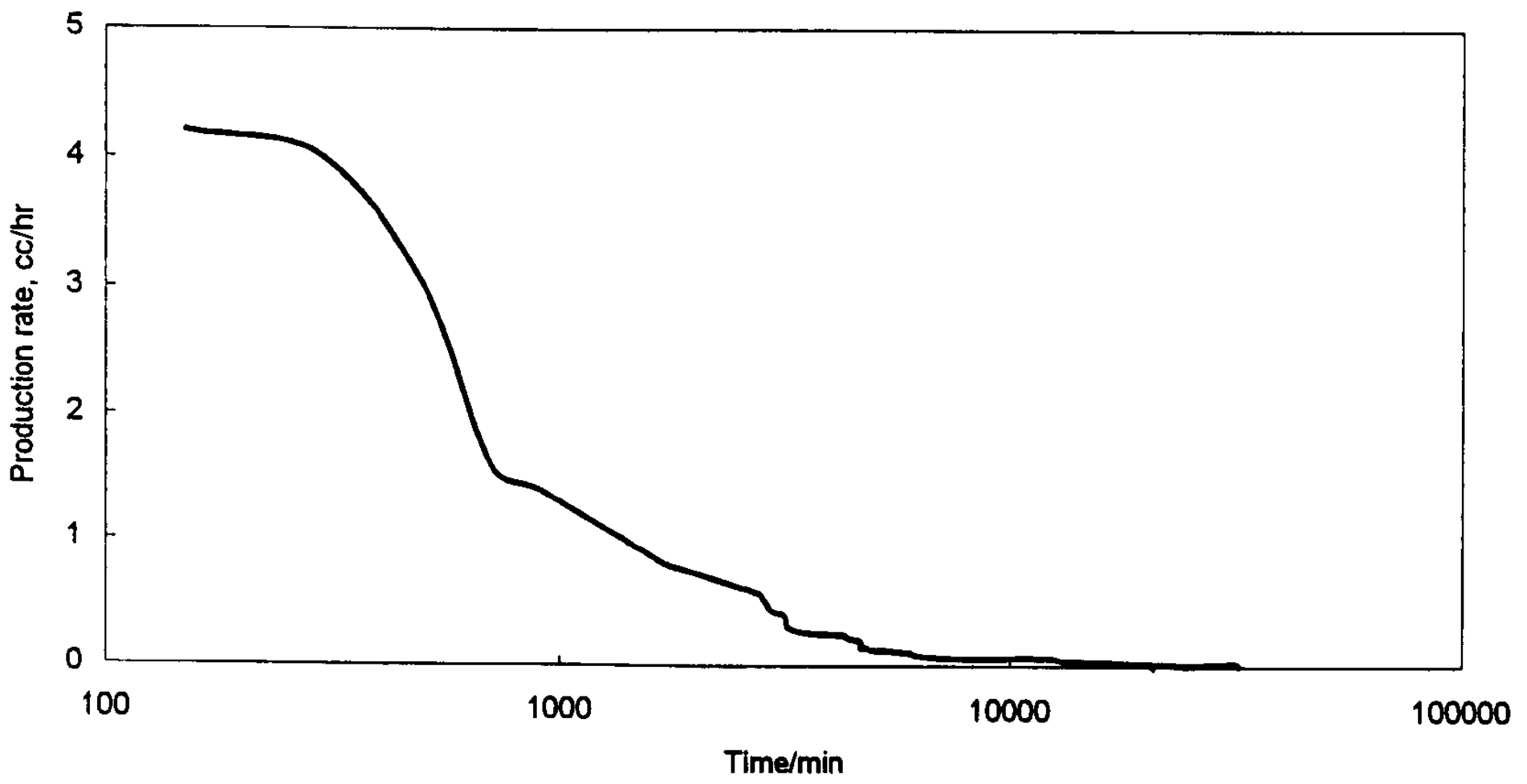

Figure 5.7-6b Production rate vs. time (log scale) for Experiment 5.7-5.

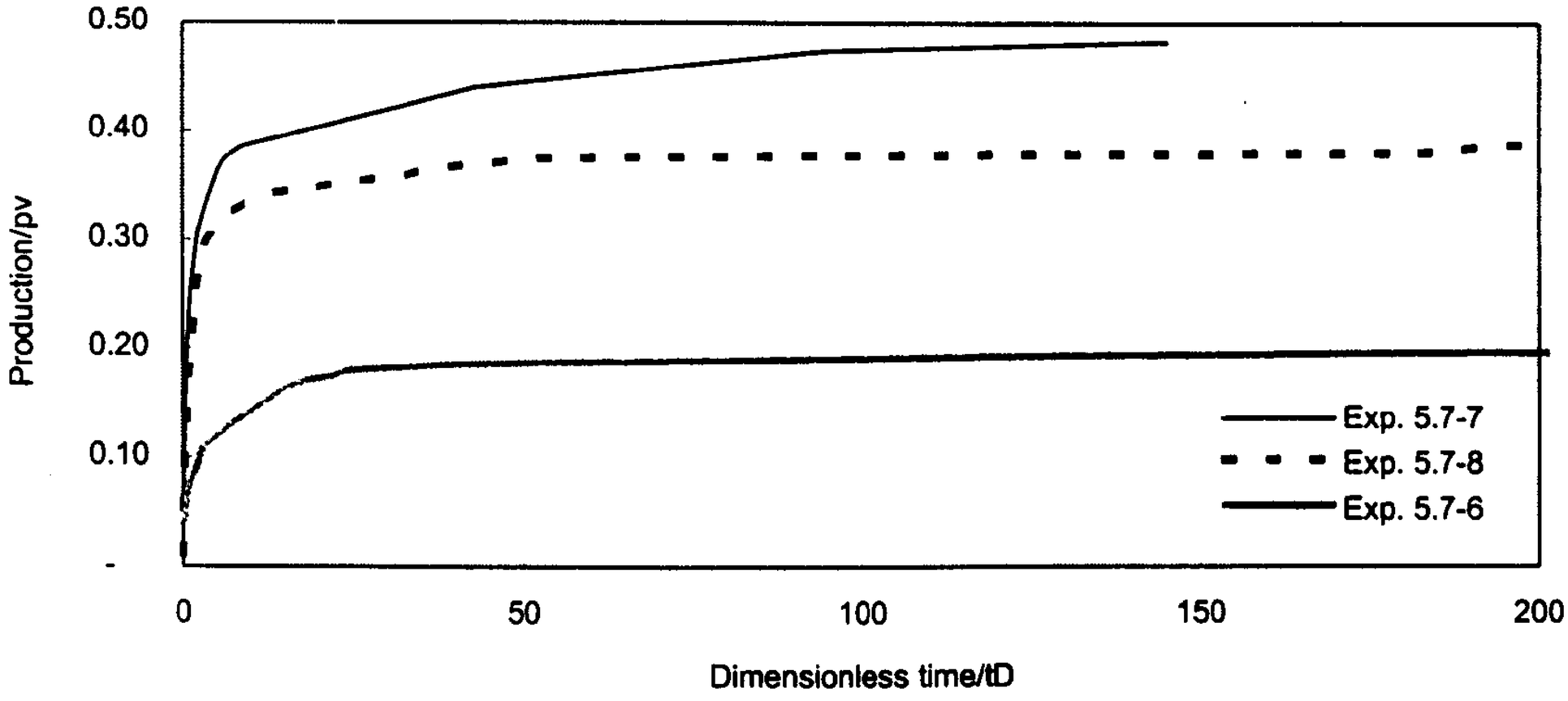

Figure 5.7-7a Production vs. time (linear scale) for Experiments 5.7-6, 5.7-7, 5.7-8.

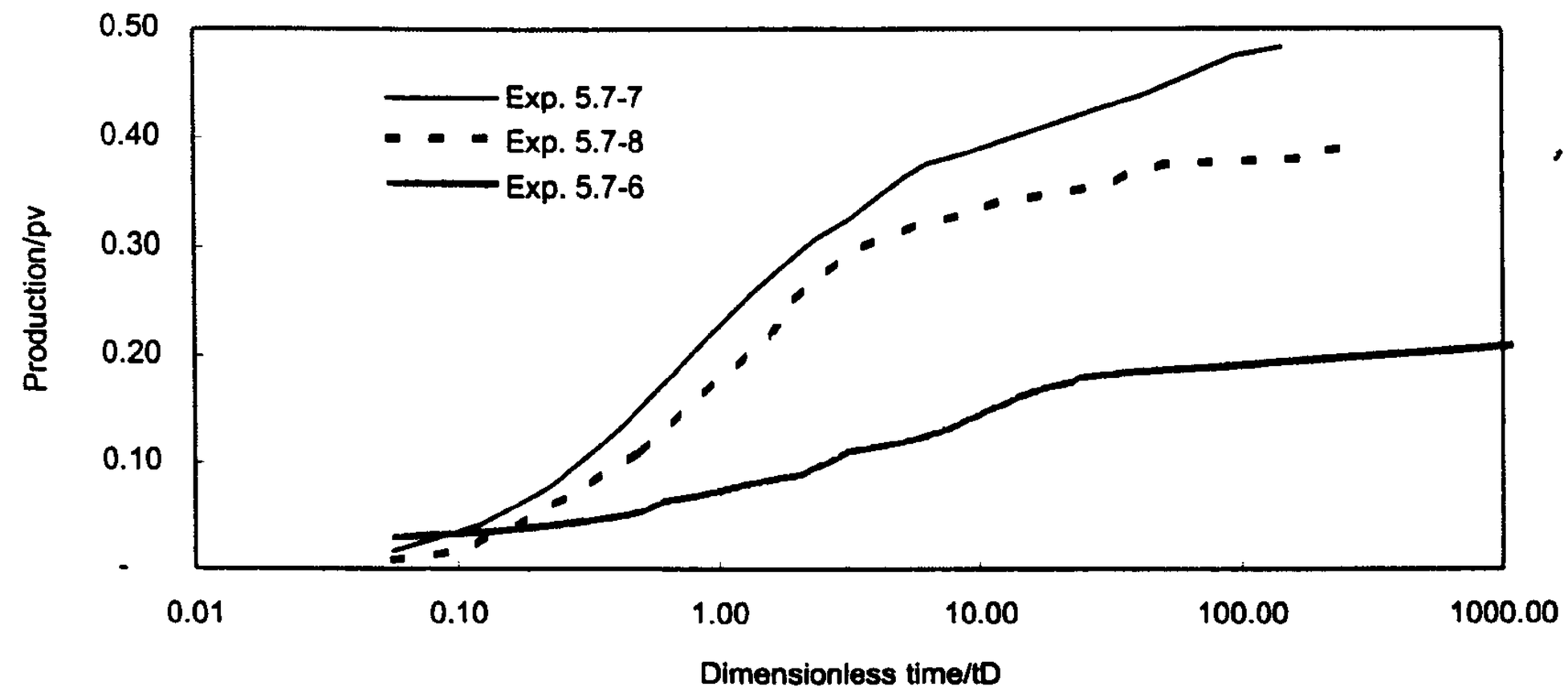

Figure 5.7-7b Production vs. time (log scale) for Experiments 5.7-6, 5.7-7, 5.7-8.

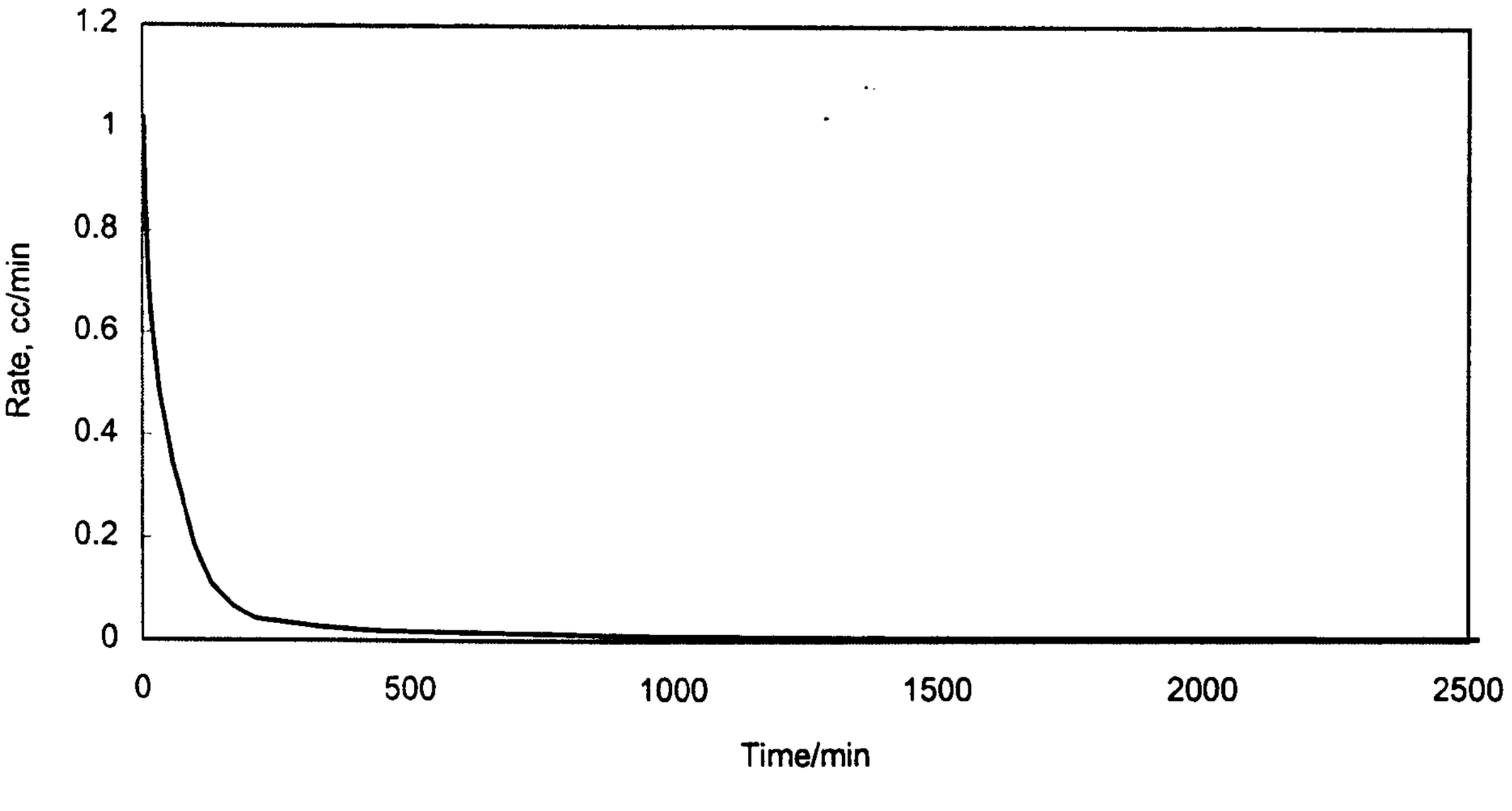

Figure 5.7-8a Production rate vs. time (linear scale) for Experiment 5.7-6.

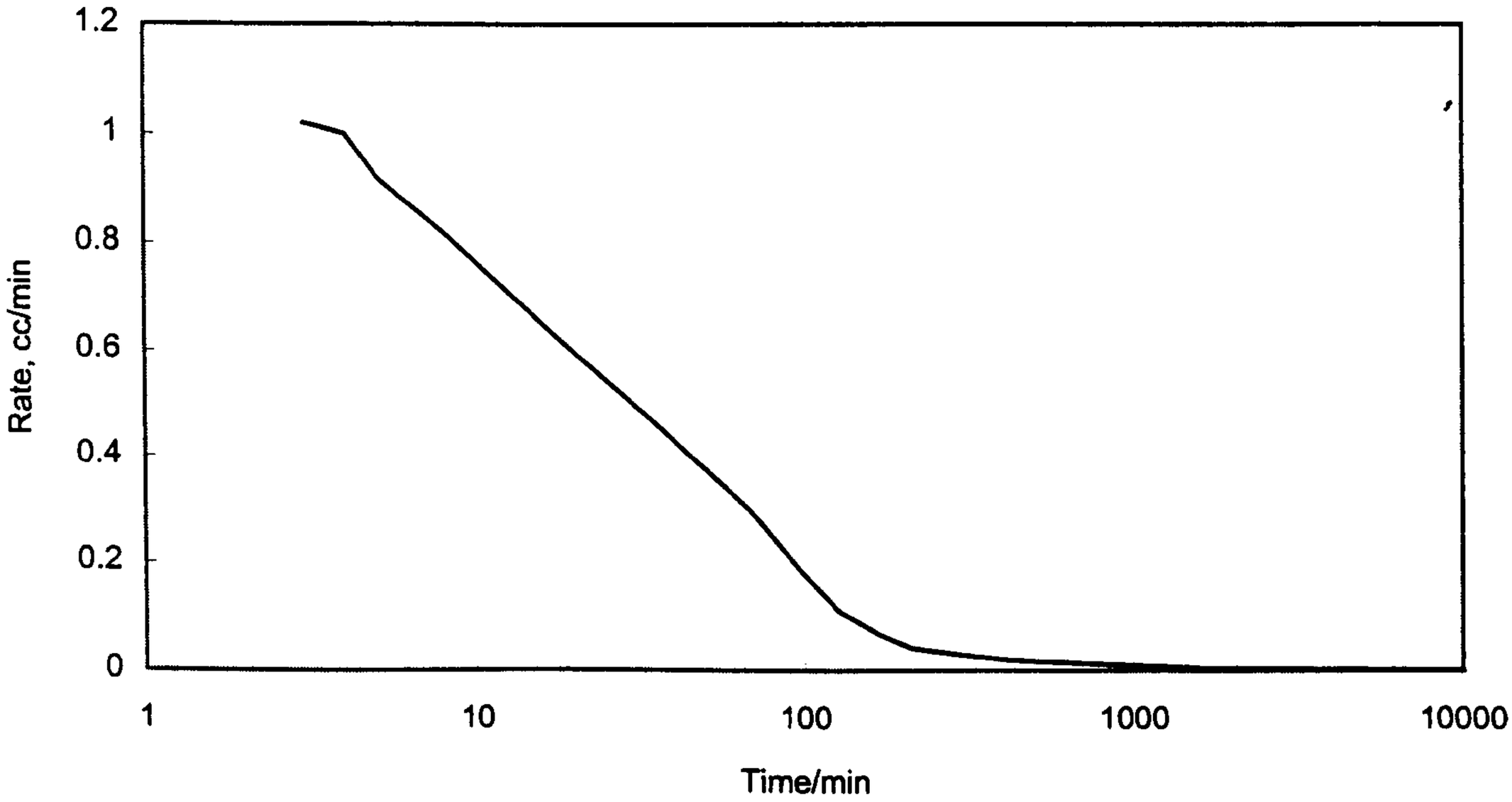

Figure 5.7-8b Production rate vs. time (log scale) for Experiment 5.7-6.

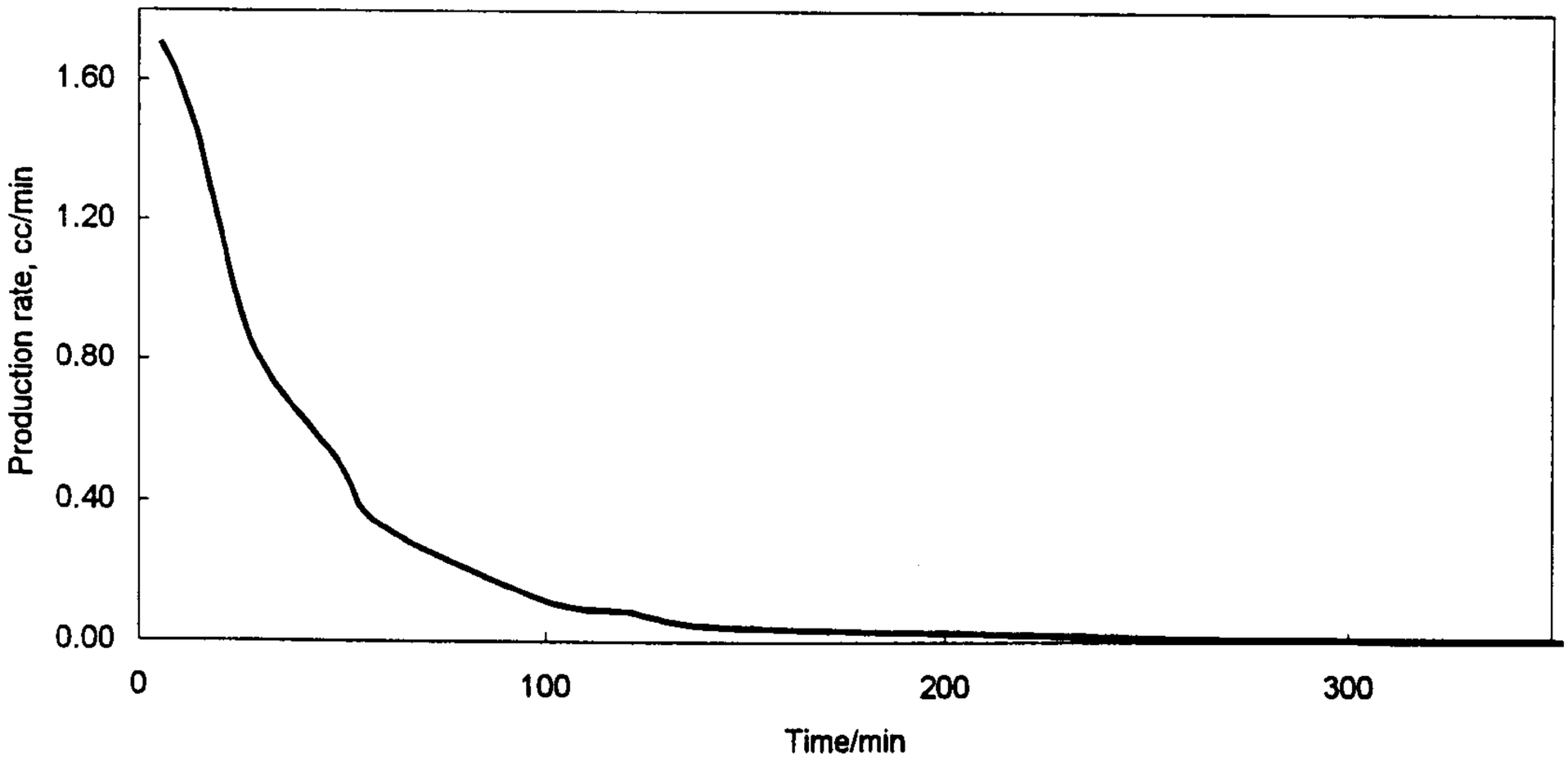

Figure 5.7-9a Production rate vs. time (linear scale) for Experiment 5.7-7.

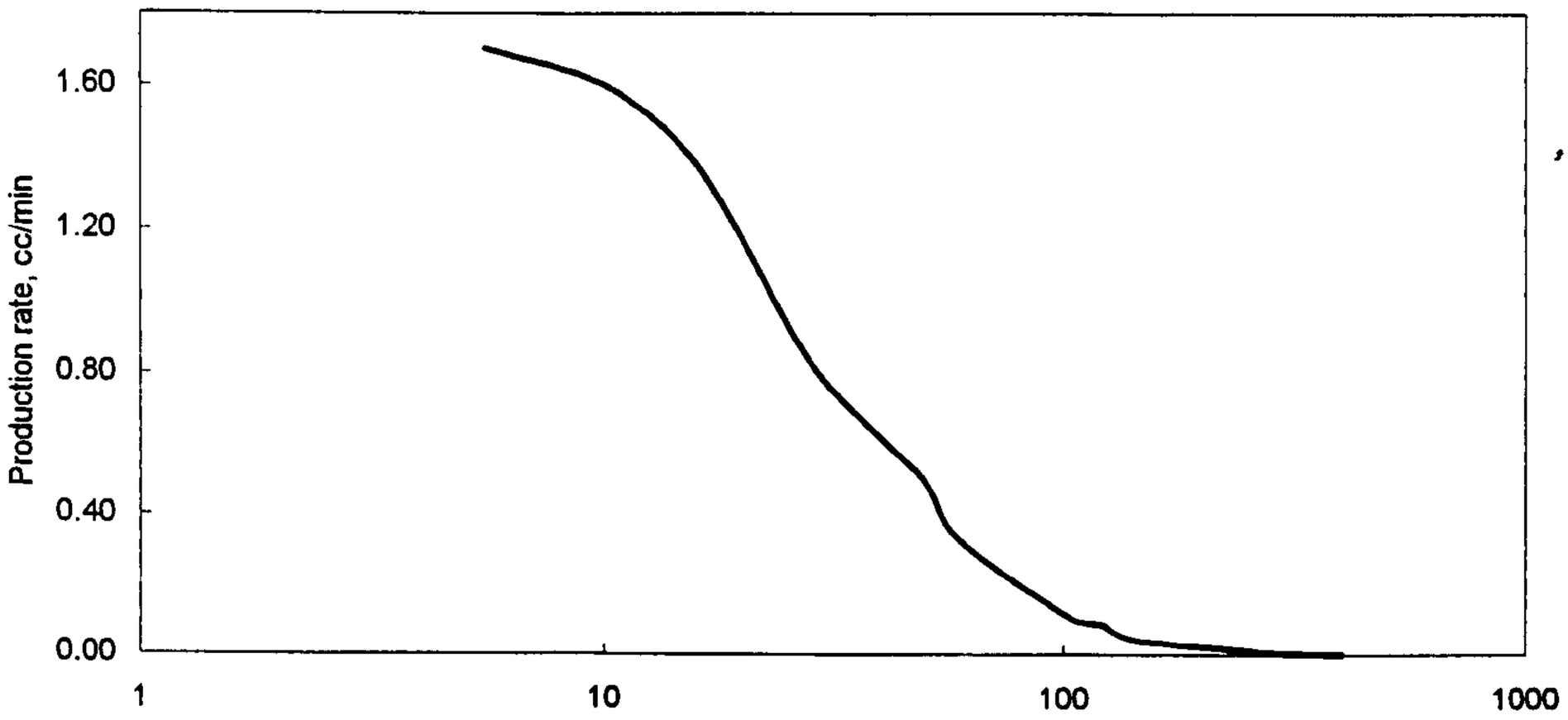

Figure 5.7-9b Production rate vs. time (log scale) for Experiment 5.7-7.

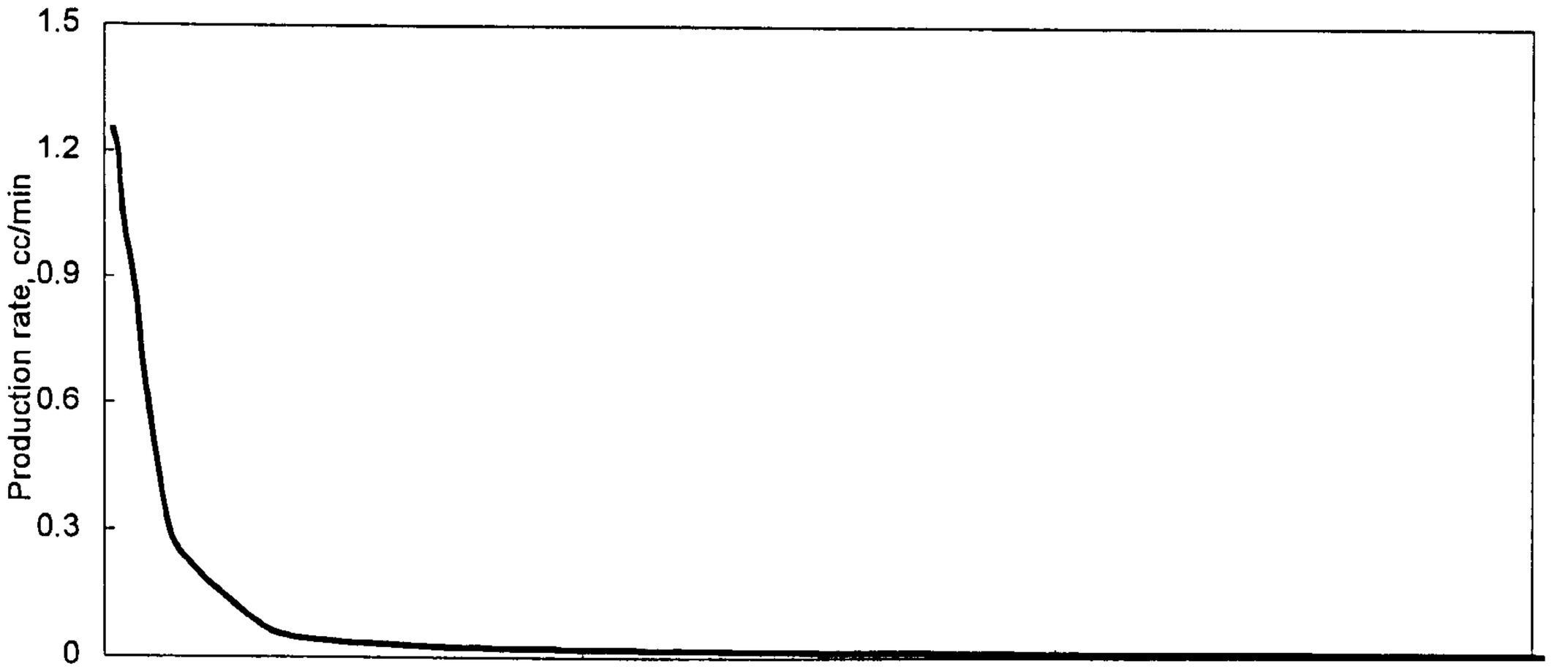

Figure 5.7-10a Production rate vs. time (linear scale) for Experiment 5.7-8.

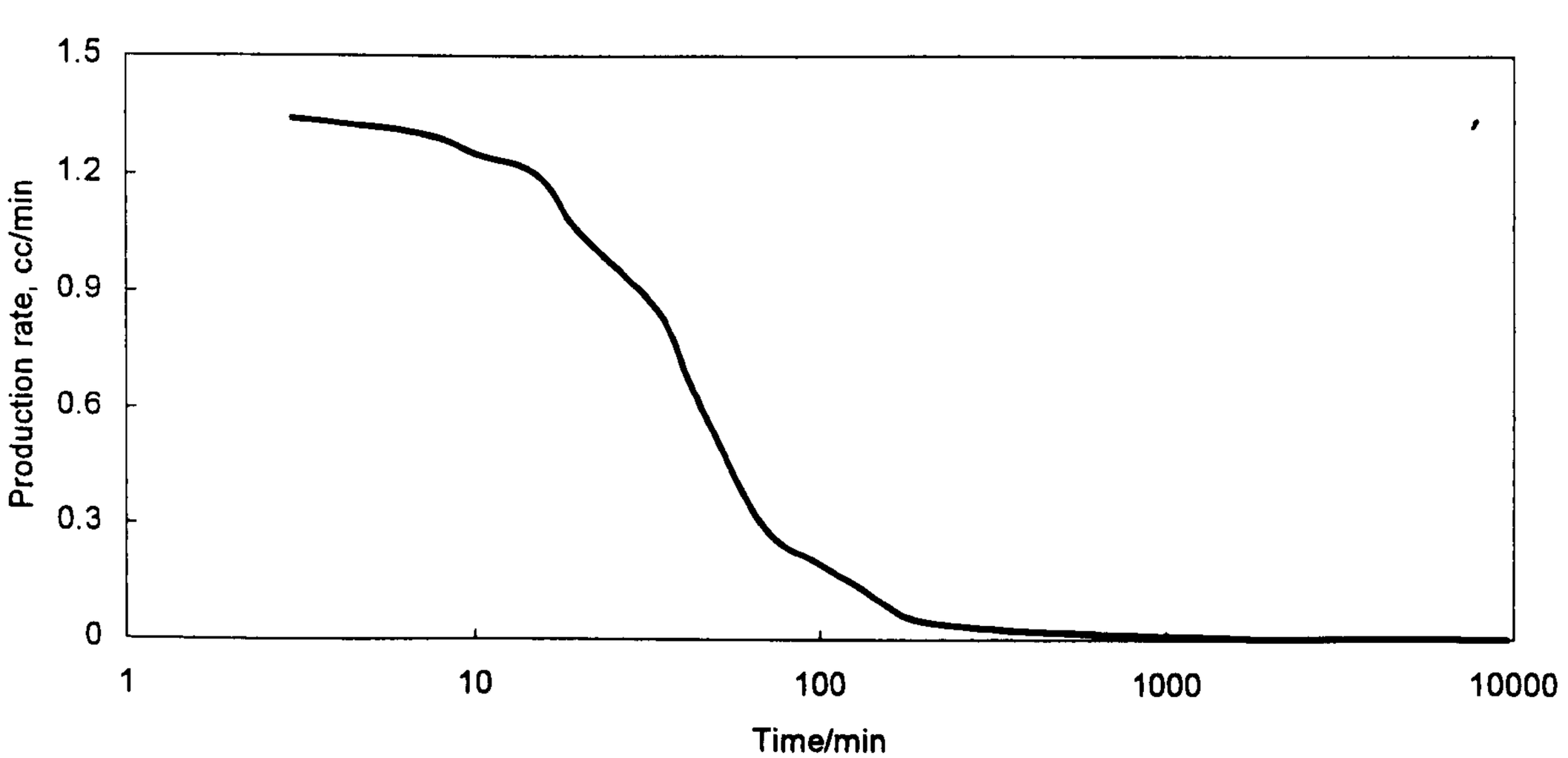

Figure 5.7-10b Production rate vs. time (log scale) for Experiment 5.7-8.

CHAPTER-6

NUMERICAL SIMULATION

6.1 INTRODUCTION

In general simulation refers to the representation of some process by either a theoretical or a physical model. One of the primary objectives of a reservoir study is to predict future performance of a reservoir and find ways and means of increasing ultimate recovery. Reservoir simulation by computers allows a more detailed study of the reservoir by dividing the reservoir into a number of grid cells (sometimes several thousand) and applying fundamental equations for flow in porous media to each grid cell. Digital computer programs that perform the necessary calculation to do such model studies are called simulators.

Choice of the proper simulator to simulate the performance of a particular reservoir requires an understanding of the reservoir and a careful examination of the data available. A simulator that is suitable for reservoir *A* may not be appropriate for reservoir *B*, in spite of apparent similarities between reservoirs *A* and *B*.

A reservoir or part of it could be modeled in one, two or three dimensions depending on the objective of the study. For gas injection and water studies (simple ones) mostly (x-z) models are used, but the (x-y) and the radial (r-z) geometries are also used quite often.

Simulators can be classified also according to the type of reservoir or process they are intended to simulate. There are, for example, gas, black oil (e.g. Eclipse 100), chemical (e.g. Eclipse 200), compositional (e.g. Eclipse 300), thermal (e.g. Eclipse 500), gas condensate, and miscible displacement reservoir simulators. Moreover, there are one-, two- and three-phase reservoir models. Simulators are designed to simulate the physics of fluid flow. Their accuracy depends on their formulations and the input data.

Although reservoir modelling was developed to study overall field performance and to predict that performance following matching, it has many other applications. Typical sections of field can be analyzed, and by assigning the best known values to that section, its mechanism can be studied. Then, some of the parameters can be changed to learn what effect they may have on the overall mechanism. In turn, it may be found that what parameter needs most study to better understand the performance of the field.

Reservoir models may be used to study well problems such as pressure buildup and draw down behavior, gas/oil ratio behavior, and water/oil ratio histories. It has application in studying the coning and fingering of water and gas into oil-producing wells.

6.2 SIMULATION OF NATURALLY FRACTURED RESERVOIRS

Naturally fractured reservoirs are characterized as having two distinct porosity system: a primary system associated with the reservoir matrix and a secondary system associated with the fractures. The fractures serve as highly conductive flow paths for the reservoir fluid, increasing the reservoir's effective permeability significantly compared to the rock matrix. The fracture volume is usually small, so the porous rock matrix serves as the primary source of hydrocarbons. The fluid production mechanisms of fractured reservoirs are significantly different from that of single-porosity systems. Fluid expansion pushes hydrocarbon from the high-porosity low permeability matrix to the low-volume high permeability fractures, while gravity and capillary forces may enhance or inhibit hydrocarbon recovery from the matrix system.

Numerical simulation of naturally fractured reservoirs allows one to evaluate complex reservoir systems and to make reservoir performance predictions without being restricted to simplifying assumptions that normally accompany analytical solutions. In 1993, Aguilera, pointed out that, the best way to estimate recoverable volumes of fractured reservoir is with the use of a numerical simulator for dual porosity/dual permeability

system. He also argued that, even if a good history match is obtained, the forecasting might lead to disastrous results because the conventional simulator does not take into account the interaction between matrix and fractures and the large permeability contrasts between matrix and fractures.

It should however, be mentioned that the greatest weakness of dual porosity models is the lack of data on fracture sizes, distributions, orientations, permeabilities, porosities and matrix block properties, which usually vary greatly in the reservoir. In addition since the block to block phenomena are not well known, simulation of gravity and/or imbibition mechanisms are not straight forward processes.

In a single-block model, a concept on which many reservoir simulators have been based, it is assumed that, the individual matrix blocks are completely isolated from their neighbors. Moreover, it is assumed that, in view of the extremely large permeability contrast between the fracture network and the matrix rock, oil produced from a matrix block, flows via the fracture system to the gas-oil contact, without any interaction with matrix blocks passed. Consequently, the matrix blocks in gas invaded part of the reservoir behave independently and the overall reservoir performance can be the sum of all the single matrix blocks, in that region.

Although the actual matrix blocks have irregular shapes and varying sizes, for the interpretation of reservoir behavior, a simple geometric shape (e.g. a rectangular box) and average matrix block size is assumed.

Barenblatt (1960), proposed a dual-media approach for modelling naturally fractured systems. The fractures and matrix are treated as separate continua throughout the reservoir. Every point in the reservoir contains fracture pressures/saturations and matrix pressures/saturations. Fluid may flow through the fracture and matrix continua. The two continua are connected through an exchange term on the basis of the differences in matrix and fracture pressures. Kazemi (1976) and Rossen (1987) presented simulators for

modelling fluid flow in naturally fractured reservoirs. The matrix/fracture fluid exchange mechanism is an important component in naturally fractured reservoir simulation. Reiss (1980) and van Golf-Racht (1982) analyzed fluid segregation in detail for the matrix and fracture systems to identify matrix-block production rates and ultimate recoveries.

Fluid flows through the matrix to the fracture system causes nonuniform saturation and pressure profiles throughout the matrix block. Capillary forces produce profiles that vary radially out from the center of a matrix block, while gravity forces create profiles that vary in the vertical direction. Saidi (1983) accounted for both radial and vertical variations by subdividing each matrix block into a cylindrical set of grid cells and simulating the varying saturation and pressure profiles. Pruess and Narasimham (1985) modeled radial-like profiles using a multiple-interacting-continua grid cells that was discretized symmetrically about the center of the matrix block.

6.2.1 Dual-Porosity Approach

The Dual-porosity concept, initially proposed by Barenblatt (1960), assumes the simultaneous existence of two continuous porous systems of distinctly different porosities and permeabilities (i.e. matrix and fracture systems), at each point of a reservoir.

The matrix continuum consists of the intergranular pore space of the rock, which comprises the majority of the storage in the reservoir. The fracture continuum consists of the interconnected network of fractures and/or solution vugs that constitute the primary conduits for fluid flow. Warren and Root (1963), proposed the idealization of using two domains, one for matrix and the other for the fracture, to describe the heterogeneity for well test analysis. The fracture domain has a low storativity and high permeability whereas the matrix domain is the exact opposite. It is assumed that fluid will flow to the well only through the fracture domain. This idealization is called dual-porosity model. Warren and Root assumed a quasi-steady state interporosity flow between the fracture and

matrix. Early dual-porosity models include those of Kazemi (1976) and Saidi (1983). Kazemi discretized the fracture continuum into grid cells and simulated fluid flow by a set of fracture mass-balance equations. The matrix was assumed to act as a source or sink to the fracture, and the flow between the two continua was represented by a single matrix/fracture transfer term. With the assumption that the matrix blocks were isolated, the transfer term was constructed from a representative matrix block located at the center of the grid cell. No gravity terms were included for matrix/fracture flow and they used the same fracture capillary pressure and upstream relative permeability for both matrix/fracture and fracture flow. Saidi (1983) modeled a fractured reservoir by dividing it into sectors in which the fracture was assumed to have infinite transmissibility. The matrix block was represented by several cylindrical grid cells that were suitably distributed vertically and horizontally. These matrix blocks were girded with boundary conditions imposed on them by the fracture, which was under the gravity segregation assumption.

The dual-porosity theory assumes that all flow takes place in the fractures. The matrix acts only as a storage medium for the reservoir fluids, where a transfer function describes the flow from the matrix to the fracture network. Mathematically, the dual-porosity theory assumes that a point in the reservoir is part of both matrix and fracture continua. A dual-continuum approach better represents the actual flow taking place between the matrix and the fractures. Each point in the reservoir has the properties of either the matrix or the fracture continuum. This is a more realistic representation of the reservoir, but it is not suitable for an analytical solution of the pressure distribution in the reservoir.

The Dual-porosity model is classified into two categories, depending on the nature of the flow from the matrix blocks to the fractures, or interporosity flow: one assumes pseudo-steady state, or restricted interporosity flow e.g. Barenblatt (1960), Warren and Root (1963), and the other assumes transient, or unrestricted interporosity flow e.g. Kazemi

(1969), Boulton and Streltsova (1977). The major difference between the two assumptions is in the transition period. Pseudo-steady state interporosity flow gives a flatter response while the transient interporosity flow gives a much steeper curve. Moench (1984) incorporated a fracture skin in the dual-porosity model. He considered that mineral deposits at the surface of the fractures may obstruct interporosity flow, and he quantified this obstacle by a new parameter, the fracture skin. Without a fracture skin, Moench's model is identical to the transient interporosity flow model. When fracture skin becomes large, Moench's solution changes to the pseudo steady state interporosity flow model. Intuitively, a very high fracture skin would mean that no flow is possible from the matrix to the fractures. Although transient interporosity flow is more realistic from a physical point of view, pseudo-steady state interporosity flow behavior may be obtained if there is more obstacle to flow at the matrix-fracture interface than in the matrix itself.

The shape factor

The communication between matrix block and fractures are controlled by the matrix-fracture interporosity transmissibility, which is defined as:

$$T_{maf} = (V_b k \sigma_f)_{ma} \tag{6.1}$$

where V_b, k, and σ_f are bulk volume, permeability, and shape factor of the matrix block, respectively. In order to evaluate the interporosity transmissibility, σ_f will have to be known. Thomas (1983), outlined three methods of calculating σ_f.

$$\sigma_f = \frac{4N_f\,(N_f+2)}{L^2} \tag{6.2}$$

$$\sigma_f = \frac{A}{LV} \tag{6.3}$$

$$\sigma_f = 4\left(\frac{1}{L_x^2}+\frac{1}{L_y^2}+\frac{1}{L_z^2}\right) \tag{6.4}$$

where N_f, L_x, L_y, and L_z are the number of normal sets of fractures, the lengths of the grid cells in x, y, and z direction, respectively. The shape factor can be derived from a conservative finite-difference expansion for flow between fractures and cubical grid cells. For fractures in three dimensions, Equations 6.2 and 6.4 will give the apparent matrix block size and for flow in one or two dimensions, the corresponding L terms are deleted. If there is a fracture along only one side of the matrix block for one dimensional ($1D$) system, the coefficient in Equation 6.4 is 2.0. Equation 6.2 was originally proposed by Warren and Roots (1963). Kazemi et al. (1992) presented a shape factor, σ_f, to compensate for the effect of shapes and boundary conditions.

$$\sigma_f = \frac{1}{V_b} \sum_{i=1}^{n} \frac{A_i}{L_{A_i}} \tag{6.5}$$

where V_b, A_i, L_A, A_i, and n are the bulk volume of the matrix, the area open to imbibition with respect to the ith direction, the distance from to the center of the matrix, and the total number of surfaces open to fracture, respectively.

For field scale models, the value of σ_f is a property of the system and for uniformly fractured media would be independent of simulation cell size. The "correct" value of σ_f does not depend on the assumption of matrix block shape. Equations 6.2 and 6.4 are used only to deduce an apparent matrix block size, L, from the value of σ_f. If matrix block shape were known exactly, then the value of σ_f could be calculated from Equation 6.4. Practically speaking, σ_f is just a matching parameter and can be estimated by history matching.

6.2.2 Improvement in The Dual-Porosity Model

Much of the more recent literature on dual porosity modelling is devoted to developing enhancements for modelling the gravity effects in the transfer calculation. These can be

classified into three groups, i.e., gravity-segregated, subdomain, and dual-permeability models.

The gravity-segregated model

The dual porosity model which assumes dispersed fluid phases in the matrix and fracture cannot represent matrix-fracture transfer due to gravity displacement since the matrix and fracture are assumed to be at the same depth for each grid cell. The gravity segregated model accounts for the drainage mechanism by a gravity head, in the matrix-fracture potential.

The subdomain approach

This model does not assume gravity equilibrium in the matrix and the vertical fluid flow within the matrix blocks in one computational cell is accounted for by subdividing the matrix blocks into layers or fine grid cells. Within the fracture, complete vertical segregation of fluid phases is assumed and the phase-contact depths are evaluated similar to that used in the gravity segregated model. The fracture pressure at the subdomain elevations can then be evaluated based on the assumptions of constant fracture potentials and zero fracture capillary pressure within the grid cell.

The dual-permeability model

This is the most appropriate model to use when capillary continuity is important. The matrix-matrix flow term represents both the transfer of fracture oil (drained from the matrix above) to a lower matrix block due to reinfiltration as well as the matrix flow through the permeable matrix block contacts (see Figure 6.1).

6.3 NUMERICAL MODELLING OF THE LABORATORY EXPERIMENTS

A commercial simulator, Eclipse 100, was calibrated and used to numerically model the experiments. The simulation provided data on pseudo permeabilities and capillary pressure for glass pack and sand pack models. Also, fracture capillary pressure for gravity

drainage process, was generated by matching experimental data of the stack matrix block. The purpose of the work were, to generate pseudos relative permeability and capillary pressure for glass pack and sand pack models for using in gravity drainage calculation, simulation of gravity drainage of single block and stack block experiments, and to generate fracture capillary pressure by matching data of stack block experiments, and compare it to the theory of Chapter 5.

6.3.1 Properties of The Eclipse100 Simulator

Eclipse 100 is a commercial simulator capable of simulating the black-oil, primary depletion, water flooding, steam injection, gas injection, geothermal reservoirs, dual porosity and dual porosity-dual permeability systems. It is also capable of simulating laboratory scale experiments.

The dual porosity-dual permeability option has been used throughout the simulation studies of the laboratory experiments. For dual porosity-dual permeability runs, dual porosity system properties must be defined. Once the dual porosity option is used, the number of grid cells is doubled and a dual grid is set up. The first *N/2* grid cells represent the matrix system and the last *N/2*, the fracture system (*N* is the total number of grid cells). The grid parameters, such as grid cell sizes and formation tops are automatically doubled. Each grid cell in the fracture system is connected to the equivalent grid cell in the matrix system by a special interaction, namely the matrix-fracture interaction.

6.3.2 Simulation of The Gravity Drainage Experiments in Fractured System

Eclipse 100 was utilized to simulate and match the laboratory experimental results using the laboratory scale data. In other words, exact properties as in the laboratory experiments were used in the simulator.

The cubical core samples used in the experimentation were defined as cylindrical with the same height (z-direction) and volume. Fluid viscosities, densities, and other *PVT* properties were defined at the room temperature and atmospheric pressure at which the experiments were conducted.

The simulation runs were performed for different pseudo capillary pressure and pseudo relative permeability curves until a good match was obtained with experimental results of glass pack and sand pack models. As input relative permeabilities, straight lines were used for fractures, whereas, sandstone matrix permeabilities were based on measurements.

6.3.3 Simulation Method

a- Fine grid method: In fine grid simulation since the grid cells have the same dimensions as the core plug which were used for measuring physical properties of matrix block, i.e. capillary pressure and relative permeability, the measured laboratory data were used directly in the model. There was a good match between fine grid simulation and experimental recovery data.

b- Single block simulation: As the oil flow in gravity drainage process is mainly in vertical direction, a one dimensional model should be adequate to represent its performance. To simulate a gas/oil transfer function i.e. the curve representing the oil expelled from a matrix element as a function of time, the dual porosity-dual permeability system was used. To model such systems, two simulation cells are associated with each block in the geometric grid, representing the matrix and fracture volume of the cell. Four regions are defined in the single block model (see Figure 6.2), the bottom matrix region *M2*, consists of a single cell that is made inactive. Initially the top matrix region *M1*, is saturated with oil and two fracture regions *F1* and *F2* are filled with gas. The increase in oil saturation in the bottom fracture *F2* is equivalent to the produced oil from the top matrix region.

c- Generation of pseudo's: To generate pseudo relative permeability and capillary pressure for each grid cell, the grid cell dimensions were specified equal to the matrix block dimensions and the recovery data was matched by tuning the new pseudo relative permeability and pseudo capillary pressure.

d- Stack block simulation: For simulating stack of two matrix blocks which were separated by a horizontal fracture, eight regions are defined (see Figure 6.2). The grid cells *M1* and *M3* have the same dimensions as the matrix blocks, porous spacers are simulated by grid cell *M2*, and grid cell *M4* is made inactive. Initially *M1*, *M2*, and *M3* are saturated by oil and four fracture regions are filled with gas. The increase in oil saturation in the lowest fracture (i.e. *F4*) is equivalent to the amount of drained oil from the stack block.

6.3.4 Simulation Results

a- Preparation of simulator

Single block simulation using the fine grid approach: to investigate the accuracy of the laboratory measured capillary pressure and relative permeability of sand stone block, Experiment 6.1 (see Table 6.1) was simulated by fine grid technique. The physical properties of sandstone matrix blocks were measured by using core plug. The matrix block (i.e. *L3*) is subdivided into 10 grid cells, where the measured physical properties were applied directly to each grid cell. The graphs of experimental *FGD* of matrix block *L3* and output of its simulation are shown in Figure 6.3. A good match between simulation output and experimental data indicates that the accuracy of measured physical properties is good enough for free gravity drainage calculation which have been done in Chapter 5.

b- Generating pseudos relative permeabilities and capillary pressure

The dual-porosity dual-permeability option of Eclipse 100, was used to generate pseudos for sand pack and glass pack models (i.e. *SP*, *G1*, and *GL2*).

b.1- Sand pack model

The grid cell is defined with the same dimensions and physical properties as matrix block. Free gravity drainage production data generated from laboratory experiments of sand pack model was used for tuning exponent n and λ of Corey's and Land's expressions, respectively. A good match was achieved between the experimentally gravity drainage data of block and the simulation output (see Figure 6.4). The results of tuned relative permeabilities and capillary pressure for the sand pack model are shown in Table 6.2.

b.2- Glass pack models G1 and GL2

In order to establish pseudo relative permeability and pseudo capillary pressure data for the glass pack blocks *G1* and *GL2*, Corey's and Land's exponents were tuned until a reasonable match was achieved between the gravity drainage production of block and simulation output (see Figures 6.5 and 6.6). The tuned pseudos for *G1* and *GL2* models are shown in Table 6.2.

Table 6.1 Specifications of Experiment 6.1.

Block L3		Free Gravity Drainage Specifications	
X, Y, Z, cm	3.311*2.953*24.3	Ultimate Recovery, pv	0.077
Porosity, %	22.12	Duration, hr	1250
Permeability, mD	741	Characteristic Time, hr	12.29
Test fluids	Oil-2/Air	Characteristic Rate, cc/hr	3.45

Table 6.2 Relative permeability and capillary pressure of physical models, generated by matching the recovery data.

a- *Sand pack model* (Sim. 5.3-4, Fig. 6.4)

S_g	P_c *(atm)*	S_o	k_{ro}
0.000	0.002	0.00	0.000
0.126	0.003	0.25	0.000
0.252	0.004	0.33	0.003
0.378	0.005	0.40	0.018
0.504	0.010	0.48	0.050
0.63	0.020	0.55	0.100
		0.63	0.180
		0.70	0.280
		0.78	0.410
		0.85	0.570
		0.93	0.770
		1.00	1.00

b- Glass pack, block G1 (Sim. 5.4-3, Fig. 6.5)

S_g	P_c *(atm)*	S_o	k_{ro}
0.000	0.0000	0.00	0.0000
0.126	0.0144	0.10	0.0000
0.252	0.1024	0.20	0.0001
0.378	0.3024	0.25	0.0016
0.504	0.5144	0.30	0.0081
0.630	0.5500	0.40	0.0250
0.720	0.6459	0.50	0.062
0.810	0.7144	0.60	0.1300
0.900	0.8019	0.70	0.2400
1.000	0.1597	0.80	0.4100
		0.90	0.6600
		1.00	1.0000

c- Glass pack, block GL2 (Sim. 5.7-6, Fig. 6.6)

S_g	P_c *(atm)*	S_o	k_{ro}
0.00	0.0107	0.00	0.0000
0.09	0.0120	0.10	0.0000
0.18	0.0126	0.19	0.00001
0.27	0.0154	0.28	0.00032
0.36	0.0178	0.37	0.00240
0.45	0.0223	0.46	0.01000
0.54	0.0267	0.55	0.03100
0.63	0.0407	0.64	0.08000
0.72	0.0437	0.73	0.17000
0.81	0.0467	0.82	0.33000
0.90	0.0707	0.91	0.59000
1.0	0.1597	1.00	1.00000

c- Stack block simulation

The purposes of stack block simulation were, 1- To show the capability of simulators to match free gravity drainage from a stack block only by tuning the fracture capillary pressure, 2- To prepare some generated fracture capillary pressure for comparing to that which was presented in Chapter 5.

c.1- Simulation of stack block (L3/L6)

The stack block consists of two similar sandstone blocks (i.e. *L3* and *L6*). The physical properties based on Experiments 5.7-1, 5.7-2 and 5.7-3 (see Table 5.7-1) and the generated pseudos (i.e. k_{ro} and P_c) were used as input data for these runs (see Figures 6.7, 6.8 and 6.9). All physical variables were known for these runs, therefore the only tuning parameter which may be used for matching was the fracture properties. A straight line relative permeability was used for fracture and the capillary pressure was tuned for matching experimental results. The generated fractured capillary pressure that caused a reasonable match for Experiment 5.7-2 is shown in Table 6.3.

c.2- Simulation of stack block (GL1/GL2)

The stack block consists of two similar glassbeads pack blocks (i.e. *GL1*, *GL2*) which were separated by a horizontal fracture. The physical properties based on Experiments 5.7-7 and 5.7-8 have been applied as input data for these runs (see Figures 6.10 and 6.11). A straight line relative permeability was used for the fracture and the fracture capillary pressure was tuned for matching experimental results. The generated fractured capillary pressure that caused a reasonable match for Experiment 5.7-8 is given in Table 6.3.

6.3.5 Fracture Capillary Pressure

In our laboratory experiments, due to high transmissibility of the vertical fracture, the gas oil contact inside the vertical fracture dropped to the bottom of the stack block quickly. In Experiment 5.7.8, the horizontal fracture aperture was more than its critical value and based on the theory of Section 5.4, the fracture capillary pressure was controlled by capillary pressure of the oil drops. At each time, it is more likely to have different drops at their different stages of enlargement. Therefore in most of the time the capillary pressure of horizontal fracture is less than the maximum capillary pressure of drop before its detachment (i.e. 2.5E-4 psi).

When aperture of the horizontal fracture is less than its critical value (e.g. Experiment 5.7-2), there exists capillary continuity between blocks. By assuming that the capillary pressure at the gas oil contact in vertical fracture to be negligible and based on presented theory in Section 5.7, the capillary pressure of horizontal fracture will be constant and equal to $\Delta\rho\, g\, h$. For Experiment 5.7-2, h is equal to the height of lower block (i.e. the height of horizontal fracture from level of $P_c = 0$), and $P_{cf} = 0.463$ psi.

Since all physical parameters (i.e. block height, physical properties of rock and test fluids) are known, the only tuning parameter for matching the experimental data by simulation was fracture capillary pressure. The generated fracture capillary pressures that caused a reasonable match for Experiments 5.7-2 and 5.7-8 are given in Table 6.3. The difference

between fracture capillary pressure sets generated by simulation and those calculated based on theory of Chapter 5 (see Table 6.3 and Figure 6.12), is due to difference in the physics behind them.

In gas invaded zone of actual fractured reservoirs, the oil flow in vertical fracture is different from that of horizontal fracture. The oil flow in vertical fractures is mainly in direction of fracture plane, while inside the horizontal fracture it is mainly perpendicular to fracture plane. In all simulators, the dual-porosity dual-permeability option accepts only one set of capillary pressure data for fractures. In our opinion, due to difference in physics of oil flow between these two cases, it will be more convenient if two sets of fracture capillary pressure be used. When gravity drainage process is not active, the Young-Laplace form of fracture capillary pressure, and when gravity drainage mechanism plays the main role in oil production, the fracture capillary pressure based on the theory of Section 5.7 are recommended.

Table 6.3 Horizontal fracture capillary pressure, generated by matching the recovery data (i.e. Experiments 5.7-2 and 5.7-8).

Simulated P_{cf}, for Exp. 5.7-2		***Simulated P_{cf}, Exp. 5.7-8***	
S_{gas}	***Pc (atm)***	S_{gas}	***Pc (atm)***
0.00	0.132	0.00	0.00
0.10	0.147	0.10	0.00
0.20	0.148	0.20	0.00
0.25	0.150	0.25	0.00
0.30	0.151	0.30	0.00
0.40	0.156	0.40	0.00
0.50	0.160	0.50	0.00
0.60	0.162	0.60	0.00
0.70	0.163	0.70	0.00
0.80	0.176	0.80	0.01
0.90	0.250	0.90	0.02
1.00	0.294	1.00	0.04

6.4 Conclusions

1. Experimental recovery data or fine grid cells technique can be used for generating pseudo relative permeability and capillary pressure for grid cells. To produce pseudos, Corey's and Land's coefficients were tuned until a good match was obtained with experimental data or fine grid results. In reservoir simulation, the generated pseudos can be used later for prediction recovery performance under different production scenarios.

2. A numerical simulator with dual porosity-dual permeability option can be used to simulate gravity drainage process in a stack of matrix blocks. It handles the problem by assigning some pseudo properties to fracture. These pseudo properties of fracture are useful for sensitively analysis and history matching of the system.

3. It should however, be mentioned that the greatest weakness of dual porosity models are the lack of data on fracture sizes, distributions, orientations, permeabilities, porosities and matrix block properties, which usually vary greatly in the reservoir.

4- It must be clear that there is some inconsistency between the generated fracture capillary pressure and the actual fracture capillary pressure.

5. It is recommended that after more research based on the concept of Section 5.7-7, a new algorithm for generation fracture capillary pressure be used in simulators.

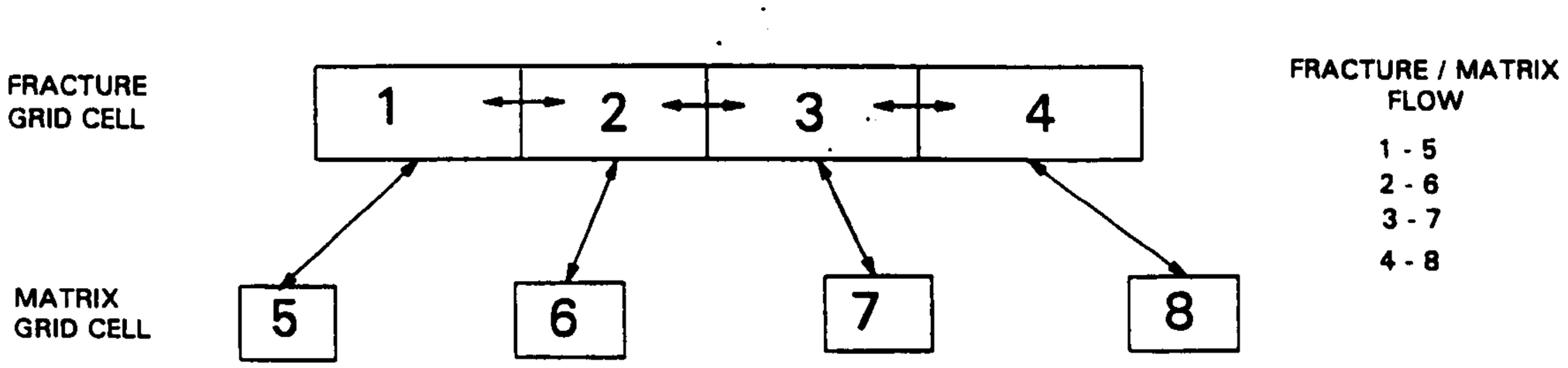

a: Dual-porosity system.

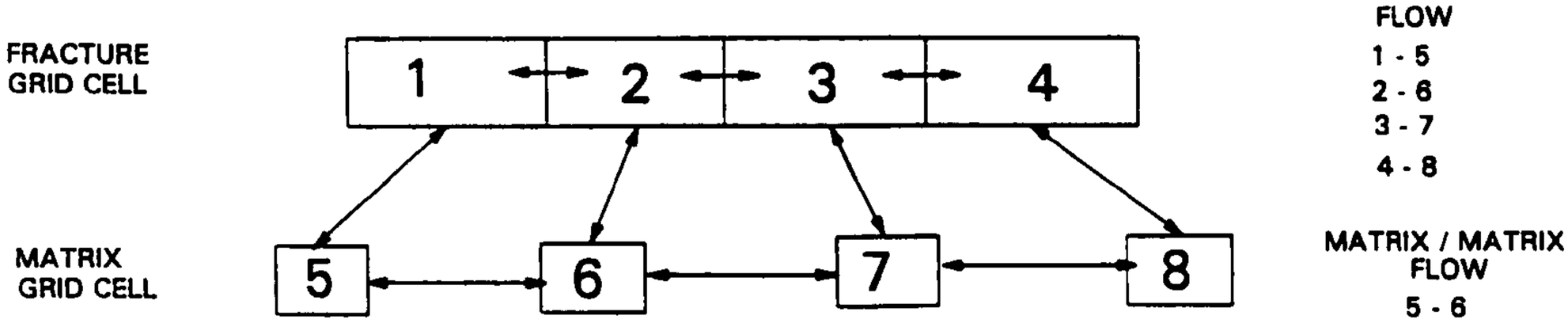

b: Dual-porosity dual-permeability system.

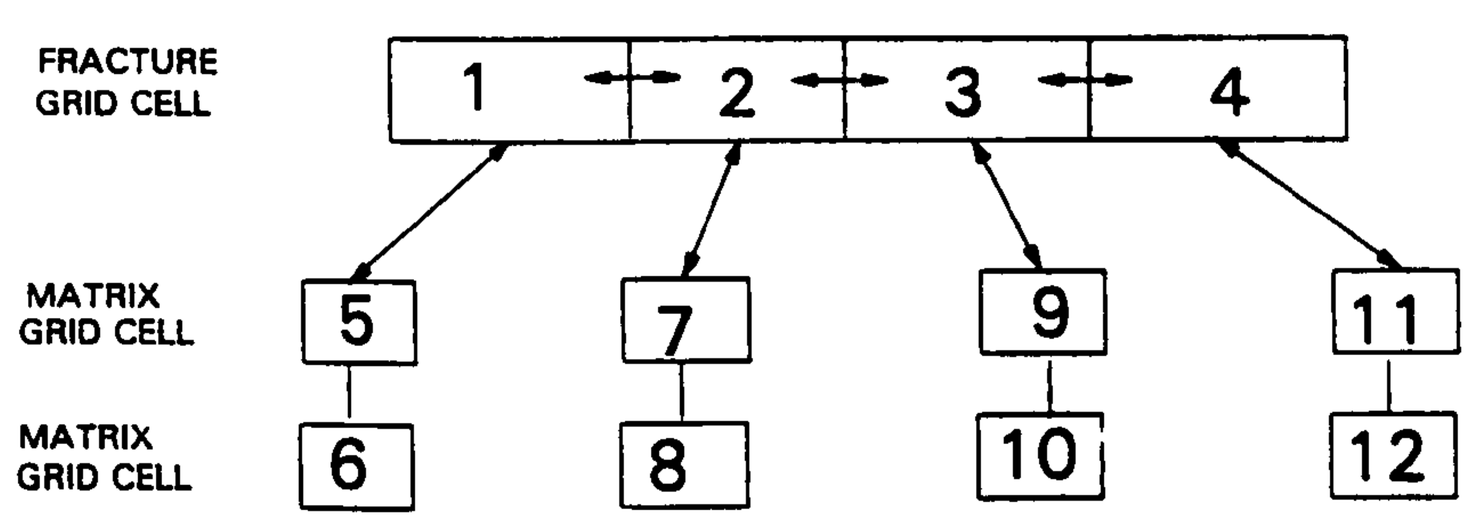

c: Dual-porosity system with subdivision of matrixdomain.

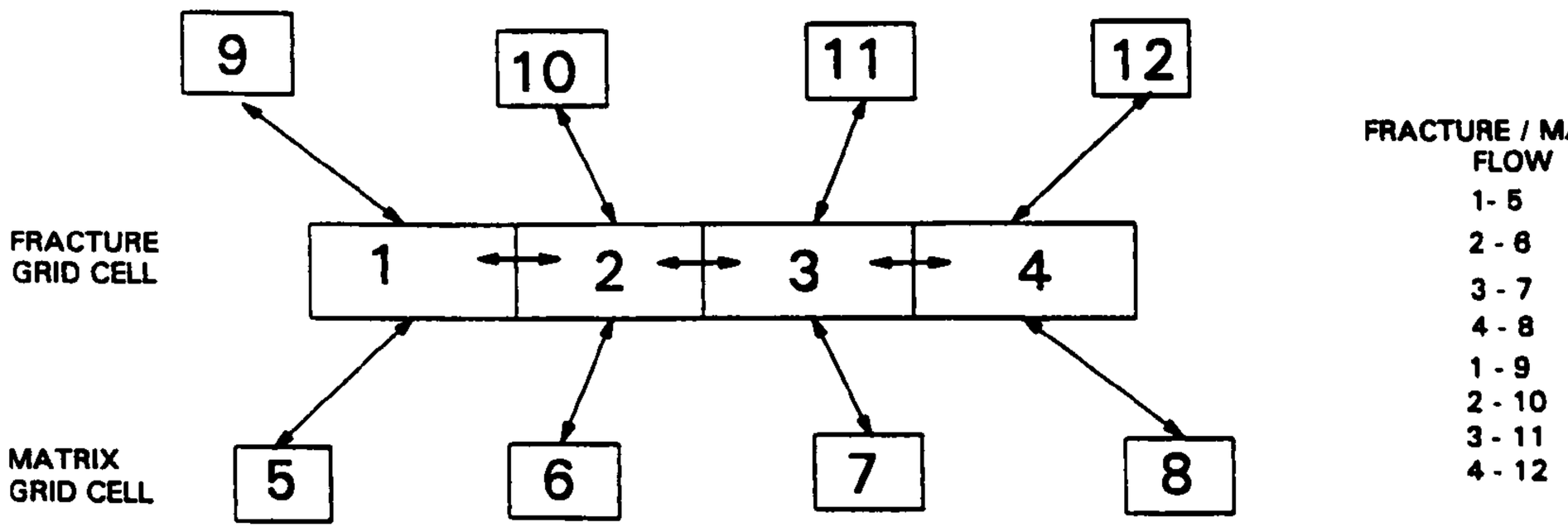

d: Triple-porosity system.

Figure 6.1 Simulation of grid cell for different configuration.

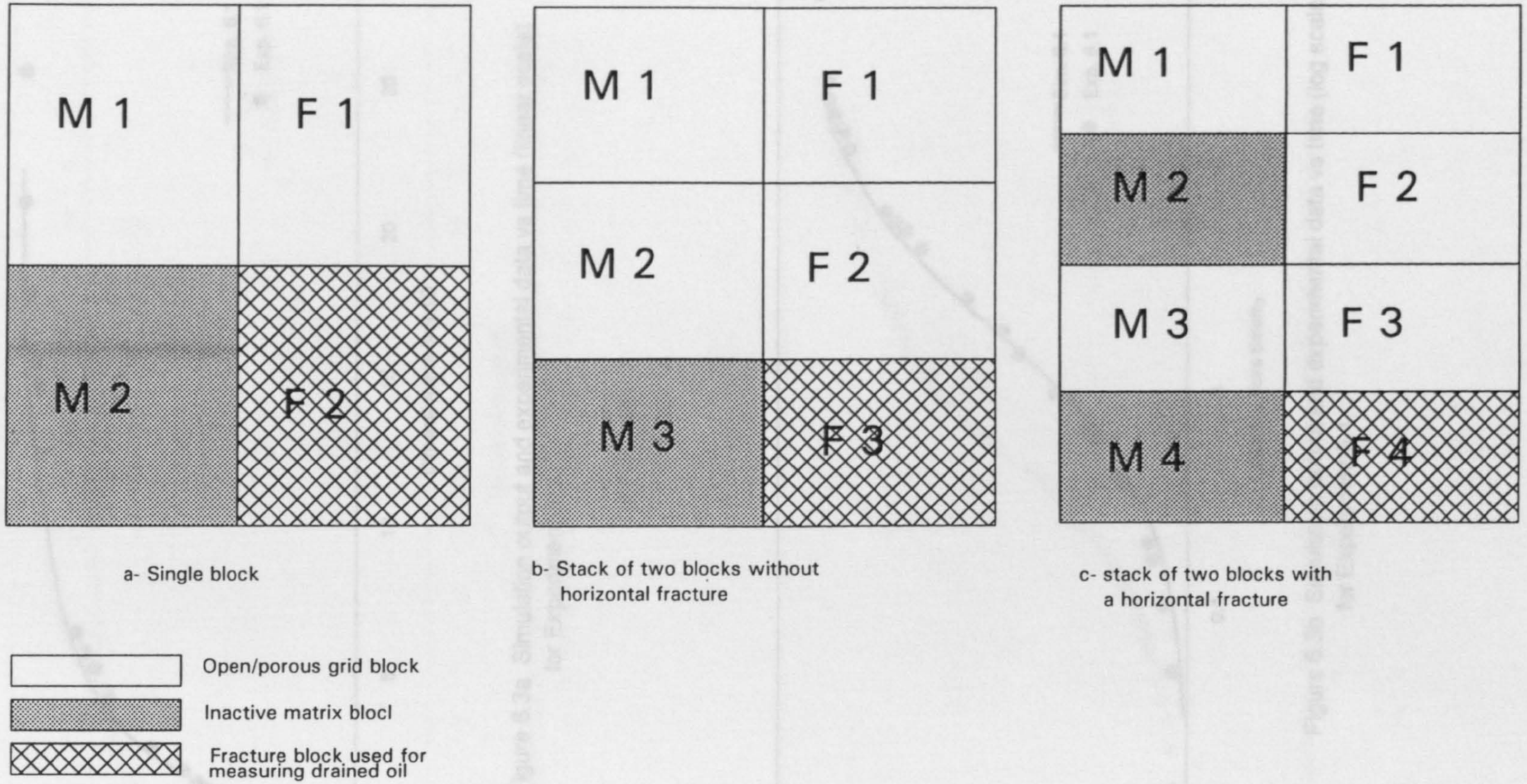

Figure 6.2 Fracture/matrix grid block for different configuration.

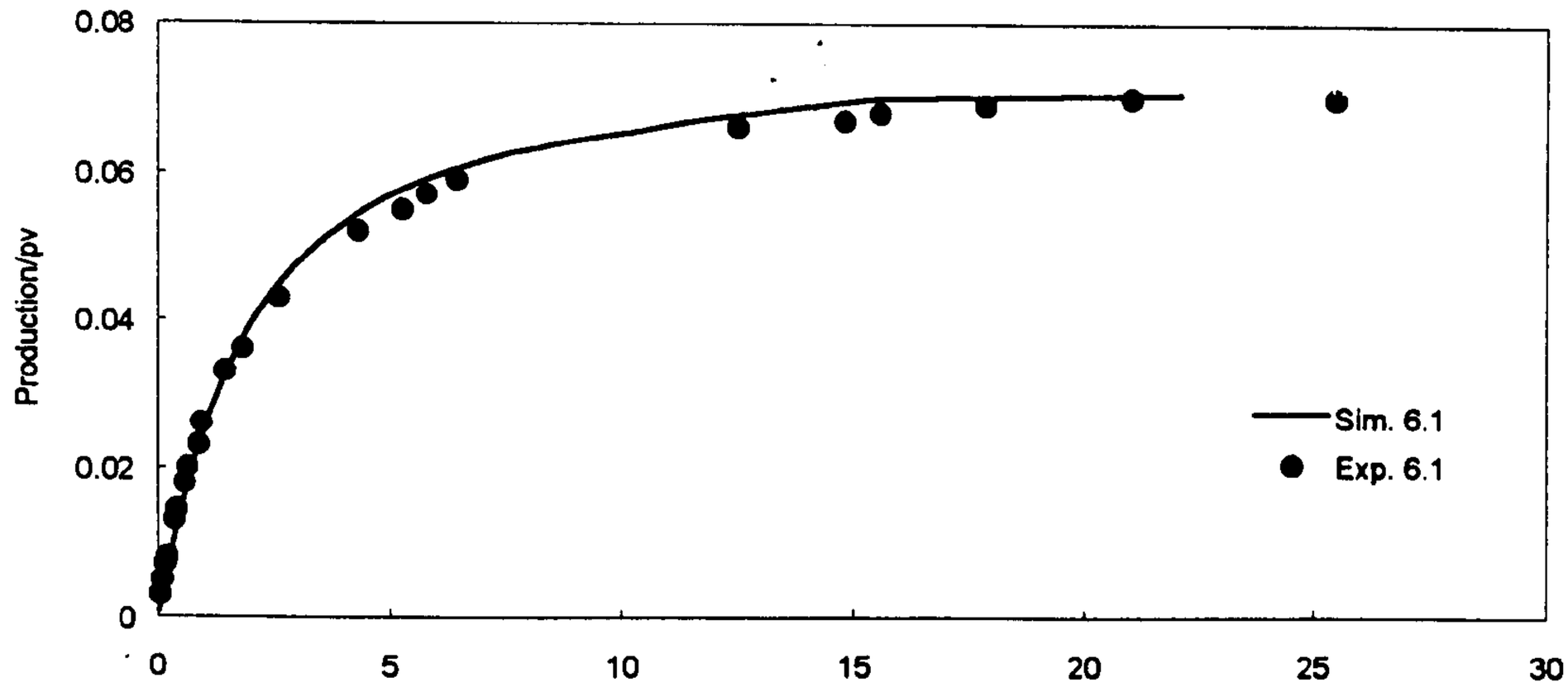

Figure 6.3a Simulation output and experimental data vs time (linear scale) for Experiment 6.1.

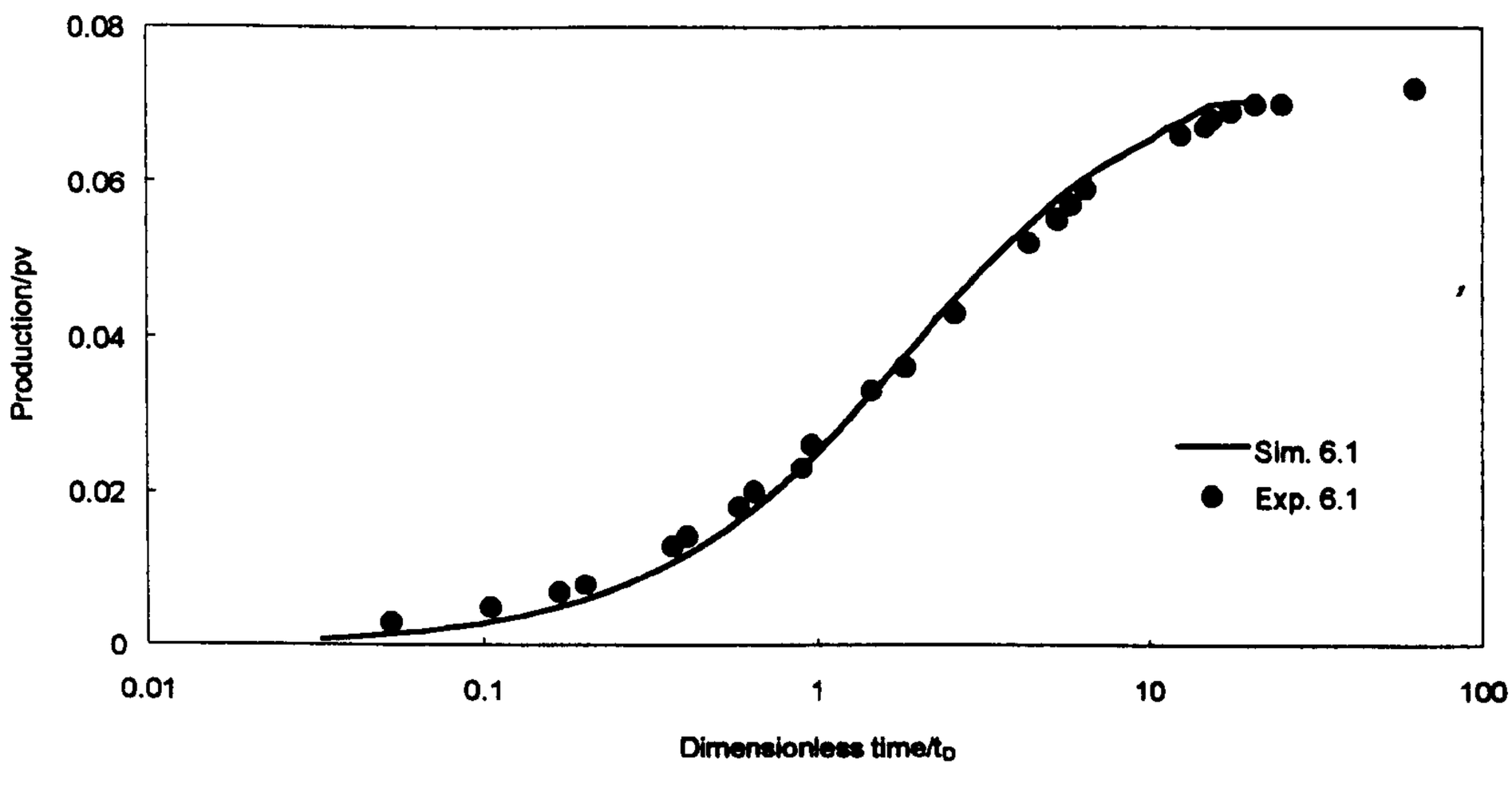

Figure 6.3b Simulation output and experimental data vs time (log scale) for Experiment 6.1.

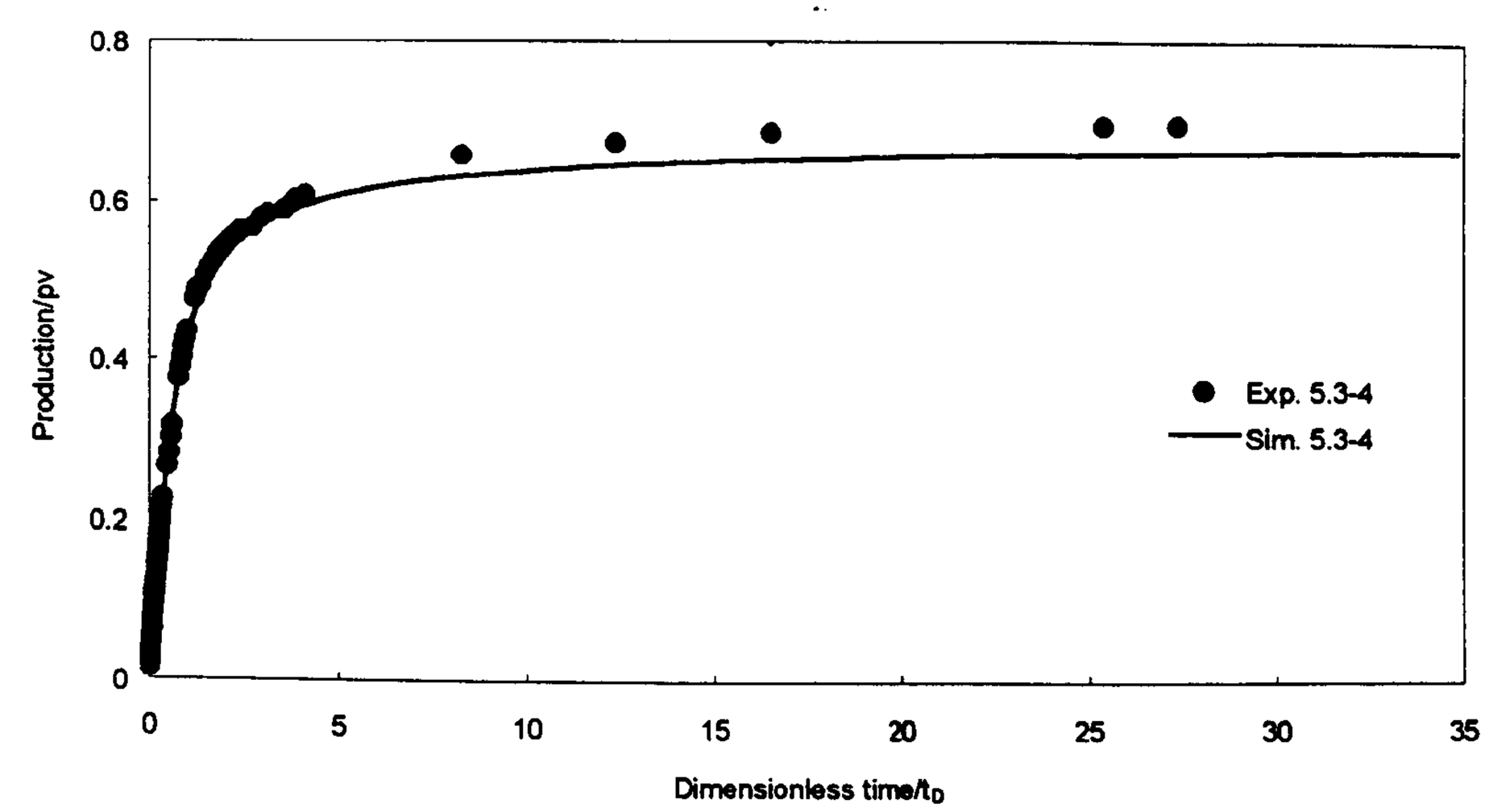

Figure 6.4a Simulation output and experimental data vs. time (linear scale) for Experiment 5.3-4.

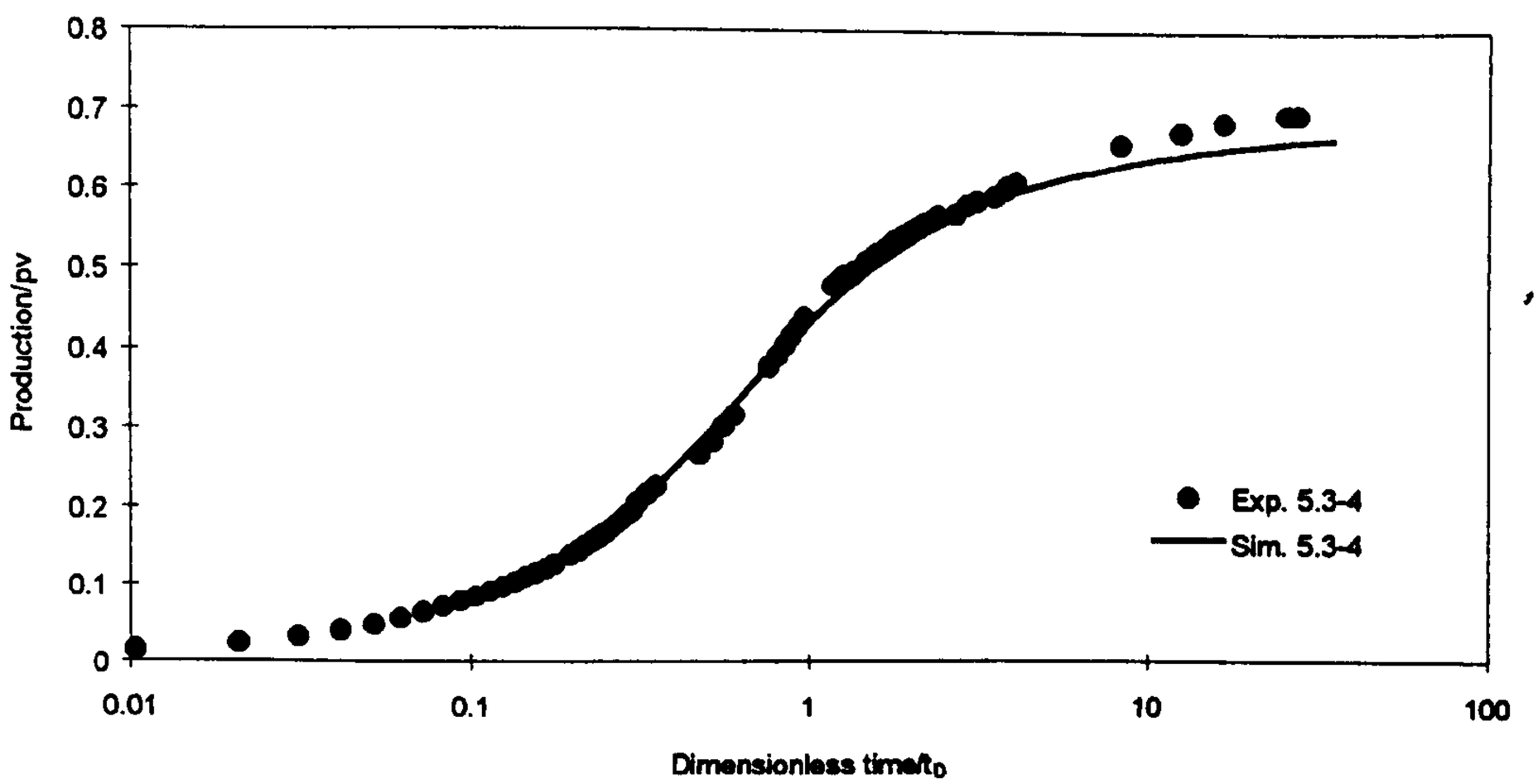

Figure 6.4b Simulation output and experimental data vs. time (log scale) for Experiment 5.3-4.

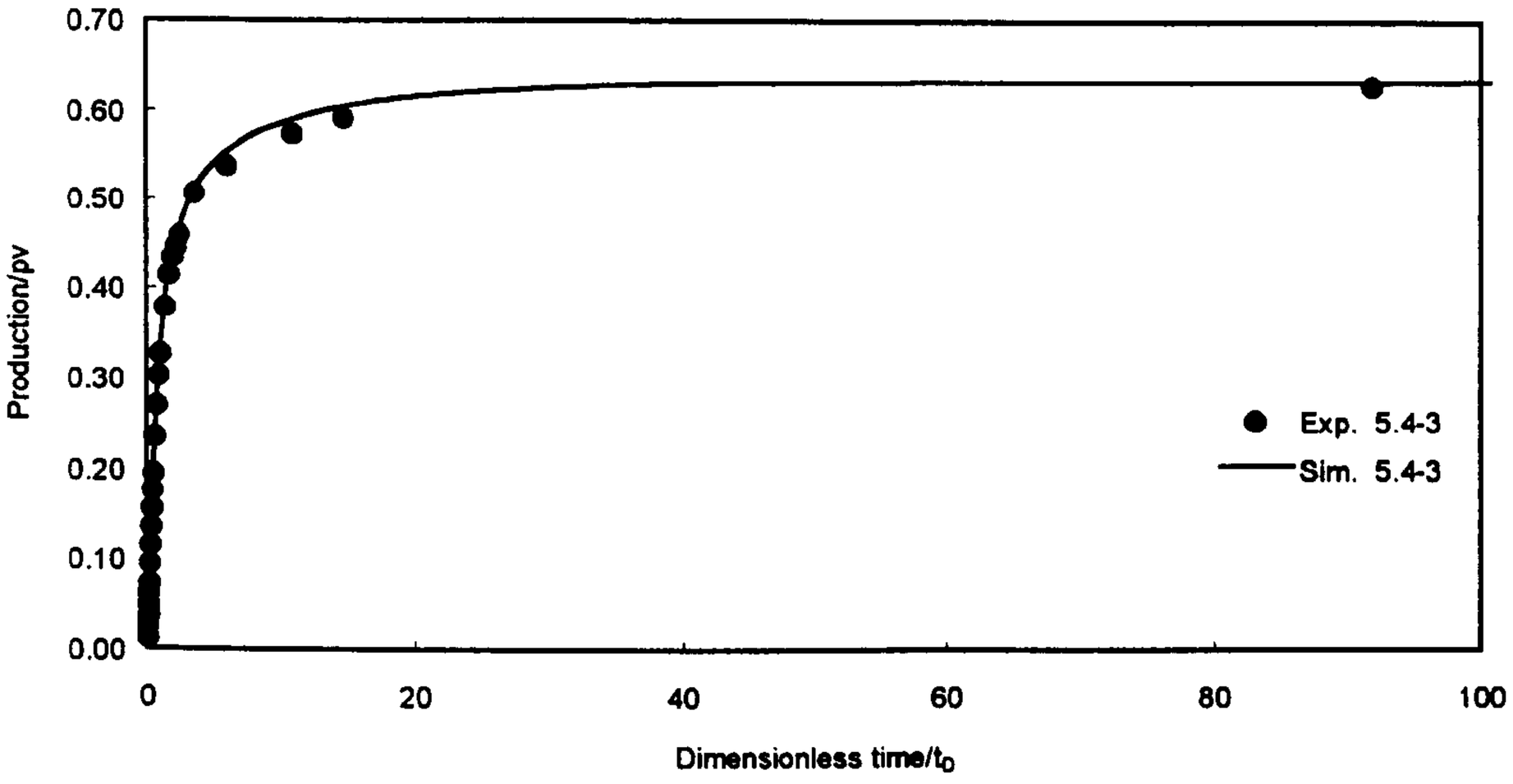

Figure 6.5a Simulation output and experimental data versus time (linear scale) for Experiment 5.4-3.

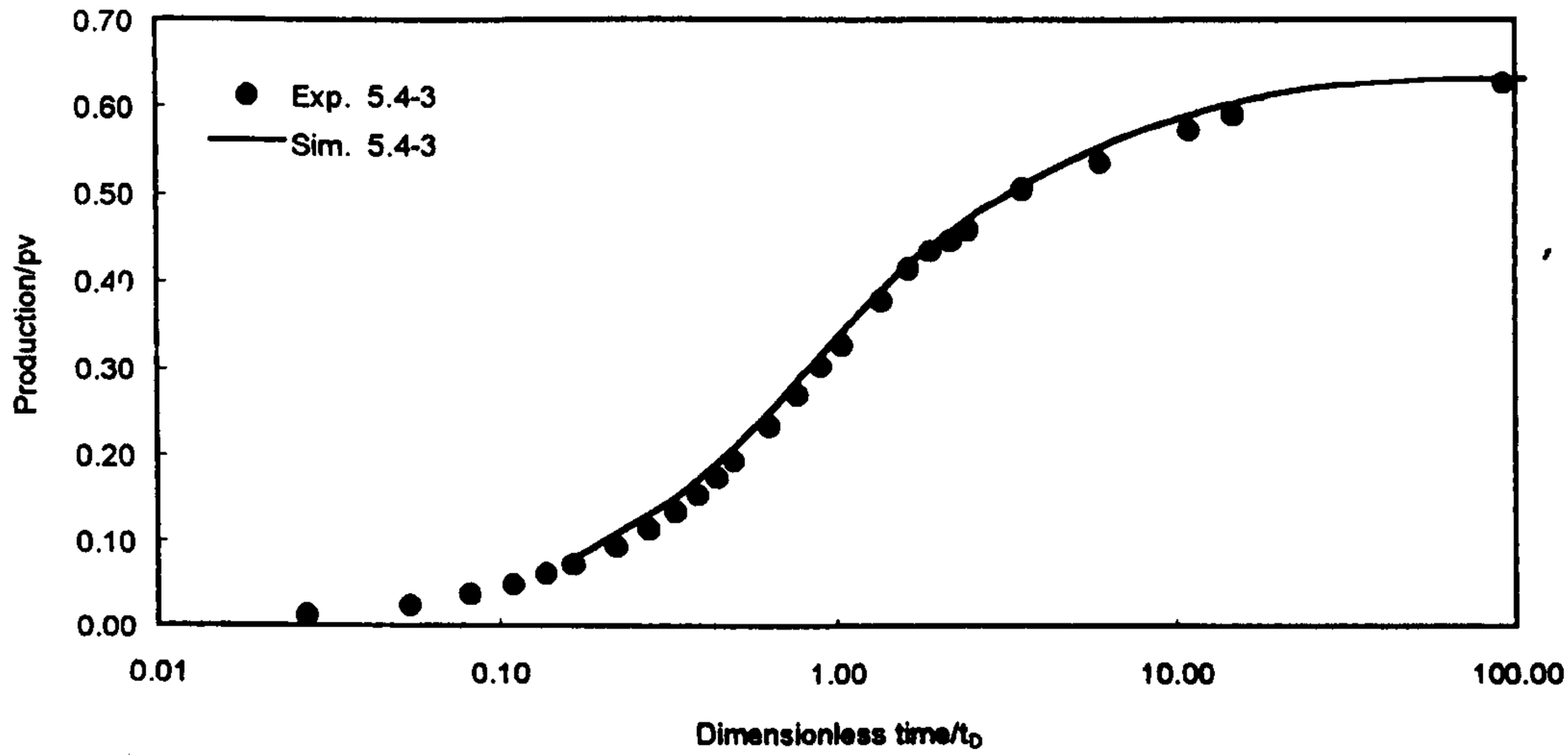

Figure 6.5b Simulation output and experimental data versus time (log scale) for Experiment 5.4-3.

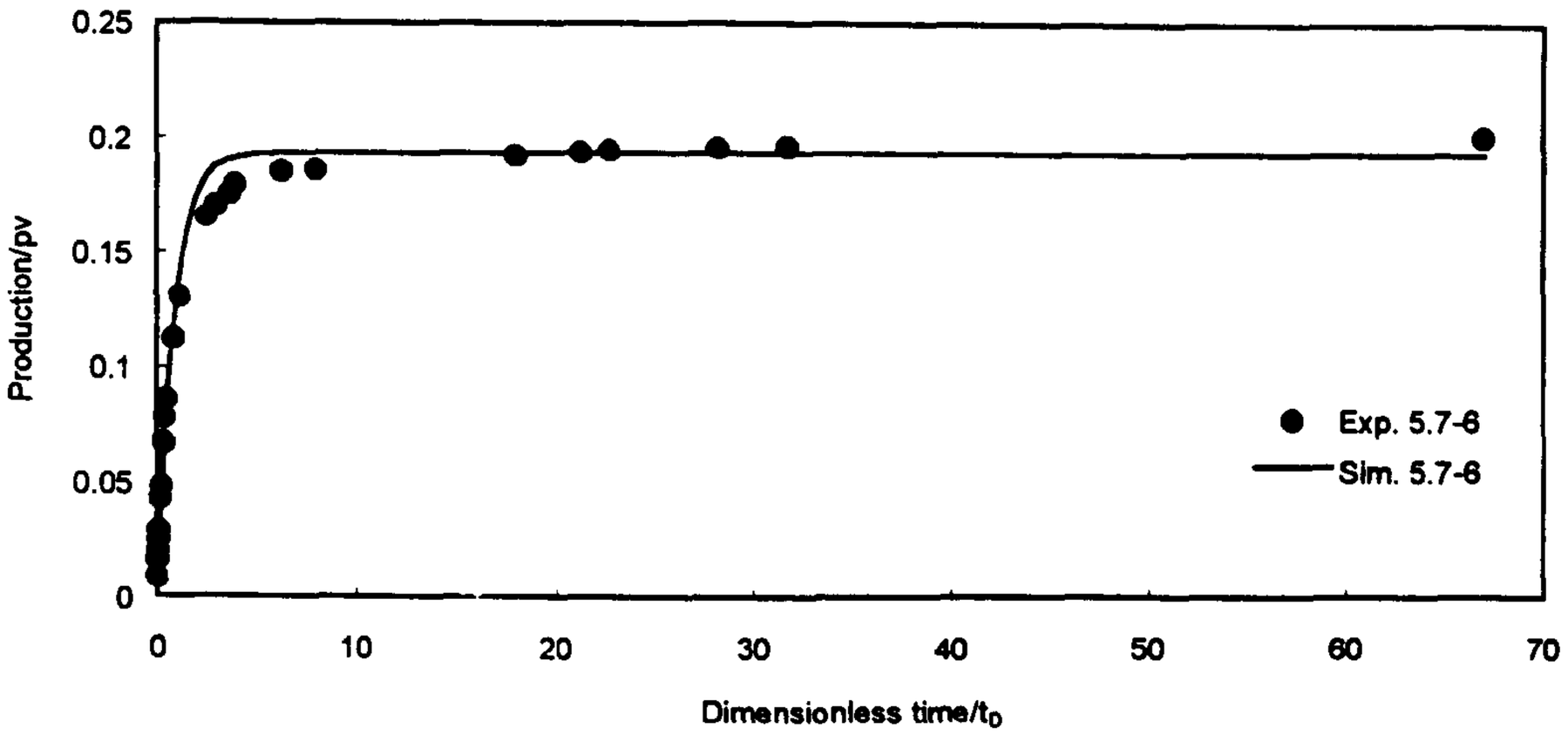

Figure 6.6a Simulation output and experimental data vs. time (linear scale) for Experiment 5.7-6.

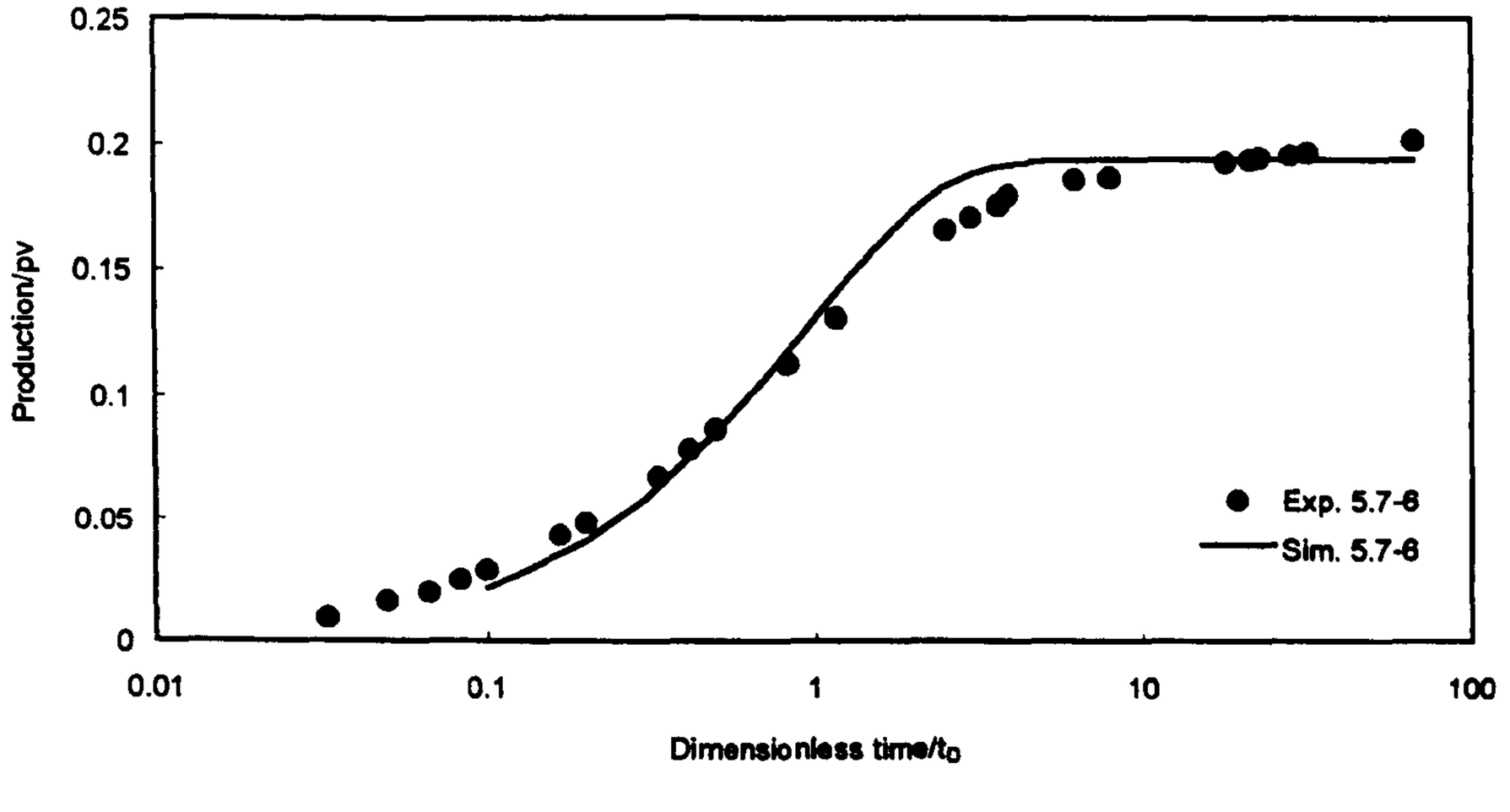

Figure 6.6b Simulation output and experimental data vs. time (log scale) for Experiment 5.7-6.

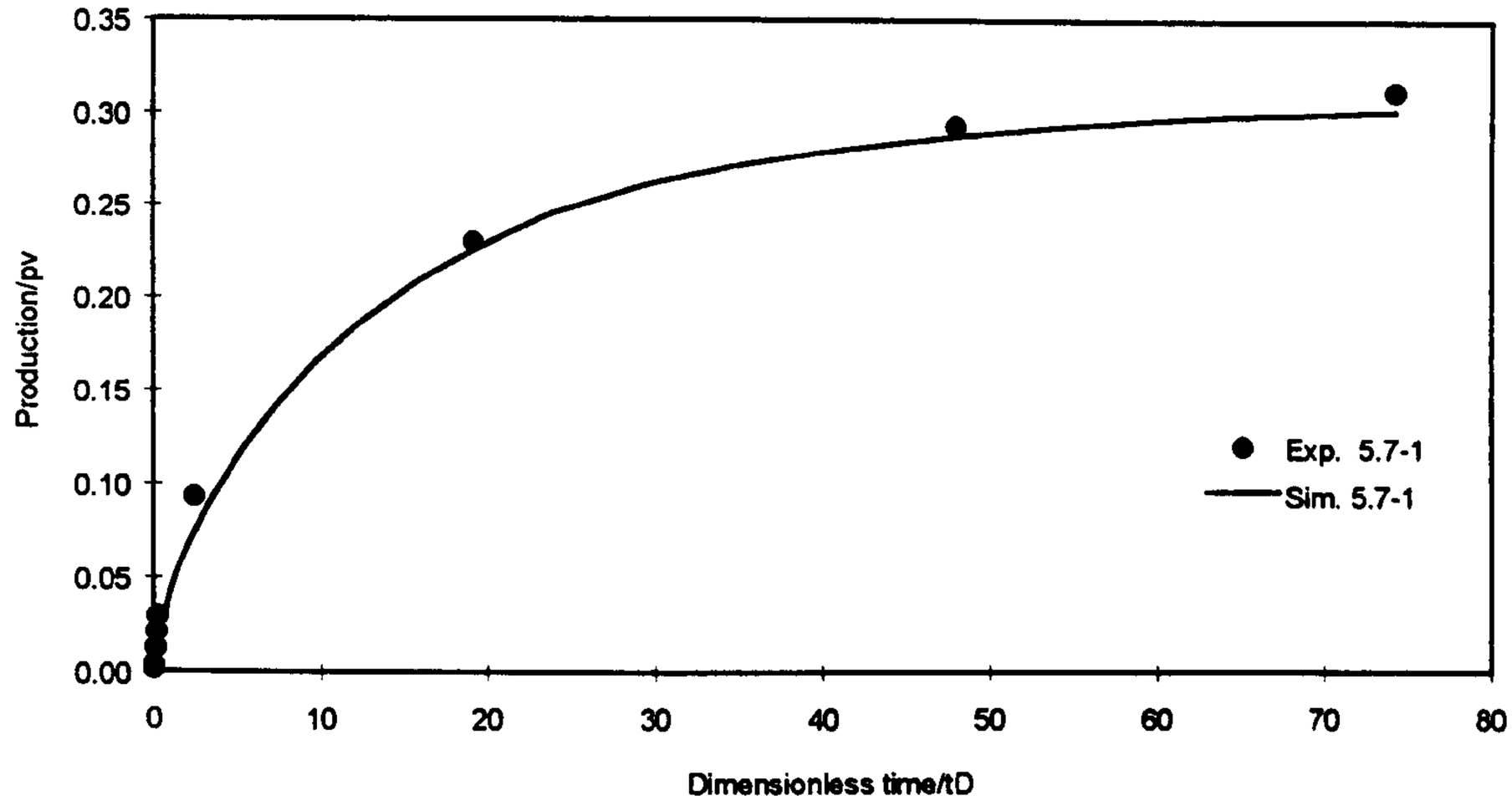

Figure 6.7a Simulation output and experimental data vs. time (linear scale) for Experiment 5.7-1.

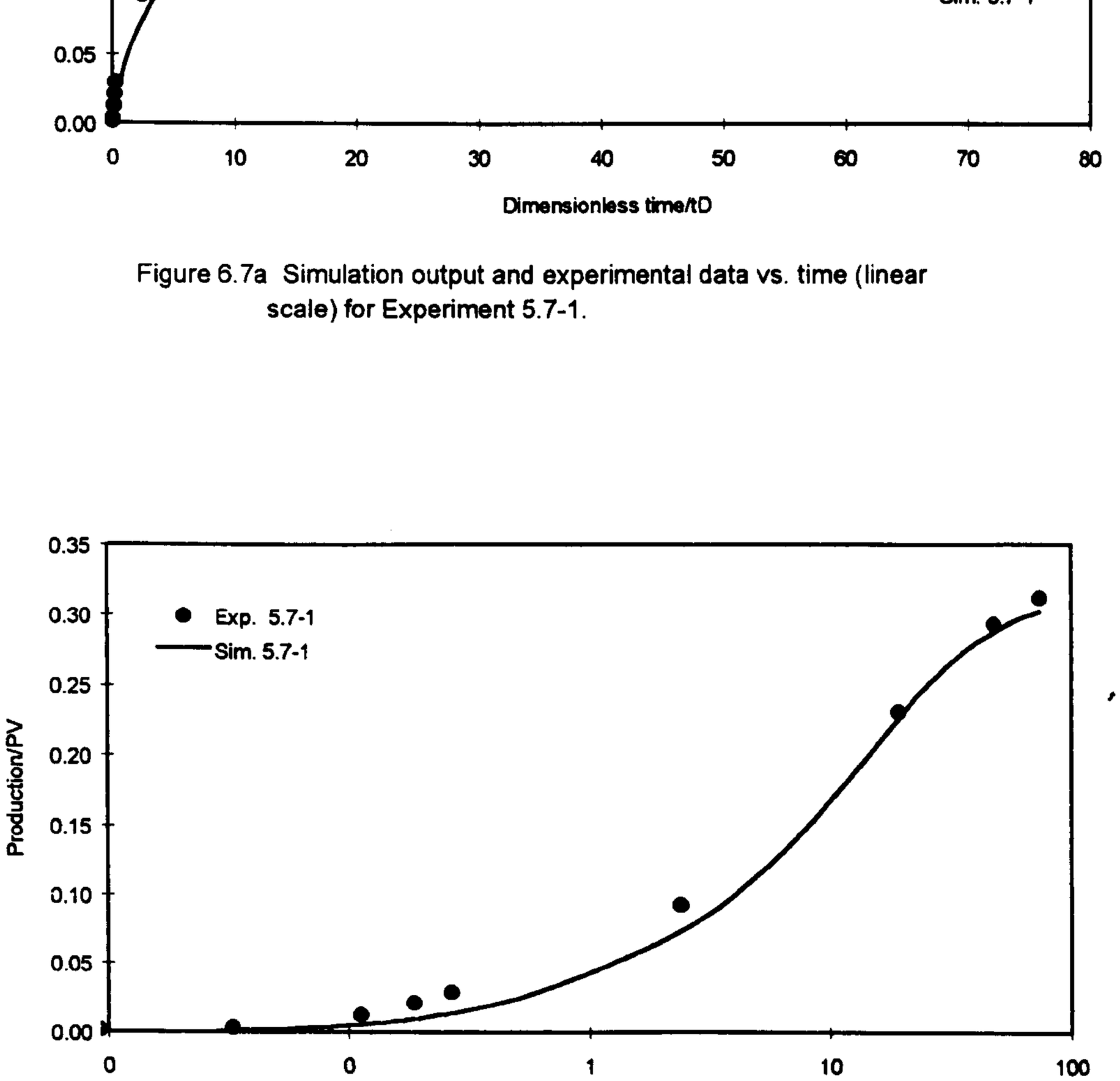

Figure 6.7b Simulation output and experimental data vs. time (log scale) for Experiment 5.7-1.

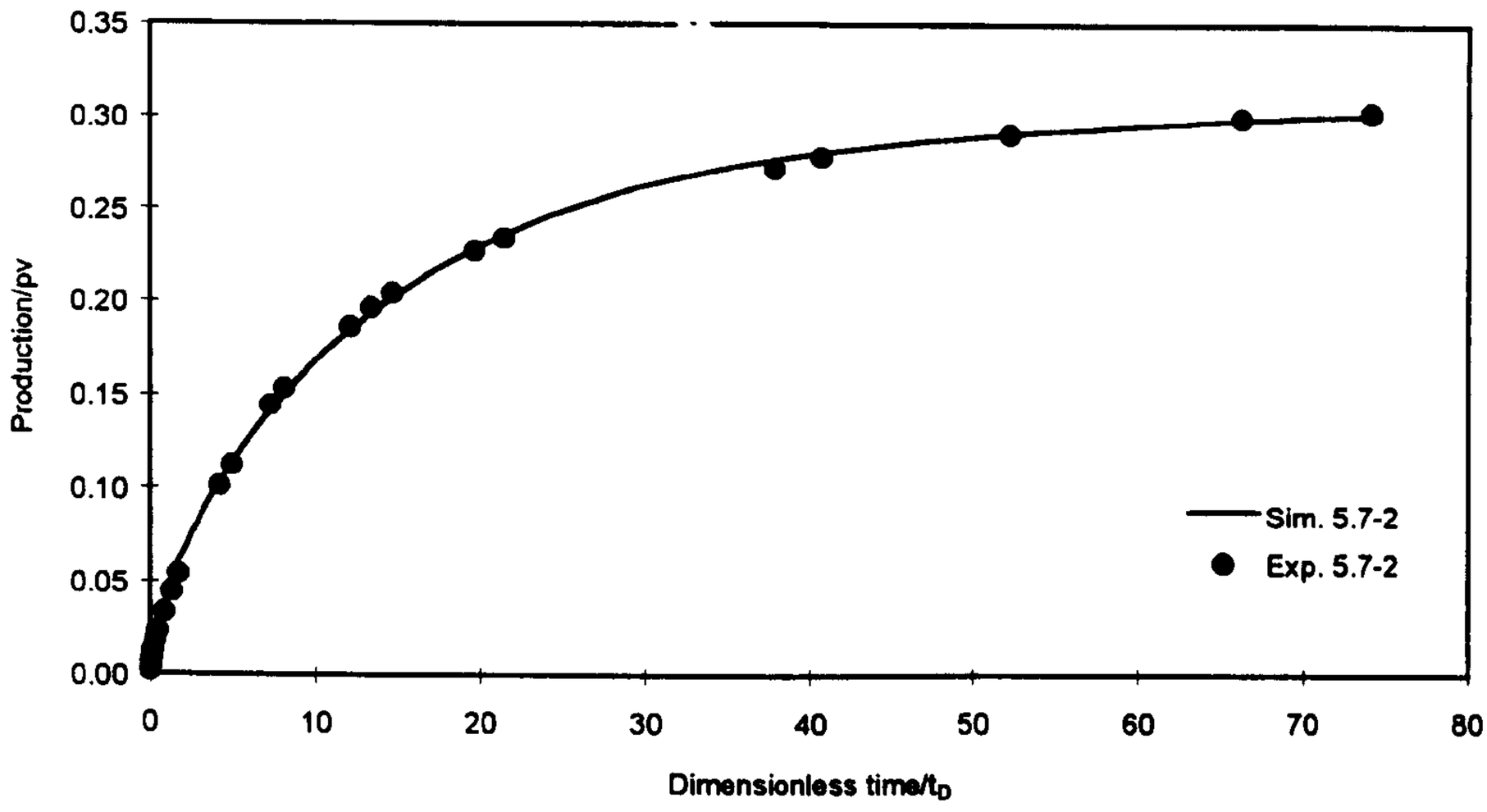

Figure 6.8a Simulation output and experimental data vs. time (linear scale) for Experiment 5.7-2.

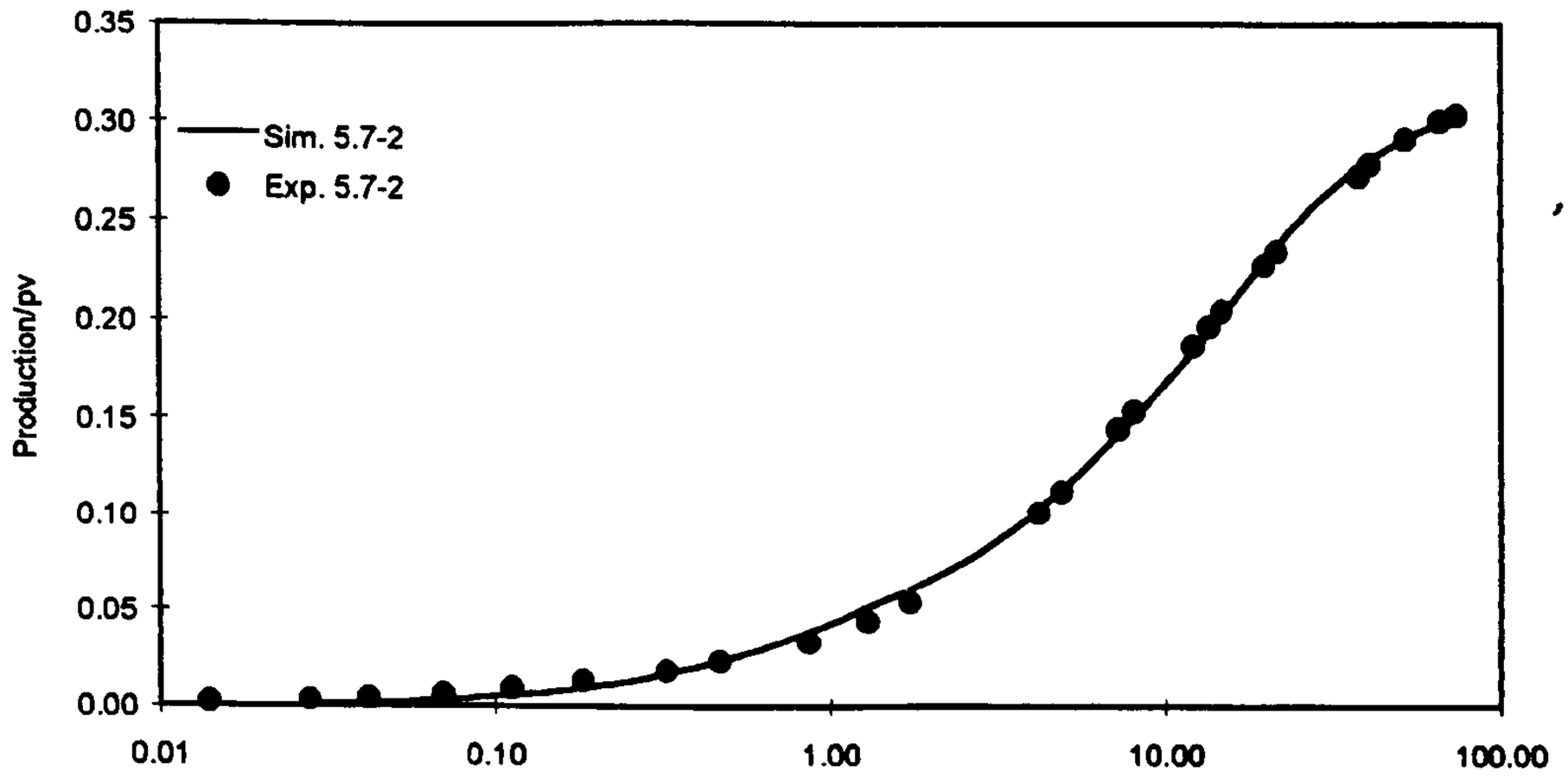

Figure 6.8b Simulation output and experimental data vs. time (log scale) for Experiment 5.7-2.

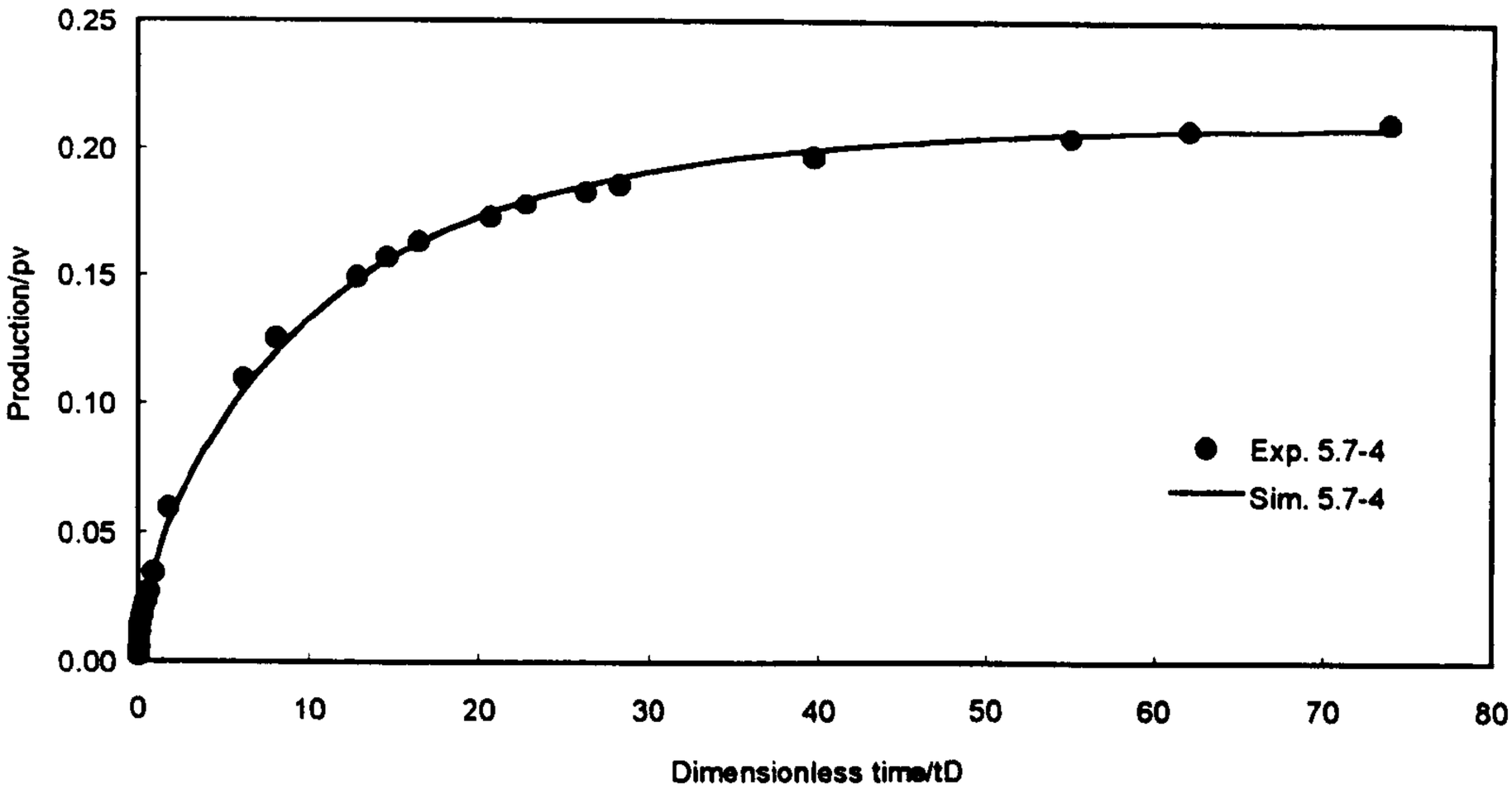

Figure 6.9a Simulation output and experimental data vs. time (linear scale) for Experiment 5.7-4.

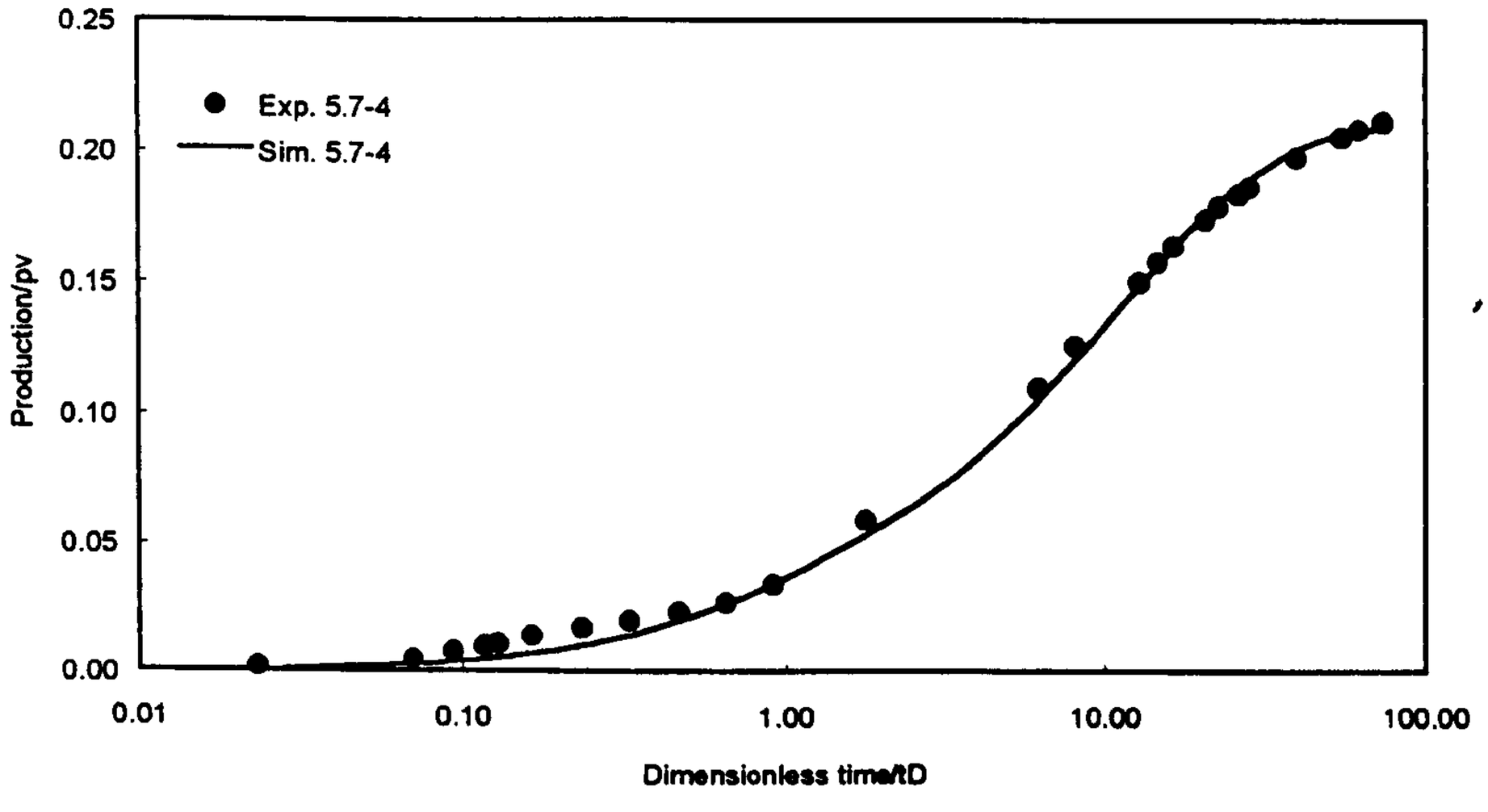

Figure 6.9b Simulation output and experimental data vs. time (log scale) for Experiment 5.7-4.

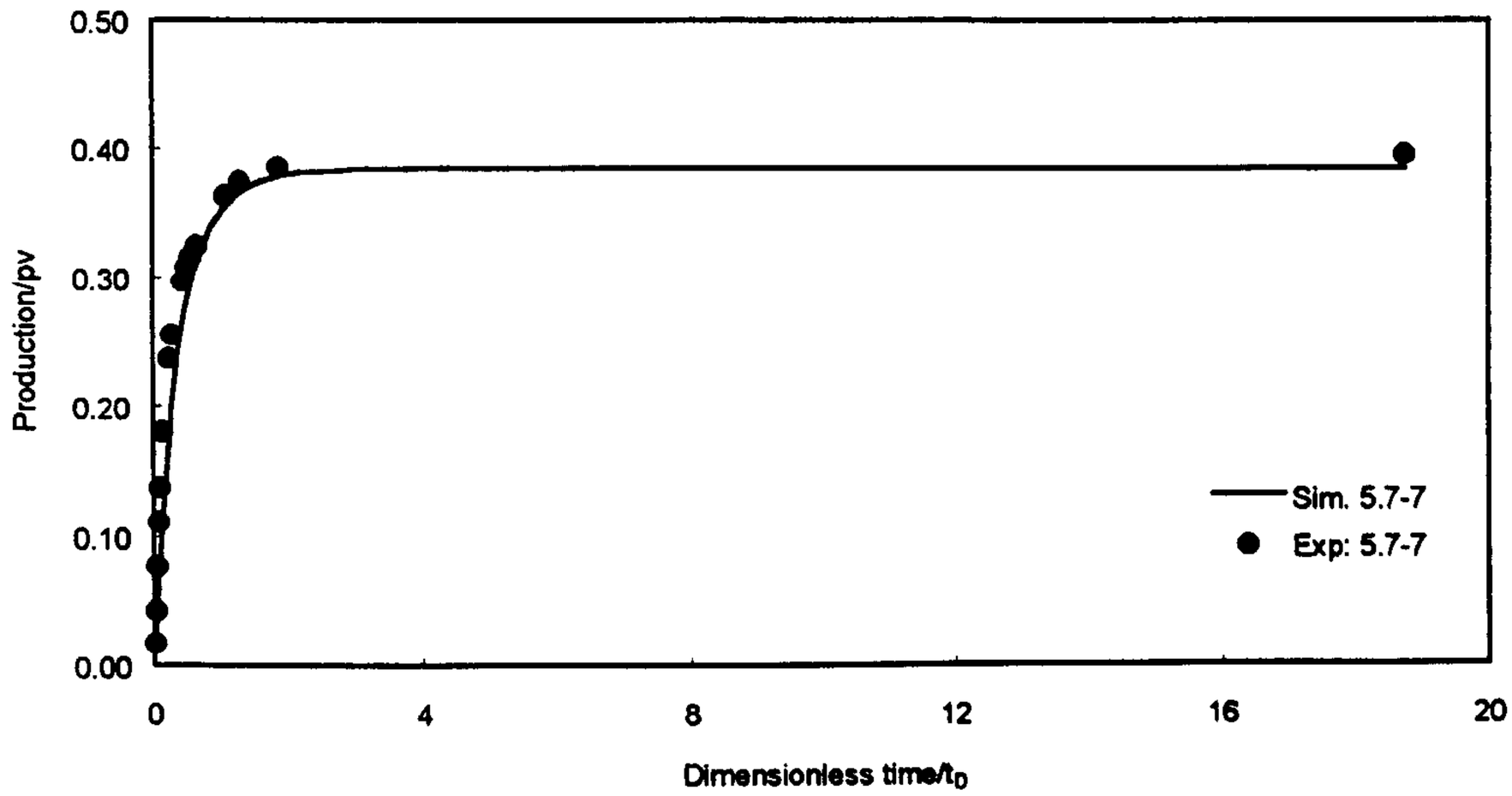

Figure 6.10a Simulation output and experimental data vs. time (log scale) for Experiment 5.7-7.

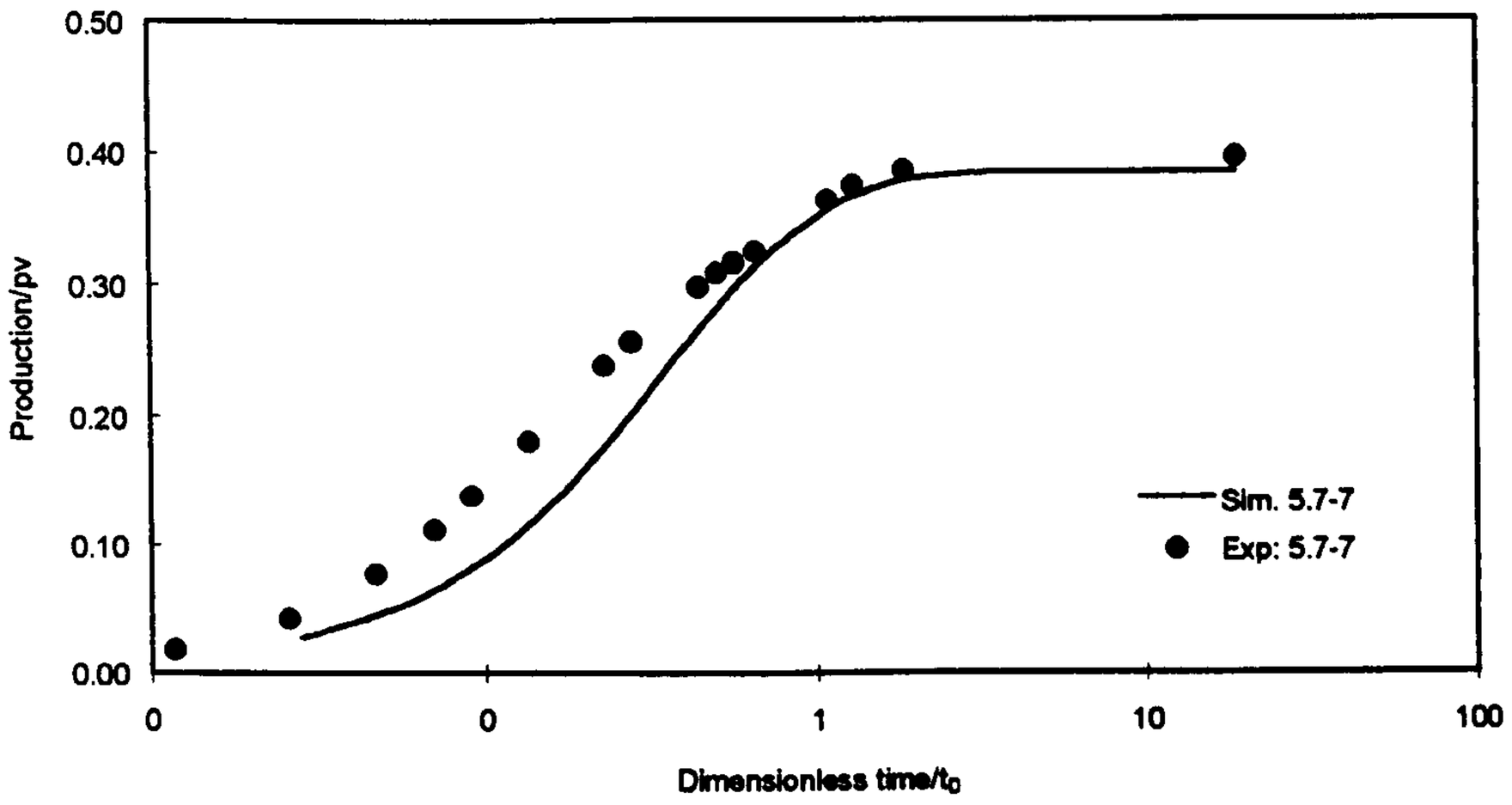

Figure 6.10b Simulation output and experimental data vs. time (log scale) for Experiment 5.7-7.

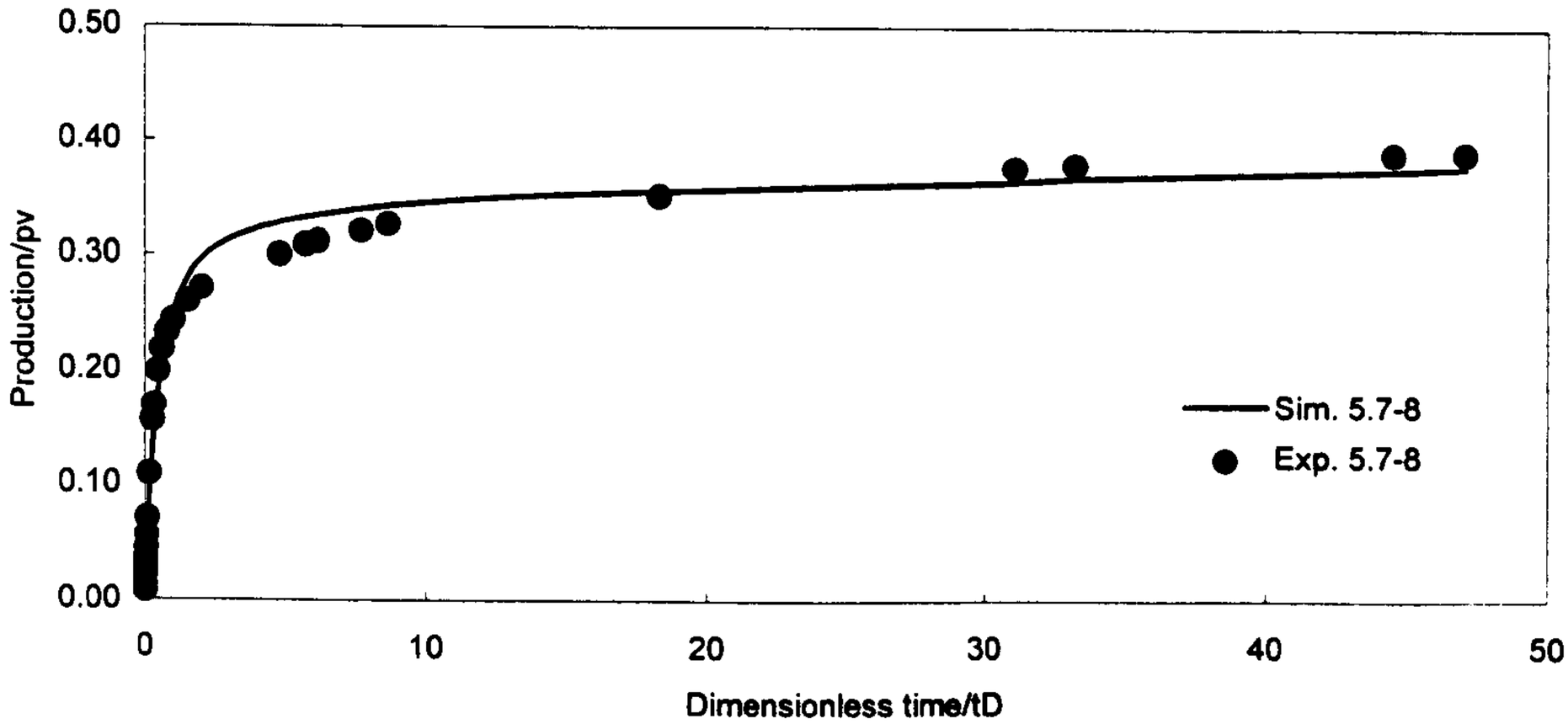

Figure 6.11a Simulation output and experimental data vs. time (linear scale) for Experiment 5.7-8.

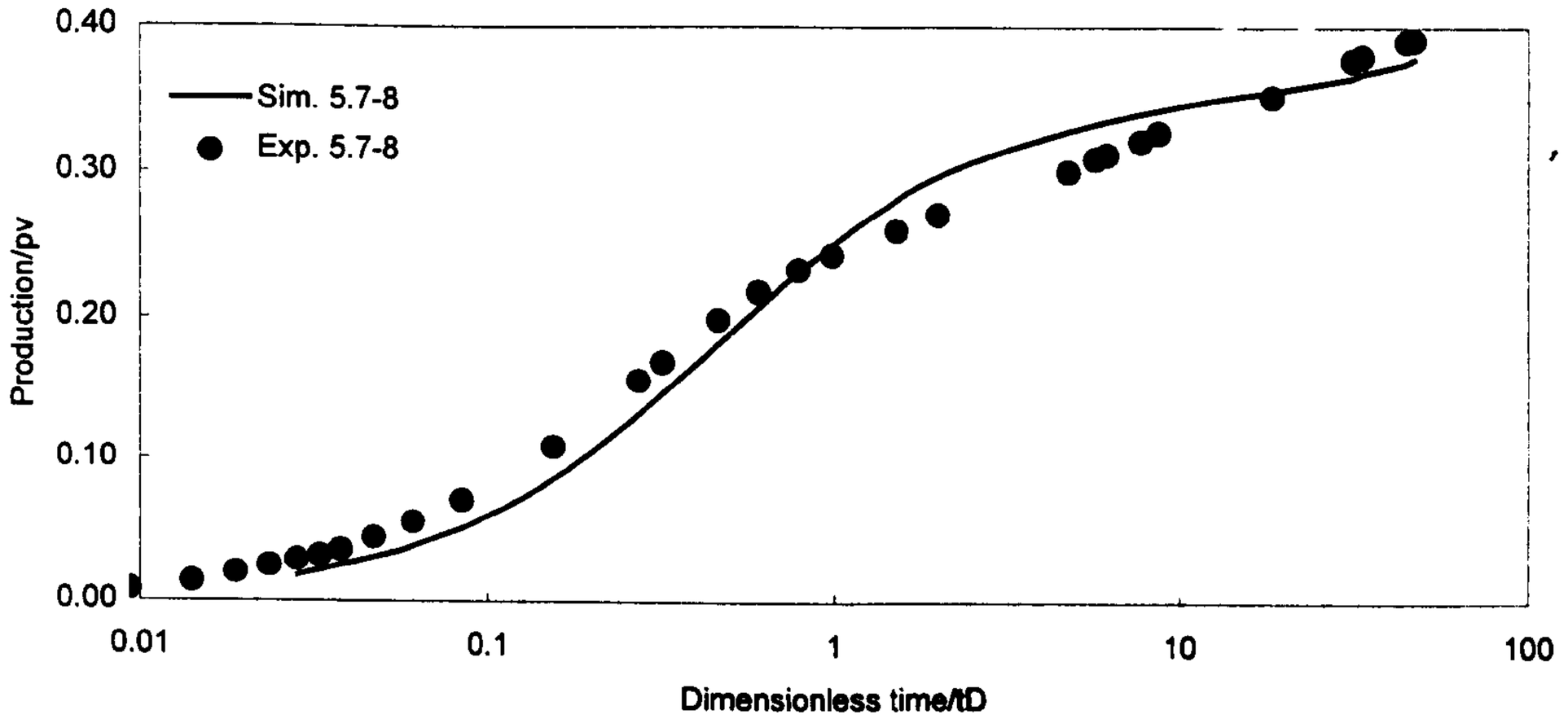

Figure 6.11b Simulation output and experimental data vs. time (log scale) for Experiment 5.7-8.

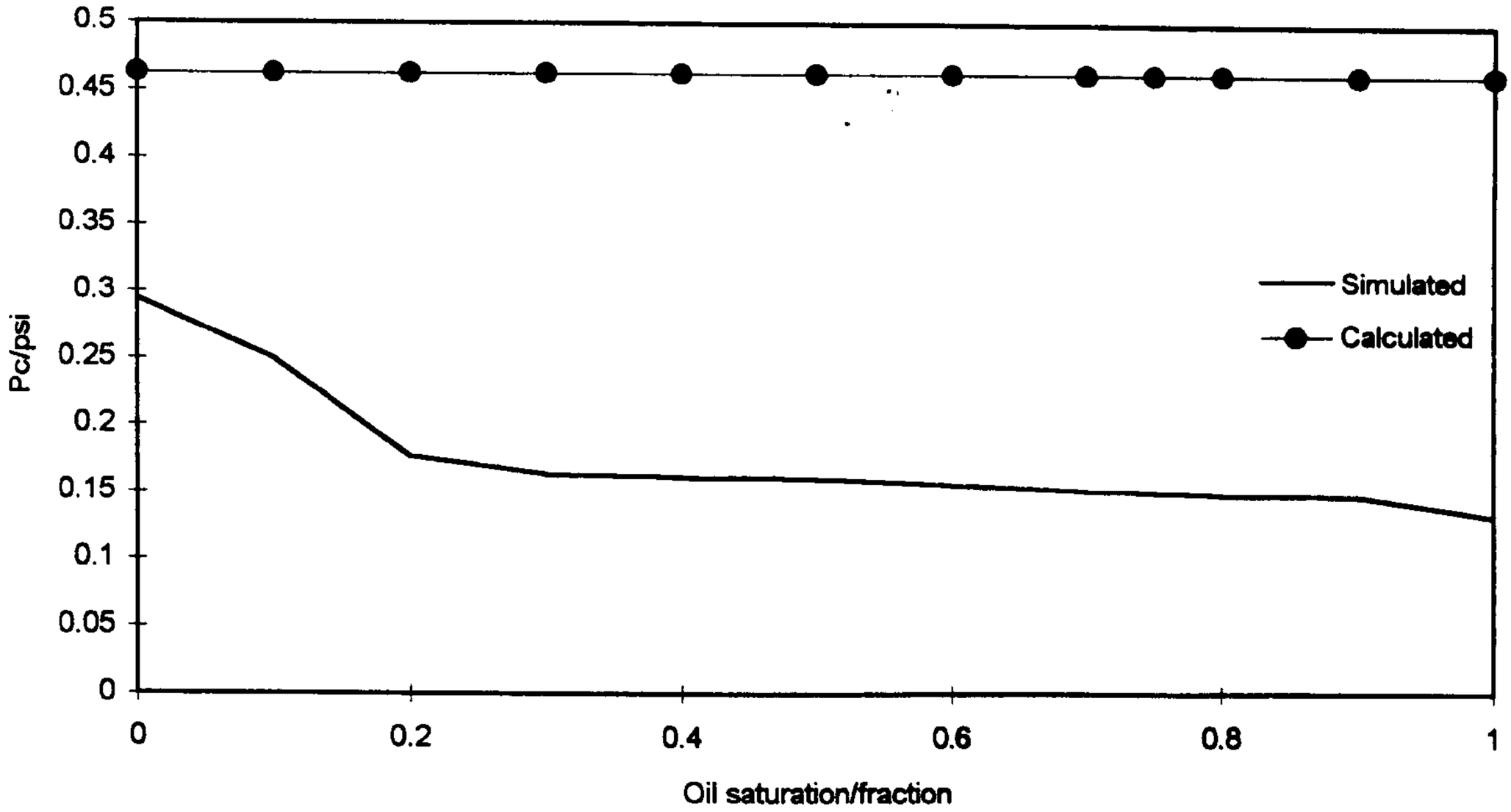

Figure 6.12 Comparison betweencalculated and simulated fracture capillary pressure for Experiment 5.7-2.

CHAPTER-7

CONCLUSIONS AND RECOMMENDATIONS FOR FUTURE WORK

7.1 CONCLUSIONS

Gravity drainage can result in recovery of substantial quantities of oil in primary, secondary and tertiary recovery periods of a fractured reservoir. The results of the micromodel observations can be used in conjunction with core flow experiments and mathematical modelling to improve our capabilities to predict the recovery performance of a reservoir. Based on this study, the following conclusions can be drawn. These conclusions are presented under the following three topics.

7.1.1 Gravity Drainage at Pore Scale

An investigation in microscopic displacement processes can be used to help understanding the macroscopic behavior of oil displacement which would in turn help in modelling flow mechanisms in large scales. The conclusion for this part are discussed under secondary and tertiary displacement processes.

a- Secondary process; The following conclusions were obtained when gas was injected, at very low rates (i.e. gravity stable), in a micromodel that was saturated with oil in the presence of irreducible connate water.

1- The irreducible water in the rock is generally considered immobile when gas injection studies are conducted using reservoir simulators. Our experiments revealed that this may not be valid (see Section 4.3). The injected gas changes the balance between gravity and capillary forces and may result in mobilization of water and redistribution of all phases. Therefore the current practice of using simple two-phase and three-phase relative permeabilities, with constant immobile water saturation is not adequate to describe the physical process of oil recovery by gas injection accurately.

2- With positive, or near zero spreading coefficient, which is generally the case for most oils and reservoir-waters, oil spreads over water and forms a film between gas and water phases. This oil film provides an efficient conduit for flow of oil between various pores under the combined effect of gravity and capillary forces.

3- Gravity drainage process in a layered porous medium is less efficient in comparison to a homogeneous medium with the same overall average permeability. Early arrival of the gas phase underneath the less permeable layer and its propagation there, causes entrapment of oil and some restriction in oil flow from the less permeable layer.

4- For gravity drainage of residual oil in the form of discontinuous blobs, the velocity is affected by the vertical length of the blobs, contact angle hysteresis, the liquid density to viscosity ratio and the geometry of the conducting spaces.

5- Oil drainage occurred both, ahead of the gas phase front and behind it in the gas invaded zone. As the gas front moves deeper in the model, the pressure difference between the gas and oil phases in the gas invaded part increases. Therefore, gas can overcome higher values of capillary pressure and enter smaller pore openings and result in further drainage of oil.

6- When gas breaks through the bottom of micromodel, several big clusters of oil are still present throughout the model, all being by-passed by loops of gas. After the gas breakthrough, gas leaves the model intermittently. Once the gas pressure overcomes the threshold pressure of the oil saturated throats at the exit, it rushes out of the micromodel. The oil recovery in this period is mainly by film flow process and gas continuous to flow intermittently.

b- Tertiary process; The observations stated here are the results of gravity stable gas injection into micromodels that had been initially water flooded and their oil saturation had been reduced to residual values.

1- In a mixed-wettability system, parts of the pores and throats surfaces are oil-wet, while the rest are water-wet. Movement of both oil and water in one pore as wetting phase was recognized, and by this arrangement of wettability the oil would be mobilized in the most pores. This implies that recovery of oil at a given level of water cut could be higher in mixed-wet system than in completely water-wet system.

2- The residual oil remaining in the pore space, after water flooding, can be re-mobilized by injection of gas. The oil blobs are generally invaded by gas phase and form a film of oil between gas and water phases. This process facilitates the flow of oil through its own film between the pores.

3- Depending on the balance of forces, the oil and water could flow concurrently or counter-currently with gas, when they flowed through their own films.

4- When two fingers of gas approach each other by drainage of liquid phase, liquid lamella between the two gas tips vanish quickly. But for the case of two oil fingers approaching each other, in most cases, a water lamella between the two oil tips stays there for a long time and moves with the bulk of the oil.

5- The capillary pressure largely dictates the residual phase saturation during the displacement process. It also provides the driving force for some of the liquid lamella rupture and coalescence events that occur between adjacent non-wetting (gas and/or oil) tips.

6- Although some large oil blobs or clusters were formed in the model, they were often by-passed by gas. The general view that oil bank is formed and pushed ahead to be recovered was not observed in our experiments. The start of oil production occurred together with gas breakth+rough and, thereafter, by the film flow process. This might be the artifact of the small size of the micromodel and its two dimensional feature.

7- When the spreading coefficient is negative the volume of trapped oil blobs remains almost constant for a long time, after they have been invaded by gas i.e. no significant oil

drainage takes place by film flow process. For the case of positive spreading coefficient, decrease in oil volume of one cluster, and at the same time an increase in the oil volume of another separate nearby oil cluster is observed. This event indicates that there is a good communication between different individual oil clusters via a continuous oil film for positive spreading coefficient.

7.1.2 Free Gravity Drainage in Fractured Reservoir

One of the most important issues in studying a fractured reservoir is to investigate block-to-block interaction. To improve our understanding of the block-to-block interaction the main phenomena i.e. free gravity drainage of single block, capillary pressure of horizontal fracture, infiltration process, effect of contact area and capillary continuity were investigated.

Free gravity drainage of single block

1- If a single block is surrounded instantaneously by gas, the oil will leave the block at a rate determined by the density difference between gas and oil, the oil permeability, the capillary pressure and the oil viscosity.

2- For the free gravity drainage of a single block, the oil production rate has the highest value in the beginning, and gradually reduces to zero when the oil saturation profile approaches its ultimate value (equilibrium between capillary and gravitational forces). As long as the gradient in gravity potential for the oil exceeds the gradient in capillary pressure, the oil flow continues.

3- During drainage the gas front travels rapidly downwards to reach the threshold height, whereas oil saturation at the upper part of the block approaches the ultimate drainage saturation profile very slowly due to the reduced oil mobility at lower oil saturation.

4- If the vertical permeability of the rock and the fluid properties are known, the gravity drainage velocity can be estimated from the theory presented in Section 5.3.3. This provides a method of estimating gravity drainage rates which are difficult to measure directly because of the long blocks necessary to obtain measurements for the region above the transition zone.

Capillary pressure of horizontal fracture

1- The results of the experiments of stacked of two blocks (when lower block is non-effective), revealed that there exist a critical fracture thickness for each set of physical conditions of the fracture system.

2- When the fracture aperture is more than the critical value, the drainage takes place by formation and detachment drop process. In this case the pressure difference between gas and oil in horizontal fracture (i.e. the fracture capillary pressure) is governed by the radius of curvature of the hanging drop. The hanging drop has two effects on drainage performance of the upper block by its length and by its capillary pressure. The combination of these two effects (which have different signs) is such that at the bottom surface of the upper block the capillary pressure has a very small value.

3- When the fracture aperture is less than its critical value, the enlarging drops deformed to liquid bridges between the upper and the lower blocks. When the lower block is impermeable, the amount of fracture capillary pressure (both for the liquid bridge and the hanging drop) is closed to zero and compared to capillary pressure of the matrix block in an actual reservoir condition is negligible.

Infiltration process

1- The required condition for the infiltration process is that the wetted region of trickled oil must be above the capillary hold-up zone. When geological conditions (along-dip and cross-dip barriers, flat and open fractures) are such that the wetted region is below the

threshold height, since all pores are filled by wetting phase, there is no capillary force for the infiltration process.

2- For a pile of two blocks, the oil which leaves the upper block can penetrate through the top and side boundaries of the lower block, thus delaying the drainage of the lower block and/or causing resaturation. Initially, it extends as a film over the wall surface before being imbibed in the rock, and the capillary pressure in that film reduces to zero. Since the capillary pressure at the bottom of the block is also close to zero, a potential gradient for oil is formed and causes the oil to be imbibed into the matrix. The effect of saturation change at the wetted region of the block is extended by film and/or bulk flow through the pores network to lower parts of the block, and gradually the oil saturation, relative permeability, and drainage rate of the block are increased.

3- In the gas invaded zone, when the flow rate of the oil from or passing upper blocks exceeds the characteristic drainage flow rate, q^*, of a lower saturated block, the infiltration rate at the top of the block will be equal to q^*, while the surplus will pass through the fracture network. When the oil flow rate from upper block is less than the q^* of the lower block, all of it will infiltrate into the lower block, and after a transitional period, stabilized oil saturation and distribution is reached, again.

4- When the top boundary of a desaturated block comes into contact with the constant oil trickled rate, the oil saturation around the wetted region instantaneously increases to $1\text{-}S_{gc,}$ while oil saturation in lower region is still at its initial (lower) value. The difference in the infiltration rate at the top and the drainage rate at the bottom of a block determines the rate of change of the average oil saturation of the block. The oil saturation and distribution inside the block and drainage flow rate will increase until a steady-state saturation is approached (depending on the capillary-pressure, relative permeability, and rate of oil supply). Once the system is stabilized, there is no further changes in oil

saturation and fluid distribution in the block remain constant and the infiltration and drainage rates become equal.

5- Due to the capillary force, in all of the performed infiltration experiments, the trickled oil preferred to move through the matrix instead of flowing through highly transmissible fractures. The oil produced from the upper blocks had to travel through all the neighboring blocks before being produced at the bottom of the lowest block.

6- When the blocks are tilted, as long as the angle of inclination is less than 45°, the trickled oil preferred to move through the porous media rather than slipped over the fracture surfaces. The inclination reduces the effective height of the block (H_b) by the amount of $H_b.(1-\sin\theta)$, where θ is the angle of inclination. When the width of the inclined blocks is large enough, the upper corner of the top block may undergo some drainage process.

It should be borne in mind that in the experiments reported in Section 5.5, oil was the wetting phase and there was no water present. In real reservoirs, however, some connate water is present and the capillary pressure of oil and gas in presence of water does not act exactly the same way as that of oil and gas. Moreover, most of reservoir rocks are of mixed wettability rather than completely oil wet or water wet.

Effect of contact area

1- At reservoir conditions, asphaltene precipitation, scale deposition and strong erosion are responsible for reduction in contact area between two neighbouring blocks to a fraction of the available surface area. While, the existence of rubbles of small pieces of permeable rocks within the fractures, which is a dominant feature in most fractured reservoir rocks, provides a degree of capillary continuity. As long as the contact area provides a capillary continuity between upper and lower blocks, the ultimate recovery will be the same as that of a single block with the same total height, but with a delay time.

2- There is a non-linear relationship between the gravity drainage rate and the contact area between the two blocks. To match the measured drainage rate of a stack with different contact areas, the time scale of drainage rate of full contact stack must be multiplied by a constant factor.

3- For each stack block system there is a lower limit value for the contact area, beyond which the transmissibility of the oil is so low that the production takes an unacceptable long time.

4- A new definition for constriction coefficient is presented; $C = t_c/t_u$, where t_c, and t_u are the drainage duration of the constricted case and the unconstricted case, respectively. Once C is tuned, it is possible to match the production data of a restricted block from the data of the unrestricted case, only by multiplying the time scale by the constriction coefficient.

Capillary continuity

1- In a stack of interacting equal and oil saturated blocks, which is surrounded by the gas, the oil produced from the upper blocks travels through the complete stack before being produced at the bottom of the lowest block. For the case of non-capillary contact between the blocks (thick fracture), the total amount of ultimate recovery will be equal to the number of blocks times the ultimate recovery of a single block. But for full capillary continuity between blocks, the ultimate recovery of a stack block is similar to a single block with the same height.

2- The main parameter that must be considered in capillary continuity is the 'drainage duration'. By increasing the degree of capillary continuity between two blocks, the starting time of shifting from bulk-flow through the liquid and/or porous bridge, to film flow over and/or through the spacers, will be increased.

3- When the fracture aperture is thick and spreading coefficient is positive, the oil drainage behind the gravity/capillary equilibrium of the upper block (single block case),

drains mainly by film flow process. The film flow process over the non/less porous spacers cannot provide adequate liquid transmissibility for flow across the fracture between the matrix blocks. The oil transmissibility by film flow is so small that production of oil from the threshold zone of the upper block takes an extremely long time. Since the drainage flow rate by film flow is very small, this kind of capillary continuity is recommended to be considered as non-effective.

4- When the fracture aperture is small enough for the existence of stable liquid bridges, the draining oil flows through them as bulk flow. Based on the high transmissibility via liquid bridges, it could be considered as an effective continuity. Still, there exists some delay time between the recovery performance of a stack block with the effective capillary continuity compare to that of a single block with the same height.

5- When there is no liquid bridge between the blocks, the fracture capillary pressure may be considered to be zero (discontinuous blocks). If during its enlargement process the oil drop attaches to the upper surface of the lower block (a narrow fracture) the pressure difference between oil and gas changes suddenly. In this case, the capillary pressure of fracture (capillary pressure of the liquid bridge) is comparable with the capillary pressure of the matrix at that elevation. The two radii of curvature of the liquid bridge would be adjusted, such that they represent a capillary pressure which is a function of density difference between oil and gas and height of the fracture from zero level capillary pressure.

6- when the fracture aperture is less than its critical value, as long as, the continuity between matrix blocks are through the stable liquid bridges, the capillary pressure of horizontal fracture has no relation with the amount of fracture aperture. In this condition, fracture capillary pressure can be calculated from the equation $P_{cf} = \Delta\rho.g.h$, where h is the elevation of the horizontal fracture from the level of zero capillary pressure.

7- There exists a maximum capillary pressure for the liquid bridge ($P_{c\text{-}l\text{-}max}$), such that beyond this $P_{c\text{-}l\text{-}max}$, the liquid bridge will disintegrate. If the capillary pressure of the fracture exceeds this value the liquid bridges that contact the adjacent matrix block will disintegrate and capillary continuity will shift to discontinuity.

8- Although different degrees of capillary continuity have the same effect from ultimate recovery point of view, but their transmissibility are not the same. The weakest degree of capillary continuity (capillary continuity through oil film over the boundary of solid spacers), results the smallest transmissibility. At the best conditions (narrow fracture aperture), due to a larger number of liquid bridges the transmissibility of a stack block is such that its flow rate is close to that of a single block with the same height.

7.1.3 Simulation Study

1- When the grid cells are larger than the matrix blocks, experimental recovery data or fine grid technique can be used for generating pseudo relative permeability and capillary pressure for grid cells. To produce pseudos, Corey's and Land's coefficients were tuned until a good match was obtained with experimental data or fine grid results. In reservoir simulation, the generated pseudos may be used later for predicting recovery performance under different production scenarios.

2- A numerical simulator with dual porosity-dual permeability option can be used to simulate gravity drainage process in a stack of blocks. It handles the problem by assigning some pseudo properties to fracture. These pseudo properties of the fracture are useful for sensitivity analysis and history matching of the system.

3- It should, however, be mentioned that the greatest weakness of dual porosity models are the lack of data on fracture sizes, distributions, orientations, permeabilities, porosities and matrix block sizes and properties, which usually vary considerably in the reservoir.

7.2 RECOMMENDATIONS FOR FUTURE WORK

1- Based on the microscale gravity stable gas injection experimental results, it is recommended that more micromodel experiments should be performed using micromodels with characteristics more similar to real reservoir conditions. These should include micromodels with rough texture, mixed wet, heterogeneity and layering.

2- Important phenomena to be investigated by physical model experiments are:

. Free gravity drainage from a single block, followed by trickling of oil droplets on top and/or along the sides of the block for different tilts and trickling rates.

. The possibility of precipitation of asphaltenes or other impermeable materials on matrix block surfaces and the possible effect on the flow by plugging the pores.

. The effect of reduction in the formation pressure on physical properties of the fracture network.

3- To Perform mechanistic modeling and network modeling of the flow processes in the fractured porous media. The observations made in physical micromodel experiments should be considered by such mathematical modeling. The modeling should be formulated to handle flow of three fluid phases in three dimensional space and it should be capable of simulating the micromodel experiments in two-dimensional models.

4- To carry out a more systematic investigation of the fracture aperture, in particular to investigate the following processes;

. The way oil is flowing through the inclined fracture system with different inclination angle, when gas is present there (film flow, bulk flow or through preferential paths).

. Studies at the microscale, at which two-phase flow through fractured porous media are suitable for investigation, are required to be pursued in order to obtain a more complete mechanistic understanding of the block-to-block interaction.

. Also, stability of liquid bridges at small draining rate of oil for different fracture aperture is recommended.

5- As an extension of this work, gravity drainage under non-equilibrium gas injection conditions should be examined. The process of gas diffusion and variation of interfacial tension will then become the critical issues affecting the drainage rate and recovery.

6- The actual degree of interaction and the effective height of the stack of reservoir blocks that interfere needs further investigation.

7- Based on the ideas presented in Section 5.7-7, more research is suggested, to establish a new algorithm, to obtain the values of fracture capillary pressure which can be included in computer simulations of fractured reservoirs.

REFERENCES

Abrams, A., (1975). "The Influence of Fluid Viscosity, Interfacial Tension, and Flow Velocity on Residual Oil Left by Waterflood." Society of Petroleum Engineers J., 15, October, p. 437-47.

Acuna, J.A., Y.C. Yortsos, (1991). "Numerical Construction and Flow Simulation in Networks of Fractures Using Fractal Geometry." SPE 22703, presented at the SPE Annual Technical Conference and Exihibition, Dallas, October 6-9. Richardson, TX: Society of Petroleum Engineers.

Acuna, J.A., I. Ershaghi, Y.C. Yortsos, (1992). "Practical Application of Fractal Pressure Transient Analysis of Naturally Fractured Reservoirs." SPE 24705, presented at the SPE Annual Technical Conference and Exihibition, Washington D.C., October 4-7. Richardson, TX: Society of Petroleum Engineers.

Adamson, A.W., (1990). "Physical Chemistry of Surfaces." 5th Edition, Wiley-Interscience, New York.

Aguilera, R., (1991). "An Approximate Solution of Linear flow in Naturally Fractured Reservoirs." The Journal of Canadian Petroleum Technology, May.

Aguilera, R., (1993). "Advances in the study of Naturally fractured Reservoirs." The Journal of Canadian Petroleum Technology, Volume 32, No. 5, May.

Aleman-Gomez, M., T.R. Ramamohan, and J.C. Slattery, (1984). "A Statistical Model for Unsteady-State Displacement in Porous Media." SPE paper 13265 presented at the 59th Technical Conference and Exhibition of the Society of Petroleum Engineers, Houston,.

Anderson, W.G., (1986-A). "Wettability Literature Survey - Part 1: Rock-Oil-Brine Interactions, and the Effects of Core Handling on Wettability." Journal of Petroleum Technology, 38, pp. 1125, October.

Anderson, W.G., (1986-B). "Wettability Literature Survey - Part 2: Wettability Measurement." Journal of Petroleum Technology, 38, November.

Anderson, W.G., (1986-C). "Wettability Literature Survey - Part 3: The Effect of Wettability on the Electrical Properties of Porous Media." Journal of Petroleum Technology, 38, December.

Anderson, W.G., (1987-A). "Wettability Literature Survey - Part 4: The Effect of Wettability on Capillary Pressure." Journal of Petroleum Technology, October.

Anderson, W.G., (1987-B). "Wettability Literature Survey - Part 5: The Effect of Wettability on Relative Permeability." Journal of Petroleum Technology, November.

Anderson, W.G., (1987-C). "Wettability Literature Survey - Part 6: The Effect of Wettability on Water flooding." Journal of Petroleum Technology, December.

Archie, G.E., (1942). "The Electrical Resistivity Log as an Aid in Determining Some Reservoir Characteristics." AIME Tech. Pub., vol. 142.

Armitage, P., R.A. Dawe, (1989). "What is the Rheology of Foam in Porous Media, A Micromodel study." paper SPE 18495, presented at the International Symposium on Oil field Chemistry in Houston. TX, 8-10 February.

Aronofsky, J.S., L. Masse, and S.G. Natanson, (1958). "A Model for the Mechanism of Oil Recovery from the Porous Matrix Due to Water Invasion in Fractured Reservoirs." Trans., AIME vol. 213, pp. 17-19.

Babadagli, T., I. Ershaghi, (1993). "Improved Modelling of Oil/Water Flow in Naturally Fractured Reservoirs Using Effective Fracture Relative Permeabilities." SPE 26076, presented at the SPE Western Regional Meeting, Anchorage, May 26-28, Richardson, TX: Society of Petroleum Engineers.

Bahralolom, I., R.E. Bretz, and F.M. Orr Jr., (1988-A). "Experimental Investigation of the Interaction of Phase Behaviour with Microscopic Heterogeneity in a CO_2 Flood." SPE Reservoir Engineering, v. 3, n.2, pp. 662-672.

Bahralolom, I., F.M. Orr Jr, (1988-B). "Solubility and Extraction in Multiple-Contact Miscible Displacement: Comparison of N_2 and CO_2 Flow Visualisation Experiments." SPE Reservoir Engineering, v. 3, n.1, pp. 213-219.

Baker, L.E., (1988). "Three Phase Relative Permeability Correlations." SPE 17369. Paper presented at the SPE/DOE EOR Symposium in Tulsa, Ok, April 17-20.

Bardon, C., D.G. Longeron, (1980). "Influence of Very Low Interfacial Tensions on Relative Permeability." Society of Petroleum Engineers J., October, 391-401.

Barenblatt, G.E., I.P. Zheltov, and I.N. Kochina, (1960). "Basic Concepts in the Theory of Seepage of Homogeneous Liquids in Fissured Rocks." J. Appl. Math. and Mech., pp. 1286-1303.

Bech, N., O.K. Jensen, and Birger Nielsen, (1991). "Modeling of Gravity-Imbibition and Gravity-Drainage Processes: Analytical and Numerical Solutions." SPE Reservoir Engineering, February.

Beckner, B.L., K. Ishimoto, S. Yamaguchi, (1987). "Imbibition-Dominated Matrix-Fracture Fluid Transfer in Dual Porosity Simulators." SPE no. 16981.

Beckner, B.L., A. Firoozabadi, and K. Aziz, (1988). "Modeling Transverse Imbibition in Double-Porosity Simulators." paper SPE 17414, presented at the 1988 SPE California regional Meeting, Long Beach, C.A., March 23-25.

Bentsen, R.G, (1977). "Conditions Under which Capillary Terms may be Neglected." paper presented at 28th Annual Tech. Meeting of Pet. Soc. of CIM, Edmonton, May 30 - June 3.

Bentsen, R.G., and H.K. Sarma, (1989). "The External-Drive Technique: Its Use and Abuse." The AOSTRA Journal of Research, Vol. 5, No. 1, 61-74.

Birks, J., (1957). "A Reservoir Engineering Study of the Masjid-i-Sulaiman reservoir." BP report KH/PE/77.

Bikeman, J.J., (1958). "Surface Chemistry." Academic Press. New York, p. 65.

Botset, H.G, (1940). "Flow of Gas-Liquid Mixtures Through Consolidated Sand." Trans. AIME, vol. 136, pp. 91-103.

Bourbiaux B.J., F.J. Kalaydijian, (1990). "Experimental Study of Cocurrent and Countercurrent Flows in Natural Porous Media." paper SPE 18283 presented at the 63rd Annual Tech. Conf. and Exh. of SPE, Houston, TX, October 2-5.

Brownell, L.E., and Katz, D.L., (1947). "Flow of Fluids Through Porous Media." Chem. Eng. Progr., vol. 43, pp. 601.

Buckingham, E., (1907). "Studies in the Movement of Soil Moisture." U. S. Depart. Agr. Bur. Soils Bull. 38, Washington D.C., PP. 29-61.

Buckley, S.E., and M.C. Leverett, (1942). "Mechanism of Fluid Displacement in Sands." Trans. AIME, vol. 146, pp. 107-116.

Buckley J.S. , Takamura K., and Morrow, N.R., (1987). "Influence of Electrical Surface Charges on the Wetting Properties of Crude Oils." paper SPE 16964 presented at Annual Fall Technical Conference, Dallas, TX, September, 27-30.

Campbell, B.T. and F.M. Orr, (1985). "Flow Visualization for CO2/Crude Oil Displacements." Society of Petroleum Engineers J., v. 25, no. 5, pp. 665-678, October.

Cardwell, W.T., R.L. Parsons, (1948). "Gravity Drainage Theory." Trans. AIME, vol. 179, pp. 199-215.

Carman, P.C, (1937). "Fluid Flow through Granular Beds." Trans. Inst. Chem. Engrs., London, vol. 15, pp. 150 ff.

Catchpole, J.P. and G. Fulford, (1966). "Dimensionless Groups." Ind. and Eng. chem., 58, 46.

Caudle, B.H., R.L. Slobod, and E.R. Brownscombe, (1951). "Further Developments in the Laboratory Determination of Relative Permeability." Trans. AIME 192, pp. 145-150.

Chatenever, A. and J. C. Calhoun, (1952). "Visual Examination of Fluid Behavior in Porous Media." Trans. AIME 195, pp. 149-156.

Chatzis, I., N.R. Morrow, and H.T. Lim, (1983). "Magnitude and Detailed Structure of Residual Oil Saturation." Society of Petroleum Engineers Journal, pp. 311-326, April.

Chatzis, I. , A. Kantzas, and F. A. L. Dullien, (1988). "On the Investigation of Gravity-Assisted Inert Gas Injection using Micromodels, Long Berea Sandstone Cores, and Computer-Assisted Tomography." paper SPE 18284, presented at 63rd Annual Technical Conference and Exhibition of SPE Houston, October 2-5.

Chuoke, R.L., P. van Meurs, and C. van der Poel, (1959). "The Instability of Slow, Immiscible, Viscous Liquid-Liquid Displacements in Permeable Media." Trans. AIME, vol. 216, pp. 188-194.

Cinco-Ley, H. and F.V. Samaniego, (1982). "Pressure Transient Analysis for Naturally Fractured Reservoirs: "paper SPE 11026, presented at the 57th Annual Fall Technical Conference and Exhibition of the SPE-AIME, New Orleans, san Francisco, Mar 24-26.

Coats, K.H., J.R. Dempsey, and J.H. Henderson, (1971). "The Use of Vertical Equilibrium in Two- Dimensional Simulation of Three-Dimensional Reservoir Performance." Society of Petroleum Engineers J., March.

Coats, K.H, (1989). "Implicit Compositional Simulation of Single-Porosity and Dual-Porosity Reservoirs." paper SPE 18427, presented at the 1989 SPE Symposium on Reservoir Simulation, Houston, TX., February. 6-8.

Codreanu, Dimitrie Bossie, P.R. Bia, J.C. Sabathier, (1983). "The 'Checker Model,' An Improvement in Modeling Naturally Fractured Reservoirs with a Tridimensional, Triphasic, Black-oil Numerical Model." Society of Petroleum Engineers J., October.

Collins, R.E, (1961). "Flow of Fluids Through Porous Materials." McGraw Hill Company, New York, 143.

Corey, A.T., Rathjens, and C.H., Henderson, J.H., and Wyllie, M.R.J., (1956). "Three-phase relative permeability." JOURNAL OF PETROLEUM TECHNOLOGY, pp. 63-65, November.

Danesh, A. , J.M. Peden, D. Krinis, G.D. Henderson, (1987). "Pore Level Visual Investigation of Oil Recovery by Solution Gas Drive and Gas Injection." paper SPE 16956, presented at 62nd Annual Tech. Conf. and Exh. of SPE, Dallas, TX, 27-30 September.

Danesh, A. , D. Krinis, G.D. Henderson and J.M. Peden, (1988-A). "Asphaltene Deposition in Miscible Gas Flooding of Oil Reservoirs." Chem. Eng. Res. Des. v. 66, pp. 339-344.

Danesh, A. , D. Krinis, G.D. Henderson and J.M. Peden, (1988-B). "Experimental Investigation of Retrograde Condensation in Porous Media at Reservoir Conditions." paper SPE 18316, presented at the 63rd Annual Technical Conference and Exhibition of SPE, Houston, October 2-5.

Danesh, A. , D. Krinis, G.D. Henderson and J.M. Peden, (1989). "Pore-Level Visual Investigation of Miscible and Immiscible Displacements." J. Petroleum Science and Engineering, V. 2, pp. 167-177.

Darcy, H., (1856). "Les Fontaines publiques de la ville de Dijon." Victor Dalmont, Paris.

Davis, J.A., and S.C. Jones, (1968). "Displacement mechanisms of micelle solutions." Journal of Petroleum Technology, 20, (December), pp 1415-1428.

Dawe, R.A., R.J. Wright, (1983). "Oil Recovery Behaviour: The Microscale." The Royal Scholl of Mines Journal, 33, pp. 25-30.

de Laplace, P.S., (1806). "Mechanique Celeste." Supplement to Book 10.

de Silva, F.V., B. Meyer, (1990). "Analysis of Gravity Capillary Equilibrium in Chalk Fractured Reservoirs." Third North Sea chalk Symposium.

de Swaan, A., (1978). "Theory of Water flooding in Fractured Reservoir." Society of Petroleum Engineers J., pp. 117-128, April.

Dean, R.H., and L.L. Lo, (1988). "Simulations of Naturally Fractured Reservoirs." SPE Reservoir Engineering, May, pp. 638-648.

Delclaud, J.P, (1972). "New Results on the Displacement of a Fluid by Another in a porous Medium." paper SPE 4103, presented at 47th Annual Fall SPE meeting, San Antonio, October 8-11.

Dombrowski, H.F., and L.E. Brownell, (1954). "Residual Equilibrium Saturation of Porous Media." Ind. Engineering Chem., 46, pp. 1207-19.

Donaldson, E.L., B.P. Lorenz, and R.D Thomas, (1966). "The Effects of Viscosity and Wettability on Oil and Water Relative Permeabilities." Paper SPE 1562 presented at 41st Annual Fall SPE Meeting, Dallas, October 2-5.

Donaldson, E. C. , and R.D Thomas, (1971). "Microscopic Observations of Oil Displacement in Water-wet and Oil-wet Systems." SPE 3555, presented at 46th Annal Fall Meeting of Society of Petroleum Engineering, New Orleans, La., October 3-6.

Donaldson, E.L., M.B. Kayser, (1981). "Three-Phase Fluid Flow in Porous Media." DOE/BETC/IC-80/4, report published by the US Department of Energy, Bartlesville, Okla., April.

Dullien, F.A.L, (1979). "Porous Media: Fluid Transport and Pore Structure." Academic Press, New York.

Dumore, J.M., (1970). "Development of Gas Saturation During Solution Gas Drive in an Oil Layer Below a Gas Cap." Trans. AIME , Vol. 244, P. 211.

Dumore, J.M., and R.S. Schols, (1974). "Drainage Capillary-Pressure Functions and the Influence of Connate Water." SPEJ, 437, November.

Dykstra, H., (1978). "The prediction of Oil recovery by gravity Drainage." paper SPE 6548, Journal of Petroleum Technology, pp. 813-830, June.

ECLIPSE, (1994). "ECLIPSE 100 Reference Manual." no. 94a, Intera Information Technologies Limited.

Ehrlich, R. and F.E. Crane, (1969). "A Model for Two-Phase Flow in Consolidated Materials." SPEJ, 221-231 June.

Ehrlich, R., H.H. Hasiba, and P. Raimondi, (1974). "Alkaline Water flooding for wettability Alteration-Evaluating a Potential Field Application." SPE no. 4905, JOURNAL OF PETROLEUM TECHNOLOGY p. 1335.

Ershaghi, I., and R. Aflaki, (1985). "Problems in Characterisation of Naturally Fractured Reservoirs from Well Test Data." SPE Journal, June.

Fatt, I., (1956). "The network model of porous media." Trans. AIME, 207, pp. 144-159.

Festoy, S., and T.D. van Golf-Racht, (1987). "Gas Gravity Drainage in Fractured Reservoirs Through New Dual-Continuum Approach." paper SPE 16980 presented at the 1987 SPE Annual Technical Conference and Exhibition, Dallas, TX., September, 27-30.

Firoozabadi, A., and L.K. Thomas, (1989). "Sixth SPE Comparative Solution Project :A Comparison of Dual-Porosity Simulators." SPE Symposium on Reservoir Simulation in Houston, TX, February 6-8.

Firoozabadi, A., and J. Hauge, (1990). "Capillary pressure in Fractured porous media." Journal of Petroleum Technology, pp. 784-791, June.

Firoozabadi, A., (1991). "Aurthor's Reply to Discussion of Capillary Pressure in Fractured Porous Media" SPE 22212, February.

Firoozabadi, A., and T. Markeset, (1992-A). "An Experimental Study of Capillary and Gravity Cross-flow in Fractured Porous Media." paper SPE 24918 presented at the 67th Annual Technical Conference and Exhibition, Washington, DC, October 4-7.

Firoozabadi, A., Tore Markeset, (1992-B). "An Experimental study of the Gas-Liquid Transmissibility in Fractured Porous Media." SPE 24919, presented at the SPE Annual Technical Conference and Exhibition, Washington, D.C., October 4-7.

Firoozabadi, A., and K. Ishimoto, (1994-A). "Reinfiltration in Fractured Porous Media: Part 1- One Dimensional Model." SPE 21796, paper SPE Advanced Technology Series, Vol. 2, pp. 35-44.

Firoozabadi, A., K. Ishimoto, and B. Dindoruk, (1994-B). "Reinfiltration in Fractured Porous Media: Part 2- Two Dimensional Model." paper SPE 21798, SPE Advanced Technology Series, Vol. 2, pp. 45-51.

Firoozabadi, A., T. Markeset, (1994-C). "Fracture-Liquid transmissibility in Fractured Porous Media." SPE 24919, SPE Reservoir Engineering, August.

Foster, W.R, (1973). "A Low-Tension Waterflooding Process." Journal of Petroleum Technology, 25, 205-210.

Fulcher Jr, R.A., T. Ertekin, C.D. Stahl, (1985). "Effect of Capillary Number and Its Constituents on two-phase Relative Permeability Curves." Journal of Petroleum Technology, pp. 249-260, February.

Fung, Larry S.K., and D.A. Collins, (1991). "An Evaluation of the Improved Dual Porosity Model for the Simulation of Gravity Effects in Naturally Fractured Reservoirs." JPCT Vol. 30, No.3.

Geertsma, J., (1956). "Theory of Dimensionally Scaled Models of Petroleum Reservoirs." Trans., AIME vol. 207, pp. 118, Journal of Petroleum Technology, pp. 1125, June.

Geffen, T.M., W.W. Owens, D.R. Parish, and R.A. Morse, (1951). "Experimental Investigation of Factors Affecting Laboratory Relative Permeability Measurements." Trans. AIME, vol. 192, pp. 99-110.

Gilman J.R., and H. Kazemi, (1988). "Improved Calculations for Viscous and Gravity Displacement in Matrix Blocks in Dual-Porosity Simulators." SPE 16010, Journal of Petroleum Technology, pp. 60-70, January.

Gray, J.D., R.A. Dawe, (1989). "Modelling Low Interfacial Tension (<1mN/m) Hydrocarbone Phenomena in Porous Media with Particular Relevance to Gas Condensate and Volatile oil Reservoirs." paper SPE 19695, presented at the 64th Annual Tech. Conf. and Exhibition, San Antonio, Tex., October 8-11.

Habermann, B, (1960). "The Efficiency of Miscible Displacement as a Function of Mobility Ratio." Trans. AIME, v. 219, p. 264.

Hagoort , J., (1978). "Oil Recovery by Gravity Drainage." paper SPE 7424, SPE Journal, pp. 139-150.

Halbouty, M.T., (1969). "The Future of the Domestic Oil and Gas Industry." Journal of Petroleum Technology, 149, February.

Hall A.C., S.H. Collins, and J.C. Melrose, (1983). "Stability of Aqueous Wetting Films in Athabasca Tar Sands." Society of Petroleum Engineers J., pp. 249-258 April.

Hall, H.N., (1961). "Analysis of Gravity Drainage." Journal of Petroleum Technology, pp. 927-936, September.

Handy, L.L., and P. Datta, (1966). "Fluid Distribution During Immiscible Displacement in Porous Media." Trans. AIME, 237, 261.

Hammon, G., J. Vidal, (1988). "Scaling-up the Capillary Imbibition Process from Laboratory Experiments on Homogeneous and Heterogeneous Samples." paper SPE 15852 presented at the SPE European Petroleum Conference, London, 20-22 October.

Harkins, W.D, (1952). "The Physical Chemistry of Surface Films." Reinhold, New York, in 'Physical Chemistry of Surfaces', A.W.Adamson, John Wiley & Sons, Inc., 1990, p. 110.

Hewett, T. A. and R. A. Behrens, (1991). "Reservoir characterization." II, eds. L.W. Lake, H. B. Carroll, Academic Press, San Diego.

Higgings, R.V., G.B. Shea, (1949). "Laboratory Studies of Gravitational Drainage of Oil from Unconsolidated Sands." U.S. Bureauof Mines, RI 4391.

Hirasaki G.J., (1988). "Wettability: fundamentals and surface forces." paper SPE/DOE 17367 presented at the SPE/DOE enhanced oil recovery symposium, Tulsa, OK, April 17-20.

Homsy, G. M, (1987). "Viscous Fingering in Porous Media." Ann. Rev. Fluid Mechanics, v. 19, pp. 271-311.

Honarpour, M., L. Koederitz and A.M. Hawey, (1986). "Relative Permeability of Petroleum Reservoirs." CRC Press, Florida.

Horie, Tadashi, Abbass Firoozabadi, (1988). " Capillary Continuity in Fractured Reservoirs." paper SPE 18282.

Horie, T., A. Firoozabadi, K. Ishimoto, (1990). "Laboratory Studies of Capillary Interaction in Fracture/Matrix Systems." SPE Reservoir Engineering, August.

Hornof, V., N.R. Morrow, (1988). "Flow Visualisation of the Effective of Interfacial Tension on Displacement" , SPERE 3:251-256, February,

Hovanessian, S.A. and F.J. Fayers, (1961). "Linear Waterflood with Gravity and Capillary Effects." Society of Petroleum Engineers J, Mar. 32-36.

Huh, D.G. , T.D. Cochrane, F.S. Kovarik, (1988). "The Effect of Microscopic Heterogeneity on CO_2 Foam Mobility: Part 1- A Mechanistic study." paper SPE/DOE Sixth Symposium on Enhanced Oil Recovery, Tulsa, OK, 17-29 April.

Huitt, J. L., (1956). "Fluid Flow in Simulated Fractures." A.I.Ch.E. Jour., 2, No. 2:259-264.

Johnson, R.F., Jr., and Dettre, R.H., (1969). "Wettability and Contact Angles, in Surface and Colloid Science." Ed. E. Matijevic, Wiley - Interscience, New York.

Johnson, E.F., D.P. Bossler, and V.O. Naumann, (1959). "Calculation of Relative Permeability from Displacement Experiments." Trans. AIME, 219, pp. 370-372,

Jones., F.O., Jr. (1975). "A Laboratory Study of the Effects of Confining Pressure on Fracture Flow and Storage Capacity in Carbonate Rocks." paper SPE 4569, Journal Of Petroleum Technology, January.

Jones, T.A., S.O. Wooten and T.J. Kaluza, (1988). "Single-Phase Flow Through Natural Fractures." paper SPE 18175, presented at the SPE 63 Annual Tech. Conf. and Exhibit., Houston, TX.

Kantzas, A., I. Chatzis, and F.A.L. Dullien, (1988). "Enhanced Oil Recovery by Inert Gas Injection." paper SPE 17379, in proceeding of the SPE/DOE Symposium on Enhanced Oil Recovery, Society of Petroleum Engineers, Tulsa, OK, April 17-20.

Kazemi, H.: "Pressure Transient Analysis of Naturally Fractured Reservoirs" AIME , pp. 451-461. Richardson, TX, (1969).

Kazemi, H., L.S. Merrill, JR, K.L. Porterfield, and P.R. Zeman, (1976). "Numerical Simulation of Water-oil Flow in Naturally Fractured Reservoirs.", Society of Petroleum Engineers J., pp. 317-326, December, Trans., AIME, vol. 261.

Kazemi, H., J.R. Gilman, (1992). "Analytical and Numerical Solution of Oil Recovery From Fractured Reservoirs with Empirical Transfer Functions." SPE Reservoir Engineering, May.

Kimbler, O.K. and B.H. Caudle, (1957). "New Technique for Study of Fluid Flow." Oil & Gas J. 55 (50), December 16, pp 85-88.

Kleppe, J. , R.A. Morse, (1974). "Oil production from fractured reservoirs by water displacement." paper SPE 5084 presented at the SPE-AIME 49th Annual Fall Technical Conference and Exhibition, Houston, October 6-9.

Klikenberg, L.J., (1941). "The Permeability of Porous Media to Liquids and Gases." API Drill. and Prod. Practice, p. 200.

Kozeny, J, (1927). "Uber Kapillare Leitung des Wassers im Boden." Sitzber. Akad. Wiss. Wien, Math-naturew. kł., vol. 136-2A, pp.271ff.

Krohn, C.E., (1988). "Fractal Measurements of Sandstones, Shales, and Carbonates." J. Geophys. Res., 93(B4): PP. 3297-3305.

Kuhlman, M.I., (1988). "Visualizing the Effect of Light Oil on CO2 Foams." paper SPE/DOE 17356, Proceedings of the SPE/DOE Sixth Symposium on Enhanced Oil Recovery, Tulsa, OK, 17-29 April.

Kulander, B.R., C.C. Barton, and S.L. Dean, (1979). "The Application of Fractography to Core and Outcrop Fracture Investigations." U.S. DOE, METC/SP-79/3.

Kyte, J.R., (1970). "A Centrifuge Method to Predict Matrix-Block Recovery in Fractured Reservoirs." SPE Journal, PP. 164-170, June, Richardson, TX. Society of Petroleum Engineers.

Kyte, J.R. and D. W. Berry, (1975). "New Pseudo Functions to Control Numerical Dispersion." Soc. of Petroleum Eng. J. 15, 269-276.

Labastie, A., M. Guy, J.P. Delclaud, R. Iffly, (1980). "Effect of Flow Rate and Wettability on Water-oil Relative Permeabilities and Capillary Pressure." paper SPE 9236 presented at 55th Annual Fall SPE Meeting, Dallas, September, 21-24.

Labastie, A., (1990). "Capillary Continuity Between Blocks of a Fractured Reservoir." SPE 20515, presented at the SPE Annual Technical Conference and Exihibition, New Orleans, September, 23-26.

Land, C.S., (1968). "Calculation of Imbibition Relative Permeability for Two- and Three-Phase Flow from Rock Properties." SOCIETY OF PETROLEUM ENGINEERS June, 6, 149.

Lee, B.Y.Q., T.B.S. Tan, (1987). "Application of a Multiple Porosity/Permeability Simulator in Fractured Simulation." paper SPE 16009 presented at the 1987 SPE Symposium on Reservoir Simulation, San Antonio, February. 1-4.

Lefebvre du Prey, E., (1973). "Factors Affecting Liquid-Liquid Relative Permeabilities of a Consolidated Porous Medium." Society of Petroleum Engineers J., 13, pp. 39-47, February.

Lefebvre du Prey, E., (1976). "Cascade Drainage of Blocks in a Fissured Reservoir." Revue. Institute Francais du Petrole, pp. 173-78, January-February.

Lefebvre du Prey, E., (1978). "Gravity and Capillary Effects on Imbibition in Porous Media." paper SPE 6192, SPE Journal, pp. 195-206, June.

Lenormand R., C. Zarcone, (1984). "Role of Roughness and Edges During Imbibition in Square Capillaries." 59th Annual Technical Conference and Exhibition of SPE of AIME, Houston, Texas, September, pp. 16-19.

Leroy, G., (1976). "Cours de Geologie de Production" Ref. 24, p. 429. Institute Francais du Petrole.

Leverett, M.C., (1941). "Capillary Behavior in Porous Solids." Petroleum Trans, AIME, vol. 142, pp.152-69.

Levine, J.S., (1954). "Displacement Experiments in a Consolidated Porous System." Trans., AIME, vol. 201, p. 57.

Liu, C, (1982). "The unsteady Radial Flow of Compressible Liquids Through a Medium with Multiple Porosity." paper SPE 10580, presented at the SPE-AIME International Meeting on Petroleum Engineering, Beijing, China, March, 19-22.

Long, Jane C.S., Paul A. Witherspoon, (1985). "The Relationship of the Degree of Interconnection to Permeability in Fracture Networks. "Journal of Geophysical Research, Vol. 90, No. B4, pp 3087-3098, March 10.

Loremze, J.C., N.R. Warpinski, and P. T. Branagan, (1989). "Fracture Characteristics and Reservoir Behaviour of Stress-Sensitive Fracture Systems in Flat-Lying Lenticular Formations." Journal of Petroleum Technology, June.

Mahers, E.G., and R.A. Dawe, (1982). "The Role of Diffusion and Mass Transfer Phenomena in the Mobilisation of Oil During Miscible Displacement." proceeding of the Second European Symposium on Enhanced Oil Recovery, Paris, France, pp. 279-288, 8-10 November..

Mahers, E.G., and R.A. Dawe, (1984). "Diffusion Inside Porous Media for EOR Process by Micromodel and Holography." paper SPE 12679 presented at the 4th SPE_DOE Symposium on Enhanced Oil Recovery, Tulsa, Oklahoma, 15-18 April.

Mahers, E.G., and R.A. Dawe, (1985). "Visualisation of Microscopic Displacement Processes Within Porous Media in EOR Capillary Pressure Effects." Proceedings of the Third European Meeting on Improved Oil Recovery, Rome, 16-18 April.

Maini, B.B., G. Coskuner, and K. Jha, (1989). "A Comparison of Steady-State and Unsteady-State Relative Permeabilities of Viscous Oil and Water in Ottawa Sand." Paper presented at the 40th Annual Technical Meeting of the Petroleum Society of C.I.M., Banff, May 28-31.

Mandelbrot, B.B., (1975). "Stochastic Models for the Earth's Relief, the Shape and the Fractal Dimension of the Coastlines, and the Number-Area Rule for Islands." Proc. Nat. Acad. Sci., 72, pp. 3825-3828.

Manjnath, A., and M.M. Honarpour, (1984). "An Investigation of Three Phase Relative Permeability." SPE 12915. Paper presented at the Rocky Mountain Regional Meeting in Casper, WY, May 21-23.

Marle, C.M., (1981). "Multiphase Flow in Porous Media." Technip, Paris, Chapter 7.

Martine, F.D., (1988). "Gels for CO_2 Profile Modifications." paper SPE/DOE 17330, presented at the Sixth Symposium on Enhanced Oil Recovery, Tulsa, OK., April 17-20.

Mast, R.F., (1972). "Microscopic Behavior of Foam in Porous Media." paper SPE 3997.

Mattax, Calvin C., J.R. Kyte, (1962). "Imbibition Oil Recovery from Fractured, Water Drive Reservoir." Society of Petroleum Engineers J., pp. 177-184, June.

McCaffery, F.G: "The Effect of Wettability on Relative Permeability and Imbibition in Porous Media." Ph.D. Thesis, Chem. Eng. Dept. Univ. of Calgary (1973).

McCaffery, F.G., and D.W. Bennion, (1974). "The Effect of Wettability on Two-phase Relative Permeabilities." The Journal of Canadian Petroleum Technology, 13, 42.

McDonald, I.F., and F.A.L. Dullien, (1976). "Correlating Tertiary Oil Recovery in Water-Wet Systems." Society of Petroleum Engineers J. Vol. 16, pp.7-9.

McDonald, A.E., B.L. Beckner, H.M. Chan, T.A. Jones, and S.O. Wooten, "Some Important Considerations in the Simulation of Naturally Fractured Reservoirs." paper SPE 21814, 1991.

McKellar, M. and N.C. Wardlaw, (1982). "A Method of Making Two-dimensional Glass Micromodels of Pore System." Journal of Canadian Petroleum Technology, v.21, n. 4, pp 39-41.

McQuillan, H., (1973). "Small-Scale Fracture Density in the Asmari Formation of Southwest Iran and its Relation to Bed Thickness and Structural Setting." AAPG Bulletin, v. 47, No. 12, pp. 2367-2385. Tulsa, OK: American Association of Petroleum Geologists.

McQuillan, H., "Fracture-Controlled Production from the Oligo-Miocene Asmari Formation in Gachsaran and Bibi Hakimeh Fields, Southwest Iran." in 'Carbonate Petroleum Reservoirs', Edited by ; Perry O. Roeh land P. W. Choquette, New York, Springer-Verlag.

Melrose, J.C., (1965). "Wettability as Related to Capillary Action in Porous Media." Trans. AIME, 234, pp. 259-271.

Melrose, J.C., C.F. Brandner, (1974). "Displacement Efficiency for Oil Recovery by Water Flooding." The Journal of Canadian Petroleum Technology, 13, p. 42, October-December.

Melrose J.C., (1982). "Interpretation of Mixed Wettability States in Reservoir Rocks." paper SPE 10971 presented at the Annual Fall Technical Conference, New Orleans, LA, September, 26-29.

Michaels, A.S., (1964). "Effect of Chromatographic Transport in Hexylamine on Displacement of Oil by Water in Porous Media." Trans., AIME vol. 231, SPE Journal, pp.231, September.

Moench, A.F., (1984). "Double Porosity Models for a Fissured Groundwater Reservoir with Fractured Skin", Water Resources Res. , 831, 7 July.

Mohanty, K.K., H.T. Davis, L.E. Scriven, (1987). "Physics of Oil Entrapment in Water-wet Rock." SPE Reservoir Engineering, February.

Moore, T.F., R.L. Slobod, (1956). "The Effect of Viscosity and Capillarity on the Displacement of Oil by Water." Prod. Monthly, pp. 20-30. Auguest.

Morrison, T.E., J.H. Henderson, (1960). "Gravity Drainage of Oil Into Large Horizontal Fractures." Petroleum Transaction, AIME, pp. 7-15, vol. 219.

Morrow, N.R. and, B. Songkran, (1979). "Displacement Mechanisms in Oil Recovery Processes." paper presented at 3rd International Conf. on Surface and Colloid Science, Stockholm, August 20-25.

Morrow, N.R., H.T. Lim, J.S. Ward, (1986). "Effect of Crude-Oil-Induced Wettability Changes on Oil Recovery." SPE Formation Evaluation, vol. 1, no. 1, pp. 89-105, February.

Naar, J. and, R.J. Wygal, (1961). "Three-Phase Imbibition Relative Permeability." Society of Petroleum Engineers J. , 12, 254.

Nelson, R.A., (1982). "An Approach to Evaluating Fractured Reservoirs." Journal of Petroleum Technology September.

Odeh, A.S., (1959). "Effect of Viscosity Ratio on Relative Permeability." trans. AIME 216, 346. of Fractures Using Fractal Geometry." paper SPE 22703.

Odeh, A.S., (1965). "Unsteady-state Behaviour of Naturally Fractured Reservoirs." Society of Petroleum Engineers J., March.

Oh, S.G., J.C. Slattery, (1976). "Interfacial Tension Required for Significant Displacement of Residual oil ." paper D-2, Proc. of ERDA Symposium on Enhanced Oil and Gas Recovery, Tulsa, Oklahoma, September, 9-10, Published by the Petroleum Publishing Co. of Tulsa, Oklahoma.

Ojeda, E., F.W. Preston, J.C. Jr Calhoun, (1953). "Correlation of Oil Residuals Following Surfactant Floods." Prod. Monthly 18, 20.

Oren, P.E., W.V. Pinczewski, (1990). "The Effect of Film Flow on the Mobilization of Waterflood Residual Oil by Gas Flooding." Proceeding of the 6th European Symposium on Improved Oil Recovery, pp. 705-716, Stavanger, Norway, May 21-23.

Owete, O.S. , W.E. Brigham, (1987). "Flow Behaviour of Foam: A Porous Micromodel Study." SPE Reservoir Engineering, v. 2, n. 3, p. 315.

Paillet, F.L., (1985). "Problems in Fractured Reservoir Evaluation and Possible Routes to Their Possible Solution." The Log Analyst, v.26, No. 6.

Parmeswar, R. and N.L. Maerefat: "A Comparison of Methods for the Representation of Three Phase Relative Permeabilities." SPE 15061. Paper presented at the 56 California Regional Meeting in Oakland CA, April 2-4 (1986).

Parsons, R.W., (1966). "Permeability of Idealised Fractured Rock." SPE Journal, June.

Paterson, L., V. Hornof, and G. Neale, (1984). "Visualization of a Surfactant Flood of an Oil-saturated Porous Medium." SPE Reservoir Engineering Journal, V. 24, n. 3, P. 325 June.

Pavone, D., P. Bruzzi, and R. Verre, (1989). "Gravity Drainage at Low Interfacial tension." proceeding of the Fifth European Symposium on Improved Oil Recovery, Budapest, pp. 165-174, April.

Peden, J.M., M.I. Husain, (1985). "Visual Investigation of Multiphase Flow and Phase Interactions Within Porous Media." paper SPE 14307, presented at 60th Annual Technical Conference and Exhibition of SPE, Las Vegas, NV, 22-25 September.

Peters, J.E., and D.L. Flock, (1981). "The Onset of Instability During Two-Phase Immiscible Displacement in Porous Media." Society of Petroleum Engineers J. April, 249-258.

Peters, J.E., and C.A. Reid, (1990). "A Microcomputer-Based Imaging System for the Visualisation of Fluid Displacements.", Journal Of Petroleum Technology, v. 42, n. 5, pp. 558-563, May.

Philip, J.R., (1955). "Numerical Solution of Equations of Diffusion Type with Diffusivity-Concentration dependent." Trans. Faraday Soc. 51, 885-892.

"Photofabrication Methods with Kodak Photoresists." Eastman Kodak Company, 1979.

Por, G.J., P. Boerrigter, J.G. Maas, and A. de Vries, (1989). "A Fractured Reservoir Simulator Capable of Modeling Block-Block Interaction." paper SPE 19807.

Pruess, K. and T.N. Narsimhan, (1985). "A Practical Method for Modeling Fluid and Heat Flow in Fractured Porous Media." SPEJ, February. 14-26, Richardson, TX, Society of Petroleum Engineers.

Pruess, K., Y.W. Tsang, (1990). "On two phase relative permeability and capillary pressure of rough-walled rock fractures." Water Resources Research, 26 No. 9:1915-1926, September.

Pozzi, A.L., R.J. Blackwell, (1963). "Design of Laboratory Models for Study of Miscible Displacement." Trans., AIME vol. 228, II-28, SPE Journal, pp.28, March.

Purcell, W.R, (1949). "Capillary Pressures - Their Measurement using Mercury and the Calculation of Permeability therefrom." Trans. AIME, vol. 186, 39-48.

Qasem, F., I. Ershaghi, (1994). "IPR of Naturally Fractured reservoirs." Presented at the SPE western Regional Meeting, Long Beach, CA (March 24-25), Richardson, TX. Society of Petroleum Engineers.

Quandalle, P. and J.C. Sabathier, (1987). "Typical Features of a New Multipurpose Reservoir Simulator." paper SPE 16007 presented at the 1987 SPE Symposium on Reservoir Simulation, San Antonio, TX., February. 1-4.

Rapoport, L.A., Leas, W.J, (1953). "Properties of Linear Waterfloods." Trans., AIME, vol. 198, pp. 139-148.

Rayleigh, Lord, (1916). "On Convection Currents in a Horizontal Layer of Fluid when the Higher Temperature is on the Underside." Phil. Mag., 32, P.529.

Reed, R.R., and R.N. Healy, (1976). "Some Physicochemical Aspects of Microemulsions Flooding: A Review" in 'Improved Oil Recovery by Surfactant and Polymer Flooding.' (D. Shah, O. and R. S. Schechter, eds.), Academic Press, New York.

Reid, A.M., S.A. Reid, and S.J. Mazzullo, (1990). "Lowstand Carbonate Reservoirs." Bull. Am. Assoc. Pet. Geologists, 74:221.

Reiss, L.H, (1980). "The reservoir Engineering Aspects of Fractured Formations." Gulf Publishing Co., Houston 108.

Richardson, J.G, (1957). "The Calculation of Waterflood Recovery from Steady-State Relative Permeability Data." Trans. AIME, vol. 210, pp. 373-375.

Romm, E.S., (1966). "Fluid Flow in Fractured Rocks." in Russian, Nedra, Moscow.

Romm, E.S., (1972). "Fluid Flow in Fractured Rocks." English Translation by Blake, W.R., Phillips Petroleum Co., Bartles-Ville, OK.

Rose, W.D, (1972). "Some Problems Connected with the Use of Classical Description of Fluid/Fluid Displacement Processes." in Fundamentals of Transport Phenomena in Porous Media, edited by IAHR, Elsevier Publ. Co. New York.

Rossen, R.H., E.I. Shen, (1987). "Simulation of Gas/Oil Drainage and Water/Oil Imbibition in Naturally Fractured Reservoirs." paper SPE 16982 presented at the 1987 SPE Annual Technical Conference and Exhibition, Dallas, TX, September 27-30.

Saffman, P.G. and Sir Geoferey Taylor, (1958). "The penetration of a fluid into a porous medium or Hele-Shaw cell containing a more viscous liquid." Proc. Roy. Soc. A, volume 245, plate 3.

Saidi, A.M., (1975). "Mathematical Simulation Model Describing Iranian Fractured Reservoirs and Its Application to Haft Kel Field." Proc. , Ninth World Pet. Cong., Tokyo, 4, pp. 209-219.

Saidi, A.M., D.H. Tehrani, and K. Wit, (1979). "Mathematical Simulation of Fractured Reservoir Performance." Proc. 10th World Petroleum Congress, Romania, Vol. 3, 1-9.

Saidi, A.M, (1983). "Simulation of Naturally Fractured Reservoirs." paper SPE 12270 presented at the SPE Symposium on Reservoir Simulation, San Francisco, November 16-18.

Saidi, A.M., (1987). "Reservoir Engineering of Fractured Reservoirs- Fundamental and Practical Aspects." TOTAL Edition Press., Paris.

Saidi, A.M., (1989). "Discussion of Improved Calculations for Viscous and Gravity" Displacement in Matrix Blocks in Dual-Porosity Simulators." Journal of Petroleum Technology, January.

Saidi, A.M., (1990). "Discussion of Gas Gravity Drainage in Fractured Reservoirs Through New Dual-Continuum Approach." SPE Reservoir Engineering, May.

Saidi, A.M., (1991-A). "Discussion of Capillary Pressure in Fractured Porous Media." SPE 21892, Journal of Petroleum Technology, February.

Saidi, A.M., (1991-B). "Discussion of Valid Capillary Pressure Data at Low wetting-Phase Saturation." SPE Reservoir Engineering, August.

Sajjadian, V.A. (1989). "An Experimental Study of Convection Mechanism in The Naturally Fractured Reservoirs." MSc Thesis, University of Petroleum Industry, Ahwaz, Iran.

Sajjadian, V.A., H. Golshan, (1990). "An Experimental Study of the Influence of Connate Water on Gravity Drainage Mechanism in Oil Reservoirs." Fifth Iranian Chemistry & Chemical Engineering Congress, Tehran, 27-30 Auguest.

Sajjadian, V.A., D.H. Tehrani, (1998-A). "Displacement Visualization of Gravity Drainage by Micromodel." paper SPE 49557, 8th Abu Dhabi International Petroleum Exhibition and Conference, 11-14 October.

Sajjadian, V.A., A. Danesh, and D.H. Tehrani, (1998-B), "Laboratory Studies of Gravity Drainage Mechanism in Fractured Carbonate Reservoir-Capillary Continuity." paper SPE 49497, 8th Abu Dhabi International Petroleum Exhibition and Conference, 11-14 October.

Sajjadian, V.A., A. Danesh, and D.H. Tehrani, (1999), "Laboratory Studies of Gravity Drainage Mechanism in Fractured Carbonate Reservoir-Reinfiltration." paper SPE 54003, to be presented at the Sixth Latin American and Caribbean Petroleum Enginneering Conference, Caracas, 21-23 April 1999.

Sarem, A.M., (1966). "Three-Phase Relative Permeability Measurements by Unsteady-State Method." SPE Journal, September, pp. 199-205, Trans. AIME, vol. 237.

Schechter, D.S., B. Guo, (1994). "Parachore Based on Modern Physics and Their Uses in IFT Prediction of Reservoir Fluids." paper SPE 30785.

Schneider, F.N. and W.W. Owens, (1970). "Sandstone and Carbonate Two- and Three-phase Relative Permeability Characteristics." Society of Petroleum Engineers J., 75-84, March.

Shirley, A.I., (1988). in "Surfactant Based Mobility Control (D.H. Smith, ed., ACS Symposium Series 373, American Chemical Society, Washington, D.C., Chapter 12, pp. 234-257.

Sonier F., P. Souillard, and F. T. Blaskovich, (1986). "Numerical Simulation of Naturally fractured Reservoirs." paper SPE 15627 presented at the 1986 SPE Annual technical Conference and Exhibition, New Orleans, October 5-8.

Stahl, R.F., W.A. Martin, and R.L. Huntington, (1943). "Gravitational Drainage of Liquid from Unconsolidated Wilcox Sand." Trans., AIME vol. 151, pp. 138.

Stegemeier, G.L., (1976). "Mechanisms of Oil Entrapment and Mobilization in Porous Media." in 'Improved Oil Recovery by Surfactant and Polymer Flooding' edited by D.O. Shah and R.S. Schechter, eds., Academic Press, New York, in press.

Stones, E.J., S.A., Zimmerman, C.V. Chien, and S.S. Marsden, (1992-A). "The Effect of Capillary Connectivity Across Horizontal Fractures on Gravity Drainage From Fractured Porous Media." paper SPE 24920.

Stones, E.J., Marsden, S.S., and Zimmerman, S.A, (1992-B). "Gravity-Induced Drainage From Fractured Porous Media." paper SPE 24042.

Stone, H.L., (1970). "Probability Model for Estimating Three-Phase Relative Permeabilities." Journal of Petroleum Technology, February., 2, pp. 214-218, Tran. AIME, vol. 249.

Taber, J.J., (1969). "Dynamic and Static Forces Required to Remove a Discontinuous Oil phase from Porous Media Containing Both Oil and Water." Society of Petroleum Engineers J. , March 3-12.

Tan, C.T., A. Firoozabadi, (1995-A). "Theoretical Analysis of Miscible Displacement in Fractured Porous Media by a One-dimensional Model: Part I - Theory." Journal of Canadian Petroleum Technology, February, pp. 17-27.

Tan, C.T., A. Firoozabadi, (1995-B). "Theoretical Analysis of Miscible Displacement in Fractured Porous Media by a One-dimensional Model: Part II - Features." Journal of Canadian Petroleum Technology, February, pp. 18-35.

Tehrani, D. H., V. A. Sajadian, A. Danesh, and G. Henderson, (1995). "Micromodel Studies of Secondary and Tertiary Recovery of Oil by Gas Injection." Conference and Exhibition, Modern Exploration and Improved Oil and Gas Recovery Methods, Cracow, Poland, 12-15 September.

Terwilliger, P.L., L.E. Wilsey, H.N. Hall, P.M. Bridges, and R.A Morse, (1951). "An Experimental and Theoritical Investigation of Gravity Drainage Performance." Trans. AIME, vol. 192, pp. 285-296.

Thomas, L. Kent, T.N. Dixon, and R.G. Pierson, (1983). "Fractured Reservoir Simulation." Society of Petroleum Engineers J., pp. 42-54, February.

Thomas, L. Kent, T.N. Dixon, and R.G. Pierson, (1991). "Ekofisk Nitrogen Injection." SPE Formation Evaluation, June.

Tiffin, D.L., and Yellig, W.F., (1983). "Effects of Mobile Water on Multiple-Contact Miscible Gas Displacement." Society of Petroleum Engineers J., pp. 447-455, June.

Touboul, E., R. Lenormand, and C. Zarcone, (1987). "Immiscible Displacements in Porous Media: Testing Network Simulators by Micromodel Experiments." paper SPE 16954, presented at 62nd Annual Technical Conference and Exhibition of SPE, Dallas, TX, 27-30 September.

Treiber, L.E., D.L. Archer, and W.W. Owens, (1972). "A Laboratory Evaluation of the Wettability of Fifty-five Oil Producing Reservoirs." Trans., AIME vol. 253, pp. II-138, Society of Petroleum Engineers J., 12, 6, pp. 531-540, December.

Van Golf-Racht, T.D, (1982). "Fundamentals of Fractured Reservoir Engineering." Elsevier/North Holland Inc., New York City, p. 710.

Wagner, O.R., R.O. Leach, (1966). "Effect of Interfacial Tension on the Displacement Efficiency" Society of Petroleum Engineers J., 6(4) 335-44.

Wardlaw, N.C., J.P. Cassan, (1978). "Estimation of Recovery Efficiency by Visual Observation of Pore Systems in reservoir Rocks." Bul. Canadian Petroleum Geology, 26, pp. 572-585, December.

Wardlaw, N. C, (1980). "The Effects of Pore Structure on Displacement Efficiency in Reservoir Rocks and in Glass Micromodels." paper SPE 8843, Proceedings First Joint SPE/DOE Symposium on Enhanced oil Recovery, Tulsa, OK, 20 April, P. 345.

Warren, J.E., P.J. Root, (1963). "The Behaviour of Naturally Fractured Reservoirs.", Tans. AIME, vol. 228, pp. 245-254.

Watson, A. Ted, J. Michael Gatens III, W. John Lee, Zillur Rahim, (1990). "An Analytical Model for History Matching Naturally Fractured Reservoir Production Data." SPE Reservoir Engineering, August.

Welge, H.J., (1952). "A Simplified Method for Computing Oil Recovery by Gas or Water Drive." Trans. AIME, vol. 195, pp. 91-98.

Wheeler, E.L: "Scientific Glassblowing." John Wiley & Sons, New York.

Williams, J.K., R.A. Dawe, (1987). "Modelling Pore Scale Displacement Processes at Near Critical Conditions." 4th European Symposium on Enhanced Oil Recovery, Hamburg, Germany, October 27-29.

Wilson, J.L., (Jan 1980). "Facts and Principles of World Petroleum Occurrence." A. D. Mail, editor, CSPG Memoir No. 6, pp. 95-115.

Witherspoon, P.A., (June 1980). "Validity of Cubic Law for Fluid Flow in a Deformable Rock Fracture." Water Resources Research, v. 16, p. 1016.

Wyckoof, R.D., Botset, (1937). "The Flow of Gas-Liquid Mixtures through Unconsolidated Sands." Petroleum Trans, AIME, vol. 123, pp.247-74.

Yortsos, Y.C., and A. Fokas, (1980). "An Analytical Solution for Linear Waterflood Including the Effect of Capillary Pressure." paper SPE 9407 presented at 55th Annual Fall SPE Meeting, Dallas, September, 21-24.

Young, T., (1855). "Miscellaneous Works." G. Peacock, ed., J. Murray, London, Vol. I, P. 418.

Yuster, S.T, (1951). "Theoretical Considerations of Multiphase Flow in Idealized Capillary System." Proc. 3rd World Pet. Congr., pp. 437.

Zerhboub, M. ,H. Bertin, M. Quintard, (1987). "Visualisation of Miscible or Partially Miscible Fluid Displacement Through Porous Media." Presented at 4th European Symposium on Enhanced Oil Recovery, Hamburg, West Germany, October 27-19.

Zhi- An Luan, (1994). "Some Theoretical Aspects of Gravity Drainage in Naturally fractured Reservoirs." paper SPE 28641,

Zimmerman, R.W., G.S. Bodvarsson, (1989). "An Approximate Solution for One-Dimensional absorption in Unsaturated Porous Media." Water resources Research vol. 25, pp. 1422-1428.

Zimmerman, R.W., G.S. Bodvarsson, (1995). "Effective block size for Imbibition or Adsorption in Dual-porosity Media." Geophysic Research Letter., 22, pp. 1461-1464.